An Engineered *Escherichia coli* Consortium for Studying Quorum Sensing

Yuwei Li

Submitted in accordance with the requirements for the degree of
Doctor of Philosophy

University of Leeds
School of Food Science and Nutrition

January 2024

I confirm that the work submitted is my own, except where work which has formed part of a jointly authored publication has been included. My contribution and the other authors to this work has been explicitly indicated below. I confirm that appropriate credit has been given within the thesis where reference has been made to the work of others.

Chapters 2, 3, and 6 contain the work published in Li, Y., Clarke, J.E., O'Neill, A.J., Goycoolea, F.M., and Smith, J. 2023. An Engineered Escherichia coli Community for Studying Quorum Sensing. *SynBio*. **1**(2), pp.144-157. Regarding this jointly authored publication, I conceptualised the project, designed the strains, determined the gene sequences for the designed plasmids, designed and conducted the experiments, analysed and presented the data, and drafted, reviewed, and edited the manuscript. James Smith and Francisco M. Goycoolea conceptualised and supervised the project. Justin E. Clarke determined the gene sequences for the designed plasmids and provided feedback on the design of some of the experiments. James Smith, Francisco M. Goycoolea, and Alex J. O'Neill provided laboratory resources. All the other authors provided feedback on the design of the strains and reviewed and edited the manuscript.

Acknowledgements

I am grateful to my supervisors, Dr James Smith, Prof. Francisco M. Goycoolea, and Dr Helen F. Chappell, for their support and guidance.

I am grateful to Prof. Alex J. O'Neill for allowing me to work with his group and for his support and advice. I would like to thank the members of Alex's group. Special thanks to Dr Justin E. Clarke for his support and advice, especially for guiding me in determining the gene sequences for the designed plasmids. Special thanks to Dr Luiza Galarion for her help and suggestions.

I am grateful to the members of my supervisors' groups. Special thanks to Mengqi Wu for the equal collaboration from the preparation of the microfluidic chips to the generation of the compiled microscopic images. Special thanks to Isaac Noble for helping proofread this thesis and for his suggestions. Special thanks to Mengqi Ma for the helpful discussions.

My gratitude also goes to Franziska Schulze Bockeloh, Dr Hans Kleine-Brüggeney, and Dr Christoph Engwer for their support in the microfluidic experiments and in generating the compiled microscopic images.

I would like to thank the staff at the School of Food Science and Nutrition, especially Dr Joanna H. Sier and Miles Ratcliffe, for their help.

I am indebted to my family and friends for their support and encouragement.

Abstract

In bacterial communities, quorum sensing (QS) is a generalised cell-to-cell communication strategy individuals use to coordinate their collective behaviour via chemical signalling. Typically, QS involves the production and accumulation of QS signalling molecules to sufficient concentrations to regulate gene expression. A number of bacterial behaviours, such as biofilm formation and virulence factor production, were found to be regulated by QS. In natural environments, bacteria live in niches and form intricate consortia where QS plays an important role in controlling their collective behaviour. Studies using model bacterial communities could be a promising approach to provide insight into how bacteria interact with each other and with the environment, which may aid in the development of new antivirulence strategies based on QS. From design and construction to performance assessment, an *E. coli* consortium consisting of three fluorescent strains was established. The consortium was designed based on the LuxI/LuxR system of *Vibrio fischeri*. Three strains possess OHHL (a QS autoinducer) sensing, production, and degradation abilities, respectively, and were constructed as reporters to study the activation and attenuation of QS responses. Meanwhile, these abilities could be regulated by supplementing three inducers and assessed by detecting three fluorescent signals, respectively. The performance of the strains was assessed in the planktonic and encapsulated states. The plasmids of the engineered strains can be modified to study other genes via subcloning. This work can serve as a basis for future studies of QS using an engineered bacterial consortium.

Table of contents

List of Figures

List of Tables

List of Abbreviations

QS	Quorum sensing
OHHL	N-(3-oxohexanoyl)-L-homoserine lactone
AI-1	Autoinducer-1
AIP	Autoinducing peptide
AI-2	Autoinducer-2
AHL	Acyl-homoserine lactone
Ti	Tumour-inducing
OOHL	N-3-oxooctanoyl-L-homoserine lactone
OdDHL	N-3-oxododecanoyl-homoserine lactone
BHL	N-butanoyl-homoserine lactone
DPD	4,5-dihydroxy-2,3-pentanedione
HAI-1	Harveyi autoinducer 1
CAI-1	Cholerae autoinducer 1
σ^{54}	Sigma-54
sRNA	small RNA
DPO	3,5-dimethylpyrazin-2-ol
PQS	Pseudomonas quinolone signal
QQE	Quorum quenching enzyme
PDMS	Polydimethylsiloxane
RBS	Ribosome binding site
EGFP	Enhanced green fluorescent protein
EBFP2	Blue fluorescent protein variant
IPTG	Isopropyl-beta-D-thiogalactopyranoside
aTc	Anhydrotetracycline
Amp	Ampicillin
LB	Lysogeny broth
FI	Fluorescence intensity
OD_{600}	Optical density at $\lambda = 600$
a.u.	Arbitrary units
NAD(P)H	Nicotinamide adenine dinucleotide (phosphate) (reduced form)
ara$^-$	In the absence of arabinose

ara^{+}	In the presence of arabinose
S	Sensor strain
P	Producer strain
R	Regulator strain
T	Tuner (DE3) strain
NS	Not significant
IR	Anhydrotetracycline-induced regulator strain
Non-IR	Non-induced regulator strain
CFU	Colony-forming units
Evos	EVOS FL Auto 2 Imaging System
P1 - 5	Pressure port 1 - 5
CH1 - 4	Chip channel 1 - 4

Chapter 1 Introduction

1.1 Discovery of quorum sensing

Quorum sensing (QS) is a generalised cell-to-cell communication strategy that enables microbial individuals, such as bacteria and fungi, to coordinate their collective behaviour via the production and detection of chemical signalling molecules known as autoinducers (Whitehead et al., 2001; Rutherford and Bassler, 2012; Mehmood et al., 2019). In bacterial communities, QS regulations are dependent on autoinducer concentrations that are related to bacterial density in environments. At low cell density, autoinducer concentrations are insufficient to alter the bacterial phenotypes. As the bacterial communities grow, autoinducers accumulate to sufficient concentrations and are detected by regulators, thereby collectively altering the expression of QS regulons (Whitehead et al., 2001; Rutherford and Bassler, 2012; Schuster et al., 2013). Typically, QS regulons contain genes encoding enzymes that produce the corresponding autoinducers (Rutherford and Bassler, 2012). Additionally, QS regulons also include genes that regulate bacterial behaviour, e.g., bioluminescence (Miyashiro and Ruby, 2012), antibiotic resistance (Zhao et al., 2020), biofilm formation (Papenfort et al., 2017), and the production of virulence factors (Dong et al., 2000).

The QS communication mechanism was first identified in the bioluminescent marine bacterium *Vibrio fischeri*, where it enables the establishment of a symbiotic relationship between *V. fischeri* and *Euprymna scolopes* (Hawaiian bobtail squid). As shown in Figure 1.1, this bacterium employs a LuxI/LuxR QS system for bioluminescence. At low cell density, the autoinducer N-(3-oxohexanoyl)-L-homoserine lactone (OHHL) is synthesised and freely diffuses. At high cell density, OHHL accumulates and binds to the transcriptional regulator LuxR, resulting in the activation of LuxR. The activated LuxR subsequently binds to *lux box*, leading to the expression of *luxICDABEG* and bacterial luminescence. The LuxI catalyses the synthesis of OHHL, forming a positive feedback loop (Kaplan and Greenberg, 1985; Shadel and Baldwin, 1991; Whitehead et al., 2001; Urbanowski et al., 2004; Miyashiro and Ruby, 2012). Besides, it should be noted that in addition to the core LuxI/LuxR system, bioluminescence in *V. fischeri* is also under the control of other systems, such as the ArcA/ArcB two-component regulatory system which was shown to repress luminescence (Bose et al., 2007; Miyashiro and Ruby, 2012).

E. scolopes takes advantage of the bioluminescence of *V. fischeri* as a part of its survival strategy. The squid evolved a special bilobed organ for *V. fischeri* proliferation and control of its own luminescence intensity. Briefly, *E. scolopes* acquires *V. fischeri* from seawater. *V. fischeri* then aggregates and migrates into the bilobed organ and colonises it. When the cell

density reaches a sufficient level, the bioluminescence of *V. fischeri* is activated. During the nocturnal feeding period, the squid adjusts the bilobed organ to emit light that is similar in brightness to moonlight to avoid casting a shadow. Each day at dawn, the squid expels most of *V. fischeri* from its organ. The bioluminescence decreases dramatically. The remaining *V. fischeri* repopulates the organ during the day to glow again (Wilson and Hastings, 1998; Visick and McFall-Ngai, 2000; Visick and Ruby, 2006).

This type of cell density-dependent and autoinducer-mediated QS systems was subsequently discovered in many species other than *V. fischeri*, shedding light on a range of regulatory pathways in microorganisms.

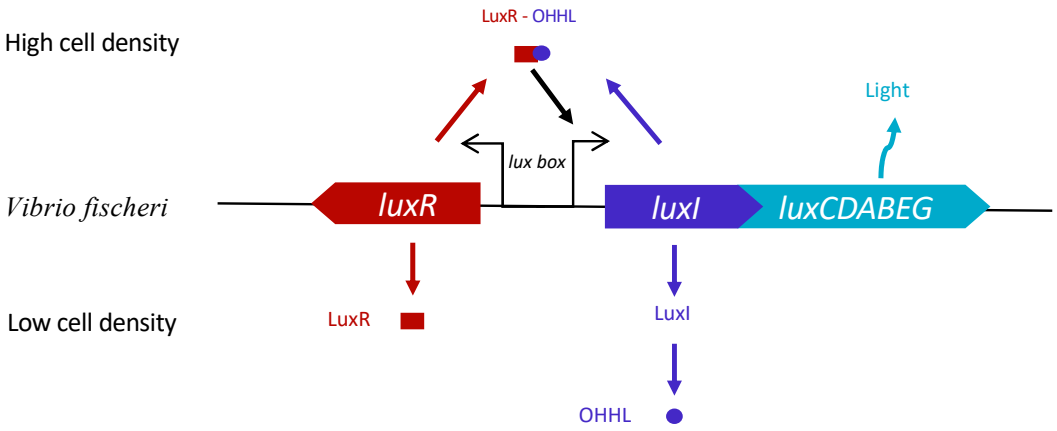

Figure 1. 1 Regulation of bioluminescence in *V. fischeri*. At low cell density, the synthesised autoinducer OHHL diffuses away. At high cell density, OHHL binds to and activates the transcriptional regulator LuxR. The activated LuxR activates the transcription of *luxICDABEG*. The *luxI* encodes the synthase LuxI that catalyses the synthesis of OHHL. The *luxCDABEG* are responsible for bioluminescence.

1.2 Quorum sensing in bacterial communities

In bacterial communities, three main types of QS systems have been discovered (Boo et al., 2021). They are (i) autoinducer-1 (AI-1)-mediated systems commonly employed by Gram-negative bacteria (e.g., the above-mentioned LuxI/LuxR system of *V. fischeri*); (ii) autoinducing peptides (AIPs)-mediated systems commonly employed by Gram-positive bacteria (e.g., Agr system of *Staphylococcus aureus* (Sturme et al., 2002)); (iii) autoinducer-2 (AI-2)-mediated systems that have been discovered in Gram-negative bacteria (e.g., *Vibrio harveyi* (Defoirdt et al., 2008)) and Gram-positive bacteria (e.g., *S. aureus* (Yu et al., 2012)). In addition to these three typical QS systems, other QS signalling molecules have also been identified, such as the QS diffusible signal factor family and dialkylresorcinols (Deng et al., 2014; Brameyer et al., 2015; Defoirdt, 2018).

1.2.1 Quorum sensing mediated by autoinducer-1

Gram-negative bacteria commonly communicate using small molecules, among which acyl-homoserine lactones (AHLs), also known as AI-1, are widely used (Rutherford and Bassler, 2012). As introduced in Section 1.1, this type of QS mechanism typically involves three stages: (i) the synthase catalyses the synthesis of an autoinducer; (ii) when the autoinducer accumulates to a sufficient concentration, it can be detected by its cognate transcriptional regulator, thereby activating the regulator; (iii) the activated regulator can then activate the expression of a QS regulon, which includes the gene encoding the AHL. Of note, some regulators were found to be active in the absence of their cognate AHLs, which blocks their activity (Tsai and Winans, 2010). Besides, some AHLs were found to be detected by other regulators in addition to their cognate regulators (Patankar and González, 2009).

Figure 1.2a below shows the structures of some AHLs, of which OHHL is used by *V. fischeri* while BHL and OdDHL are used by *Pseudomonas aeruginosa* for communication. AHLs may have different acyl chain lengths and different side-chain decorations. The binding of AHLs to their cognate receptors is usually highly specific and is affected by the structure of AHLs (Rutherford and Bassler, 2012). Figure 1.2b shows the general features of the OHHL synthesis reaction. OHHL is produced by the acylation and lactonization of an acyl-acyl carrier protein and an S-adenosyl-L-methionine (Watson et al., 2002). The OHHL synthesis requires synthases such as LuxI, EsaI, or ExpI (Tsai and Winans, 2010).

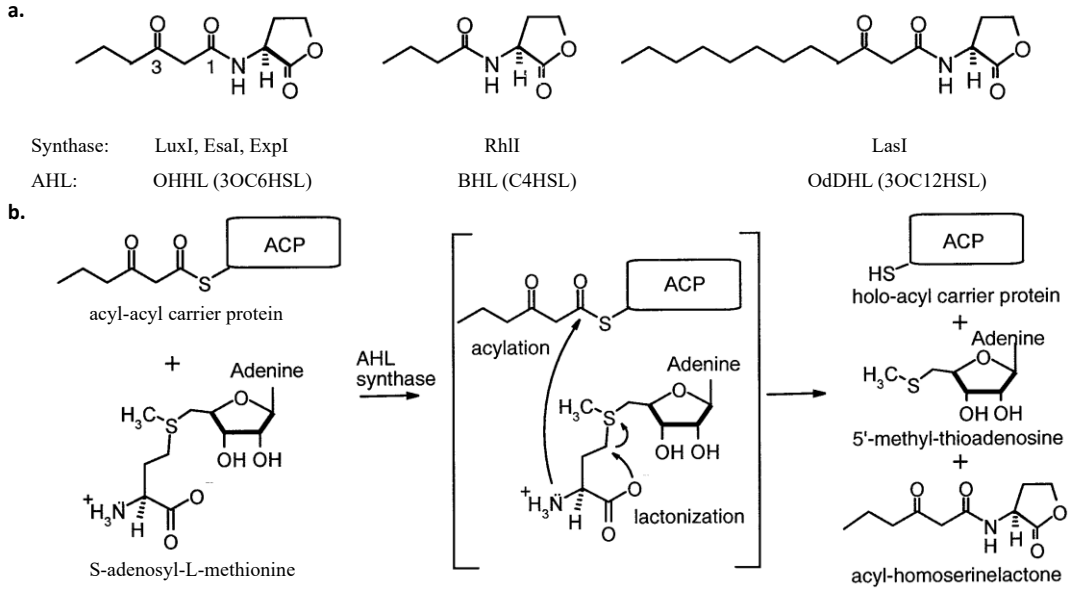

Figure 1. 2 Features of AHL synthesis. **a.** Examples of AHL structures and synthases. **b**. General features of the OHHL synthesis reaction. This figure was modified from the figure published by Watson et al. (2002).

The LuxI/LuxR quorum sensing system

A paradigm AI-1-mediated QS system is the above-mentioned LuxI/LuxR system of *V. fischeri*. The regulation of this LuxI/LuxR system is shown in Figure 1.1 above. This system consists of a bidirectional promoter *lux box*, *luxR,* and *luxICDABEG*. The *luxR* encodes the transcriptional regulator LuxR. The *luxI* encodes the synthase LuxI that catalyses the synthesis of OHHL. The *luxCDABEG* are responsible for the bioluminescence. When the OHHL accumulates to a sufficient concentration, the LuxR-OHHL complex is formed, which can bind to the *lux box* and activate the transcription of the *luxICDABEG* (Kaplan and Greenberg, 1985; Shadel and Baldwin, 1991; Whitehead et al., 2001; Urbanowski et al., 2004; Miyashiro and Ruby, 2012).

The *lux box* is a sequence of 20 base pairs. LuxI is a synthase of 193 amino acid residues that catalyses the synthesis of OHHL (Miyashiro and Ruby, 2012). The transcriptional regulator LuxR consists of 250 amino acid residues. The region between residues 79 to 127 of LuxR is hypothesised for autoinducer binding. The region between residues 184 to 230 is hypothesised for DNA binding (Slock et al., 1990). Of note, the residues 196 to 210 contain a predicted helix-turn-helix motif, which is thought to be required for DNA binding (Brennan and Matthews, 1989; Choi and Greenberg, 1992). In addition, LuxR in the absence of residues 2 to 162 was found to be active and autoinducer-independent (Choi and Greenberg, 1991). Moreover, the binding of LuxR to OHHL has been found to be reversible (Urbanowski et al., 2004).

Figure 1.3 shows the role of the proteins encoded by the lux genes in bioluminescence. The *luxA* and *luxB* encode subunits of a luciferase, respectively. This luciferase catalyses Reaction 1.1 to release light. The reduced form of flavin mononucleotide is indicated as $FMNH_2$; long-chain aldehyde is indicated as RCHO; flavin mononucleotide is indicated as FMN; and long-chain fatty acid is indicated as RCOOH. The FMN reductase responsible for $FMNH_2$ production is encoded by *luxG*. The *luxCDE* encodes acyl-coenzyme A reductase, acyl transferase, and long-chain-fatty-acid ligase, respectively, and are responsible RCHO production (Ruby et al., 2005; Miyashiro and Ruby, 2012).

$$RCHO + FMNH_2 + O_2 \xrightarrow{\text{luciferase}} RCOOH + FMN + H_2O + light \quad \text{---} \quad \text{Reaction 1.1}$$

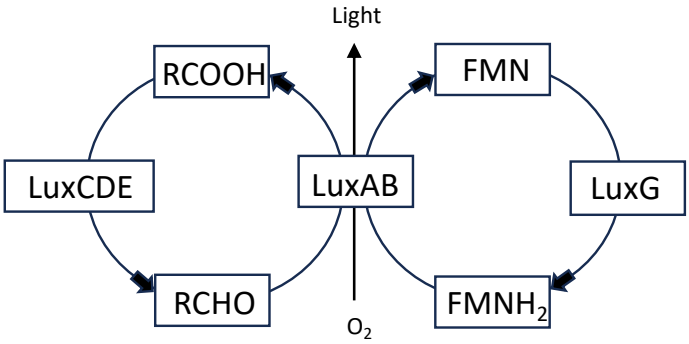

Figure 1. 3 Role of the proteins encoded by the lux genes in bioluminescence. This figure was modified from the figure published by Miyashiro and Ruby (2012).

LuxI/LuxR-type quorum sensing systems

Apart from LuxI/LuxR, QS systems EsaI/EsaR and ExpI/ExpR also rely on OHHL for communication. In the EsaI/EsaR system of *Erwinia stewartii*, EsaI catalyses the synthesis of OHHL, and the *esaR* encodes the transcriptional regulator. Unlike the LuxR, EsaR seems not to regulate the EsaI expression. Besides, EsaR was found to repress its own expression. The OHHL was found to be a critical component that regulates the pathogenicity of *E. stewartii*, where the mutants unable to produce OHHL were found to be non-pathogenic (Bodman and Farrand, 1995; Tsai and Winans, 2010). In *Erwinia carotovora*, the ExpI/ExpR system is involved in the expression of enzymes capable of macerating plant tissues. The *expI* mutant was not found to cause obvious maceration, and autoinducer addition was found to restore the virulence of the *expI* mutant (Pirhonen et al., 1993; Tsai and Winans, 2010).

The TraI/TraR system of *Agrobacterium tumefaciens* is another representative LuxI/LuxR-type QS system. This system controls the expression of genes involved in the conjugation and replication of the tumour-inducing (Ti) plasmid (Hwang et al., 1994; Pappas and Winans, 2003; Lang and Faure, 2014). *A. tumefaciens* contains octopine- and nopaline-type Ti plasmids that express the transcriptional regulator TraR and the synthase TraI that catalyses the syntheses of autoinducer N-3-oxooctanoyl-L-homoserine lactone (OOHL) (Lang and Faure, 2014). It was found that the N-terminal domain of TraR contains an alpha-beta-alpha sandwich that can bind OOHL. The C-terminal domain of TraR contains a helix-turn-helix DNA-binding motif and can bind the tra box (Zhang et al., 2002). Besides, the TraR-OOHL complex was found to activate the expression of TraI, forming a positive feedback loop in OOHL synthesis (Lang and Faure, 2014). Furthermore, it was found that the TraR could rapidly degrade in the absence of

the autoinducer, which may prevent the premature activation of the QS (Zhu and Winans, 2001; Papenfort and Bassler, 2016).

Pseudomonas aeruginosa is a ubiquitous bacterium that colonises diverse niches by exploiting different compounds as energy sources. This bacterium can cause infections in immunocompromised humans, such as those with severe burns and cystic fibrosis (Lyczak et al., 2000). The QS gene expression in *P. aeruginosa* was found to be in a highly interconnected regulatory network including three QS systems. These three QS systems are LasI/LasR, RhlI/RhlR, and *Pseudomonas* quinolone signal (PQS) systems, of which the first two systems are LuxI/LuxR-type systems (Schuster and Peter Greenberg, 2006; Rutherford and Bassler, 2012). In the LasI/LasR system, the synthase LasI catalyses the synthesis of the autoinducer N-3-oxododecanoyl-homoserine lactone (OdDHL), which can be detected by the regulator LasR. At high cell density, the OdDHL-LasR complex activates the transcription of the genes including those encoding virulence factors and the synthase. In the RhlI/RhlR system, similarly, RhlI catalyses the synthesis of autoinducer N-butanoyl-homoserine lactone (BHL), which can be detected by the receptor RhlR. At high cell density, the BHL-RhlR complex activates the transcription of genes including those encoding virulence factors and the synthase (Tsai and Winans, 2010; Rutherford and Bassler, 2012).

Orphan LuxR homologues

In the LuxI/LuxR-type QS systems, genes encoding the autoinducer and transcriptional regulators are considered pairs. With the increasing understanding of bacterial QS, orphan LuxR homologues have been uncovered. A homologue that is not directly associated with a synthase on the genome, contains an autoinducer-binding domain in the N-terminal region, contains a helix-turn-helix DNA-binding domain in the C-terminal region, and predictably does not contain any other functional domains is defined as an orphan LuxR homologue (Patankar and González, 2009). For example, orphan QscR was found in *P. aeruginosa*. QscR was found to form inactive heterodimers with LasR and RhlR at low AHL concentrations, thereby inhibiting the expression of some genes. The inhibition would be relieved when OdDHL and BHL concentrations increase (Ledgham et al., 2003). QscR was also found to repress the expression of some genes that are not regulated by the LasI/LasR or RhlI/RhlR systems. Moreover, QscR, in the presence of OdDHL, was found to activate the transcription of the PA1897 promoter (Lequette et al., 2006). In addition, Patankar and González reviewed a number of orphan LuxR homologues that were found to expand the regulatory networks (Patankar and González, 2009).

1.2.2 Quorum sensing mediated by autoinducing peptides

Gram-positive bacteria usually use autoinducing peptides (AIPs) as signalling molecules. Similar to AI-1-mediated QS systems, typical AIP-mediated systems could be considered to have three stages: (i) autoinducer synthesis, (ii) autoinducer detection, and (iii) regulation of gene expression.

In AIP-mediated QS systems, AIPs are usually encoded as precursors and require transporters for secretion. The precursors need to be processed to become AIPs. In some cases, transporters are able to process precursors into AIPs. When the extracellular AIP concentrations are sufficient, the extracellular AIPs can be detected by two-component signal transduction systems of nearby cells (Rutherford and Bassler, 2012). Such signalling systems typically consist of (i) sensor histidine kinases and response regulators. The signal transduction cascade of these systems could be divided into four steps: (i) signal detection, (ii) kinase activation, (i) phosphotransfer, and (iv) response generation (Zschiedrich et al., 2016). In a typical AIP-mediated system, after detecting the AIP, the sensor kinase autophosphorylates at a conserved histidine, and the phosphate is passed on to a conserved aspartate of a cognate cytoplasmic response regulator. The phosphorylated regulator then activates the expression of the QS regulon. It was found that, in Gram-positive bacteria, genes encoding the AIP precursor, transporter, sensor kinase, and response regulator are typically in an operon. The expression of the operon is activated by the phosphorylated regulator, forming a positive feedback loop. Additionally, in some AIP-mediated QS systems, AIPs are transported back into cells and interact with receptors to regulate gene expression (Rutherford and Bassler, 2012).

A representative example of this type of system is the Agr system in *S. aureus*. As shown in Figure 1.4, AgrD is the precursor of AIP. The transmembrane transporter AgrB participates in the maturation and export of AIP. The sensor histidine kinase AgrC and response regulator AgrA form a two-component signal transduction system. When the concentration of AIP reaches a sufficient level, AgrC-AIP binding results in the autophosphorylation of AgrC. The phosphate is then transferred to AgrA. The phosphorylated AgrA is able to activate the transcription of *agrBDCA* and *RNAIII*, which regulates the production of virulence factors (Sturme et al., 2002; Rutherford and Bassler, 2012; Tan et al., 2018). It was also found that the Agr system regulates biofilm formation and dispersal in *S. aureus* (Boles and Horswill, 2008; Tan et al., 2018).

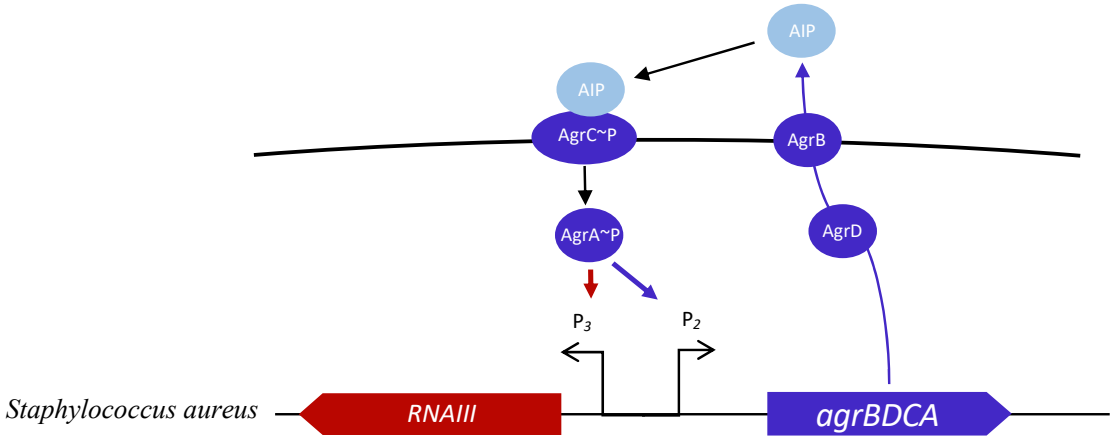

Figure 1. 4 Agr system in *S. aureus*. The precursor AgrD is transported out of the cell by the transmembrane transporter AgrB, which may also process the AgrD into AIP. When the concentration of the AIP reaches a sufficient level, AIP binds to sensor histidine kinase AgrC, resulting in the autophosphorylation of the AgrC. The phosphate is transferred to the response regulator AgrA. Phosphorylated AgrA can then activate promoters P_2 and P_3.

1.2.3 Quorum sensing mediated by autoinducer-2

In addition to the Agr system, *S. aureus* employs another typical QS system mediated by a furanosyl borate diester, also known as autoinducer-2 (AI-2). The role of the AI-2-mediated system in *S. aureus* is less understood (Le and Otto, 2015). In an AI-2-mediated QS system, *luxS* encodes S-ribosylhomocysteine lyase that converts S-ribosylhomocysteine to homocysteine and 4,5-dihydroxy-2,3-pentanedione (DPD). DPD is an AI-2 precursor that can spontaneously convert to AI-2 (Vendeville et al., 2005; Rutherford and Bassler, 2012). Furthermore, as the *luxS* has been found in a number of Gram-negative and Gram-positive species, AI-2 is considered a language that enables interspecies communication (Federle and Bassler, 2003; Rutherford and Bassler, 2012).

A representative bacterium that employs the AI-2-mediated QS system *V. harveyi*, whose QS has been shown to be regulated by three autoinducers: (i) harveyi autoinducer 1 (HAI-1) of the AI-1 type, (ii) AI-2, and (iii) cholerae autoinducer 1 (CAI-1) (Defoirdt et al., 2008). As shown in Figure 1.5, these autoinducers are synthesised by three enzymes and detected by three signal transduction systems, respectively. In contrast to the Agr system of *S. aureus*, autoinducer sensor proteins in *V. harveyi* autophosphorylate in the absence of sufficient autoinducers. The phosphate is transferred to receptor LuxO via phosphorelay protein LuxU. The phosphorylated LuxO, together with the sigma factor sigma-54 (σ^{54}), activates the transcription of genes encoding small RNAs (sRNAs). The sRNAs, together with RNA chaperone Hfq, inhibit the $LuxR_{vh}$ expression and then inhibit QS regulon expression. When autoinducers accumulate to

sufficient concentrations, autoinducer sensor proteins switch from kinases to phosphatases that dephosphorylate the receptor LuxO. Lack of the sRNAs lifts the repression of $LuxR_{vh}$ expression, thereby activating the expression of QS regulon (Lilley and Bassler, 2000; Tu and Bassler, 2007; Defoirdt et al., 2008).

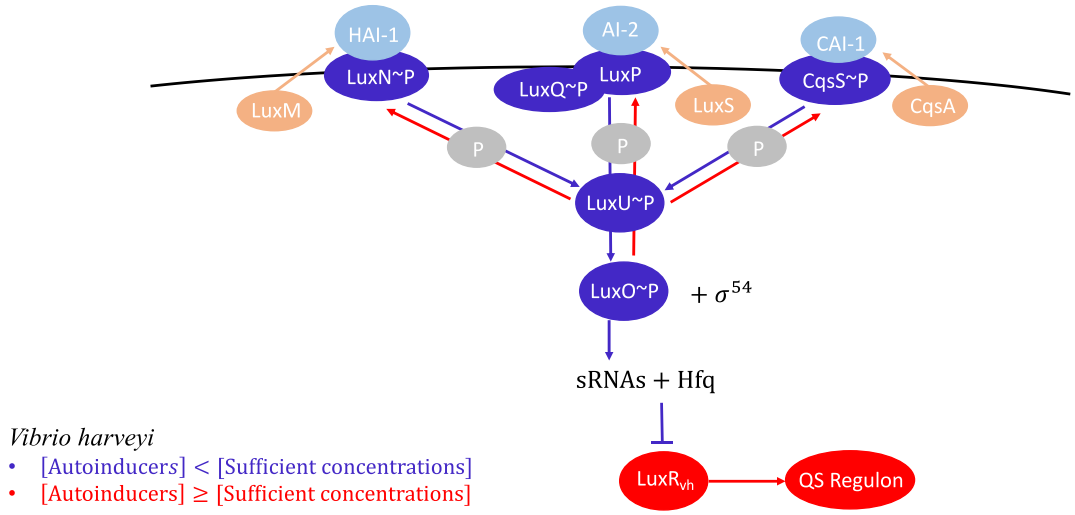

Figure 1. 5 QS systems in *V. harveyi*. Three signal transduction systems respond to autoinducers HAI-1, AI-2, and CAI-1, respectively. In the absence of sufficient autoinducers (scenarios coloured in dark blue), autoinducer sensor proteins function as kinases that pass phosphate to response regulator LuxO via phosphorelay protein LuxU. The phosphorylated LuxO, together with σ^{54}, activates the transcription of genes encoding sRNAs. The sRNAs, together with Hfq, inhibit $LuxR_{vh}$ expression and then inhibit QS regulon expression. After detecting autoinducers (scenarios coloured in red), autoinducer sensor proteins switch to phosphatases, resulting in the dephosphorylation of the LuxO. The expressed $LuxR_{vh}$ activates the expression of QS regulon.

1.2.4 Other quorum sensing systems

In addition to the three main types of QS systems introduced above, a number of other QS systems have been discovered (Papenfort and Bassler, 2016). For example, apart from the QS systems mediated by HAI-1 and AI-2, *V. harveyi* also employs a QS system mediated by CAI-1, an autoinducer synthesised by CqsA and detected by the CqsS (Figure 1.5). The human pathogen *Vibrio cholerae* also employs the QS systems mediated by AI-2 and CAI-1. In *V. cholerae*, when autoinducer concentrations are below the sufficient level, phosphorylated LuxO, together with σ^{54}, activates the transcription of genes encoding sRNAs (Lenz et al., 2004). These sRNAs, together with Hfq, activate the production of low-cell-density master regulator AphA and repress the production of high-cell-density master regulator HapR. Under this condition, biofilm formation and virulence factor production are activated. After detecting autoinducers, the production of AphA and HapR is reversed, and biofilm formation and

virulence factor production are inhibited (Papenfort et al., 2017). Additionally, HapR was found to activate the production of proteases, which may enable *V. cholerae* to detach from the epithelium and leave the host (Zhu and Mekalanos, 2003; Papenfort et al., 2017). Moreover, Papenfort et al. (2017) discovered a QS system using 3,5-dimethylpyrazin-2-ol (DPO) as an autoinducer and an orphan LuxR homologue, VqmA, as a regulator. The VqmA-DPO complex activates the expression of a sRNA VqmR, which, together with Hfq, inhibits biofilm formation (Papenfort et al., 2017). Of note, before the discovery of the DPO-mediated QS system, *V. cholerae* was considered to employ only the QS systems mediated by CAI-1 and AI-2, suggesting that even in intensively studied microorganisms, there may be QS systems that have not yet been discovered.

1.2.5 Quorum sensing in complex environments

The above are some representative QS systems that control the collective behaviour of bacteria, some of which can threaten the survival of other organisms. Moreover, the QS system mediated by the same autoinducer may have different QS mechanisms in different species, such as the QS systems mediated by AI-2 and the CAI-1 in *V. harveyi* and *V. cholerae*. However, being able to respond to the same autoinducers enables communication within and between species. A representative bacterium is *V. harveyi*. The three languages it uses may facilitate its communication with other species. To be specific, the HAI-1 (LuxM/LuxN QS system) is present in a few closely related *Vibrio* species and CAI-1 (CqsA/CqsS QS system) has been found to be conserved in many *Vibrio* species. Therefore, HAI-1 and CAI-1 may be languages that facilitate communication between *Vibrio* species. The LuxS responsible for AI-2 production has been found in many bacterial species, suggesting that AI-2 may be a widespread interspecies language (Ng et al., 2011).

In natural environments, bacteria commonly inhabit heterogeneous niches that are subject to dynamic changes such as shear flow, nutrients, and surface topography (Mukherjee and Bassler, 2019). In addition to signalling molecules, environmental conditions may also affect QS. For example, as reviewed by Mukherjee and Bassler (2019), the bacterial biomass required to initiate QS may increase with increasing fluid flow rate as fluid flow removes autoinducers. Moreover, bacteria commonly form biofilms, which are extracellular matrices mainly composed of water and extracellular polymeric substances such as polysaccharides, proteins, DNA, and lipids (Di Martino, 2018). Biofilm formation is considered part of the bacterial survival strategy that could enhance cell-to-cell communication, facilitate horizontal gene transfer, and increase resistance to external perturbations such as antibiotic treatment (Miller and Gilmore, 2020). QS responses could be stochastic, i.e., a subpopulation of cells shows QS responses while the remaining population does not. In addition, intervening in the

communication of gut microbiota by manipulating AI-2 concentration was found to shape the composition of the gut microbiota and aid in the resistance of antibiotic-induced dysbiosis in mice (Thompson et al., 2015; Mukherjee and Bassler, 2019).
In addition, a number of interkingdom interactions between bacteria and hosts were found (Verbeke et al., 2017). An AI-2 mimic was found to be produced by some mammalian epithelial cells in response to *V.harveyi* and activate the bioluminescence response of *V.harveyi* (Ismail et al., 2016). The host-derived factors could also modify, degrade, and sequester the autoinducer, thereby participating in bacterial communication (Mukherjee and Bassler, 2019). Another example is that mentioned above in Section 1.2.1, in *A. tumefaciens*, genes encoding TraI and TraR were found on octopine- and nopaline-type Ti plasmids (Lang and Faure, 2014). Indole, which can be produced by some plants and bacteria, was also found to inhibit QS in many bacterial species, as reviewed by Lee et al. (2015).

QS was also found to be involved in the emergence of bacterial cooperation and cheating. For example, in *P. aeruginosa*, QS controls the expression of elastase required for casein digestion. Secreted elastase is considered a "public good" as it is produced by individuals but could benefit the entire community. It was reported that when wild-type *P. aeruginosa* was grown in M9 minimal medium with caseinate as the sole carbon source, *lasR* mutants that were unable to grow independently in the medium emerged (Sandoz et al., 2007). Additionally, QS is considered involved in the competition in polymicrobial communities as it controls the expression of toxins that may promote competition with other bacterial species (Abisado et al., 2018).

1.3 Application of quorum sensing manipulation

With the increasing understanding of QS mechanisms, QS intervention targeting the QS system is a promising antivirulence strategy that can be applied in different fields such as aquaculture, agriculture, and human health. The application of QS-related genetic parts in biotechnology is also being explored, e.g., using these genetic parts to engineer strains for bioproduction and chemical detection (Choudhary and Schmidt-Dannert, 2010; Miller and Gilmore, 2020; Boo et al., 2021). The focus of this thesis is to engineer a bacterial consortium, including a biosensor, to study the activation and attenuation of QS responses. The application of QS in antivirulence therapy and autoinducer biosensors is introduced next.

1.3.1 Application of quorum sensing in antivirulence therapy

Antibiotics are antimicrobial substances used to treat bacterial diseases. However, antibiotic treatment commonly places strong selective pressures on the target bacterial communities and may lead to the emergence and spread of antibiotic-resistant strains. Diseases caused by these antibiotic-resistant strains are a major cause of death. Consequently, antivirulence therapy is considered an alternative approach to disease control that focuses on disarming rather than killing pathogenic bacteria (Cegelski et al., 2008; Defoirdt, 2018). As introduced in Section 1.2, a number of bacteria employ QS systems to regulate the production of virulence factors. Antivirulence via QS intervention is considered an alternative to control diseases caused by these bacteria. Screening and assessing natural and synthetic QS intervening agents, i.e., QS inhibitors and agonists, is a common approach to developing QS intervention therapy (Rutherford and Bassler, 2012; Defoirdt, 2018). Moreover, bacteria could persist under antibiotic pressure in biofilm and were reported to be more resistant to antibacterial agents when grown in biofilm than in culture (Anwar et al., 1990; Cegelski et al., 2008). Regulating biofilm formation and dispersal via QS intervention may serve as an adjunct to and may improve the efficacy of antibiotic treatments.

Quorum sensing agonists

An example of an agonist-based application is the delivery of CAI-1 for cholera treatment. Cholera is an acute diarrhoea caused by *V. cholerea* that can lead to death if untreated (Faruque et al., 1998). As introduced in section 1.2.4, in *V. cholerea*, accumulation of CAI-1 can activate the production of HapR. HapR was found to inhibit virulence factor production and biofilm formation. HapR was also found to activate the production of proteases, which may enable *V. cholerea* to detach from the epithelium and leave the host (Zhu and Mekalanos, 2003; Papenfort et al., 2017). Therefore, CAI-1 supplementation is considered a treatment that may alleviate cholera symptoms. A previous study found that (pre)treatment with engineered *E. coli* Nissle 1917 expressing CAI-1 increased the survival of mice fed with *V. cholerae* and reduced the coverage of cholera toxin in the mouse intestines (Duan and March, 2010). Additionally, encapsulating CAI-1 in nanoparticles that promote the diffusion of CAI-1 was found to increase the *V. cholera* QS responses (Lu et al., 2015). These findings suggest the potential for developing QS-based engineering probiotics and oral drugs to against cholera.

Quorum sensing inhibitors and quorum quenching enzymes

A variety of molecules, such as enzymes, non-cognate AHLs, phytochemicals, and synthetic molecules, have been shown to possess QS inhibition ability (Kalia et al., 2019). QS inhibition can be achieved by inhibiting the synthesis of autoinducers, or by degrading, modifying, or sequestering autoinducers. Additionally, it was reported QS inhibition can be achieved by interfering with the binding between autoinducers, regulators, and promoters (Fetzner, 2015; Defoirdt, 2018; Kalia et al., 2019). Of note, bacteria were found to evolve mutants to resist QS inhibitors (García-Contreras et al., 2013; Sikdar and Elias, 2020). Quorum quenching enzymes (QQEs) were found to inhibit the production of virulence factors, motility, and biofilm formation. For the AI-1, a number of QQEs, including lactonases, acylases, and oxidoreductases, that can degrade or modify AHL have been found (Fetzner, 2015; Sikdar and Elias, 2020). Compared to QQEs for AI-1, relatively few QQEs were found for AI-2 (Sikdar and Elias, 2020). The kinase LsrK was found to phosphorylate AI-2, thereby interfering with AI-2-mediated QS (Roy et al., 2010). Besides, Sikdar and Elias (2020) also reviewed some other enzymes that can degrade other QS signalling molecules.

The QQE employed in this work is an AHL lactonase AiiA. AHL lactonases can degrade AHLs by hydrolysing their lactone rings. Many AHL lactonases were found to degrade more than one AHL (Fetzner, 2015; Sikdar and Elias, 2020). The first AHL lactonase identified is the AiiA discovered in *Bacillus subtilis* 240B1 (Dong et al., 2000; Fetzner, 2015). Purified AiiA was found to inactivate OHHL, N-3-oxodecanoyl-L-homoserine lactone, and OOHL. No production of autoinducer was detected in the culture supernatant of *Erwinia carotovora* SCG1 expressing AiiA. The enzyme activities of three extracellular pectolytic enzymes of *E. carotovora* expressing AiiA were lower than those of the *E. carotovora* SCG1 strains that did not express AiiA. Plant tissues inoculated with *E. carotovora* expressing AiiA also showed attenuated soft rot disease symptoms compared with those inoculated with the *E. carotovora* SCG1 strains that did not express AiiA (Dong et al., 2000). Subsequently, AiiA homologues with varying degrees of AHL-degrading activity were identified in *Bacillus thuringiensis* subspecies (Lee et al., 2002). As AiiA has been shown to degrade AHLs and attenuate QS responses and has a library of homologues that can be used to arm an engineered strain, *aiiA* was used as a component to construct the QS regulator strain in this work.

1.3.2 Quorum sensing biosensors

As introduced in Section 1.2, QS regulations are dependent on autoinducer concentrations, and a number of QS responses have been found to be associated with the production of virulence factors. Autoinducer detection is considered an approach that could support clinic diagnostics (Miller and Gilmore, 2020). A variety of techniques are available for autoinducer detection and quantification, such as chromatography, mass spectrometry, and bacterial biosensors (Verbeke et al., 2017; Miller and Gilmore, 2020). A commonly used method is high-performance liquid chromatography-tandem mass spectrometry, which is accurate in the detection of autoinducers and can be used to evaluate the accuracy of the biosensor. However, this method requires expensive equipment and could be time-consuming. QS biosensors that are able to express quantifiable phenotypes upon induction by autoinducers are considered promising alternatives (Miller and Gilmore, 2020).

As introduced in Section 1.2.1, an AI-1-mediated QS system typically involves a promoter that controls gene transcription dependent on the concentration of an autoinducer. Therefore, a QS reporter strain could be engineered by introducing a plasmid containing such a promoter that controls the transcription of a reporter gene into a suitable host strain. The concentration of the autoinducer in the environment could then be estimated based on the intensity of the reporter signal expressed by the engineered strain.
E. coli, which inherently lacks AI-1 synthase, is widely used as a host strain. Meanwhile, *luxCDABE*, fluorescent protein genes, and *lacZ* are commonly used as reporter genes (Steindler and Venturi, 2007; Miller and Gilmore, 2020). The *lacZ* encodes beta-galactosidase, which can catalyse the hydrolysis of colourless 5-bromo-4-chloro-3-indolyl-beta-D-galactopyranoside (X-gal) into galactose and 5-bromo-4-chloro-3-hydroxyindole. 5-bromo-4-chloro-3-hydroxyindole can then oxidise into the visible blue compound 5,5'-dibromo-4,4'-dichloro-indigo (Burn, 2012). Additionally, *Chromobacterium violaceum* CV026, which can produce the purple pigment violacein upon induction by AI-1 (acyl chain lengths range from C_4 to C_8), is also a commonly used AI-1 biosensor (McClean et al., 1997; Miller and Gilmore, 2020).

For AI-2 detection, a commonly used biosensor is *V. harveyi* BB170. This mutant has been genetically modified to be unable to produce AI-1 and AI-2 and is insensitive to AI-1. Therefore, its bioluminescence intensity depends on the concentration of AI-2 (Verbeke et al., 2017; Miller and Gilmore, 2020). As for AIP detection, *Enterococcus faecalis* is widely used, and quantifiable readings are usually measured via turbidimetry (Verbeke et al., 2017). Additionally, several cell-free biosensors have been designed to quantify autoinducer concentrations (Miller and Gilmore, 2020). For example, a cell-free biosensor engineered based on QS genetic parts of *P. aeruginosa* was found to be able to quantitatively measure the concentration of OdDHL in cystic fibrosis lung sputum samples (Wen et al., 2017).

1.4 Engineered bacterial consortia

QS biosensors are valuable in screening for novel QS inhibitors and have the potential to support clinic diagnostics (Wen et al., 2017; Qin et al., 2020; Miller and Gilmore, 2020). However, single sensors may fall short of representing the real-life context of microbial communities consisting of numerous species in heterogenous niches and under continuous dynamic changes. In particular, QS regulations have been shown to be affected by the interspecies and interkingdom signals and are involved in polymicrobial cooperation, cheating, and competition (Abisado et al., 2018; Mukherjee and Bassler, 2019). Studies of QS biosensors usually focus on recreating the signal listening element of QS mechanisms but lack the signal transmission and regulation participants as a bacterial community. Consequently, it is challenging to study QS activation and attenuation activities as a complex community. Studies using engineered bacterial consortia could be a promising approach to provide insight into how bacteria interact with each other and with the environment, which may aid in the development of new antivirulence strategies based on QS. Moreover, real-life microbial communities are usually extremely complex, and engineered model communities could provide a research platform to deconstruct part of this complexity.

In addition, QS-related genetic parts can support the construction of exquisite synthetic genetic circuits. However, expressing a complex synthetic genetic circuit could impose a substantial metabolic burden on the host cell (Tsoi et al., 2018). Additionally, it was found that two modules of a circuit in a single strain showed resource competition. Decoupling the two modules into two strains reduced the adverse effects of resource competition (Zhang et al., 2021). Dividing the labour of complex circuits into engineered consortia may be a promising approach as it may reduce metabolic burden, reduce resource competition, and optimise productivity compared to accomplishing the task in a single strain (Tsoi et al., 2018; Duncker et al., 2021; Zhang et al., 2021). Freely diffusible QS autoinducers could serve as practical tools for connecting the engineered bacterial strains. Besides, managing strain ratios during co-culture is a challenge when using engineered bacterial consortia for expression. Constructing using QS-related genetic parts may be a viable approach to regulate the strain ratios (Boo et al., 2021). In addition, as an AI-1 synthase may produce more than one AHL and an AI-1 regulator may respond to more than one AHL, the orthogonality of the QS systems should be assessed when designing circuits using genetic parts from different QS systems (Davis et al., 2015; Tekel et al., 2019).

1.5 Bacteria in microfluidic platforms

Microfluidics is known as a technology that manipulates fluids at the microscale. Fluid flows at the microscale are usually laminar, which makes the fluid dynamics predictable (Weibel et al., 2007; Sackmann et al., 2014). Additionally, microfluidics enables miniaturisation, integration, precision, and automation control of experimental processes. Supported by designed devices, microfluidics provides novel platforms for biological studies (Sackmann et al., 2014; Pérez-Rodríguez et al., 2022). Soft lithography is a collection of techniques for fabricating versatile microscale and nanoscale devices based on printing, moulding, and embossing. Elastomeric polymers such as polydimethylsiloxane (PDMS) are widely used materials for soft lithography (Weibel et al., 2007). PDMS possesses a number of properties, such as chemical inertness, biocompatibility, flexibility, and optical transparency, making it a good candidate material for microfluidic studies (Weibel et al., 2007; Pérez-Rodríguez et al., 2022). A number of microfluidic devices have been developed to study bacterial behaviours, such as biofilm formation and antibiotic resistance. Microfluidics allows for sophisticated incubators, precise control of the cultivation environment, microscopic visualisation, and high-throughput studies, providing a relatively more realistic and efficient platform for studying bacterial communities compared to traditional microbiological techniques (Pérez-Rodríguez et al., 2022).

As introduced in Section 1.2.5, bacteria continuously interact with the environment they inhabit. In addition to designing synthetic genetic circuits, a number of environmental parameters, such as subpopulation distribution, community size, and nutrition supplementation, could be manipulated to investigate the phenotype and performance of engineered bacterial communities. Danino et al. (2010) designed an *E. coli* genetic clock whose fluorescent protein expression oscillated over time. The strain contains two plasmids constructed using the luxI promoter, *luxI*, *luxR*, *aiiA*, and *yemGFP*. Briefly, the *luxI*, *aiiA* and *yemGFP* are under the control of three luxI promoters, respectively. Therefore, the luxI promoter in the strain is positively and negatively regulated. The fluorescence intensity of the population was found to oscillate over time in a tailored microfluidic device. The device provided an ideal environment for achieving the oscillations. Specifically, the chamber size allowed for appropriate nutrition distribution, autoinducer density, and bacterial density. In addition, the flow rate, which was related to the effective degradation rate of AHL, was found to affect the oscillation period and amplitude (Danino et al., 2010).

Droplet microfluidics is a technique that enables the encapsulation of experimental targets, such as single molecules or single cells, into isolated compartments (monodisperse droplets) where experiments could then be conducted for further analysis (Theberge et al., 2010). The droplets are formed by mixing two immiscible phases, usually an oil phase and an aqueous phase (van Tatenhove-Pel et al., 2020; Pérez-Rodríguez et al., 2022). Monodisperse droplets are formed using different generators, such as T-junction (Nisisako et al., 2002) and flow-focusing (Kleine-Brüggeney et al., 2021) generator. Additionally, Poisson statistics can be used for single-cell encapsulation, which may aid in the study of bacteria (Kleine-Brüggeney et al., 2021; Pérez-Rodríguez et al., 2022). In this work, a macro-to-micro platform developed by Evorion Biotechnologies (Münster, Germany) for microfluidic cell culture was employed to visualise and assess the performance of engineered strains in microdroplets (Kleine-Brüggeney et al., 2019; Kleine-Brüggeney et al., 2021).

1.6 Objective and chapter summary

This work aimed to engineer a model consortium consisting of three fluorescent *E. coli* strains as the sensor, producer, and regulator of an AI-1-type autoinducer to study cell-to-cell QS communication. The QS-related abilities of these strains were expected to be tuneable by different external inducers. The genetic components associated with the designed functions were expected to be dissembled and assembled by routine cloning techniques to facilitate future studies of other QS-related proteins. Moreover, the QS-related activities were expected to be trackable and quantifiable by three distinguishable fluorescent proteins. In general, the workflow can be divided into four steps: (i) construction of the bacterial consortium (Chapter 2), (ii) characterisation of the engineered strains in the planktonic state (Chapter 3), (iii) phenotypic analysis of the strains encapsulated in agarose hydrogel microbeads (Chapter 4), and (iv) assessment of performance of the strains encapsulated in agarose hydrogel (Chapter 5).

Chapter 2 discusses the construction of the engineered bacterial consortium. To engineer the bacterial consortium, three plasmids were designed based on the LuxI/LuxR QS system of *V. fischeri*. Meanwhile, the genes of three inducer concentration-dependent promoters, three fluorescence proteins, and two restriction sites were selected as components to construct the plasmids. The strains obtained were preliminarily screened by fluorescence detection. The plasmids of the strains were sequenced and analysed.

Chapter 3 discussed the performance of the strains in the planktonic state. The bacterial growth, fluorescence intensity, and cell response levels (fluorescence intensity normalised by growth) of the strains induced at a range of inducer concentrations were characterised. The ability of

the producer to activate the sensor's response by producing OHHL, and the ability of the regulator to attenuate the sensor's response by degrading OHHL were assessed.

The sensor and producer strains were encapsulated in agarose hydrogel microbeads and cultivated overnight on microfluidic chips while being imaged under transmitted light and fluorescence channels. The phenotypes of the bacterial communities in the microbeads are discussed in Chapter 4. The colony response levels (fluorescence intensity normalised by area size) of the target colonies were digitised using Fiji-ImageJ. The QS responses of the strains encapsulated in agarose hydrogel microbeads were discussed in Chapter 5.

Chapter 6 discusses the main results and limitations of this work. This chapter also discusses some work that could be conducted in future studies.

Chapter 2 Construction of a model bacterial consortium

In this chapter, the construction of a model bacterial consortium engineered for studying quorum sensing based on the LuxI/LuxR system of *V. fischeri* is introduced. The aim was to construct an *E. coli* consortium of three fluorescent strains, where each strain performs a QS-related function, namely sensing, production, and degradation of a QS autoinducer. Three plasmids were constructed, each containing a fluorescent protein gene and at least one QS-related gene. To make the expression of the strains tuneable, three inducible promoters were used to control the transcription of the designed inserts, allowing artificial perturbation to the expression of the bacterial community during cultivation. To increase the flexibility of plasmid construction of the bacterial consortium, the designed inserts were flanked by restriction sites, allowing the plasmids of the three engineered strains to be modified to study other genes via subcloning.

2.1 Materials, equipment, and software

2.1.1 Strains and plasmids

E. coli Tuner (DE3) and DH5alpha were used as host cells for expression and storage strains, respectively. Plasmid pBAD24 in *E. coli* (ATCC 87399) was purchased from ATCC. Plasmid pZH509 was a gift from Zach Hensel (Hensel, 2017). Plasmid pET-21 (+) with the designed insert already inserted was from Twist Bioscience. The other two designed inserts were synthesised and assembled in vector pTwist Amp High Copy by Twist Bioscience. The designed inserts of producer and regulator strains were optimised using the Twist Bioscience codon optimisation tool. All plasmids used (pBAD24, pET-21(+), and pZH509) have an *ampR* that confers ampicillin resistance.

2.1.2 Genetic parts of inserts

The genetic parts *luxR* (BBa_C0062), *luxPR_4G12T* (BBa_K3205005), *aiiA* (BBa_C0160), terminator rrnB T1 (BBa_B0010), and a ribosome binding site (RBS) (BBa_K3288007) were all obtained from iGEM (https://parts.igem.org/Main_Page, accessed 30 January 2024). Two ribosome binding sites used in this work were both modified from BBa_K3288007. In addition, natural terminators ECK120033736, ECK120029600, and ECK120033737 and synthetic terminators L3S2P21 and L3S3P21, which showed good abilities in reduction in the

downstream expression (Chen et al., 2013), were used in pairs in this work to ensure termination.

The *tetR* constitutively expressed from promoter P_{N25} (Muthukrishnan et al., 2012) was derived from plasmid pZH509. The genes encoding the enhanced green fluorescent protein (EGFP) (GenBank: U55761.1) (Cormack et al., 1996), LuxI (GenBank: M19039.1) (Devine et al., 1988), mCherry (GenBank: AY678264.1) (Shaner et al., 2004), and blue fluorescent protein variant (EBFP2) (GenBank: EF517318.1) (Ai et al., 2007) were all obtained from GenBank (https://www.ncbi.nlm.nih.gov/genbank/, accessed 30 January 2024) (Clark et al., 2015).

Information on the genetic materials (Table A.1), main experimental materials and equipment (Table A.2) used in this chapter is provided in Appendix A. The sequences of the constructed plasmids are provided in Appendix B. Information on software used in this chapter is provided in Table A.3 in Appendix A.

2.2 Design and construction of the bacterial consortium

2.2.1 Design of the model bacterial consortium

The flowchart for designing the model *E. coli* consortium is shown in Figure 2.1. The aim of this work was to construct an *E. coli* consortium consisting of three fluorescent strains based on the LuxI/LuxR system of *V. fischeri* to investigate the activation and attenuation of QS responses. The strains possess OHHL sensing, production, and degradation abilities, and are therefore referred to as sensor, producer, and regulator, respectively. These QS-related abilities were expected to be concentration-dependently controlled by different external inducers other than OHHL. Therefore, the option of supplementing different concentrations of external inducers would enable manipulating the QS-related abilities of the strains and also allow for artificial perturbations to the bacterial community during cultivation. Moreover, the sensor's response upon OHHL induction, the production ability of the producer, and the degradation ability of the regulator were expected to be quantifiable by the fluorescence intensity of three distinguishable fluorescent proteins, which also allows for simultaneous tracking of the cells. Furthermore, as the sensor was expected to be co-culture with the other two strains, the same selectable marker was required. Meanwhile, two restriction sites were also required for insert assembly and disassembly, which also allows the plasmids to be reconfigurable to facilitate the future study of other genes. Taking all the above requirements into account, three inserts were designed based on the available genetic parts and backbone donor plasmids. Three plasmids containing promoters controlled by three different inducers and containing the same two restriction sites following the promoters were employed (Figure 2.2 and Table 2.1). Given that a promoter requires the *E. coli* Tuner (DE3) strain as the host strain to achieve inducer

concentration-dependent expression (Merck KGaA, 2011), this strain was chosen as the host strain for all designed plasmids to prevent metabolic inconsistencies caused by choosing different host strains.

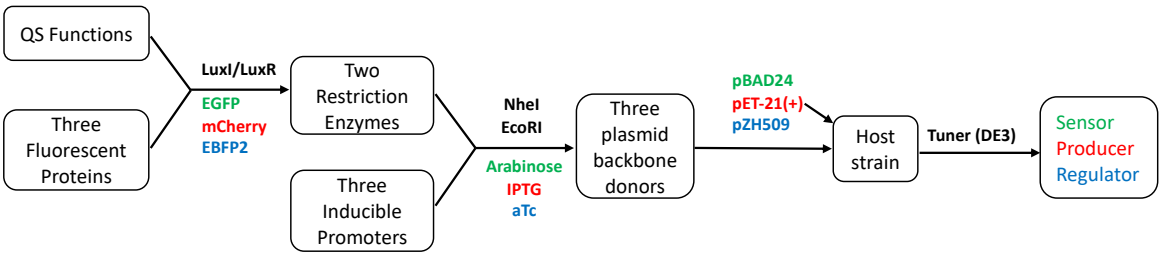

Figure 2. 1 Design scheme of the model bacterial consortium. Names are coloured according to the fluorescent signal of the strains. The QS functions and fluorescent proteins to be used were first determined and assigned to three strains. Taking into account the requirements of two restriction sites and three inducible promoters, three backbone donor plasmids were selected. The host strain that is required for an inducible promoter to achieve concentration-dependent expression was then determined.

The schematic structures of the designed plasmids and the major components of the three strains are shown below in Figure 2.2 and Table 2.1, respectively. The designed inserts are located above the plasmid backbones (Figure 2.2). When designing the strains, firstly, an appropriate QS system needs to be determined as the basis for plasmid construction. The LuxI/LuxR system of *V. fischeri*, as an extensively studied QS system with many identified inhibitors and homologues that could be further studied, was preferred. Then, in order to possess the autoinducer sensing, production and degradation abilities, genetic parts from and related to the LuxI/LuxR system were employed, which are *luxI*, *luxR*, and *aiiA*. Additionally, for the sensor strain, apart from the arabinose-inducible promoter on the plasmid backbone controlling the transcription of *luxR*, promoter luxPR_4G12T was also employed for the transcription of *egfp*. This promoter was modified from the lux pR promoter of *V. fischeri* (BBa_R0062) and displayed lower basal expression (Han, 2019), i.e., lower expression when uninduced. Therefore, the sensor employing promoter luxPR_4G12T may be more tightly controlled than the sensor employing lux pR promoter.

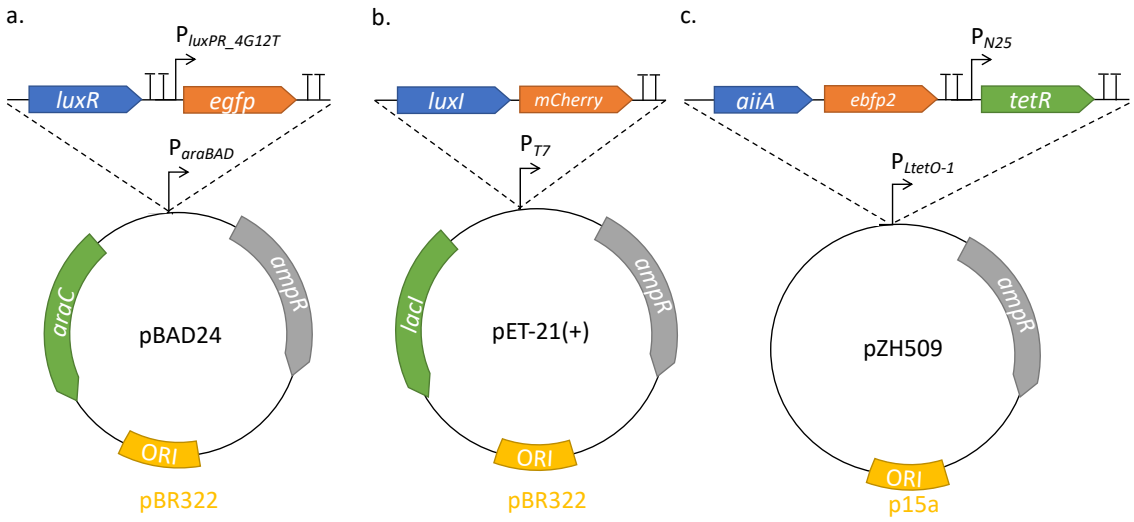

Figure 2. 2 Schematic structures of the plasmids of (**a**) sensor, (**b**) producer, and (**c**) regulator strains. Genes encoding QS-related proteins are represented as blue arrows, encoding fluorescent proteins are represented as orange arrows, encoding promoter regulatory proteins are represented as green arrows, and conferring ampicillin resistance are represented as grey arrows. The replication origins are represented as yellow ribbons. Black arrows indicate the promotors. T-shaped symbols indicate the terminators.

Table 2. 1 Major components of the three engineered strains used in this work

Strain	**Host**	**Backbone**	**Insert**
Sensor	Tuner (DE3)	pBAD24	*NheI+luxR+luxPR_4G12T+egfp+EcoRI*
Producer		pET-21(+)	*EcoRI+luxI+mCherry+NheI*
Regulator		pZH509	*EcoRI+aiiA+ebfp2+*P_{N25}*+tetR+NheI*

To be able to simultaneously monitor the fluorescent signals of three strains, three distinguishable fluorescent proteins, EGFP, mCherry, and EBFP2 were used. Three proteins have at least a 59 nm distance between emission maximum wavelengths and at least a 99 nm distance between excitation maximum wavelengths. These proteins also have close brightness (approximately 34, 16, and 18 units) and mature time (25, 15, and 25 minutes), according to FPbase (https://www.fpbase.org/table/, accessed 30 January 2024) (Lambert, 2019).

The genes responsible for the above-mentioned properties constitute the main bodies of the inserts. In addition to the main bodies, combined terminators were used for transcription termination. Ribosome binding sites were added preceding the coding sequences for translation initiation. Of note, in order to estimate the production of LuxI and AiiA based on the intensity of downstream fluorescent proteins, the plasmids of the producer and regulator strains were

designed for bicistronic expression with the same RBSs. Besides, restriction sites (NheI and EcoRI) were used to flank the inserts for insert assembly and disassembly.

When choosing plasmid backbones for the inserts, those containing promoters which are concentration-dependently controlled by common inducers and containing required restriction sites downstream to the promoters were preferred. Furthermore, to be able to co-culture the engineered strains, the same selectable marker was required. Meanwhile, in order to prevent the metabolic burden that may be caused by a high plasmid copy number, replication origins with similarly low plasmid copy numbers were preferred. Taking these requirements into account, P_{araBAD}/arabinose/pBAD24, P_{T7}/isopropyl-beta-D-thiogalactopyranoside (IPTG)/pET-21(+), and $P_{LtetO-1}$/anhydrotetracycline (aTc)/pZH509 (listed as promoter/inducer/plasmid) were chosen. The origin of replication of pBAD24 and pET-21(+) is pBR322 origin, whose copy number was reported to be approximately 15-20 copies/cell (Morgan and Patrick, 2014). The origin of replication of pZH509 is p15a, which was reported to be approximately 13 copies/cell in *E. coli* MG1655 (Shao et al., 2021). Of note, the P_{T7} is not directly induced by IPTG. P_{T7} requires the *E. coli* Tuner (DE3) strain for IPTG concentration-dependent expression. This strain is a *lacZ* (encoding beta-galactosidase) and *lacY* (encoding lactose permease) deletion mutant of *E. coli* BL21 (DE3), allowing concentration-dependent control by IPTG. Moreover, 'DE3' indicates this strain is a λDE3 lysogen that carries the T7 RNA polymerase gene under the control of the lacUV5 promoter. When induced by IPTG, the expression of T7 RNA polymerase, which is required for P_{T7} transcription, is activated. IPTG concentration-dependent expression of the P_{T7} is then attained (Merck KGaA, 2011). Meanwhile, to minimise the difference in the host cell metabolism, this strain was used as the host strain for all designed plasmids.

For the sensor strain (Figure 2.2a), promoters luxPR_4G12T and P_{araBAD} were used. The transcription from P_{araBAD} was reported to be approximately 300-fold promoted within 3 s after adding arabinose (Schleif, 2010). This promoter controls the expression of LuxR, which can be activated upon binding to OHHL. The activated LuxR can bind to the luxPR_4G12T promoter, resulting in the expression of EGFP. Therefore, the concentration of OHHL in the environment was expected to be estimated based on EGFP intensity.

The main function of the producer strain (Figure 2.2b) is to express the synthase LuxI to produce OHHL. Promoter P_{T7} was used to control the bicistronic expression of LuxI and mCherry with identical RBSs. Therefore, the production of LuxI and mCherry was expected to be regulated by IPTG concentration. The relative production of LuxI was expected to be estimated based on mCherry intensity.

The main function of the regulator strain (Figure 2.2c) is to express AHL lactonase AiiA to degrade OHHL. Promoter $P_{LtetO-1}$ was used to control the bicistronic expression of AiiA and EBFP2 with identical RBSs. The transcription of $P_{LtetO-1}$ is repressed by TetR, and the repression was found to be relieved by adding aTc (Hensel, 2017). Although the backbone donor plasmid pZH509 contains *tetR*, this gene is located between restriction sites NheI and EcoRI and would be removed during subcloning. Therefore, a constitutive promoter P_{N25} and *tetR* were added to the insert designed for the regulator strain. Additionally, previous studies found that the expression controlled by promoter $P_{LtetO-1}$ could be expressed in an aTc concentration-dependent manner (Hensel, 2017; Silva et al., 2019). Therefore, the production of AiiA and EBFP2 was expected to be regulated by aTc concentration. The relative production of AiiA was expected to be estimated based on EBFP2 intensity.

The backbone donor plasmids and inserts were assembled by subcloning. The new plasmids were introduced into the host strain Tuner (DE3) via chemical transformation using the protocols described below.

2.2.2 Preparation of autoinducer, inducer, and antibiotic stock solutions

OHHL was dissolved in acetonitrile to a stock concentration of 10^{-1} M and serially diluted to working concentrations of 10^{-8} to 10^{-2} M with Milli-Q water; L-(+)-arabinose 10 % (*w/v*) and IPTG 100 mM stocks were prepared in Milli-Q water; ampicillin (Amp) 100 mg/mL and anhydrotetracycline 100 µg/mL stocks were prepared in 50 % (*v/v*) ethanol. All stocks were sterilised using 0.22 µm syringe filters.
The culture medium for the engineered strains and lysogeny broth (LB) medium control were supplemented with 100 µg/mL Amp. The culture medium for the Tuner (DE3) strain was not supplemented with Amp.

2.2.3 Preparation of the strains

The workflow for the preparation of the engineered strains from donor strains to glycerol stocks is shown in Figure 2.3. The plasmids containing the backbones and inserts were first extracted from donor strains, followed by enzymatic digestion. The backbones and inserts were then ligated correspondingly. The ligation products were introduced into the host cells to prepare the original glycerol stocks of the three strains (Figure 2.3, grey area). The fluorescent signals of the strains were assessed before preparing them into experimental glycerol stocks for future experiments. The plasmids were extracted again for whole plasmid sequencing and preparation of storage glycerol stock (Figure 2.3, blue area).

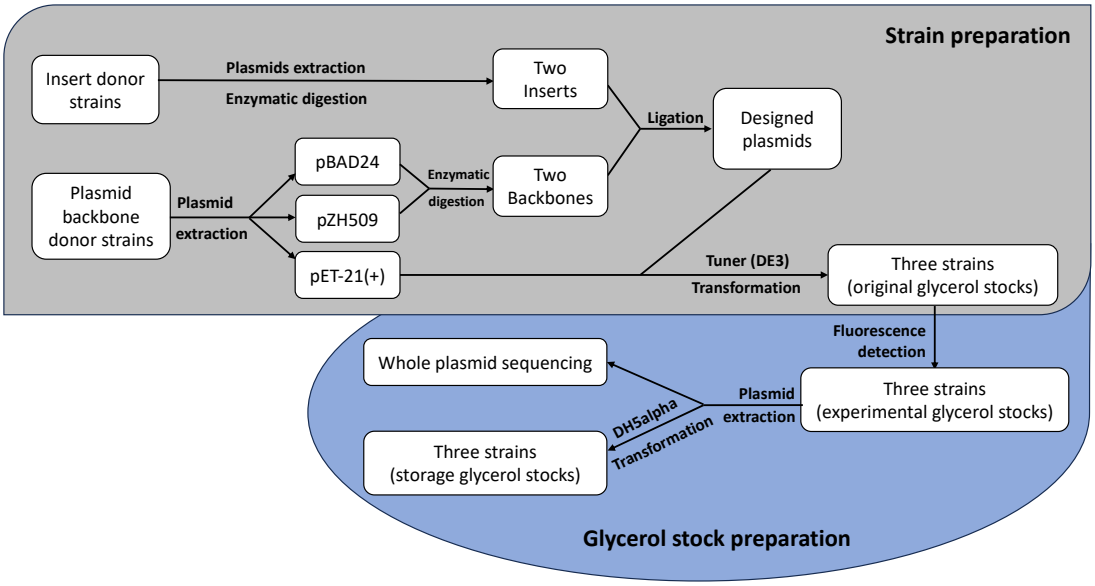

Figure 2. 3 Workflow for the preparation of the *E. coli* engineered strains

Three plasmids were extracted from their donor host cells using a QIAprep Spin Miniprep Kit. As the producer's insert had been assembled by Twist Bioscience, it was ready to be introduced to Tuner (DE3) cells. For the sensor and regulator strains, plasmids pBAD24 and pZH509 were incubated with NheI and EcoRI, separately. Digests were then purified using a DNA clean-up kit to wash out short DNA fragments. To separate long DNA sequences, digests were separated on agarose gels and purified using a QIAquick Gel Extraction Kit. Here, the backbones from plasmids pBAD24 and pZH509 were separated by electrophoresis on 1 % agarose gel at 55 volts for 90 min and 110 min, respectively. The inserts from plasmids pTwist Amp High Copy were separated by electrophoresis on 1.5 % agarose gel at 55 volts for 180 min. Backbones and the corresponding inserts (Table 2.1) were then mixed in a 1:2 molar ratio and ligated with the LigaFast Rapid DNA Ligation System at room temperature for 15 min. The experiments of plasmid extraction and digestion and digest ligation were conducted following the manufacturer's instructions.

The ligation products, that is, the plasmids of the sensor and regulator, together with the producer's plasmid, were then respectively mixed with competent cells *E. coli* Tuner (DE3) (10 ng DNA in 50 µL cell suspension). The mixtures were left on ice for 15 min, heat-shocked at 42 °C for 45 s, put back on the ice for 2 min, and then mixed with 950 µL of the LB (Amp). The cultures were then recovered at 37 °C for 1 h. Then, 100 µL of the cultures were spread on LB (Amp) agar plates and incubated at 37 °C overnight, respectively. Single colonies of three strains were inoculated into 10 mL LB (Amp) and incubated overnight with shaking,

respectively. Overnight broth cultures were then used to prepare the original glycerol stocks and stored at -80 °C.

For every strain, an overnight broth culture was prepared from a vial of original glycerol stock (protocol described in Section 2.2.4 below) and then underwent excitation and emission spectral scans (protocol described in Section 2.2.5 below). After successfully detecting the fluorescent signal, a batch of experimental glycerol stock was prepared from the overnight broth culture for future experiments (as described in Section 2.2.4 below).

Overnight broth cultures of three strains were prepared from the experimental glycerol stocks, and their plasmids were extracted. The plasmids were sequenced by the DNA Sequencing Facility, Department of Biochemistry, University of Cambridge. Using the protocol described above, the plasmids were introduced to *E. coli* DH5alpha. The overnight broth cultures were prepared into glycerol stocks for long-term storage at -80 °C using the protocol described next.

2.2.4 Preparation of overnight broth cultures and glycerol stocks

To prepare a tube of overnight broth culture, a loop of glycerol stock was streaked onto an LB (Amp) agar plate and incubated overnight. One colony was inoculated into a tube of LB (Amp) and incubated overnight with shaking. The overnight broth culture can then be harvested for experiments. To prepare a glycerol stock, overnight broth culture was mixed with sterile glycerol to 20 % - 25 % (*v/v*) and stored at -80 °C for further use. Of note, the culture medium for the Tuner (DE3) strain was not supplemented with Amp.

For overnight cultivation, cultures were incubated at 37 °C for 17±1 h, where broth cultures were shaken at 200 rpm. During incubation with the addition of OHHL or aTc, all tubes were covered with aluminium foil. The OD_{600} of overnight cultures were measured using a Jenway 6715 UV/Visible spectrophotometer.

2.2.5 Excitation and emission spectra of the strains

To quickly assess the function of the three strains, the fluorescence excitation and emission spectra of their overnight cultures were scanned. For the sensor, the culture was induced by 0.1 % arabinose and 10^{-6} M OHHL concentration and cultured overnight. Overnight induced culture (200 µL) was added onto a black microplate, covered with an optically clear, moisture-resistant, and gas-permeable seal. The plate was then measured by a CLARIOstar Plate Reader using a fluorescence intensity/spectral scan programme. The excitation and emission spectra were respectively measured at λ_{em} = 512 nm/λ_{ex} = 0 - 490 nm and at λ_{ex} = 450 nm/λ_{em} = 490 - 540 nm, where the focal height was 8.5 mm. Similarly, 200 µL of 0.1mM IPTG concentration-

induced producer overnight cultures were respectively measured at λ_{em} = 613 nm/λ_{ex} = 0 - 590 nm (excitation spectrum) and λ_{ex} = 575 nm/λ_{em} = 595 - 631 nm (emission spectrum), with 8.2 mm focal height. For the regulator strain, 100 ng/mL aTc-induced overnight cultures were used. The excitation spectrum was measured at λ_{em} = 428 nm/λ_{ex} = 320 - 390 nm, and the emission spectrum was measured at λ_{ex} = 354 nm/λ_{em} = 390 - 500 nm, with an 8.1 mm focal height. For all scans, experimental parameters also included 8 nm bandwidth, 20 flashes per well, with a gain value of 30 % determined using the first of the triplicates of the induced culture. The culture medium of all engineered strains was supplemented with 100 µg/mL ampicillin (Amp). In parallel, the overnight Tuner (DE3) culture and the LB (Amp) solution were measured as controls. Three biological replicates were performed. Of note, only on the first day were the induced cultures diluted with LB (Amp) in a 4:1 ratio. The remaining two replicates were conducted with undiluted cultures, while the other procedures of the protocol were the same.

It was found that the blue fluorescent signal could not be distinguished from the LB (Amp) medium using the above microplate reader method. Considering that the seal film might affect the reading of the fluorescence intensity, the samples were measured using a quartz cuvette and a Horiba FluoroMax-4 spectrofluorometer. The overnight (16 h) regulator culture was diluted to 3 mL with LB (Amp) (OD_{600} ~ 0.05), supplemented with and without 100 ng/mL aTc, and further overnight incubated for 16 h. Similarly, 3 mL of the Tuner (DE3) culture (OD600 ~ 0.05) was prepared. Tuner (DE3) culture and 3 mL LB (Amp) were incubated in parallel with regulator cultures as controls. After incubation, the emission spectra of 2 mL cultures were measured at λ_{ex} = 367 nm and λ_{em} = 375 - 500 nm (with 2 nm excitation and emission slits). Data were collected from at least three biological independent experiments. GraphPad Prism was used for data analysis and data presentation.

2.3 Results and discussion

2.3.1 Engineered *E. coli* consortium for studying quorum sensing

The plasmids were constructed as designed and introduced into the host Tuner (DE3) cells by chemical transformation. A model consortium of three fluorescent *E. coli* strains (OHHL sensor, producer, and regulator) was obtained to study the activation and attenuation of QS responses based on the LuxI/LuxR system of *V. fischeri*. The key features of the three strains are depicted in Figure 2.4. Each construct is under the control of its respective inducer: (i) The sensor strain contains *luxR,* whose transcription is controlled by arabinose (P_{araBAD}). Upon binding to OHHL, activated LuxR activates transcription at promoter luxPR_4G12T, resulting in the expression of EGFP. (ii) The producer strain contains the genes encoding LuxI and mCherry, both of which are under the control of IPTG (P_{lacUV5} and P_{T7}). (iii) The regulator

strain contains the genes encoding AiiA and EBFP2, both of which are under the control of aTc ($P_{LtetO-1}$).

Biosensors are fundamental tools used to study AHL QS systems and QS inhibitors (Steindler and Venturi, 2007; Defoirdt et al., 2013). The sensor is also the key strain of this work. It employs the luxPR_4G12T promoter, which was modified from the lux pR promoter of *V. fischeri* (BBa_R0062) and displayed lower basal expression (Han, 2019). The producer and regulator strains were designed as the OHHL provider and degrader. Two inducible promoters, P_{T7} and $P_{LtetO-1}$, were employed to control the expression of the enzymes responsible for OHHL production and degradation, respectively. Meanwhile, to be able to monitor the location of bacterial cells and the relative production of the enzymes, bicistronic expression was adopted, i.e., one promoter controls the expression of two separate proteins from a mRNA. The gene encoding the enzyme is followed by the gene encoding the fluorescent protein. Therefore, the fluorescent signal helps to locate the bacterial cells. The fluorescence intensity helps to estimate the production of the enzyme.

Additionally, two restriction sites were used to flank the inserts containing QS-related and fluorescent protein genes (Table 2.1). The restriction sites allow assembly and disassembly of the inserts by subcloning, enabling the plasmid to be modified to study other genes. New inserts could consider adding appropriate restriction sites to flank the coding sequences (with RBSs) to allow for more flexible assembly and disassembly.

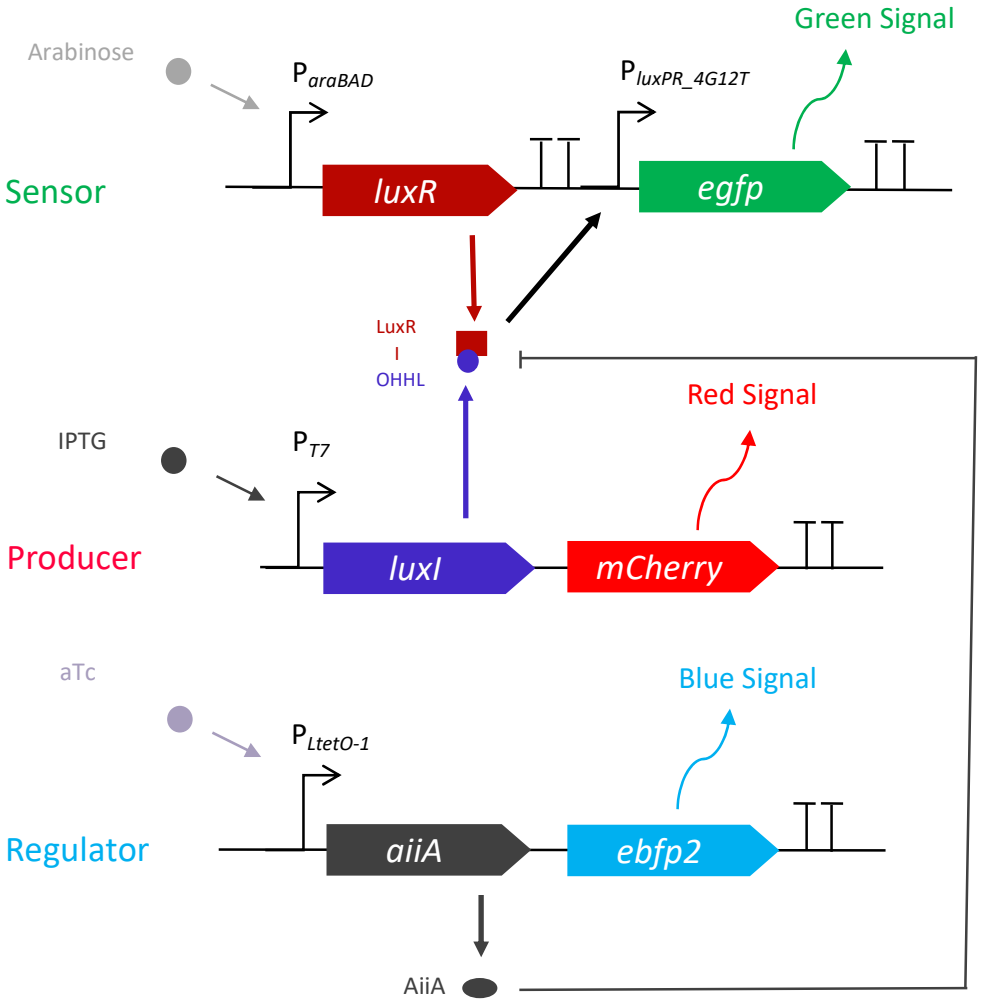

Figure 2. 4 Schematic representation of the design of the sensor, producer, and regulator strains. Functional genes are represented as arrowed ribbons. Promoters are indicated as black arrows, and terminators are indicated as T-shaped symbols.

2.3.2 Excitation and emission spectra of the strains

After obtaining the strains, the first set of experiments was to test the fluorescent signals of the strains before preparing glycerol stocks for future experiments. Samples were preliminarily scanned on microplates using a CLARIOstar Plate Reader. The excitation (right) and emission (left) spectra of induced overnight cultures of three strains compared with controls, i.e., overnight cultures of host strain Tuner (DE3) and LB (Amp) medium, are shown in Figure 2.5.

For the sensor strain (Figure 2.5a), the excitation and emission spectra of sensor culture induced at 10^{-6} M OHHL concentration, Tuner (DE3) culture, and LB (Amp) medium were measured at λ_{em} = 512 nm and λ_{ex} = 450 nm, respectively. The sensor cultures containing EGFP showed greater fluorescence intensity (FI) than the controls. It should be noted that the medium control showed greater FI than the Tuner (DE3) culture, suggesting that the turbidity resulting from the bacterial growth reduced the fluorescence reading. This result also suggests that the background fluorescence of the LB (Amp) medium would affect the readings at the tested wavelengths.

For the producer strain (Figure 2.5b), the excitation and emission spectra of producer culture induced at 0.1 mM IPTG concentration, Tuner (DE3) culture, and LB (Amp) medium were measured at λ_{em} = 613 nm and λ_{ex} = 575 nm, respectively. The FI of the producer culture was obviously higher than those of the Tuner (DE3) culture and LB (Amp) medium, of which two controls showed almost no signal compared to the producer.

For the regulator strain (Figure 2.5c), the excitation and emission spectra of regulator culture induced at 100 ng/mL aTc concentration, Tuner (DE3) culture, and LB (Amp) medium were measured at λ_{em} = 428 nm and λ_{ex} = 354 nm, respectively. The induced regulator culture showed greater FI compared to that of the Tuner (DE3). However, the readings of these cultures were found to be lower than those of the LB (Amp) medium. These results suggest there may be a fluorescent signal generated by EBFP2, but it was not distinguishable from that of the LB (Amp) medium background. It was also found that the background fluorescence caused by cells and LB (Amp) medium was higher when measuring at lower wavelengths. The measurement of the blue signal was more severely affected by this noise than the green signal, while the measurement of the red signal was least affected. This result is similar to a previous study that found that fluorescent reporters were affected by background noise caused by autofluorescence from cells and the LB medium. In particular, the green fluorescent signal was more severely affected than the red fluorescent signal (Lopreside et al., 2019). Meanwhile, it was found that the excitation and emission wavelengths of the nicotinamide moiety of NAD(P)H are around 340 nm and 460 nm, respectively (Blacker et al., 2014; Bulycheva et al., 2014), which are

similar to those of EBFP2 (Ai et al., 2007). This similarity may be a reason for the high background noise when measuring the blue signal.

The experimental design has two shortcomings. Firstly, the samples in the first biological independent experiment were diluted. Hence, the experimental protocol was inconsistent with the protocol used in the other two biological replicates, which could contribute to high standard deviation values. Secondly, the Tuner (DE3) cells (i.e., host cells without constructed plasmids) were not induced by inducers like the engineered strains. Overall, these shortcomings are unlikely to cause major issues, as the fluorescence readings of sensor and producer strains were obviously greater than those of the host strain. As for the regulator strain, it was further assessed using a spectrofluorometer.

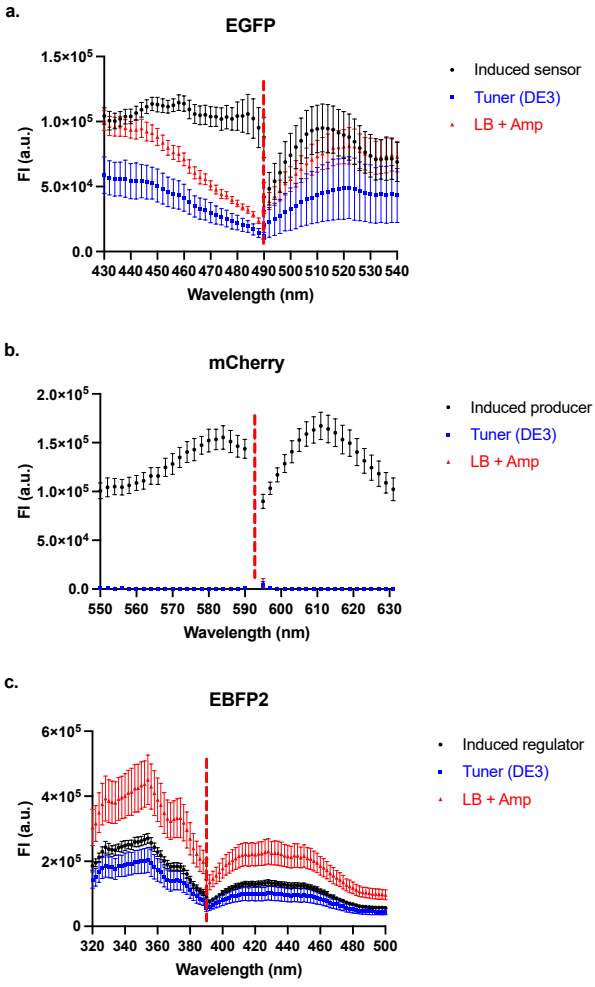

Figure 2. 5 Excitation and emission spectra of the strains. The excitation spectrum (left) and emission spectrum (right) were separated by red dashed lines. Overnight cultures of induced engineered strains, Tuner (DE3) strain, and LB (Amp) were assessed at the wavelengths of the (**a**) green signal, (**b**) red signal, and (**c**) blue signal. Data are shown as the mean values with their standard deviations (shown as error bars) of at least three independent experiments.

When testing the fluorescent signal of the regulator strain using the CLARIOstar Plate Reader, in addition to the background noise caused by cells and LB (Amp) medium, the sealing film used to cover the plate may also affect the reading of the fluorescence intensity. Therefore, the FI of overnight regulator cultures and controls were determined at λ_{ex} = 367 nm using a FluoroMax-4 spectrofluorometer and a quartz cuvette. Meanwhile, the optical density of the samples was measured at 600 nm (OD_{600}) using a Jenway 6715 UV/Visible spectrophotometer. Optical density is commonly used to estimate the cell density, i.e., growth, in liquid culture (Myers et al., 2013). The regulator was induced with aTc 100 ng/mL. The emission spectra (λ_{em} = 400 - 500 nm) of overnight cultures (initial OD_{600} ~ 0.05 and 16 h incubation) and LB (Amp + aTc) medium control are shown in Figure 2.6. In the area with the highest fluorescence readings, namely λ_{em} = 440 - 460 nm, even in the absence of aTc, the FI and the cell response level (FI/OD_{600}) of the regulator strain were significantly higher than those of the host Tuner (DE3) strain (****$p < 0.0001$, Mann-Whitney test), and those of aTc-induced regulator culture were significantly higher compared to non-induced regulator culture (****$p < 0.0001$, Mann-Whitney test). These results suggest that the regulator's plasmid showed basal expression of EBFP2 in the absence of aTc and showed enhanced expression in the presence of aTc.

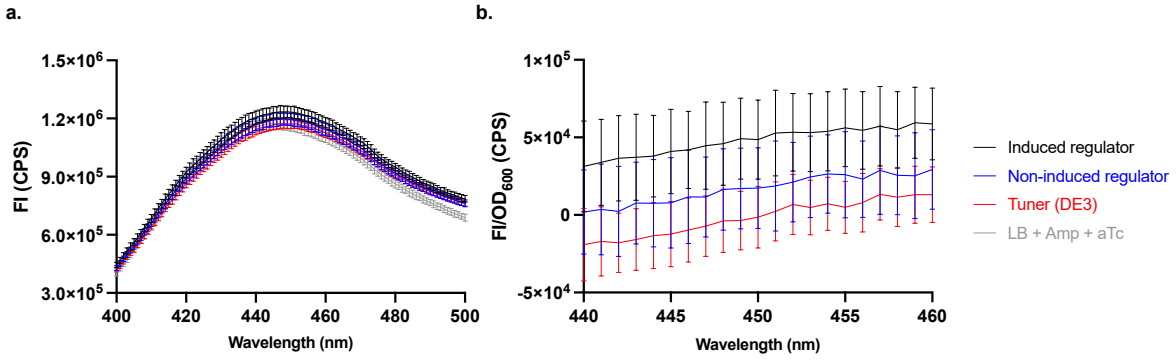

Figure 2. 6 Influence of the aTc induction on the expression of the regulator. (**a**) The emission spectra of EBFP2 at λ_{ex} = 367 nm and (**b**) the corresponding cell response levels (FI/OD_{600}) of cultures were assessed. Data are shown as the mean values with their standard deviations (shown as error bars) of at least three independent experiments.

2.3.3 Whole plasmid sequencing results

Whole plasmid sequencing was performed by the DNA Sequencing Facility, Department of Biochemistry, University of Cambridge. The sequencing results of the three constructed plasmids are shown in Appendix B. MegaBLAST (Zhang et al., 2000) was used to align the sequencing results with the designed sequences. According to the sequencing results, the strains used for experiments may have one to four mutations. The sensor may have three single-base deletion mutations at terminator L3S2P21 (site: 6255, G), at pBR322 origin (site: 2532, G), and at pBAD24 (site: 2944, C), respectively. The sensor may also have one base changed from T to G at M13 origin (site: 1715). The producer strain may have a single-base deletion mutation at terminator ECK120033737 (site: 211, A). The regulator strain may have two single-base deletion mutations at terminator L3S2P21 (site: 3539, G) and terminator ECK120033737 (site: 3601, T). The features of the mutation sites were determined according to GenBank: X81837.1 (Guzman et al., 1995) (https://www.ncbi.nlm.nih.gov/genbank/, accessed 30 January 2024) (Clark et al., 2015) and Chen et al. (2013). The sites were numbered based on the sequencing results provided in Appendix B.

Among these mutations, deletion mutations occurring at the L3S2P21 terminator, ECK120033737 terminator, and pBR322 origin are related to the designed functions of strains. In this work, all terminators used are intrinsic terminators, also known as Rho-independent terminators. Intrinsic terminators do not require Rho protein or its homologues for transcription termination. An intrinsic terminator transcribes a sequence containing a hairpin followed by a U-rich sequence for termination (Kingsford et al., 2007; Chen et al., 2013). It was found that the L3S2P21 terminator may lose one base in the hairpin area, and the ECK120033737 terminator may lose one base in the U-rich area. These two terminators showed good abilities in reducing the downstream expression (Chen et al., 2013) and were used in combination in this work to ensure termination. For the sensor and producer strains, only one terminator may be mutated. Therefore, read-through was unlikely to occur. For the regulator strain, both terminators following *ebfp2* may be mutated. Given that the EBFP2 were successfully expressed, these mutations were unlikely to have had a large effect on expression. This result is similar to a previous study that found that single-base deletion of the terminator (λtI) did not always abolish but only reduced the termination efficiency to varying degrees (Martínez-Trujillo et al., 2010). Furthermore, for the sequenced plasmids, both terminators were found mutated in two different strains, and the deletion sites of each terminator were located in the same short, direct repeat areas. This result suggests these areas are more prone to mutations, which is consistent with the finding that spontaneous deletions often occur in short, direct repeats (Weston-Hafer and Berg, 1991; Rogozin and Pavlov, 2003). Similarly, deletion at pBR322 origin was also in the short, direct repeat area. However, this strain showed reasonable functionality, suggesting that the mutation was unlikely to have a noticeable effect on function.

2.4 Conclusions

In this chapter, a model bacterial consortium consisting of three engineered strains was introduced. The strains were designed based on the LuxI/LuxR QS system of *V. fischeri* and were designed to possess OHHL sensing, production, and degradation abilities, respectively. The expression of three fluorescent proteins was designed to be activated upon induction, which aids in cell tracking. Additionally, in the sensor strain, EGFP expression can be activated by the LuxR-OHHL complex. Therefore, the concentration of OHHL in the environment was expected to be estimated based on the EGFP intensity. Fluorescent proteins mCherry and EBFP2 are downstream proteins of bicistronic expression. Their FI was expected to reflect the relative production of the upstream enzymes LuxI and AiiA, respectively. The inserts containing QS-related and fluorescent protein genes were flanked by two restriction sites (NheI and EcoRI), allowing the plasmid to be modified to study other genes via subcloning.

The abilities of the strains to express proteins upon inducer induction were quickly tested by detecting fluorescent signals. All strains showed abilities to express fluorescent proteins. The fluorescence readings were found to be affected by background noise caused by cells and LB (Amp) medium, especially at lower measurement wavelengths. The plasmids were extracted for sequencing. Sequencing data showed that one to four sing-base mutations occurred in the plasmids. The cells in the experimental glycerol stocks may also have the same mutations. The single-base deletion mutations occurring at two terminators and pBR322 origin are related to the designed functions of the strains. However, no noticeable effect on the functions of the strains has been found. The strains were further assessed on their inducer concentration-dependent expression and QS-related abilities.

Chapter 3 Characterisation of the bacterial consortium

In this chapter, the performance of the strains upon induction in the planktonic state is discussed. To better understand the performance of the sensor and producer strains, the fluorescence intensity (FI) and the optical density at 600 nm (OD_{600}) of each strain were measured during incubation under the induction of different concentrations of inducers. The cell response level (FI/OD_{600}) was also assessed. The ability of the producer supernatant to activate the response of the sensor was assessed. The ability of the regulator supernatant to attenuate the response of the sensor was also assessed. To be able to co-culture and image the strains in agarose hydrogel microbeads at the single-colony level, a conversion equation from OD_{600} to colony-forming units was obtained using the sensor strain to facilitate dilution and encapsulation of bacterial cultures.

3.1 Materials, equipment, and software

Information on the main experimental materials and equipment used in this chapter is provided in Table A.2 in Appendix A. Information on the software used in this chapter is provided in Table A.3 in Appendix A.

3.2 Characterisation of the strains

The workflow for strain characterisation is shown in Figure 3.1. Once the strains were constructed, preliminary scans were performed to confirm their excitation and emission spectra using a CLARIOstar Plate Reader, as discussed in Chapter 2. As the blue fluorescent signal was not distinguishable from background noise using the plate reader, inducer concentration-dependent expression microplate analysis was only performed for the sensor and producer strains. When assessing the QS activation and attenuation abilities, the sensor's responses induced by supernatants of the producer or regulator cultures treated under different conditions were analysed, respectively.

To be able to observe bacterial communities at the single-colony level using microfluidics, single cells are required to be immobilised in agarose hydrogel microbeads. OD_{600} to colony-forming units conversion equation was obtained using the sensor strain for the dilution step of the microfluidic experiments.

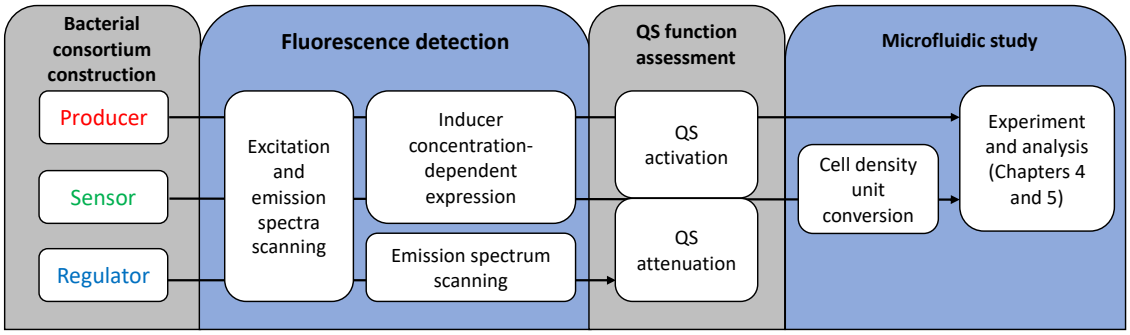

Figure 3. 1 Workflow of strain characterisation. The fluorescent protein expression abilities of three strains were first tested. The inducer concentration-dependent expression of the sensor and producer strains was then assessed. The QS activation ability of the producer strain and the QS attenuation ability of the regulator strain were assessed. OD_{600} to colony-forming units conversion equation was obtained using the sensor strain.

3.2.1 Characterisation of the sensor and producer strains

Overnight sensor and producer cultures were diluted to $OD_{600} \sim 0.05$. The sensor was incubated in the LB medium supplemented with 100 µg/mL ampicillin (LB (Amp)) and varying concentrations of OHHL. The sensor induced by OHHL in the concentration range from 10^{-10} to 10^{-4} M was tested in the absence or presence of 0.1% (*w/v*) arabinose. The producer was induced by LB (Amp) supplemented with 0.025, 0.05, 0.1, 0.3, and 0.5 mM IPTG. Cultures in a total volume of 200 µL were measured in a 96-well black plate covered with an optically clear, moisture-resistant, and gas-permeable seal. The cultures were measured every 10 min for 5 h (incubated at 37 °C, double orbital 400 rpm, top optic, 7.6 mm focal height, 2 mm scan width 2 x 2 matrix scan, and 25 flashes per well) using a CLARIOstar Plate Reader. The fluorescence intensity (FI) of EGFP of the sensor was measured with $\lambda_{ex} = 470$ (15) nm, $\lambda_{em} = 515$ (20) nm, and gain 1398. The FI of mCherry of the producer was measured with $\lambda_{ex} = 570$ (15) nm, $\lambda_{em} = 620$ (20) nm, and gain 1594. Tuner (DE3) induced by the highest tested inducer concentration and LB (Amp) were measured in parallel as controls.

3.2.2 Quorum sensing activation and attenuation abilities

The sensor in the absence of arabinose was used to test the QS activation ability of the producer and the QS attenuation ability of the regulator. To test the activation ability, producer pellets were resuspended in LB (Amp) supplemented with varying IPTG concentration and incubated for 1 - 3 h. The response of the sensor to the producer supernatant was assessed. Overnight producer culture was diluted to $OD_{600} \sim 0.5$ with LB (Amp) and supplemented with 0.025, 0.05, 0.1, 0.3, and 0.5 mM IPTG concentration in a final volume of 10 mL. The diluted cultures were covered with aluminium foil, incubated at 37 °C and shaken at 200 rpm for 3 h. Tuner (DE3)

in LB supplemented with 0.5 mM IPTG concentration (10 mL, OD_{600} ~ 0.5) and 10 mL LB (Amp) were incubated in parallel as controls. Every hour, all cultures were centrifuged at 4696 x g for 10 min, and 1 mL supernatants were taken and stored at 4 °C for subsequent mixing with sensor cultures.

To test the attenuation ability, regulator pellets (OD_{600} ~ 0.25 to 1) were resuspended in LB (Amp) supplemented with 10^{-5} M concentration of OHHL. The response of the sensor response to the regulator supernatant collected after 1 h of incubation was assessed. Overnight regulator culture was diluted to OD_{600} ~ 0.05 in a final volume of 10 mL with LB (Amp) supplemented with and without 100 ng/mL aTc. The diluted cultures were covered with aluminium foil, incubated at 37 °C and shaken at 200 rpm for 16 h. Tuner (DE3) (OD_{600} ~ 0.05) in LB was incubated in parallel. These new overnight cultures were diluted to 5 mL (OD_{600} ~ 0.25 to 1) followed by centrifuging at 4696 x g for 10 min. The pellets were resuspended with 5 mL LB (Amp) supplemented with 10^{-5} M OHHL concentration. The resuspended cultures were covered with aluminium foil, incubated at 37 °C and shaken at 200 rpm for 1 h. LB (Amp) with and without 10^{-5} M OHHL concentration in a final volume of 5 mL were incubated in parallel as controls. After 1 h incubation, the supernatants were used to mix with sensor cultures.

After harvesting the supernatants, 10 µL of sensor overnight cultures (OD_{600} ~ 1) were mixed with 190 µL of the supernatants and measured by a CLARIOstar Plate Reader using the protocol described in Section 3.2.1. For the sensor mixed with producer supernatants, the red fluorescent signal was measured at the same time as using the protocol described in Section 3.2.1.
After taking the supernatants, the pellets were resuspended, and their FI and OD_{600} were measured using a FluoroMax-4 spectrofluorometer and a Jenway 6715 UV/Visible spectrophotometer. For the red fluorescent signal, samples were measured at λ_{ex} = 583 nm/λ_{em} = 590 - 650 nm (1 nm excitation slit and 2 nm emission slit). For the blue fluorescent signal, samples were measured at λ_{ex} = 367 nm/λ_{em} = 375 - 500 nm (2 nm excitation and emission slits).

3.2.3 Conversion of OD_{600} to colony-forming units

Overnight sensor culture was diluted to OD_{600} ~ 0.05, 0.1, 0.2, 0.35, and 0.5 in a final volume of 1 mL. The diluted cultures were further serially diluted. Then, 100 µL of two countable successive dilutions of each OD_{600} were spread onto LB (Amp) agar plates. For OD_{600} ~ 0.05 and 0.1, 10^{-6} and 10^{-5} dilutions were used. For OD_{600} ~ 0.2, 0.35, and 0.5, 10^{-7} and 10^{-6} dilutions were used. Colonies were counted after overnight incubation. The colony-forming units of each OD_{600} value were calculated using the equation in ISO 15214:1998 (International Organization

for Standardization, 1998). The conversion equation from OD_{600} to colony-forming units was the simple linear regression line (through the origin) of the calculated colony numbers.

3.2.4 Data analysis

GraphPad Prism was used for data analysis and presentation. When comparing different treatments, the Mann-Whitney and the Kruskal-Wallis tests were used for unpaired comparisons of two or more groups, respectively. Data in Excel are stored in scientific notation (two decimal places). When transferring data to GraphPad Prism, data greater than 10^6 were automatically rounded.

3.3 Results and discussion

3.3.1 Characterisation of the sensor strain

The sensor employs an arabinose-inducible promoter, P_{araBAD}, to control the expression of LuxR. Upon binding to OHHL, activated LuxR can activate the luxPR_4G12T promoter that controls the expression of EGFP. Therefore, arabinose may be able to control the sensitivity of the sensor to OHHL concentration, and the concentration of OHHL in the environment could be estimated based on the FI of EGFP. In this section, the ability of the sensor to sense OHHL concentration was assessed. To this end, the FI and OD_{600} of the sensor induced by OHHL concentrations in the range 0 to 10^{-4} M in the absence (ara^-) or the presence (ara^+) of arabinose during 5 h of incubation were measured.

In the absence of arabinose (ara^-) (Figure 3.2a), the sensor showed an OHHL concentration-dependent response (EGFP intensity normalised by OD_{600}) when treated at concentrations greater than 10^{-7} M. In addition to OHHL, LuxR is also required for the activation of luxPR_4G12T promoter to express EGFP. Therefore, the concentration-dependent response here indicates an intrinsic leakage of the P_{araBAD} promoter, leading to basal expression of LuxR. At lower doses, the FI of the sensor was indistinguishable from that of the OHHL untreated sensor. Moreover, the uninduced sensor and sensor induced at OHHL concentrations lower than 10^{-8} M showed lower FI than LB (Amp) medium control. This phenomenon may be caused by turbidity and background fluorescence (discussed in Section 2.3.2). When calculating cell response levels (FI/OD_{600}) of these cultures, the FI was 'zeroed', resulting in the sensor in some treatments showing no response (Figure 3.2a, third column). This method was also used to calculate the cell response level of the sensor in the presence of arabinose (Figure 3.2b, third column).

In the presence of arabinose (ara$^+$), higher LuxR expression resulted in enhanced responses of the sensor in some treatments (Figure 3.2). As shown in Figure 3.2b, the sensor induced by OHHL concentrations greater than 10^{-8} M showed distinctly greater FI than the LB (Amp) medium control. The FI of the sensor induced at lower concentrations was lower than that of the LB (Amp) medium but higher than that of the Tuner (DE3) induced at the highest tested OHHL concentration. Additionally, the FI of the sensor induced at OHHL concentrations 10^{-10} and 10^{-9} M were similar but higher than that of the sensor without OHHL induction. These results indicate that EGFP was expressed at lower OHHL concentrations. However, the FI readings were lower than that of LB (Amp) medium control, which may be due to the turbidity and background fluorescence (discussed in Section 2.3.2). The turbidity may also be the reason the FI of the sensor induced at 10^{-8} M gradually decreased after 3 h of incubation. During this period, the change in FI may be dominantly affected by the increase in cell density rather than the accumulation of EGFP. Of note, the growth in ara$^+$ was noticeably affected by OHHL induction, especially at higher concentrations, while the sensor (ara$^-$) was less affected (Figure 3.2).

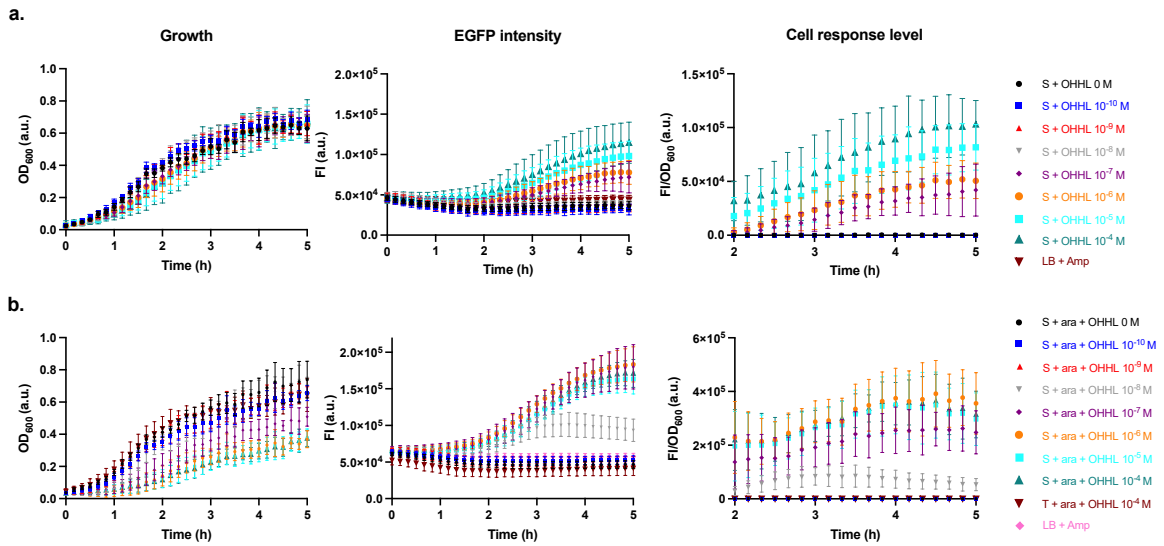

Figure 3. 2 Response of the sensor to OHHL induction. The growth (optical density at λ = 600 nm, OD_{600}), fluorescence intensity (FI) of EGFP (λ_{ex} = 470 (15) nm and λ_{em} = 515 (20) nm), and cell response levels (FI/OD_{600}) (as indicated by the column labels) of the sensor (S) induced at varying OHHL concentrations in the absence (**a**) and presence (**b**) of arabinose were measured during 5 h of incubation. Tuner (DE3) (T) and LB (Amp) were incubated in parallel as controls. Data are shown as the mean values with their standard deviations (shown as error bars) of at least three independent experiments.

Additionally, as shown in Figure 3.2 above, the expression controlled by the promoter luxPR_4G12T appeared inactive at early stages and became active after a period, which is similar to what was found in *Vibrio fischeri* (Nealson et al., 1970; Boo et al., 2021). Similarly,

a previous study showed that the expression controlled by the lux2 promoter may be inactive at early stages when used to detect OHHL (Lopreside et al., 2019). For the whole-cell sensor, this early inactivity could be attributed to several factors, such as low cell density and the time required for fluorescent protein expression and maturation.

Figure 3.3 shows the endpoints of the third column of Figure 3.2. When the sensor was induced at OHHL concentrations ranging from 10^{-8} to 10^{-4} M, the cell response levels of the sensor in ara^+ were significantly higher than those of the sensor in ara^-. One reason for the higher responses in ara^+ may be due to faster LuxR expression, which maximised the binding of OHHL to LuxR before OHHL degradation. A previous study showed that OHHL is unstable and could be degraded non-enzymatically at a high temperature and under aerobic conditions in a complex medium (Byers et al., 2002). However, in ara^+ with high expression of LuxR, although the sensor could detect OHHL concentration down to 10^{-8} M, there was no concentration-dependent EGFP expression when the OHHL concentrations were greater than 10^{-7} M. The cell response levels were similar when the OHHL concentrations were $\geq 10^{-6}$ M, indicating the possibility of reaching saturation (Figures 3.2b and 3.3). These results are similar to a previous study that found, in *V. fischeri*, a clear luminous response occurred at OHHL concentration 10^{-8}, and the response increased with the increase of OHHL concentration until 2×10^{-7} M (Kaplan and Greenberg, 1985). Moreover, a previous study found that the formation of the LuxR-OHHL complex is reversible, and the effective equilibrium constant for the formation is approximately 10^{-7} M (Urbanowski et al., 2004). Of note, the response of the sensor in ara^- did not seem to reach saturation even at 10^{-4} M OHHL concentration, suggesting sensor (ara^-) may be able to detect OHHL concentrations greater than 10^{-4}. Additionally, the sensor in ara^- showed a clearer concentration-dependent response compared to that of the sensor in ara^+ (Figure 3.3). These results suggest that the sensor has a wider detection range in ara^-, and the sensor in ara^+ could be more sensitive to lower OHHL concentrations. Moreover, these results showed that the sensitivity of the sensor could be tuned by adding or not adding arabinose, which enhances the functionality of the sensor.

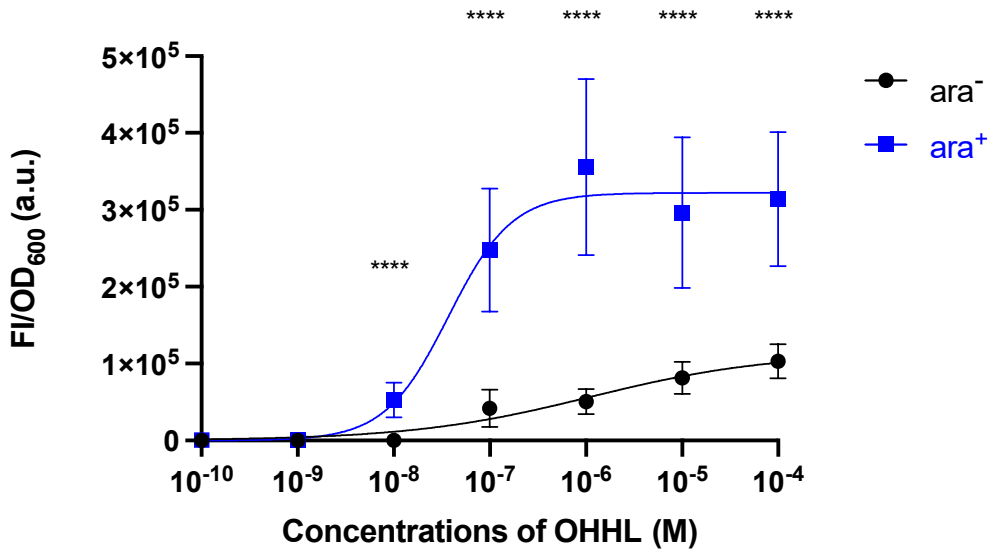

Figure 3. 3 Variation of the cell response levels (FI/OD_{600}) of the sensor as a function of OHHL concentrations in the absence (ara^-) and presence (ara^+) of arabinose. Data were obtained after 5 h of incubation (Figure 3.2, endpoint data of the 3rd column). The lines are non-linear regression best fit of the Hill equation (Equation 3.1, Table 3.1). Data are shown as the mean values with their standard deviations (shown as error bars) of at least three independent experiments. Statistical analysis was performed using Mann-Whitney test (****$p < 0.0001$).

As shown in Figure 3.3, the FI/OD_{600} values of the sensor induced for 5 h in ara^- and ara^+ were fitted to a specific binding equation with a Hill slope as shown below in Equation (3.1) (Neubig et al., 2003),

$$y = V_{max}\frac{x^h}{k_{Hill}^h + x^h} \qquad (3.1)$$

where V_{max} is the maximum specific binding in the same units as y, h is the Hill slope, and k_{Hill} is the OHHL concentration required for half-maximum binding at equilibrium in the same units as x. The best-fit values of the parameters determined using GraphPad Prism are shown in Table 3.1. The best-fit V_{max} values could not be determined and were returned as 'unstable'. However, it is noticeable that the sensor in ara^+ showed a greater response to OHHL induction compared with that in ara^- (the concentration required for half-maximal binding was two orders of magnitude lower and the slope was approximately three-fold greater in ara^+, compared to those in ara^-).

Table 3. 1 Non-linear best-fit values of the Hill equation (Equation 3.1) for the response of the sensor to OHHL induction

Response	Treatment	V_{max}	k_{Hill} (M)	h	R^2
FI/OD_{600}	ara^-	Unstable	1.124 x 10^{-6}	0.4640	0.8545
	ara^+	Unstable	3.701 x 10^{-8}	1.3140	0.8310

In conclusion, the sensor strain showed OHHL concentration-dependent EGFP expression behaviour. The sensor (ara^+) showed obviously higher response levels to OHHL induction compared to the sensor (ara^-) at most of the tested concentrations. Furthermore, the option to tune LuxR expression by adding or not adding arabinose was found to increase the flexibility of the sensor's detection range. The sensor (ara^-) showed a wider detection range from 10^{-7} to 10^{-4} M and may be able to detect OHHL concentrations greater than 10^{-4} M. The sensor (ara^+) was more sensitive to lower OHHL concentrations from 10^{-8} to 10^{-7} M. In addition, the growth of the sensor (ara^-) was less affected by the OHHL induction. These results suggest that the sensor (ara^-) may be more suitable for detecting OHHL concentrations and was used in subsequent experiments.

3.3.2 Characterisation of the producer strain

The main function of the producer (Figure 2.2b) is to express the LuxI that can catalyse the synthesis of OHHL. Additionally, LuxI and mCherry were designed to be bicistronically expressed with the same RBSs. Therefore, the relative production of LuxI was expected to be estimated based on the FI of mCherry. This bicistronic expression is under the control of P_{T7}. As discussed in Section 2.2.1, the expression of P_{T7} in Tuner (DE3) is under IPTG concentration-dependent control (Merck KGaA, 2011). Consequently, the IPTG concentration-dependent expression of the producer was assessed.

Responses of the producer strain to IPTG induction

This section discusses the performance of the producer strain regarding its ability to express mCherry upon IPTG induction at concentrations ranging from 0 to 0.5 mM. As shown in Figure 3.4, the FI and cell response level (FI/OD_{600}) of the non-induced producer were distinctly higher than those of the Tuner (DE3) induced at the highest tested IPTG concentration of 0.5 mM. This result suggests intrinsic leakage of the producer's plasmid. Moreover, the producer showed IPTG concentration-dependent expression. Compared with the non-induced producer, the FI and cell response levels slightly increased when the producer was induced by IPTG

concentrations of 0.025, 0.05 and 0.1 mM and sharply increased when the producer was induced by IPTG concentrations of 0.3 and 0.5 mM. However, the growth was sharply reduced when the producer was induced at 0.3 and 0.5 mM, which may be caused by increased expression of LuxI and mCherry. It also should be noted that the producer response to IPTG induction may approach saturation at 0.3 mM. In addition, similar to the sensor strain, the differences in FI of the producer cultures became more noticeable over time.

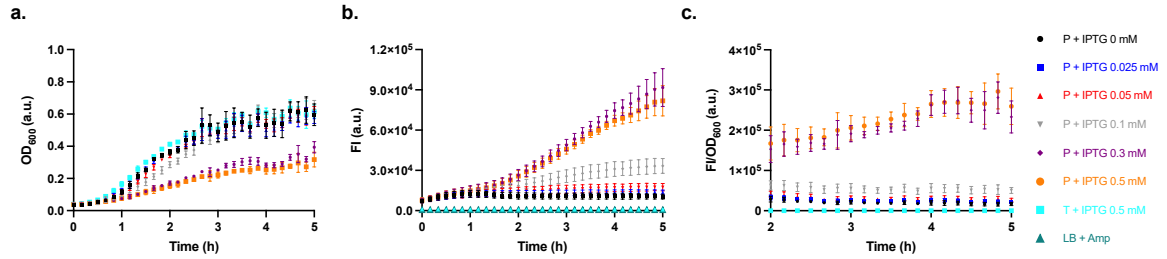

Figure 3. 4 Response of the producer to IPTG induction. (**a**) The growth (optical density at λ = 600 nm, OD_{600}), (**b**) fluorescence intensity (FI) of mCherry (λ_{ex} = 570 (15) nm, λ_{em} = 620 (20) nm), and (**c**) cell response levels (FI/OD_{600}) of the producer (P) induced at varying IPTG concentrations were measured during 5 h of incubation. Tuner (DE3) (T) and LB (Amp) were incubated in parallel as controls. Data are shown as the mean values with their standard deviations (shown as error bars) of at least three independent experiments.

Activation ability of the producer strain

When testing the activation ability of the producer, it was induced at IPTG concentrations of 0.025 to 0.5 mM for 3 h. LB (Amp) medium and the host Tuner (DE3) cultures induced at the highest tested IPTG concentration were incubated in parallel as controls. Every hour, the supernatants of all cultures were taken. After 3 h, all supernatants were mixed with the sensor (ara^-) to assess the activation ability based on the response levels of the sensor.

At all induction times, the growth of the sensor incubated with the culture supernatants was similar but was slower than that of the sensor incubated with the medium control (Figure 3.5, first column). The FI and FI/OD_{600} of the sensor incubated with the supernatants of Tuner (DE3) culture and medium control were similar and noticeably lower than those of the sensor incubated with the producer supernatants. Furthermore, even induced by IPTG for only 1 h, the activation ability of the producer supernatants was approximately two-fold greater than that of OHHL concentration 10^{-4} M (comparing Figures 3.3 and 3.6), suggesting the producer strain has good activation efficiency. However, higher IPTG concentration did not bring higher activation ability. This may be due to the strong activation ability of the producer causing the sensor to saturate even in ara^-. Future studies could include testing the activation ability of the producer at smaller initial OD_{600} values as well as different incubation times and IPTG concentrations.

On the other hand, a previous study found that increasing the incubation temperature (15, 25, and 37 °C) decreased the amount of the protein expressed from the IPTG-induced T7 promoter in BL21 Star™ (DE3) *E. coli* cells (Namdev et al., 2019). This finding suggests that the expression of the producer may not be at its most productive state at 37 °C used in this work. Nevertheless, this is unlikely to cause a major problem as all producer supernatants showed strong QS activation ability.

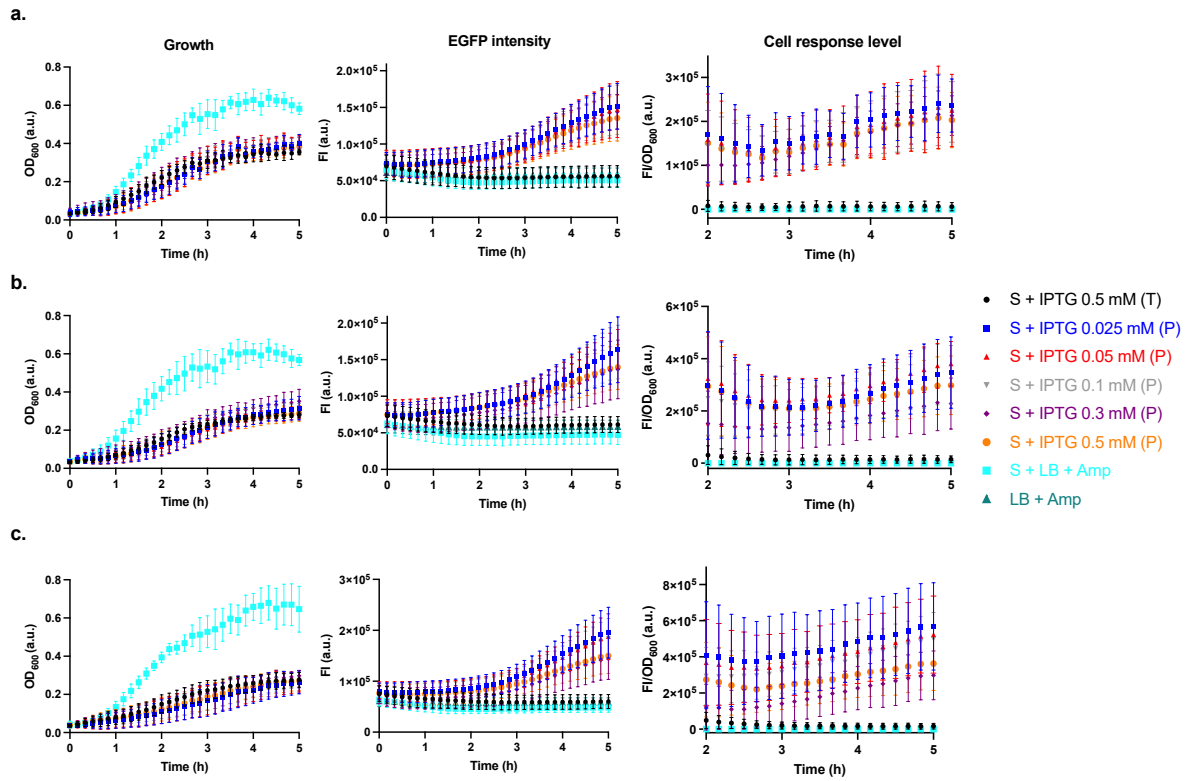

Figure 3. 5 Response of the sensor induced by the producer supernatants. The producer (P) was induced at varying IPTG concentrations. The growth (optical density at λ = 600 nm, OD_{600}), fluorescence intensity (FI) of EGFP (λ_{ex} = 470 (15) nm and λ_{em} = 515 (20) nm), and cell response levels (FI/OD_{600}) of the sensor (ara^-) (S) induced by supernatants were measured during 5 h of incubation. The supernatants were obtained after (**a**) 1 h, (**b**) 2 h, and (**c**) 3 h of incubation. Tuner (DE3) (T) and LB (Amp) were incubated in parallel as controls. Data are shown as the mean values with their standard deviations (shown as error bars) of at least three independent experiments.

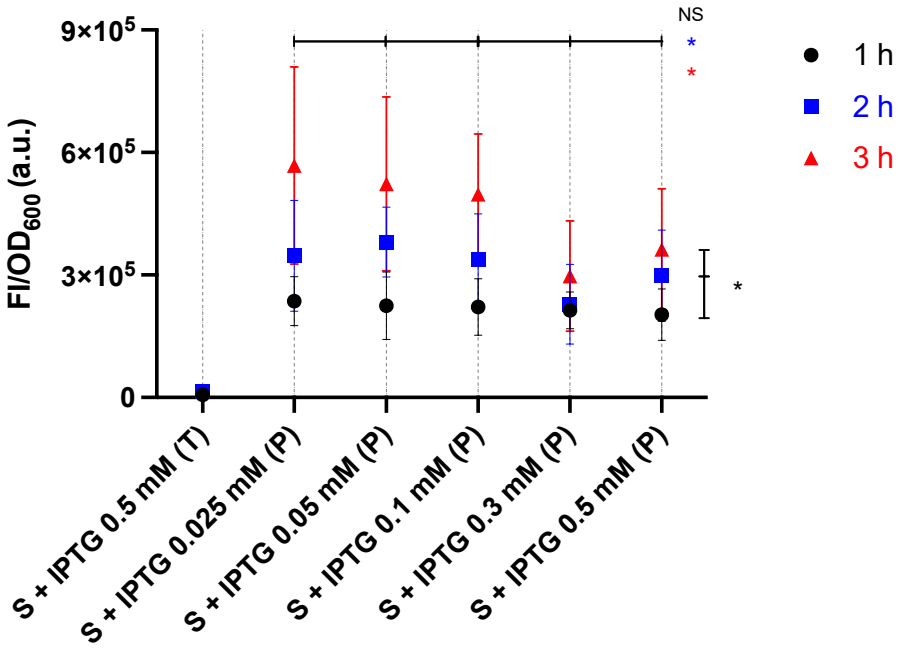

Figure 3. 6 Cell response levels of the sensor induced by the producer supernatants. The sensor (ara$^-$) was incubated for 5 h with supernatants of 1 h (black), 2 h (blue), and 3 h (red) IPTG-induced Tuner (DE3) (T) and producer (P). Data are shown as the mean values with their standard deviations (shown as error bars) of at least three independent experiments. Statistical analysis was performed using Kruskal-Wallis test (*$p < 0.05$, NS = not significant), where arrowheads indicate the groups being compared.

The red fluorescent signals of the sensor (ara$^-$) induced by the producer supernatants were simultaneously measured. As shown in Figure 3.7, the FI did not show a distinct increase over time, indicating that the invasion of the producer into the sensor culture through the supernatant was unlikely. However, the FI of the sensor incubated with the producer supernatants was higher than those incubated with the controls, which may be due to the fluorescence bleed-through of EGFP.

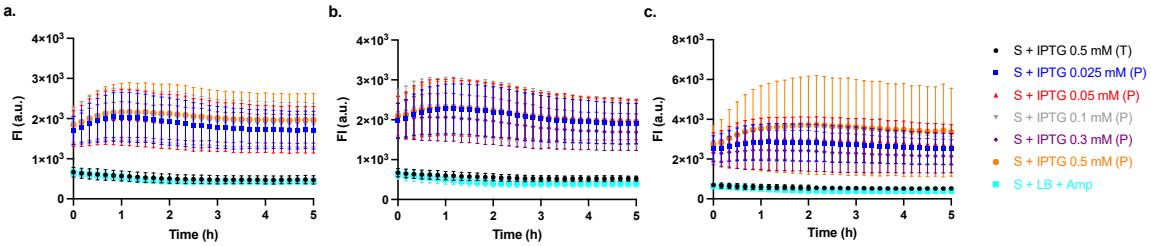

Figure 3. 7 Red fluorescence intensity of the sensor incubated with the producer supernatants. The fluorescence intensity (FI) of mCherry (λ_{ex} = 570 (15) nm and λ_{em} = 620 (20) nm) of sensor (ara$^-$) incubated with (**a**) 1 h, (**b**) 2 h, and (**c**) 3 h-induced producer (P) and Tuner (DE3) (T) supernatants were mseasued during 5 h of incubation (corresponding to the **a**, **b**, and **c** in Figure 3.5, respectively). Data are shown as the mean values with their standard deviations (shown as error bars) of at least three independent experiments.

After taking the supernatants, the FI of the resuspended producer pellets was measured using a FluoroMax-4 spectrofluorometer, and the OD_{600} was measured using a Jenway 6715 UV/Visible spectrophotometer. Generally, the FI/OD_{600} of the pellets were IPTG concentration-dependent, except for the 0.1 mM IPTG concentration-induced pellet whose FI/OD_{600} was close to that of the pellet induced at 0.5 mM IPTG concentration (Figure 3.8). This is inconsistent with the results shown in Figure 3.4, where the producer induced at 0.1 mM IPTG concentration showed an obviously lower response than the produce induced at IPTG concentrations of 0.3 and 0.5 mM. The inconsistency may be related to different initial OD_{600} and IPTG depletion. Besides, a previous study found that the expression in the Tuner (DE3) strain was not always positively correlated with IPTG concentration (Mühlmann et al., 2017).

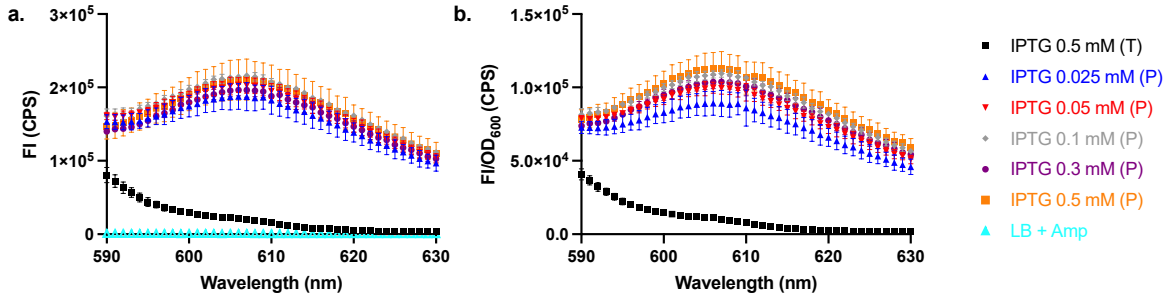

Figure 3. 8 Fluorescence intensity and cell response levels of the producer and Tuner (DE3) in remaining cultures after taking supernatants. (**a**) The red fluorescence intensity (FI) at λ_{ex} = 583 nm and (**b**) the cell response levels (FI normalised by the corresponding growth (optical density at λ = 600 nm, OD_{600})) of the resuspended producer (P) and Tuner (DE3) (T) pellets were measured. Data are shown as the mean values with their standard deviations (shown as error bars) of at least three independent experiments.

3.3.3 Characterisation of the regulator strain

Similar to the producer, the $P_{LtetO-1}$ of the regulator controls a bicistronic expression of AiiA that can degrade OHHL and fluorescent protein EBFP2 with the same RBSs. Therefore, the relative production of AiiA was expected to be estimated based on the FI of EBFP2. Although it is not yet possible to measure its FI over time, the regulator showed the ability to attenuate the response of the sensor (ara^-) by degrading OHHL (Figure 3.9). When testing the attenuation ability of the regulator, overnight cultures of the Tuner (DE3) and aTc-induced and non-induced regulator were centrifuged. The pellets were resuspended in LB (Amp) supplemented with 10^{-5} M OHHL concentration. The suspensions were incubated for 1 h and then centrifuged. The supernatants were incubated with the sensor (ara^-) for 5 h.

The sensor incubated with cell-treated supernatants showed lower growth than the sensor incubated with non-cell-treated supernatants (Figure 3.9a). The sensor incubated with Tuner

(DE3) (initial OD_{600} ~ 1) treated OHHL 10^{-5} M supernatant showed a significantly higher response than the sensor incubated with non-treated OHHL 10^{-5} M (Figure 3.9 cf. cyan and purple) (**$p < 0.01$, Mann-Whitney test). This result suggests that the Tuner (DE3) strain may produce molecule(s) that could activate the sensor's response, which may affect the accuracy of the sensor. *E. coli* was reported to inherently lack AI-1 synthase (Michael et al., 2001; Steindler and Venturi, 2007; Miller and Gilmore, 2020). However, a previous study found that diketopiperazines produced by *P. aeruginosa* were able to activate a LuxR-based *E. coli* AHL biosensor (Holden et al., 1999). Currently, it can only be speculated that there was at least one metabolite, yet to be identified, in the supernatant of the Tuner (DE3) treated with OHHL 10^{-5} M that could cause the enhanced response of the sensor. This speculation may also explain why the sensor incubated with IR0.25 (i.e., aTc-induced regulator with initial OD_{600} ~ 0.25)-treated OHHL 10^{-5} M supernatant showed a greater response level than the sensor incubated with untreated OHHL 10^{-5} M supernatant (Figure 3.9 cf. black and purple). This result suggests that, under the experimental protocol used, initial OD_{600} greater than 0.25 is required to observe the QS attenuation ability of the regulator. On the other hand, the regulator was able to degrade OHHL even in the absence of aTc due to the intrinsic leakage of the $P_{LtetO-1}$ promoter, but the attenuation ability was increased in the presence of aTc (Figure 3.9 cf. red, grey, and cyan) (****$p < 0.0001$, Kruskal-Wallis test).

In this work, the attenuation ability of the regulator at varying initial OD_{600} was tested, where the regulator with higher initial OD_{600} showed higher degrading ability (Figure 3.9 cf. black, blue, and red) (****$p < 0.0001$, Kruskal-Wallis test). As it was found that expression controlled by promoter $P_{LtetO-1}$ could be expressed in aTc concentration-dependent manner (Hensel, 2017; Silva et al., 2019), future studies could include the optimisation of the use of regulator strain by exploring this concentration-dependent expression behaviour.

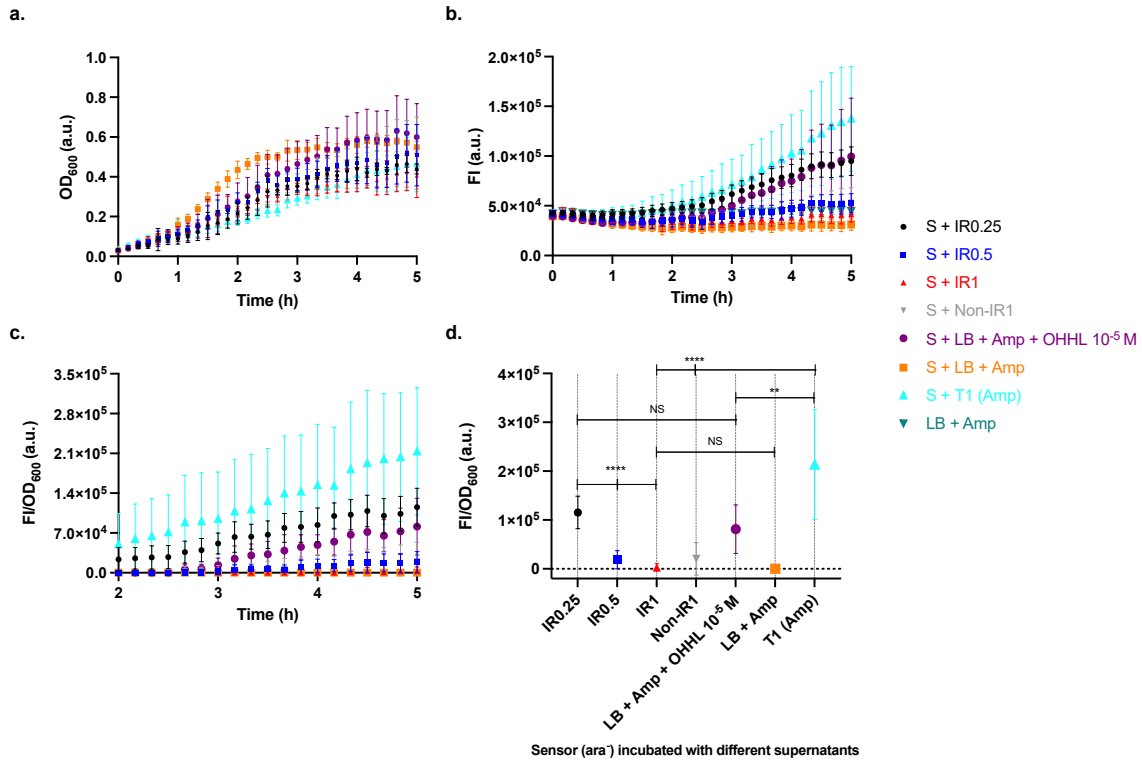

Figure 3. 9 Ability of the regulator to attenuate the response of the sensor. LB (Amp) supplemented with OHHL 10^{-5} M was used to assess the degrading ability of the regulator over 1 h incubation. The supernatants were then incubated with the sensor (ara$^-$). (**a**) The growth (optical density at λ = 600 nm, OD_{600}), (**b**) fluorescence intensity (FI) of EGFP (λ_{ex} = 470 (15) nm and λ_{em} = 515 (20) nm), and (**c**) cell response levels (FI/OD_{600}) of the sensor induced by the supernatants were measured during 5 h of incubation. (**d**) The cell response levels at the endpoints (5 h). Tests included the aTc-induced regulator (initial OD_{600} ~ 0.25, 0.5, and 1, indicated as IR0.25, IR0.5, and IR1, respectively), non-induced regulator (initial OD_{600} ~ 1, indicated as Non-IR1) and Tuner (DE3) (initial OD_{600} ~ 1, indicated as T1 (Amp)). Data are shown as the mean values with their standard deviations (shown as error bars) of at least three independent experiments. Statistical analysis was performed using Mann-Whitney test for two groups and using Kruskal-Wallis test for three groups (**p < 0.01, ****p < 0.0001, and NS = not significant), where arrowheads indicate the groups being compared.

Similar to the producer activation ability analysis, after taking the supernatants, the FI and OD_{600} of the resuspended regulator pellets were measured. As shown in Figure 3.10, the FI of cultures was higher than that of media. However, the FI of different bacterial cultures were similar. This could be caused by different initial OD_{600} in different cultures. Of note, as discussed in 2.3.2, the fluorescence readings could be affected by the turbidity and background fluorescence. When comparing the FI/OD_{600}, the cell response level of the aTc-induced regulator with initial OD_{600} ~ 1 (IR1) was significantly greater than that of the non-induced regulator with the same initial OD_{600} (Non-IR1) (*p < 0.05, Mann-Whitney test), where that of the non-induced regulator was significantly greater than that of the Tuner (DE3) (T1) (**p <

0.01, Mann-Whitney test). Additionally, in the presence of aTc, the regulator with lower initial OD_{600} showed higher cell response levels, contrary to their QS attenuation ability (comparing Figures 3.9 and 3.10b). One reason for this discrepancy could be the higher turbidity at higher OD_{600} reduced the fluorescence reading.

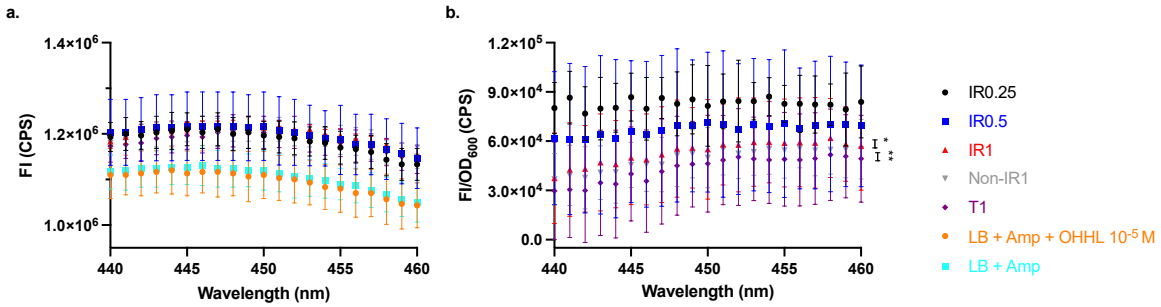

Figure 3. 10 Fluorescence intensity and cell response levels of the regulator and Tuner (DE3) in remaining cultures after taking the supernatants. (**a**) The blue fluorescence intensity (FI) at λ_{ex} = 367 nm and (**b**) cell response levels (FI normalised by the corresponding growth (optical density at λ = 600 nm, OD_{600})) of the resuspended pellet cultures were measured. Pellets include the aTc-induced regulator (initial OD600 ~ 0.25, 0.5, and 1, i.e., IR0.25, IR0.5, and IR1, respectively), non-induced regulator (initial OD600 ~ 1, i.e., Non-IR1) and Tuner (DE3) (initial OD600 ~ 1, i.e., T1). Data are shown as the mean values with their standard deviations (shown as error bars) of at least three independent experiments. Statistical analysis was performed using Mann-Whitney test (*p < 0.05 and **p < 0.01), where arrowheads indicate the groups being compared.

3.3.4 Conversion of OD_{600} to colony-forming units

In order to enable single-cell encapsulation based on Poisson statistics, the overnight culture needs to be diluted to a specific volume containing a certain number of bacterial cells. The conversion equation from OD_{600} to colony-forming units (CFU) was obtained using the sensor strain for dilution. The colony-forming units calculated using the equation in ISO 15214:1998 of OD_{600} ~ 0.05, 0.1, 0.2, 0.35, and 0.5 are shown in Figure 3.11. The conversion equation from OD_{600} to CFU (Equation 3.2) was the simple linear regression line (through the origin) of the calculated colony numbers:

$$\mathrm{CFU} = 2277600356 \times \mathrm{OD}_{600} \quad (3.2)$$

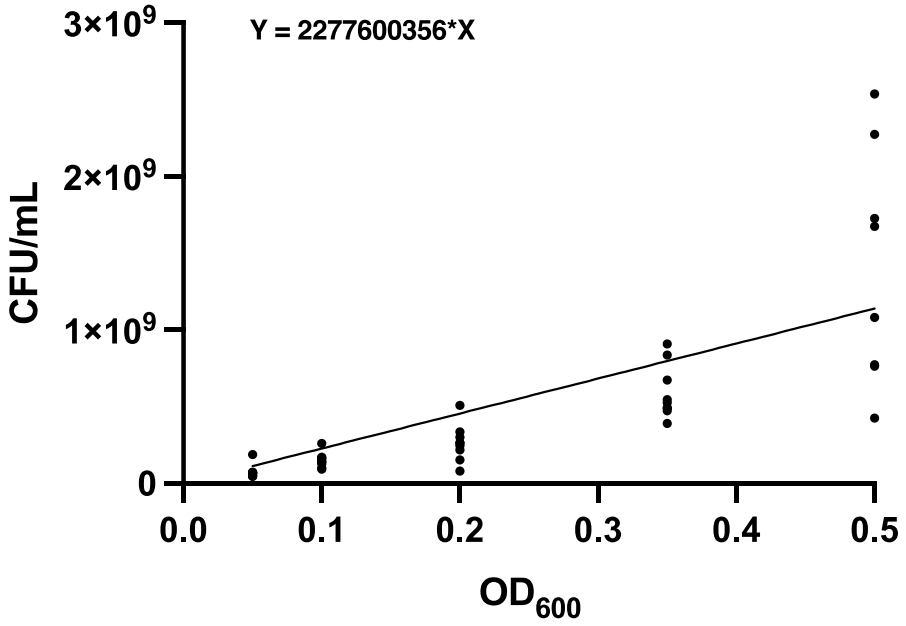

Figure 3. 11 Conversion equation from OD_{600} to colony-forming units obtained using the sensor strain. Data are shown as calculated colony numbers (black dots) and the corresponding simple linear regression line with equation. Data are collected from at least three independent experiments.

As OD_{600} increased, the difference in the calculated number of colonies obtained at the same OD_{600} also increased (Figure 3.11). This increase in difference may be caused by greater human error in the serial dilutions at greater OD_{600}. In addition, the retention of a pair of successive dilutions whose counts were less than 15 and the merging of colonies could also affect the accuracy of the conversion equation. All the engineered strains used Tuner (DE3) as the host strain. Although the growth rate of different strains may be different, Equation 3.2 was used to dilute all strains in microfluidic experiments.

3.4 Conclusions

In this chapter, the performance of the three engineered strains in the planktonic state was assessed. Both the sensor and producer strains showed inducer concentration-dependent expression behaviour and may reach saturation at high inducer concentrations. This expression behaviour of the regulator strain has not been assessed since it was not possible to distinguish the blue signal from the background noise caused by cells and LB (Amp) medium in the microplate experiments. However, the expression from the promoter, $P_{LtetO-1}$, employed by the regulator was reported to be in an aTc concentration-dependent expression manner, suggesting the attenuation ability of regulator strain may be able to be regulated by aTc concentration. Future studies could include testing the aTc concentration-dependent expression behaviour of the regulator strain using a more sensitive reader.

The sensitivity of the sensor could be tuned by adding (ara^+) or not adding (ara^-) arabinose. The sensor (ara^-) showed a wider detection range, from 10^{-7} to 10^{-4} M and may be able to detect greater OHHL concentrations. Meanwhile, the growth of the sensor (ara^-) was less affected by the OHHL induction. Therefore, the sensor (ara^-) may be more suitable for detecting the concentration of OHHL in the environment. The sensor (ara^+) may be more suitable for detecting lower OHHL concentrations ranging from 10^{-8} to 10^{-7} M. Additionally, the sensor strain was used to obtain the conversion equation from OD_{600} to colony-forming units required for single-cell encapsulation in microfluidic experiments.

The producer strain showed IPTG concentration-dependent expression but may be approaching saturation at 0.3 mM. Moreover, the producer supernatant showed good efficiency in activating the sensor's response. The activation ability of the 1 h IPTG-induced supernatants was approximately two-fold greater than that of 10^{-4} M OHHL concentration. However, the activation ability of the producer was found to be inconsistent with its IPTG concentration-dependent expression behaviour. It is speculated that this inconsistency might be due to the saturation of the sensor (ara^-). Future studies could include determining the cause of this inconsistency by adjusting experimental protocols, such as lowering the initial OD_{600} or reducing the incubation time.

The regulator strain showed the ability to attenuate the sensor's response to environmental OHHL, although its host strain, Tuner (DE3), showed the opposite ability to activate the sensor's response. In addition, the turbidity resulting from cell growth was found to interfere with the accuracy of fluorescence readings, and the detection of blue signal was more severely affected than the other two signals.

Chapter 4 Phenotypic analysis of the bacterial consortium by microfluidics

This chapter focuses on the phenotypic analysis of the engineered bacterial consortium using a microfluidic platform developed for microfluidic cell culture by Evorion Biotechnologies (Münster, Germany) (Kleine-Brüggeney et al., 2019; Kleine-Brüggeney et al., 2021). To this end, the sensor and producer strains were immobilised in agarose hydrogel microbeads. The microbeads were captured on similar microfluidic chips with either single-bead or paired-bead traps. Bacterial communities on the chip were cultured under programmed perfusion control by a control unit and imaged over time using EVOS FL Auto 2 Imaging System.

4.1 Materials, equipment, and software

Information on the main experimental materials and equipment used in this chapter is provided in Table A.2 in Appendix A. Information on software used in this chapter is provided in Table A.3 in Appendix A.

4.2 Overnight cultivation and time-lapse imaging of bacterial communities on a microfluidic platform

Figure 4.1 shows the general workflow for immobilising and imaging bacterial communities in agarose hydrogel microbeads. The workflow mainly consists of three steps: (i) preparation of microfluidic chips containing agarose hydrogel microbeads encapsulating bacterial cells (grey area), (ii) time-lapse imaging of the bacterial communities cultured in microbeads on the chip (blue area), (iii) microscopic image compilation and analysis (red area). The CellCity microfluidic platform was used to immobilise and cultivate bacterial communities (Kleine-Brüggeney et al., 2021). The EVOS FL Auto 2 Imaging System (Evos) was used for bacterial community visualisation. The general workflow of this microfluidic technology was published by Evorion Biotechnologies (Münster, Germany) at https://www.youtube.com/watch?v=3vD9EjAn-Os (accessed 30 January 2024).

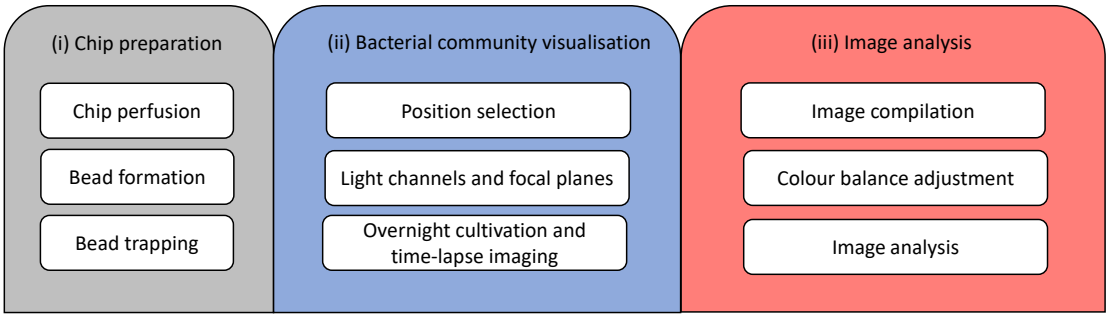

Figure 4. 1 Main steps of the workflow of this microfluidic work. The microfluidic chips containing microbeads encapsulating bacterial communities were prepared (grey area). The bacterial communities in the microbeads were then imaged over time using selected settings (blue area). The collected microscopic images were then compiled and analysed (red area).

4.2.1 Overview of the microfluidic platform

The layout of the microfluidic platform used in this work is shown in Figure 4.2. This is a macro-to-micro platform designed for microfluidic cell culture by Kleine-Brüggeney et al. (2021). This platform mainly consists of (i) a microfluidic chip for cell immobilisation and cultivation, (ii) a control unit that can be connected to the (iii) chip holder (incubation chamber) to control the pressure and temperature on the chip, and (iv) a conventional automated epifluorescence microscope for bacterial community visualisation (Kleine-Brüggeney et al., 2021).

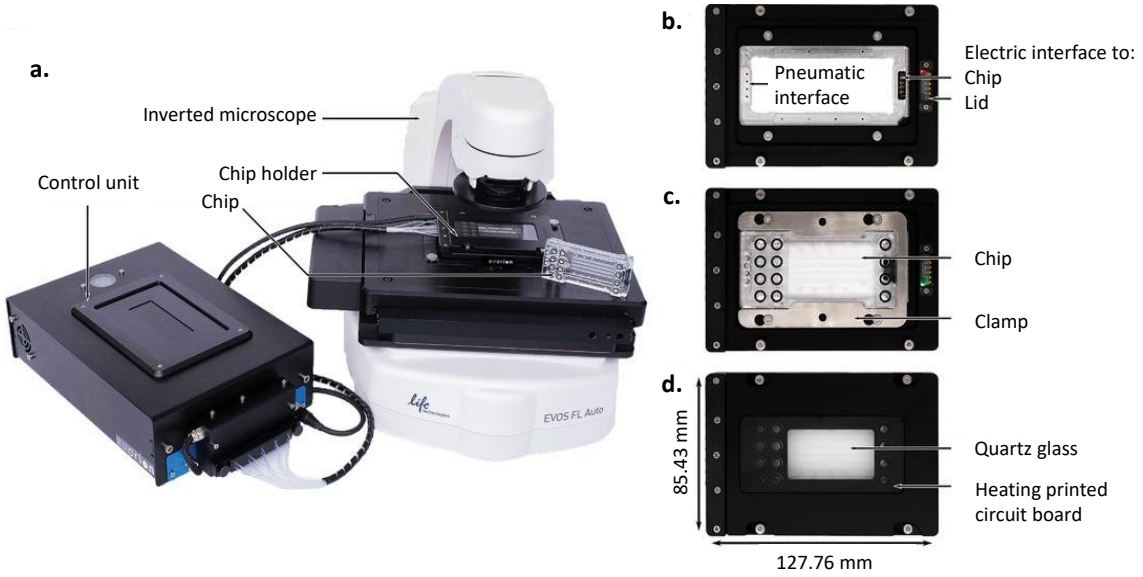

Figure 4. 2 Overview of the microfluidic platform. (**a**) The macro-to-micro cell culture platform mainly consists of a microscope, a control unit, a chip, and a chip holder (incubation chamber). (**b**) Top view of the chip holder. (**c**) Chip holder containing a chip. (d) Closed chip holder. This figure was modified from the figure published by Kleine-Brüggeney et al. (2021).

The design of the single-bead chip is shown in Figure 4.3. The chip contains three columns of four reservoirs each. The reservoirs are divided into five groups, each controlled by a pressure port (P1 - P5). The reservoirs of column A are used for bead formation and those of columns B and C are mainly used as reagent inlets and outlets, respectively (Figure 4.3a and c). In the middle area of the chip are four channels that contain a total of 2660 trapping positions. The inner diameter of the bead holder is approximately 80 µm (Figure 4.3b). Figure 4.3d shows the flow-focussing and fluid channel design of the chip. The design of the flow-focussing generator for bead formation are shown in Figure 4.3e. Reservoirs A1 and A2 are the inlets for oil and aqueous phases, respectively. Reservoir A4 is the outlet for the formed microbeads. Figure 4.3f illustrates the formation of a microbead in milliseconds (Kleine-Brüggeney et al., 2021).
The design of the paired-bead chip is similar to that of the single-bead chip, except for a smaller number of trapping positions. There are 1700 trapping positions on the paired-bead chip. Each trapping position has an additional bead holder for capturing two adjacent microbeads. The appearance of single-bead and pair-bead trapping positions is shown in Figure 4.4.

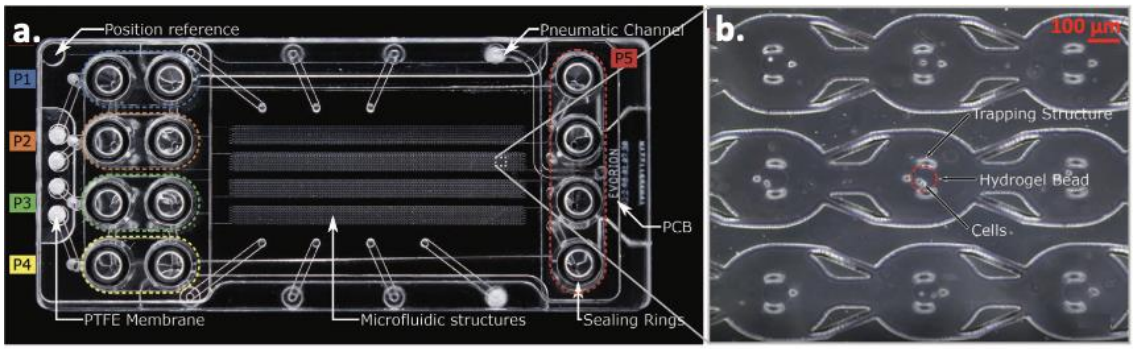
a.
Position reference
Pneumatic Channel
P1
P2
P3
P4
P5
PCB
PTFE Membrane
Microfluidic structures
Sealing Rings
b.
100 µm
Trapping Structure
Hydrogel Bead
Cells

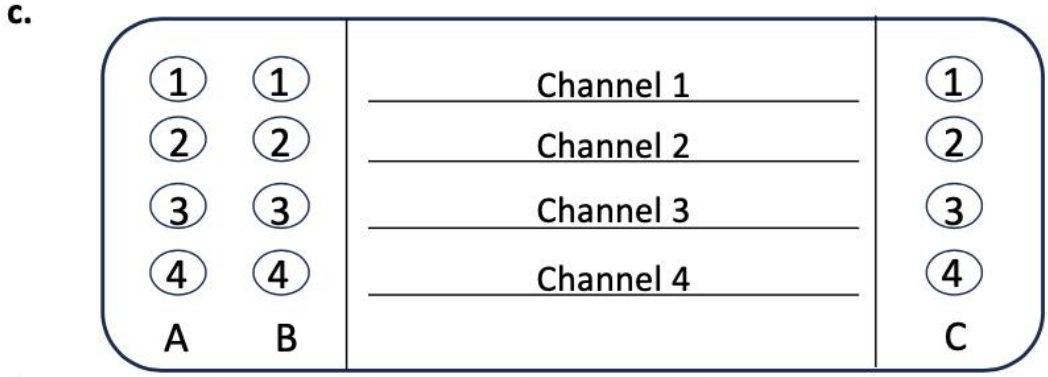
c.
1
2
3
4
A
B
Channel 1
Channel 2
Channel 3
Channel 4
1
2
3
4
C

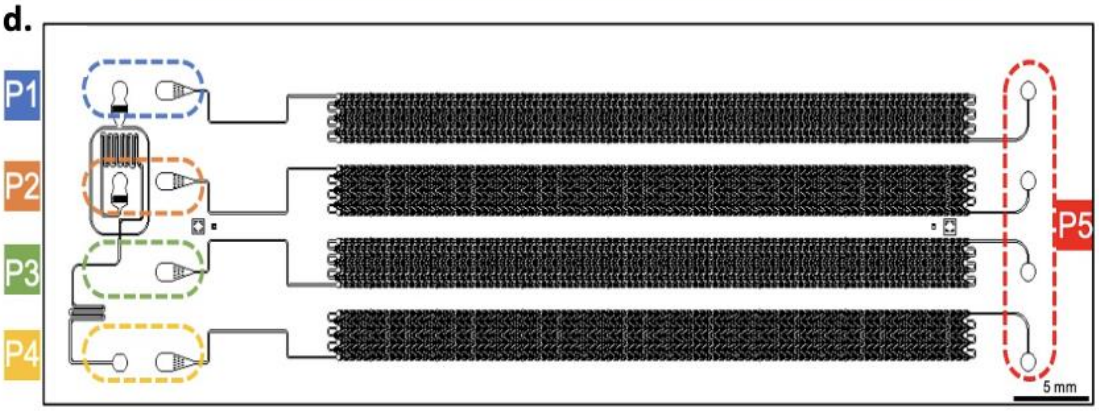
d.
P1
P2
P3
P4
P5
5 mm

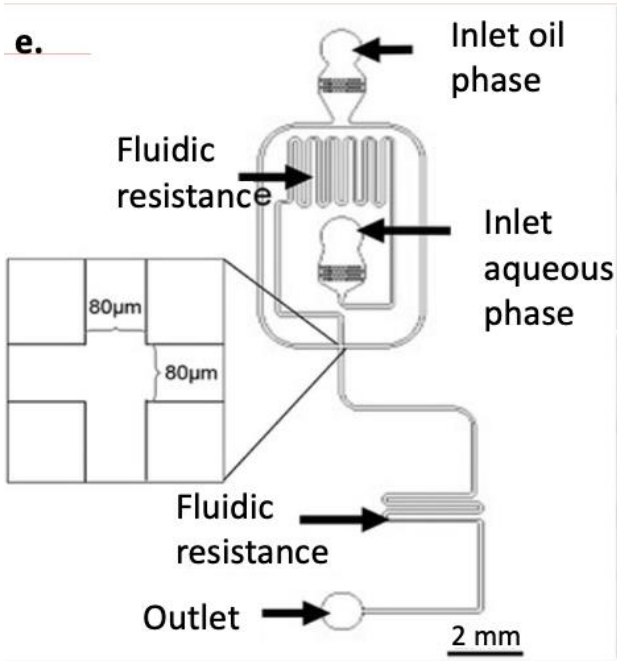
e.
Inlet oil phase
Fluidic resistance
Inlet aqueous phase
80µm
80µm
Fluidic resistance
Outlet
2 mm

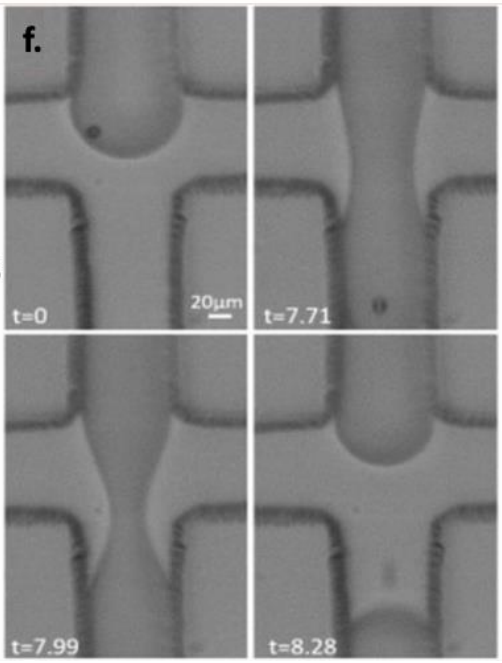
f.
t=0
20µm
t=7.71
t=7.99
t=8.28

Figure 4. 3 Design of the microfluidic chip. (**a**) Top view of the chip. The chip contains three columns of four reservoirs each. The reservoirs are divided into five groups, each controlled by a pressure port (P1 - P5). (**b**) Magnified view of the middle of a single-bead chip. Each trapping position has a bead holder (inner diameter: ~ 80 µm). (**c**) Simplified top view of the chip. (**d**) Flow-focussing generator and fluid channels of the chip. (**e**) Design of the flow-focussing generator. (**f**) High-speed recording of the formation of a microbead in millisecond. (**a**)(**b**)(**d**)(**e**)(**f**) were modified from the figures published by Kleine-Brüggeney et al. (2021).

4.2.2 Preparation of bacterial communities on microfluidic chips

In this section, the experimental protocols for preparing the single-bead and paired-bead chips are described. The protocols were provided by Evorion Biotechnologies (Münster, Germany). Briefly, overnight bacterial cultures were diluted, and the bacterial cells were encapsulated in agarose hydrogel microbeads. The beads were then trapped in bead holders on CellCity microfluidic chips for overnight cultivation and time-lapse imaging. The methods used to control the pressure and temperature on the chip were from CellCity Software provided by Evorion Biotechnologies (Münster, Germany). The temperature was controlled at 37 °C, while the pressure applied was different in different methods. Of note, the company improved the protocol and/or software after the first and second single-bead experiments, respectively. Some parameters may be different for the single-beads experiment.
The reservoirs were emptied before adding new solutions. The culture medium for the engineered strains was supplemented with 100 µg/mL ampicillin (Amp), whereas that for the Tuner (DE3) strain was not.

Pre-experimental preparation

The reagents ‘Priming Solution’, ‘Buffer B’, ‘Bead Formation Solution’, ‘Demulsification Solution’, and ‘Trapping Solution’ were stored at 37 °C. ‘Hydrogel A’ was quickly spun down and preheated to 65 °C for 30 min. Then, ‘Hydrogel A’ was thoroughly vortexed for at least 20 to 30 s and stored at 37 °C for at least 15 min before use.

Priming

Pre-warmed Priming Solution (150 µL) was added to each reservoir of column C. The ‘PrimingPreheat’ method was used to fill the channels with ‘Priming Solution’.

Bead formation

Overnight bacterial cultures were diluted to $6 - 10 \times 10^3$ cells/μL for the single-bead chip and 12×10^3 cells/μL for the paired-bead chip with LB. Dilution was carried out according to Equation 3.2 discussed in Section 3.3.4.

The diluted bacterial culture was warmed to 37 °C, and 20 μL was mixed with pre-prepared 'Hydrogel A' in 1 : 1 ratio in single-bead experiments. In paired-bead experiments, the diluted bacterial cultures of two strains were mixed in 1 : 1 ratio to a final volume of 40 μL. Then 20 μL of the mixture was mixed with 20 μL of 'Hydrogel A'.
Pre-warmed 'Buffer B' (150 μL) was added to each reservoir of column B. Pre-warmed 'Bead Formation Solution' (150 μL) was added in reservoir A1 and 'Hydrogel A'-cell mixture (8 - 12 μL) was added in reservoir A2. Monodispersed agarose microbeads encapsulating cells were formed using the 'BeadFormation' method. The beads were harvested from reservoir A4 and required to be incubated at 4 °C for 15 min before demulsification. In single-bead experiments, only the sensor cells were encapsulated. In paired-bead experiments, the mixture of the sensor and producer strains was encapsulated. The mixture of the producer and the host Tuner (DE3) strains was also encapsulated as a control.

Bead demulsification

In the collected bead solution, there was a cloudy bead-containing phase floating on the surface. Pre-warmed 'Trapping Solution' (200 μL) and 'Demulsification Solution' (100 μL) were added above and below the bead-containing phase, respectively. The mixture was inverted twice and allowed to stand for 60 s before taking 100 μL of the bead solution from the phase. Then 'Trapping Solution' (200 μL) was added into the bead-containing phase before taking 200 μL of the bead solution from the phase. The obtained bead solution was filtered through the bead filter provided in the CellCity array kit. Bead formation and demulsification steps were repeated to collect a sufficient amount of filtered bead solution for the bead trapping step described in the next section.

Bead Trapping

Before trapping the beads, the chip was washed twice. Each time, 150 μL of Buffer B or LB was added to each reservoir of Colum B, and the 'Wash_high_flow' method was used for washing. The filtered bead solution (125 - 150 μL) was then added into each reservoir of column B before performing the 'Trapping' method. Then the channels were washed twice. Each time, 150 μL of LB medium was added into each reservoir of Colum B, and then different methods were used for washing. In single-bead experiments, the 'Trapping' method was used

for the post-trapping washing. In paired-bead experiments, 'Wash_high_flow' and then 'Wash_alternating_flow' methods were used for the post-trapping washing.

Cultivation

In single-bead experiments, the culture medium was supplemented with OHHL in the concentration range from 0 to 10^{-5} M. In paired-bead experiments, the culture medium was supplemented with IPTG concentrations of 0, 0.025, and 0.3 mM. The culture medium for the engineered strains was supplemented with 100 µg/mL Amp and that for the Tuner (DE3) strain was not supplemented with Amp. These pre-prepared LB media were added to reservoirs of column B and column C, of which 200 µL was added to each reservoir of column B and 50 µL was added to each reservoir of column C. The pre-prepared culture medium added to two reservoirs of a row was the same. The chip was then ready for overnight cultivation using the 'CultivationSequence_NoCO2' method.

4.2.3 Microscopic visualisation of bacterial communities

In this section, the workflow for visualising bacterial communities encapsulated in microbeads on the chip is described. Briefly, trapping positions to be imaged were selected using the tool developed by Evorion Biotechnologies (Münster, Germany), and the imaging parameters were set. Then bacterial communities were cultivated overnight while being imaged using EVOS FL Auto 2 Imaging System (Evos).

Position selection for time-lapse imaging

Trapping positions to be imaged were selected using the Position Selection Tool developed by Evorion Biotechnologies (Münster, Germany). Firstly, 10 × objective and transmitted light were used to locate the four rectangular corners of the trapping position area. A file defining the whole imaging area was exported from Evos and imported to the Position Selection Tool to generate a calibration file containing 516 imaging areas between the four rectangular corners for pre-scanning. Then the generated images were imported to the Position Selection Tool, which then displayed individual trapping positions of the whole area. The well-formed beads that appeared to contain only one or a few cells were preferred for further imaging. Trapping positions that were appropriate for time-lapse imaging were then selected. The selected positions were exported as a scan protocol file and then imported into Evos for the time-lapse overnight imaging.

Light channels

Time-lapse imaging was performed using 40 × objective. Meanwhile, transmitted light and the green fluorescence filter (λ_{ex} = 470 (22) / λ_{em} = 510 (42)) were used in single-bead experiments. In paired-bead experiments, in addition to the transmitted light and green fluorescence filter, the red fluorescence Texas Red filter (λ_{ex} = 585 (29) / λ_{em} = 624 (40)) was used. For each light channel, according to actual situations, the light intensity, exposure time and gain were set to appropriate values. Low light intensity and high gain and exposure values were preferred to reduce photobleaching and phototoxicity (Thermo Fisher Scientific, 2018).

Focal planes

Images were iteratively taken on five focal planes over time. To set five focal planes, the 'Z-Stack Settings' of Evos was used. The relatively most focused plane of a reference position was set as the default focus position. The planes ± ~ 20 μm away from the default focus position were set as the top and bottom planes. The number of planes was set to five. Then five planes with ~ 10 μm in plane step size were set.

Overnight cultivation and time-lapse imaging

To get time-lapse images, the imaging duration was set to 24 h, where the imaging interval for single-bead experiments was 20 min and for paired-bead experiments was 30 min.
Once Evos imaging was started, the 'CultivationSequence_NoCO2' method developed by Evorion Biotechnologies (Münster, Germany) was performed simultaneously for overnight cultivation. Although the duration was set to 24 h, the cultivation was always terminated manually the next morning. The company updated the cultivation method after the first single-bead experiment. Some parameters may be different between the first single-bead experiment and the other experiments.

4.2.4 Time-lapse image analysis

The collected microscopic images were compiled into time-lapse images of each trapping position using DataViewer (version 1.0) developed by Evorion Biotechnologies (Münster, Germany). The compiled file of a trapping position contains chronologically sequenced images in each light channel and each focus plane. Then Fiji-ImageJ (Schindelin et al., 2012) was used for image analysis and digitisation.

When using Fiji-ImageJ to assess a trapping position, 'Color Balance' could be used to adjust the brightness of each light channel. When observing the overview of a bacterial community,

images taken at five focal planes of a time point could be merged into one image while maximising intensity using ‘Z Projection’. Meanwhile, ‘All time frames’ of ‘Z Projection’ could be selected to merge the focal planes by time point.

4.3 Results and discussion

To assess the performance of the engineered strains encapsulated in agarose hydrogel microbeads, first, the sensor was encapsulated in the microbeads. The beads were then trapped in single-bead chips, and the chip channels were perfused with LB (Amp) supplemented with 0 - 10^{-5} M OHHL concentrations. In the first single-bead experiment (Day 1), OHHL concentrations 10^{-10}, 10^{-8}, and 10^{-6} M and LB (Amp) medium control were tested. In the second single-bead experiment (Day 2), OHHL concentrations 10^{-9}, 10^{-7}, and 10^{-5} M and LB (Amp) medium control were tested.
To assess the activation ability of the producer encapsulated in agarose hydrogel microbeads, the sensor and producer were co-cultured in the microbeads, while the sensor and Tuner (DE3) strains were co-cultured in parallel as a control. The beads were trapped in paired-bead chips, and the chip channels were perfused with LB (Amp) supplemented with 0, 0.025 and 0.3 mM IPTG concentrations. Three biological replicates were performed, recorded as Day 1, Day 2, and Day 3.

4.3.1 Bacterial communities at different focal planes

Time-lapse images of the bacterial communities were iteratively taken on five focal planes. The relatively most focused plane of a reference position was set as the middle plane. The top and bottom planes were set to ± ~ 20 μm from the middle plane. The distance between adjacent planes was ~ 10 μm. Of note, the middle focal plane may not be the most focused plane to observe the bacterial community. Additionally, due to the ~10 μm distance between adjacent planes, the phenotype of a bacterial community on different planes may be conspicuously different. To observe the overview of a bacterial community, five focal planes could be merged into one image (projection image) using the ‘Z Projection' of Fiji-ImageJ.

Figure 4.4 below shows screenshots of two trapping positions, namely position 59 from the first single-bead experiment (Day 1) (Figures 4.4a and c) and position 216 from the second paired-bead experiment (Day 2) (Figures 4.4b and d). Screenshots were taken at time point 23. Figures 4.4a and b show five focal planes of two positions, respectively. In Figures 4.4a and b, screenshots from 1 to 5 are corresponding to the focal planes from top to bottom. The bacterial community may look different on different planes. For instance, as shown in Figures 4.4a and b, when observing screenshots from 1 to 5, some bacterial colonies become visible and clearer.

This phenomenon may be mainly due to the colony being obscured by the agarose gel. This obscuration could also affect the measurement of fluorescence intensity, resulting in the fluorescence readings of the same colony area measured on different focal planes being different, which may affect the accuracy of the digitised QS response analysis.
Figures 4.4b and d were screenshots of projection images of the two positions, respectively. The merged image may be more blurred than the most focused plane but may give an overview of the imaged communities.

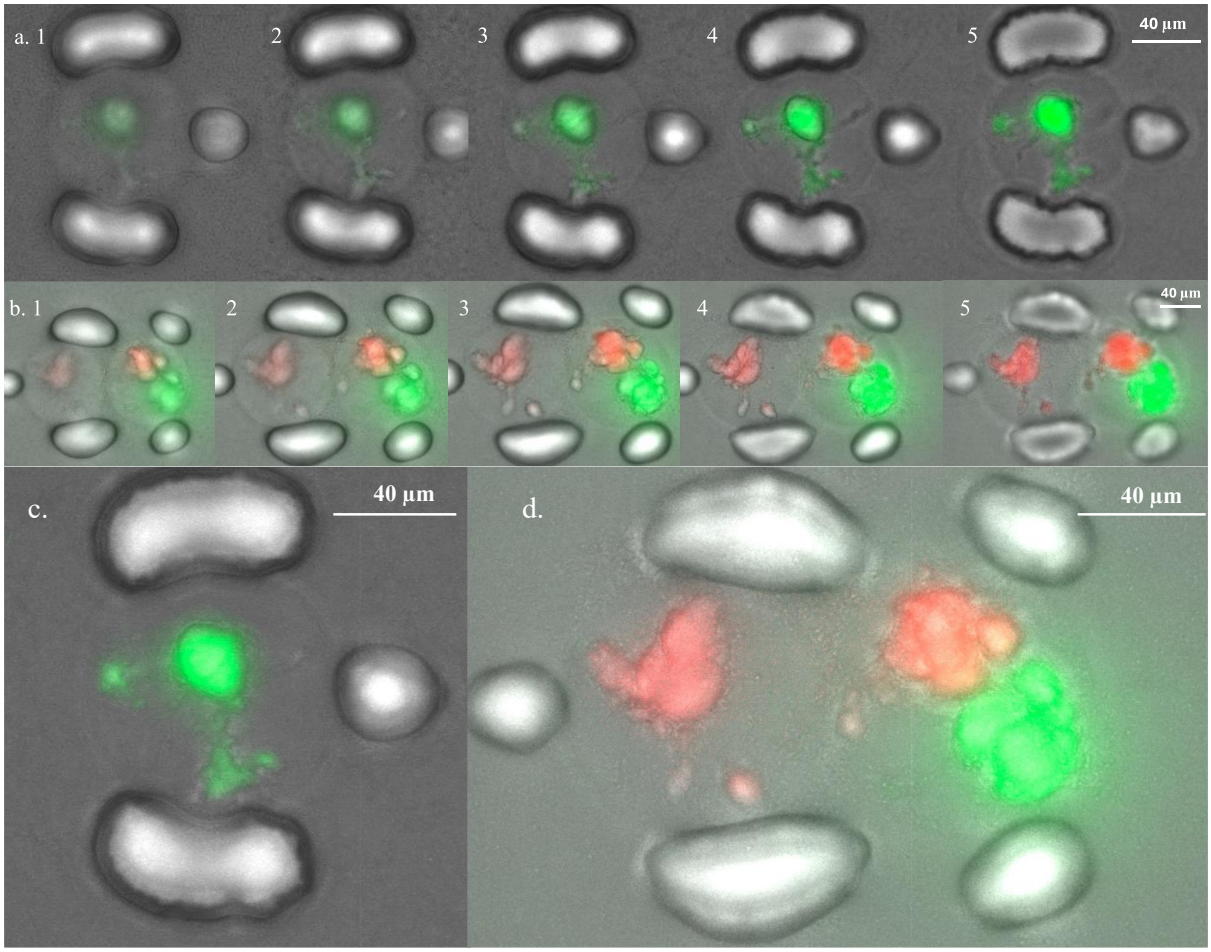

Figure 4. 4 Bacterial communities in agarose hydrogel beads imaged on different focal planes. (**a**)(**b**) Bacterial communities on different focal planes. Screenshots from 1 to 5 are corresponding to the focal planes from top to bottom. (**c**)(**d**) Projection images correspond to (**a**)(**b**), respectively. The single-bead example is position 59 (Day 1), and the paired-bead example is position 216 (Day 2). Screenshots were taken at time point 23. Scale bars were roughly measured from the most left traps.

In some trapping positions, small colonies inhabiting the edges of the beads were found. For example, in Figure 4.5, a sensor colony was found at the lower left edge of the right bead (position 99, Day 1). Of note, the distance range between the top and bottom focal planes was set to approximately 40 μm, but the average diameter of the beads was around 80 μm. This result suggests that there might be small colonies below the bottom focal plane that would not be noticed. Moreover, this sensor colony remained small till at time point 30 (30 min per time point), which may be due to the escape of the cells from the beads.

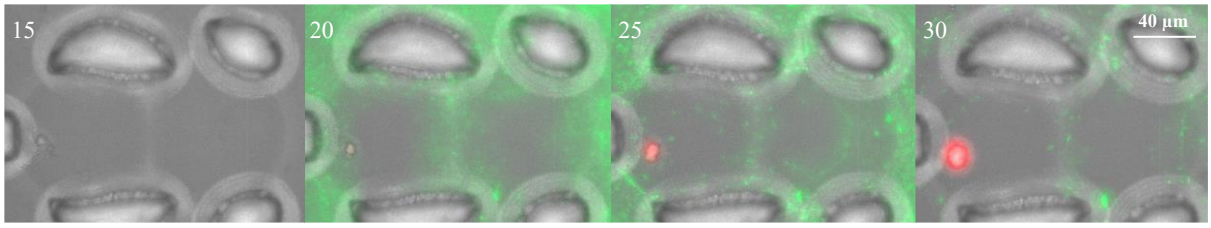

Figure 4. 5 Representative example of small bacterial colonies at the edge of the bead. Time-lapse images were taken every 30 min. Screenshots were taken at different time points, as indicated by white numbers in each screenshot. Before taking the screenshots, the focal planes and light channels of the images were merged (position 99, Day 1). Scale bar was roughly measured from the most left trap.

4.3.2 Cell escape behaviour and colony aggregation behaviour

Figure 4.6 below shows two representative examples (positions 18 and 110, Day 2) demonstrating cell escape behaviour. In Figure 4.6a, an obvious escape was observed from time points 23 to 24, which also resulted in a decrease in fluorescence intensity around the centre area. Subsequently, the shape of the community appeared relatively fixed. Figure 4.6b shows the escape behaviour from time points 12 to 13. This figure also clearly shows bacterial flagella protruding from the gel bead. The colonies within the bead merged and expanded to a larger size than the bead. One reason for this oversized expansion may be the sufficient expression of extracellular polymeric substances in the biofilm.

Moreover, it was found that bacterial colonies may also escape from the beads. For example, as shown in Figure 4.7 (position 28, Day 2), producer colonies were initially found in the left bead but completely disappeared at time point 22. This behaviour was also observed at some other positions, such as positions 172 (Day 1) and 187 (Day 1). In these two examples, the colonies seemed to disappear before their fluorescence could be detected (data not shown).

The exact reason for the escape behaviour is unknown. It is known that *E. coli* can swim using flagella and has chemotaxis, which allows it to move toward favourable environments based on chemical concentration gradients (Berg, 2000). What remains unclear is whether the tested microfluidic perfusion environment and encapsulated state would lead to the profuse

expression of *E. coli* flagella and result in *E. coli* escape. While this may provide some explanation for cell escape behaviour, only future studies will provide further insight in this regard.

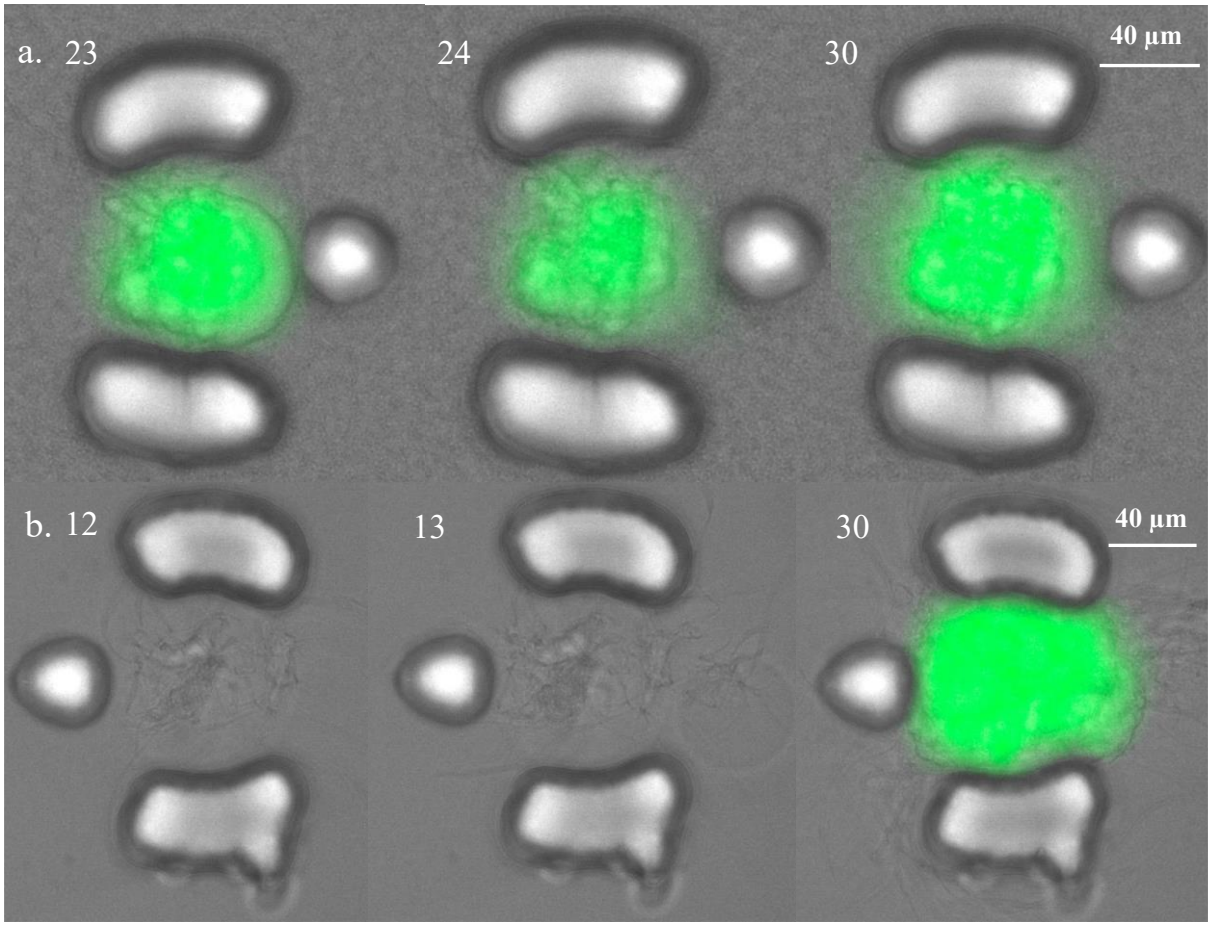

Figure 4. 6 Representative examples of cell escape behaviour and flagellar production phenotype. Screenshots were taken on a selected focal plane of (**a**) position 18 and (**b**) position 110 (Day 2), respectively. Time-lapse images were taken every 20 min. White numbers in each screenshot indicate time points. Scale bars were roughly measured from the most left traps.

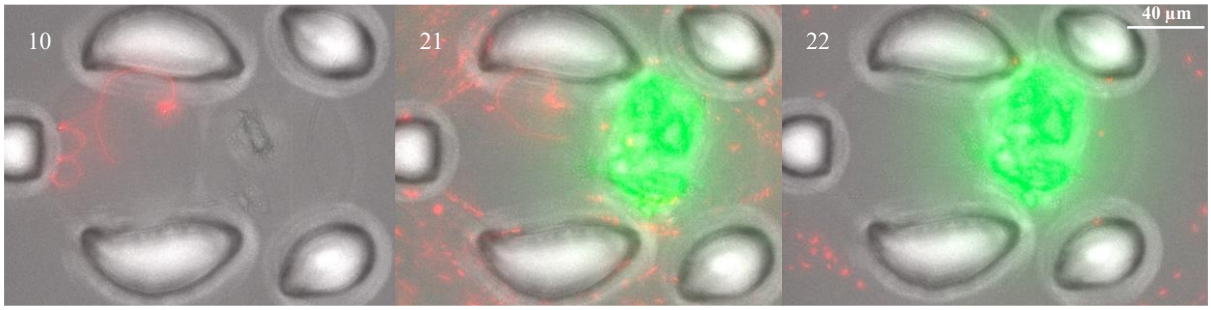

Figure 4. 7 Representative example of colony escape behaviour. Time-lapse images were taken every 30 min. Time points are indicated by white numbers in each screenshot. Before taking the screenshots, the focal planes and light channels of the images were merged (position 28, Day 2). Scale bar was roughly measured from the most left trap.

In addition to escaping from the beads, colonies were found to be able to migrate within the beads. Figure 4.8 shows a representative example where a sensor colony and a producer colony aggregated together in the left bead (position 171, Day 1). This behaviour was also found at some other positions, including positions 127 and 129 (Day 3). In these two positions, sensor colonies were found to be aggregated (data not shown). It is known that bacteria of the same strain may autoaggregate and of different strains may coaggregate (Trunk et al., 2018; Nwoko and Okeke, 2021). The aggregation behaviour may affect the accuracy of the QS response analysis using Fiji-ImageJ when the halo of one strain overlaps the colony of another strain. To minimise this effect, unmerged areas or detached colonies were preferred when selecting colonies for measurement (discussed in Chapter 5).

Moreover, it was found that the left part of the sensor colony in the left bead did not show fluorescence (Figure 4.8). Colonies or subpopulations that do not show a fluorescent phenotype are referred to as 'uninduced'. This uninduced phenotype was also found in some other positions, e.g., positions 28 and 117 (Day 1) (data not shown). The appearance of the uninduced phenotype may be due to several factors, such as mutation and plasmid loss (Bahl et al., 2004). As discussed in Section 2.3.3, mutations may have occurred in cells of experimental glycerol stocks of three strains. Loss of the ability to express the fluorescent protein due to mutation(s) could also be a cause of the uninduced phenotype. Additionally, the selectable marker used in this work is ampicillin, which may allow the sensitive cells to survive under the protection of resistant cells (Yurtsev et al., 2013). Therefore, if plasmid loss occurs, cells without plasmids may still survive.

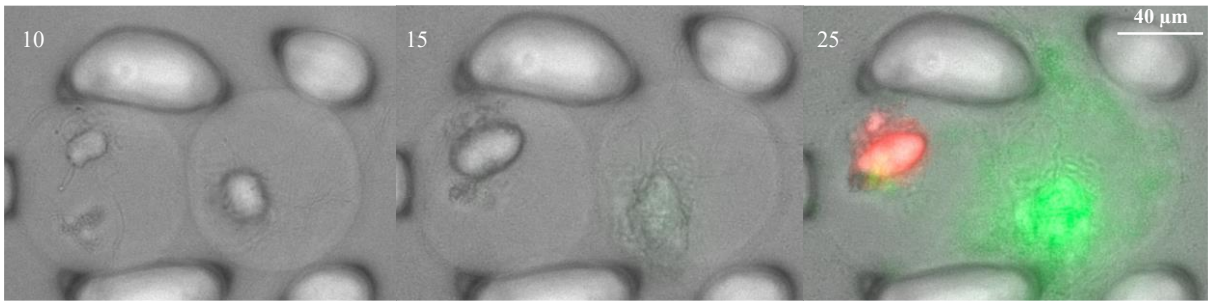

Figure 4. 8 Representative example of colony aggregation behaviour and uninduced phenotype. Screenshots were taken on one selected focal plane of position 171 (Day 1). Time-lapse images were taken every 30 min. Time points are indicated by white numbers in each screenshot. Scale bar was roughly measured from the most left trap.

4.3.3 Development of bacterial communities in microbeads

Figure 4.9 shows the development of bacterial communities in position 114 (Day 1). In this position, the channel was perfused with LB (Amp) supplemented with 0.025 mM IPTG. Figure 4.9a shows an overview of bacterial communities. Before taking screenshots, light channels and focal planes were merged. Several cells were initially encapsulated within each bead. The colonies of the sensor and producer strains clumped together while propagating, causing the fusion of the green and red fluorescence into bright yellow fluorescence.

The appearance of red fluorescence seems to be later than the appearance of green fluorescence in the merged light channel (Figure 4.9a). However, when observed in separate light channels (brightness was adjusted compared to the merged light channel), the fluorescence changes of the colonies become clearer. In Figure 4.9b, red fluorescence dots were observed at the first time point 1, which may have formed before imaging due to the intrinsic leakage of the producer's plasmid. The red fluorescence decreased over a period (usually less than 10 time points) before increasing. This initial decrease in fluorescence may be due to colony growth reducing the fluorescence intensity, as discussed in Section 2.3.2. In Figure 4.9c, no obvious green fluorescence was observed at early time points. The fluorescence appeared at around time point 5, and the brightness increased and became relatively stable at late time points. A possible reason why no obvious green fluorescence was observed at early time points may be the low expression of EGFP. As discussed in 2.3.2, higher background noise was observed at lower wavelengths in microplate experiments. This background noise may also affect the fluorescence observation in the microfluidic experiment.

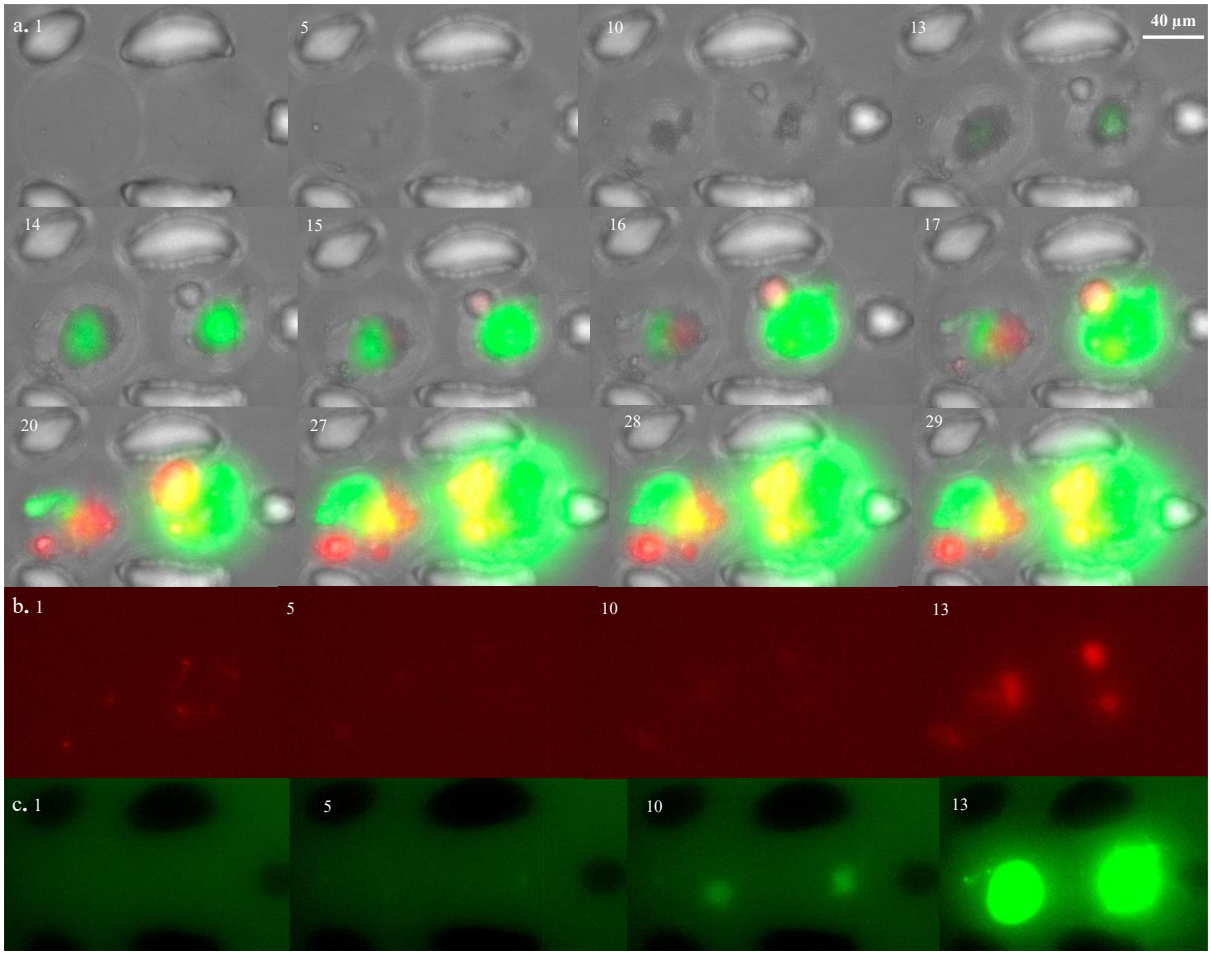

Figure 4. 9 Representative example of development of bacterial communities in paired beads. Before taking screenshots, the focal planes were merged (position 114, Day 1). Screenshots were taken (**a**) in merged light channel (transmitted light, red fluorescence, and green fluorescence channels), (**b**) in the red fluorescence channel, and (**c**) in the green fluorescence channel. Images were taken every 30 min. Time points are indicated by white numbers in each screenshot. Scale bar was roughly measured from the top left trap.

4.3.4 Scenario distributions of paired-bead experiments

The above sections discussed typical phenotypes found when observing bacterial communities in agarose hydrogel microbeads. In this section, in order to assess the ability of the producer to activate the sensor in microbeads, paired-bead trapping positions were classified according to the configuration (scenario) of strains within the beads.

In paired-bead experiments, two cell mixtures were encapsulated in agarose hydrogel beads. They were the mixture of the sensor (S) and producer (P) cultures in a 1:1 ratio (S + P) and the mixture of S and host Tuner (DE3) (T) cultures in a 1:1 ratio (S + T). Possible scenarios in all chip channels are shown in Table 4.1. The strains were indicated by their initials, S, P, and T, while the letter X indicates empty beads. The symbol '+' indicates the co-encapsulation of the strains. The symbol '/' indicates either strain, as a chip channel contained either the producer or the Tuner (DE3) strain. In a paired-bead trapping position, if one bead contained the sensor while the other bead contained either the producer or the Tuner (DE3), this position was classified as scenario 5 (Table 4.1 and Figure 4.10a). If one bead was empty and the other bead co-encapsulated the sensor and either the producer or the Tuner (DE3), this position was classified as scenario 10 (Table 4.1 and Figure 4.10b). Colonies that had disappeared were not taken into account when determining the configuration, e.g., position 28 (Day 2) (Figure 4.7) was classified as scenario 6. If a position contained an 'uninduced' colony, it was classified as scenario 11. Some positions were classified as unclear (scenario 12) if the bead contained a tiny colony or if a colony might be the uninduced phenotype. Additionally, positions with technical issues, such as beads being partially out of the imaging area or only one bead being trapped, were also classified as scenario 12. Of note, positions where only the edge of the bead was outside the imaging area were not classified as scenario 12.

Table 4. 1 Possible scenarios of positions in paired-bead experiments. Letters S, P, and T indicate the sensor producer and Tuner (DE3) strains, respectively. Letter X indicates an empty bead. Symbol '+' indicates co-encapsulation of the strains, and '/' indicates either strain.

Scenario	Bead 1	Bead 2
1	S	S
2	(P/T)	(P/T)
3	S + (P/T)	S + (P/T)
4	X	X
5	S	T/P
6	S	X
7	S	S + (P/T)
8	(P/T)	S + (P/T)
9	(P/T)	X
10	S + (P/T)	X
11	Uninduced	-
12	Unclear	-

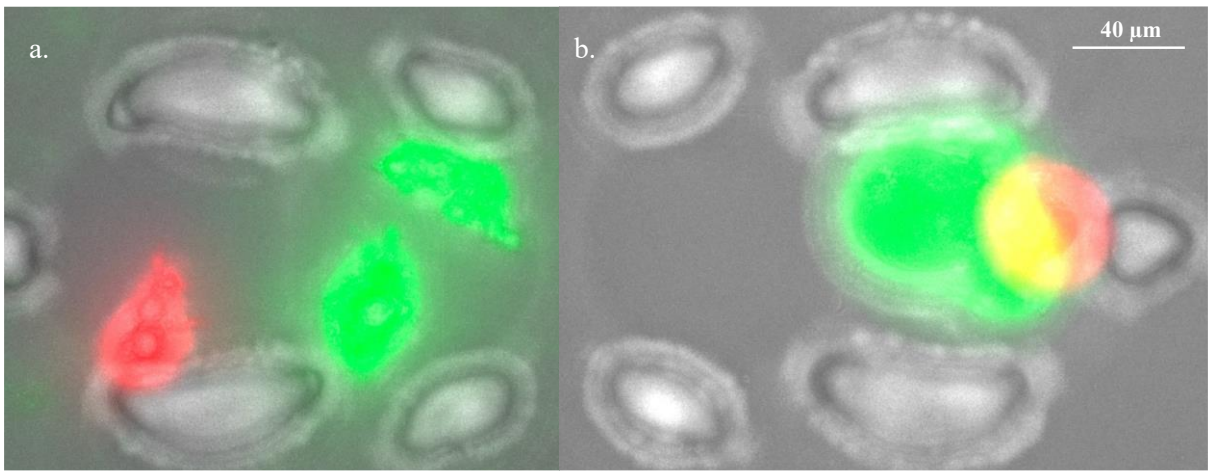

Figure 4. 10 Representative examples of paired-bead positions in scenarios 5 and 10. Before taking screenshots, the focal planes were merged. Screenshots were taken at time point 20 in (**a**) position 67 (scenario 5) and in (**b**) position 16 (scenario 10) on Day 1. Scale bar was roughly measured from the trap of the most left trap.

The scenario distribution of three paired-bead experiments was counted. In paired-bead experiments, channel 1 was the control channel, where the trapped beads encapsulated the mixture of the sensor and Tuner (DE3) cultures. Meanwhile, in channels 2, 3, and 4, trapped beads encapsulated the mixture of the sensor and producer cultures. The host strain Tuner (DE3) does not express a fluorescent protein, and its colonies appear similar to the uninduced phenotype. Besides, when the Tuner (DE3) colonies were completely covered by the sensor colonies, it was difficult to distinguish them from the sensor colonies. These factors may lead to inaccurate counting. Therefore, the distribution of channel 1 was not counted.

The scenario distributions of the channels 2 - 4 are shown in Figure 4.11. Most of the unclear positions were caused by technical issues, especially due to the beads being out of the imaging area. In general, most beads successfully encapsulated cells, as the counts of scenario 4 (both beads were empty) on three days were relatively low. The trapping positions were more evenly distributed on Day 1 and Day 2 than on Day 3. On Day 3, the counts of scenarios 1 and 7 were obviously higher than other scenarios. This result suggests that the sensor and producer cells were not mixed evenly, and there were more sensor cells than the producer cells. Additionally, small colonies may inhibit below the bottom focal plane and be overlooked, and 'uninduced' colonies may be covered by bright colonies, thus affecting the accuracy of the distributions.

In order to assess the ability of the producer to activate the sensor in agarose hydrogel microbeads, the colony area size and fluorescence intensity were required to be digitised. Scenarios 1, 2, 4, 6, and 9, in which the beads failed to encapsulate S and (P or T), were not preferred. In the remaining scenarios, 5 and 10 were preferred because their configurations are relatively simple, which may facilitate digitisation. Additionally, the distances between colonies measured in scenario 5 were expected to be greater than those in scenario 10 in most cases, which may help to evaluate the effect of OHHL diffusion on the sensor's response under the tested microfluidic condition.

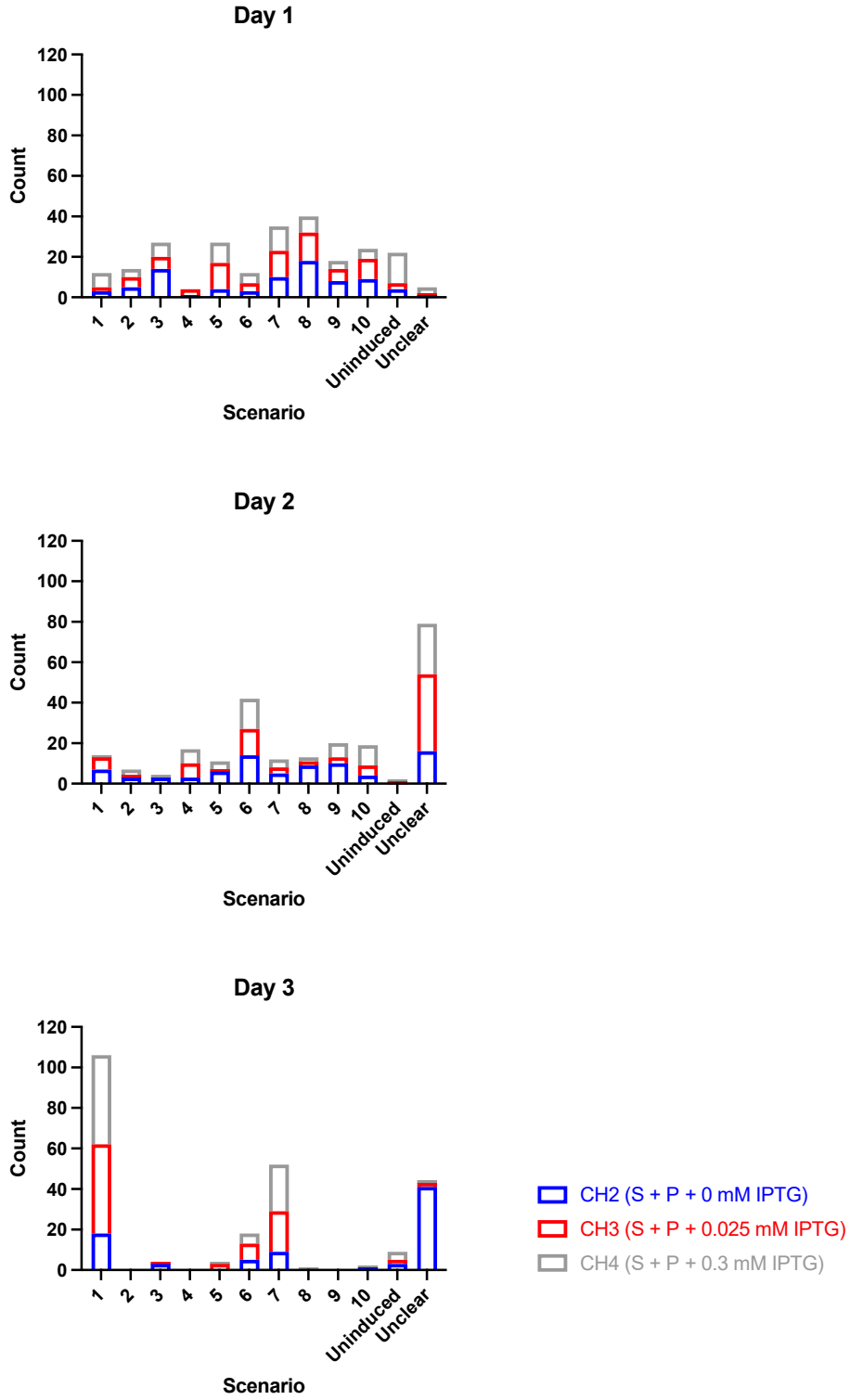

Figure 4. 11 Scenario distributions of three pair-bead experiments. Trapping positions in chip channels 2 - 4 (CH2 - 4) were classified. Microbeads in these channels encapsulated the mixture of the sensor (S) and producer (P) cultures. The strain configuration of each scenario corresponds to Table 4.1.

4.4 Conclusions

In this chapter, the sensor and producer were encapsulated in agarose hydrogel microbeads and cultivated on microfluidic chips while being imaged over time. The development of bacterial communities in microbeads was visualised.

The appearance of bacterial communities may be conspicuously different on different focal planes. It was found that cells could escape from agarose hydrogel microbeads, which may lead to relatively fixed colony shapes. Some colonies were not obviously affected by this escape behaviour and continued to develop to sizes larger than the beads. Small colonies may inhabit the edge of the beads or disappear after a period. Bacterial colonies may migrate within beads, which may result in colony aggregation. When a colony completely covers another colony, aggregation may affect the scenario classification of the trapping positions. Red fluorescence was observed at the first time point, which dimed over a period and then increased. No obvious green fluorescence was observed at early time points. Additionally, no fluorescence was observed in some colonies and subpopulations. These factors may interfere with the accuracy of image digitisation to varying degrees.

Most microbeads successfully encapsulated bacterial cells. In a paired-bead experiment, two strains can lead to 10 possible strain configurations, except for the uninduced phenotype. Uneven mixing of cells of two strains could lead to an uneven scenario distribution. Despite the complexity of the possible configurations, scenarios 5 and 10 were considered representative co-culture configurations and were preferred for QS response analysis.

Chapter 5 Assessment of the performance of the bacterial consortium in agarose hydrogel microbeads

This chapter focuses on assessing the performance of the sensor and producer strains in agarose hydrogel microbeads. The sensor encapsulated in microbeads was induced by a range of concentrations of OHHL. The sensor was then co-cultured with the producer in microbeads and induced by a range of IPTG concentrations. The performance of the strains was assessed based on their colony response levels (fluorescence intensity normalised by area) under different conditions.

5.1 Digitisation of the microscopic images

To assess the performance of the strains in microbeads, compiled microscopic images collected in the microfluidic experiments discussed in Chapter 4 were digitised using Fiji-ImageJ (Schindelin et al., 2012). As discussed in Chapter 4, cell escape behaviour may affect the size and fluorescence intensity of colonies to varying degrees. Colony expansion in the Z-axis and colony aggregation could also prevent accurate tracking of colony development over time. Consequently, the digitised analysis in this chapter focused on the colony response level of the selected area.

5.1.1 Determination of measurement area

Microscopic images of single-bead and paired-bead experiments were measured. Single-bead experiments were designed to characterise the sensor's response to OHHL induction in agarose hydrogel microbeads. OHHL concentrations of 0, 10^{-10}, 10^{-8}, and 10^{-6} M were tested on Day 1, and 0, 10^{-9}, 10^{-7}, and 10^{-5} M were tested on Day 2. Five positions of each treatment were selected for digitisation.

Paired-bead experiments were designed to assess the ability of the producer to activate the sensor's response. The mixture of these two strains was encapsulated in microbeads. The beads were then trapped on paired-bead chips and were induced at IPTG concentrations of 0, 0.025, and 0.3 mM. Three biological replicates were performed on Day 1, Day 2, and Day 3, respectively. The mixture of the host strain Tuner (DE3) and the sensor strain was also encapsulated in microbeads and cultivated in parallel as a control.

As discussed in Section 4.3.4, scenarios 5 and 10 were preferred and, therefore, selected for digitisation for QS response analysis. Trapping positions containing one or more beads (with bacterial cells) stuck outside the trap were excluded from the measurement list. Colonies that were easy to track at most time points and did not exhibit extensive escape were preferred. Small colonies (discussed in Section 4.3.1) were considered mal-developed and unmeasurable colonies. In the measurement method used, for each colony, the adopted criterion for selecting the focal plane for the measurement was to select the plane that appeared to have higher bacterial density. The measured area was fixed after a period, usually at around time point 15, unless the colony location changed greatly. When digitising co-cultured strains, detached colonies or unmerged areas were preferred.

5.1.2 Image digitisation

'Color Balance' of Fiji-ImageJ was used to select a specific light channel to be examined and measured. This function was also used to adjust the visual brightness of the images to facilitate the identification of the colonies without affecting the digitised values. 'Polygon Selections' was used to select the area to be measured. At each time point, the size and fluorescence intensity (area and integrated density in the Fiji-ImageJ, respectively) of the selected area on the selected focal plane in the selected light channel were measured. Additionally, Fiji-ImageJ allows turning off the fluorescence by adjusting the minimum value and brightness in 'Color Balance', which could facilitate the selection of the area for measurement. The colony response level was assessed as fluorescence intensity normalised by the area size. Of note, the limit of normalised fluorescence intensity measured using Fiji-ImageJ is 4095 (arbitrary units). Once the limit was reached, readings of subsequent time points were considered as 4095.

5.1.3 Data analysis

Fiji-ImageJ (Schindelin et al., 2012) was used for image digitisation. GraphPad Prism was used for data analysis and data presentation. When comparing different treatments and different days, the Mann-Whitney and the Kruskal-Wallis tests were used for unpaired comparisons of two or more groups, respectively. When comparing different scenarios, the Wilcoxon test was used for paired comparisons of two groups.

5.2 Results and discussion

5.2.1 Selection of bacterial colonies for measurement

As discussed in Section 4.3.1, the colony appearance and fluorescence intensity of bacterial communities may be different on different focal planes, which may affect the measurement of the colony response level. For each colony, the focal plane that appeared to have higher bacterial density (appeared as a black area) was selected for measurement. Besides, as the time points at which colonies could be measured may be different, colonies were not digitised from the same time points. Of note, in paired-bead experiments, the sensor and producer in a trapping position may primarily occupy different focal planes. For example, in position 71 (Day 1), the sensor and producer strains were encapsulated in two beads, respectively (Figure 5.1). The sensor located in the middle of the right bead was preferred over the sensor in the upper left corner, as the sensor in the middle showed a clearer shape and may be less likely to be affected by the cell escape behaviour. As shown in Figures 5.1b and c, the target sensor colony showed a clearer black area on focal plane 1 than on focal plane 2. Focal plane 1 was selected to measure its colony response level. The producer strain was measured on plane 2 (Figure 5.1c).

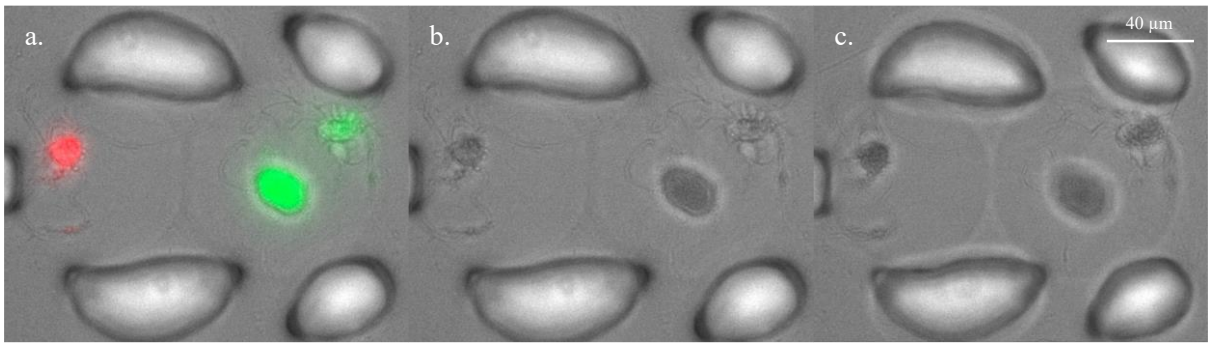

Figure 5. 1 Representative example of the selection of focal planes for measurement. Screenshots were taken in position 71 (Day 1) at time point 13. Bacterial communities on focal plane 1 with (**a**) fluorescence on and (**b**) fluorescence off. (**c**) Bacterial communities on focal plane 2 with fluorescence off. Scale bar was roughly measured from the trap of the first screenshot.

The measurement method used was not designed to track the induction response of the entire bacterial community but to assess the performance of the sensor and producer encapsulated in agarose hydrogel microbeads. Therefore, if colonies were clumped, the clear, distinct part was preferred for measurement. For example, as shown in Figure 5.2, the relatively clearer black area was selected for measurement (area marked in Figure 5.2b). In addition, colony expansion in the Z-axis and aggregation may prevent accurate tracking of colony development over time. The distinct area may become blurred or no longer distinguishable from the other areas. After a period, the measured area no longer changed unless the colony location changed greatly due to colony migration or bead movement. Besides, the size of the measured area may be reduced

if the black area became distinctly smaller due to extensive escape. In this measurement round, the time point when the size of the measured area last changed, and the corresponding size were provided in Appendix C. The average values of these time points and sizes in single-bead and paired-bead experiments are shown in Table 5.1 and Table 5.2, respectively.

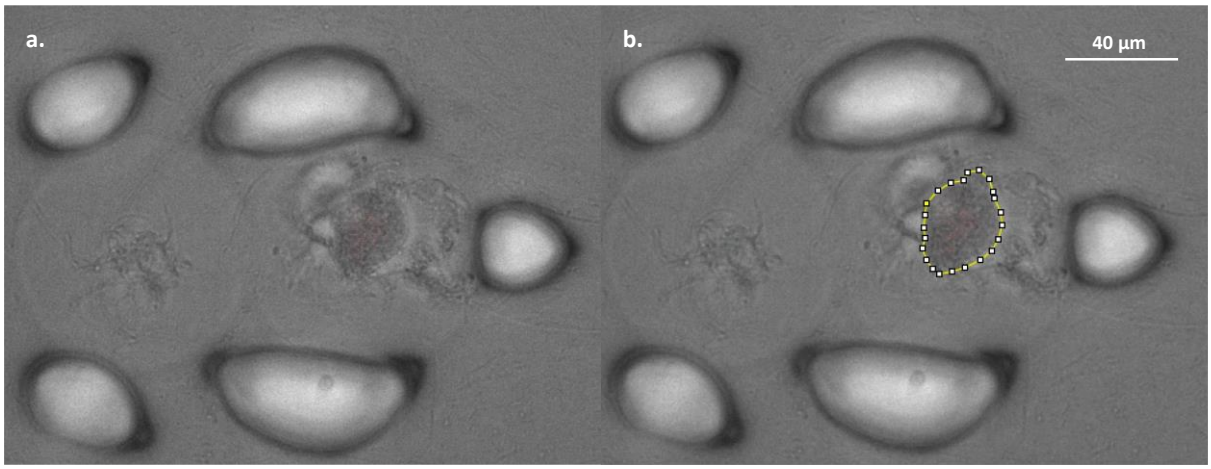

Figure 5. 2 Representative example of the selection of a distinct area for measurement. Screenshots were taken on plane 2 and time point 13 of position 192 (Day 1). (**a**) Appearance of the trapping position. (**b**) Area selected for measurement. Scale bar was roughly measured from the trap of the first screenshot.

In general, in single-bead experiments, the sizes of the measure areas were not changed at around time point 15 or 16. The average time point on Day 1 was later than that on Day 2 (Table 5.1). Meanwhile, the average size on Day 1 was smaller than that on Day 2. These differences may be due to the later development of bacterial communities on Day 1 than on Day 2. Figure 5.3 shows overviews of some bacterial communities at time point 10 on Day 1 and Day 2. The bacterial communities on Day 1 were distinctly smaller than those on Day 2, which may be primarily due to the difference in waiting time before taking the images. This difference would also interfere with the accuracy of the QS response analysis based on the digitised data.

Table 5. 1 Average time points when the sizes of the measured areas were last adjusted and the corresponding average sizes in single-bead experiments (data were rounded to two decimal places)

Experiment	Average time point	Average area size (a.u.)
Day 1	17.05	5401.35
Day 2	14.10	9296.45
Average	15.58	7348.90

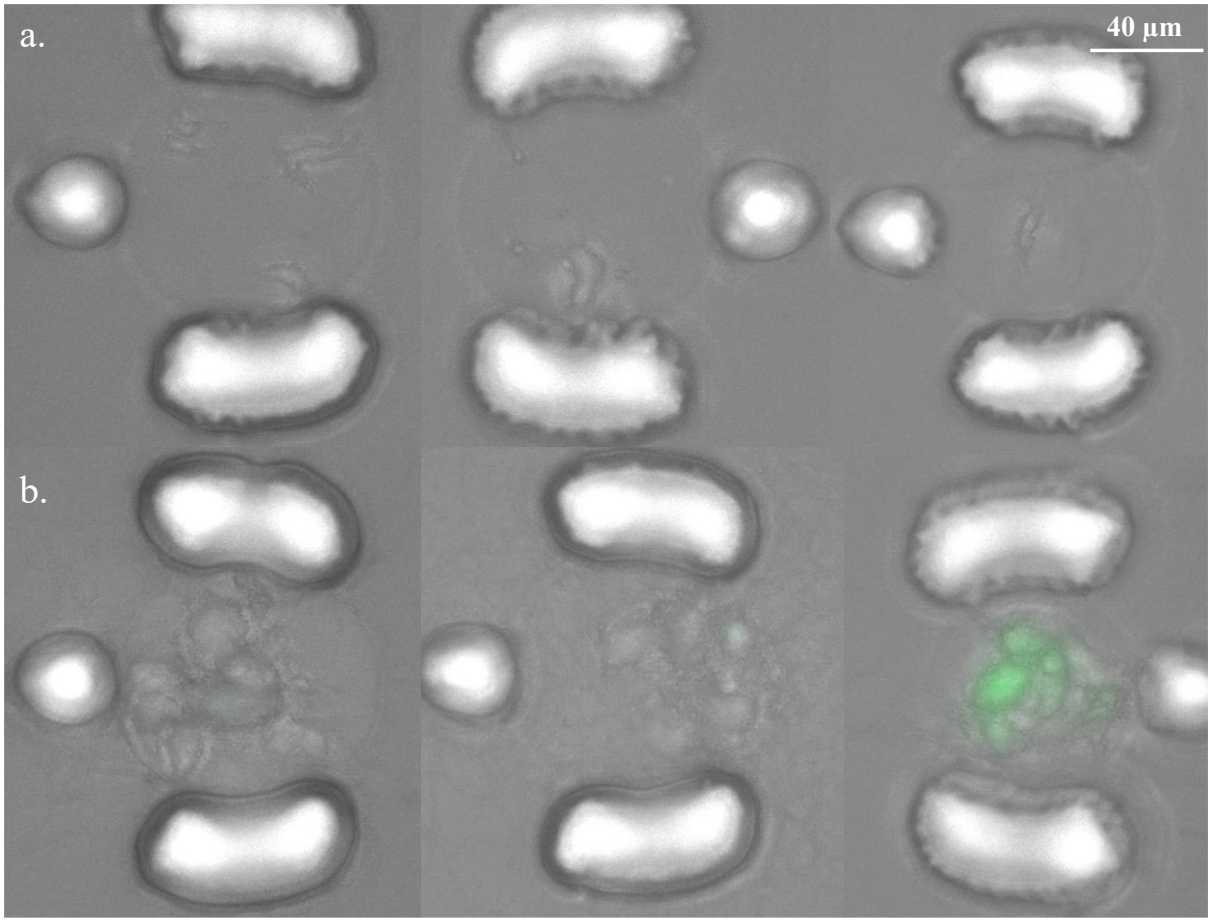

Figure 5. 3 Representative examples of bacterial communities in single-bead experiments on Day 1 and Day 2. Screenshots were taken on the merged focal plane in the merged light channel at time point 10. (**a**) From left to right, beads are in positions 31, 55, and 103 (in channels 1 - 3, respectively) on Day 1. (**b**) From left to right, beads are in positions 7, 30, and 66 (in channels 1 - 3, respectively) on Day 2. Scale bar was roughly measured from the top left trap.

In paired-bead experiments, the sizes of the measured areas were fixed at around time point 18. The time points when the sizes were fixed in scenario 10 appeared to be later than those in scenario 5 (Table 5.2). This may be due to the different strain configurations in these two scenarios. In scenario 5, two strains were encapsulated in two beads, respectively. In scenario 10, two strains were encapsulated in one bead, and the other bead was empty. Therefore, in scenario 10, two target colonies may aggregate and result in a bright yellow area, as shown in Figure 5.4 (position 170, Day 1). In order to avoid the fluorescence reading of one strain being affected by the fluorescence of the other strain, unmerged area (Figure 5.4b) and detached colony (Figure 5.4c) were preferred for digitisation. However, avoiding measuring merged areas may require adjusting selected areas at late time points, resulting in later average time points in scenario 10 than those in scenario 5. For example, in position 74 (Day 1), the measured size of the producer colony was fixed from time points 18 to 25 and adjusted at time point 26 to avoid the green fluorescence of the sensor (data not shown). Additionally, avoiding measuring merged areas may lead to limited measurable areas, resulting in smaller average sizes in scenario 10 than in scenario 5 (Table 5.2). Besides, the high fluorescence intensity of a position may interfere with area selection (Figure 5.4). For better measurement, 'Color Balance' was used in some cases to turn off fluorescence in the merged light channel (Figure 5.1).

Table 5. 2 Average time points when the sizes of the measured areas were last adjusted and the corresponding sizes in paired-bead experiments (data were rounded to two decimal places)

Experiment	Scenario	Average time point	Average area size (a.u.)
Day 1	5	17.26	12105.61
	10	18.73	5823.58
Day 2	5	18.92	8492.23
	10	21.14	4462.18
Day 3	5	15.88	7195.88
	10	16.00	3539.50
Average	-	17.99	6936.50

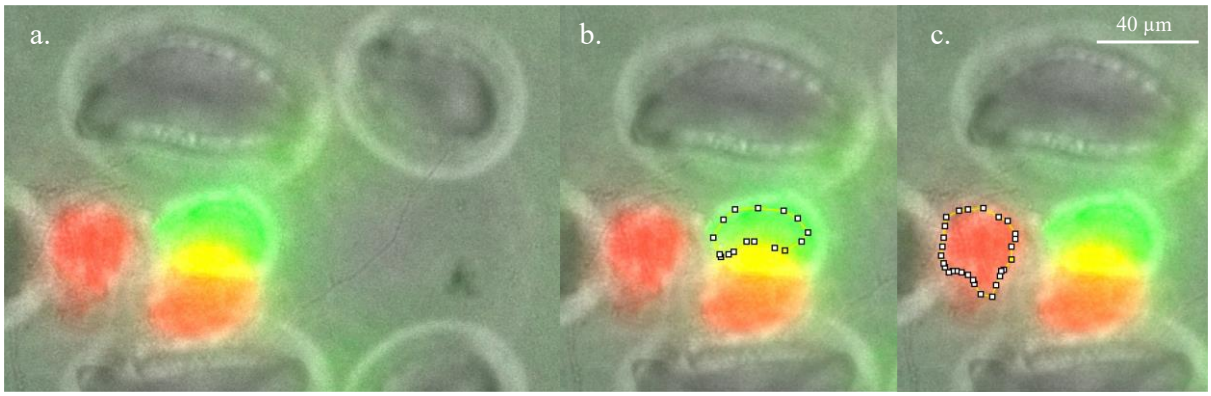

Figure 5. 4 Representative example of the selection of merged colonies for measurement. Screenshots were taken on focal plane 5 in Position 170 (Day 1) at time point 29. (**a**) Appearance of the trapping position. (**b**)(**c**) Area of the sensor and producer selected for measurement. Scale bar was roughly measured from the most left trap.

Some positions were classified as scenarios 5 or 10 but were not digitised. This is because some colonies did not show distinct expansion during cultivation and were considered mal-developed and unmeasurable colonies, such as position 99 (Day 1) (Figure 4.5). Besides, although formed microbeads were filtered before the trapping step, some beads larger than the trap were observed. These beads may be stuck outside the trap, such as positions 52 (Day 1) and 1 (Day 2) (Figure 5.5). This is unlikely to cause a major problem, as appropriate trapping of two beads was observed in most positions. However, to better understand how the strain configuration may affect the sensor's response, in the digitisation stage, these positions were excluded from the measurement list if extra beads contained bacterial colonies.

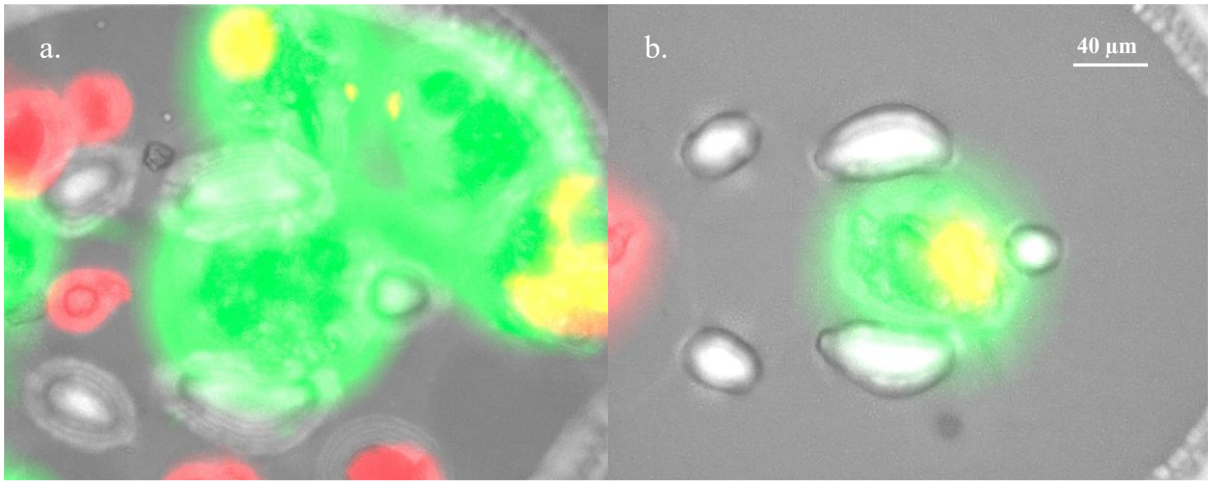

Figure 5. 5 Representative examples of trapping positions containing extra beads. Screenshots were taken on the merged focal plane in the merged light channel at time point 29. (**a**) Position 52 on Day 1. (**b**) Position 1 on Day 2. Scale bar was roughly measured from the most left trap.

5.2.2 Characterisation of the sensor strain

In this section, the sensor's colony response level upon OHHL induction in agarose hydrogel beads was assessed. In Section 3.3.1, it was found that the sensor in the absence of arabinose (ara^-) induction showed a wider OHHL concentration detection range (Figure 3.3). For this reason, microfluidic experiments were conducted under an ara^- condition. The sensor induced at 0, 10^{-10}, 10^{-8}, and 10^{-6} M OHHL were tested on Day 1, and at 0, 10^{-9}, 10^{-7}, and 10^{-5} M OHHL were tested on Day 2. The colony response levels of the sensor in five positions of each OHHL treatment were measured. The reference numbers of the positions measured are provided in Appendix C.

As shown in Figure 5.6, in general, similar to the sensor in microplate experiments (Figure 3.2a), the sensor showed a concentration-dependent response to OHHL induction. However, the sensor induced at an OHHL concentration of 10^{-7} M showed a higher colony response level than the sensor induced at a higher OHHL concentration of 10^{-6} M for the first 7 h after induction (Figure 5.6 comparing orange and cyan). In addition, the colony response level of the untreated sensor on Day 2 was higher than those of the sensor induced at 0 and 10^{-10} M OHHL concentrations on Day 1 (Figure 5.6 comparing blue, black, and red). These results indicate that the colony response levels of the sensor on Day 2 were greater than those of the sensor on Day 1, which may be due to the later development of the sensor colony on Day 1 than on Day 2 (Figure 5.3). This difference in the development speed of bacterial communities on different days may be primarily caused by different waiting times before taking the microscopic images. Nevertheless, the sensor showed an OHHL concentration-dependent response when comparing the data from Day 1 and Day 2 separately. It is not clear the highest OHHL concentration the sensor can detect under the tested microfluidic condition. The sensor may be able to detect an OHHL concentration down to 10^{-10} M when comparing the data from Day 1 (Figure 5.6 comparing red and black). More biological replicates are required to better characterise the performance of the sensor under the tested microfluidic condition. Future studies could also include testing the response levels of the sensor induced at higher concentrations.

It should be noted that Fiji-ImageJ software has a maximum measurement limit of 4095 for the integrated density normalised by the measured area. Depending on the measurement method used, once the reading of the colony response level reached this limit, the readings at subsequent time points were considered to be 4095, resulting in the plateaus of colony response levels of the sensor induced at 10^{-7}, 10^{-6}, and 10^{-5} M OHHL concentrations at later time points (Figure 5.6).

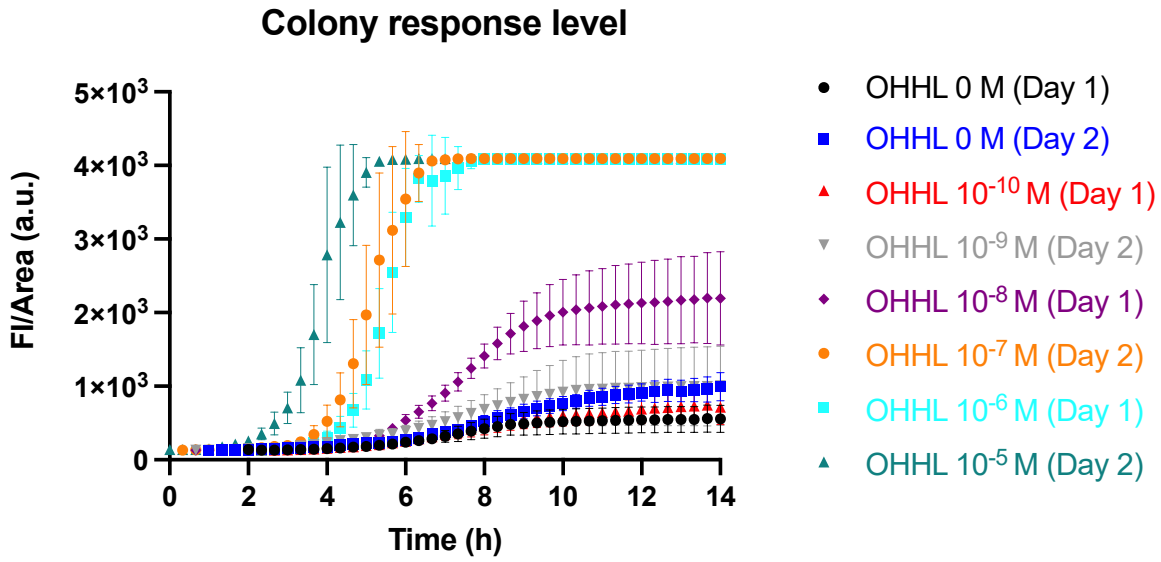

Figure 5. 6 Colony response levels of the sensor to OHHL induction in the absence of arabinose (ara^-) in agarose hydrogel beads. Data are shown as the mean values with their standard deviations (shown as error bars).

5.2.3 Activation ability of the producer strain

The focus of this section is to assess the ability of the producer to activate the sensor's response in agarose hydrogel microbeads. The sensor and producer were encapsulated in microbeads, and the microbeads were trapped in paired-bead chips for overnight cultivation and time-lapse imaging. As discussed in Section 3.3.2, the producer showed IPTG concentration-dependent expression but may approach saturation at 0.3 mM IPTG (Figure 3.4). IPTG concentrations of 0.025 and 0.3 mM, which activated the producer to distinct response levels in microplate experiments, were further tested in microfluidic experiments. Uninduced producer and host Tuner (DE3) strains were also cultivated in parallel as controls.

Microbeads from scenario 5 and scenario 10 were digitised for analysis. As discussed in Section 5.2.1, positions with extra beads containing bacterial colonies or positions where target colonies did not show distinct expansions or extensively merged with the colonies of the other strains were not preferred. The numbers of digitised positions in scenario 5 and scenario 10 of the three paired-bead experiments (Day 1, Day 2, and Day 3) are shown in Table 5.3. In channel 1, beads containing the sensor and Tuner (DE3) strains were perfused with an LB medium. Meanwhile, beads containing the sensor and producer strains were perfused with LB (Amp) supplemented with IPTG concentrations of 0 mM (channel 2), 0.025 mM (channel 3), and 0.3 mM (channel 4), respectively. The numbers of positions on Day 2 and Day 3 were lower compared to that on Day 1, which may be mainly due to the beads being partially outside the

imaging area. Additionally, an obviously uneven mixing of the sensor and producer strains on Day 3 may also have affected the numbers of measurable positions (Figure 4.11).

Table 5. 3 Numbers of positions digitised in co-culture analysis

Day	Channel	Treatment (IPTG induction)	Count	
			Scenario 5	Scenario 10
1	1	S + T (0 mM)	1	4
	2	S + P (0 mM)	4	7
	3	S + P (0.025 mM)	10	7
	4	S + P (0.3 mM)	8	2
2	1	S + T (0 mM)	4	2
	2	S + P (0 mM)	6	2
	3	S + P (0.025 mM)	1	3
	4	S + P (0.3 mM)	2	4
3	1	S + T (0 mM)	0	1
	2	S + P (0 mM)	0	1
	3	S + P (0.025 mM)	3	0
	4	S + P (0.3 mM)	1	1

To assess whether the digitised data from three days could be pooled for QS response analysis, the Mann-Whitney test and Kruskal-Wallis test were performed for two or three groups per channel, respectively. As shown in Table 5.4, in most cases, data obtained from different days did not show significant differences and were pooled according to scenarios and channels for subsequent QS response analysis.

The colony response levels of the Tuner (DE3) from three days showed significant differences in both scenarios, this treatment was the control with low readings of approximately 65. The differences may be caused by several factors, such as the different extents of cell escape and the difference in waiting time before taking the microscopic images on different days.

Table 5. 4 Comparison of colony response levels of the strains from three days. Mann-Whitney and the Kruskal-Wallis tests were performed for unpaired comparisons of two or three groups, respectively. NS = not significant, *p < 0.05, **p < 0.01, and ****p < 0.0001

Channel	Treatment (IPTG induction)	Sensor		Tuner (DE3) or Producer	
		Scenario 5	Scenario 10	Scenario 5	Scenario 10
1	S + T (0 mM)	NS	NS	****	****
2	S + P (0 mM)	NS	NS	NS	NS
3	S + P (0.025 mM)	NS	NS	NS	NS
4	S + P (0.3 mM)	*	NS	**	NS

The colony response levels of the three strains are shown in Figure 5.7. The producer showed a concentration-dependent response upon IPTG induction. The non-induced producer showed a greater response level than the non-induced host Tuner (DE3) strain, suggesting an intrinsic leakage of the producer's plasmid. These results were similar to those found in microplate experiments (Section 3.3.2). The colony response level of the producer induced at 0.025 mM IPTG concentration in microplate experiments did not show an obvious increase during cultivation. In microfluidic experiments, the colony response level of the producer induced at 0.025 mM gradually increased for hours (comparing Figures 3.4 and 5.7). This difference may be due to several factors, such as longer cultivation time and continuous supply of IPTG in microfluidic experiments. A continuous supply of IPTG could ensure the producer was induced at 0.025 mM IPTG concentration during cultivation, whereas in microplate experiments, IPTG may be depleted after a period.

In both microplate (Figure 3.5) and microfluidic (Figure 5.7) experiments, the producer showed a good ability to activate the sensor's response, even when uninduced. The sensor's colony response levels induced by the producer were shown to be significantly different in scenario 5 (*P < 0.05, Kruskal-Wallis test), but not in scenario 10. These results suggest that the sensor in scenario 5 may be more sensitive to the difference in the activation ability of the producer (where the producer induced by a higher IPTG concentration activated the sensor to a higher response level) than the sensor in scenario 10. Of note, because data from some treatments reached the measurement limit of the digitisation software at later time points, only data from the first 12 h after IPTG induction were used for comparison. Nonetheless, this method did not exclude all data that reached the limit.

It should be noted that this difference may be caused by the measurement method used. In scenario 10, two target colonies were encapsulated in one bead. The aggregation of target colonies may result in limited measurable areas, reducing the accuracy of the digitised data. This limitation also affects the assessment of whether OHHL diffusion affects the response level of the sensor under the tested microfluidic condition. Collecting more microscopic images of better quality for analysis might reduce the impact of this limitation of the measurement method used.

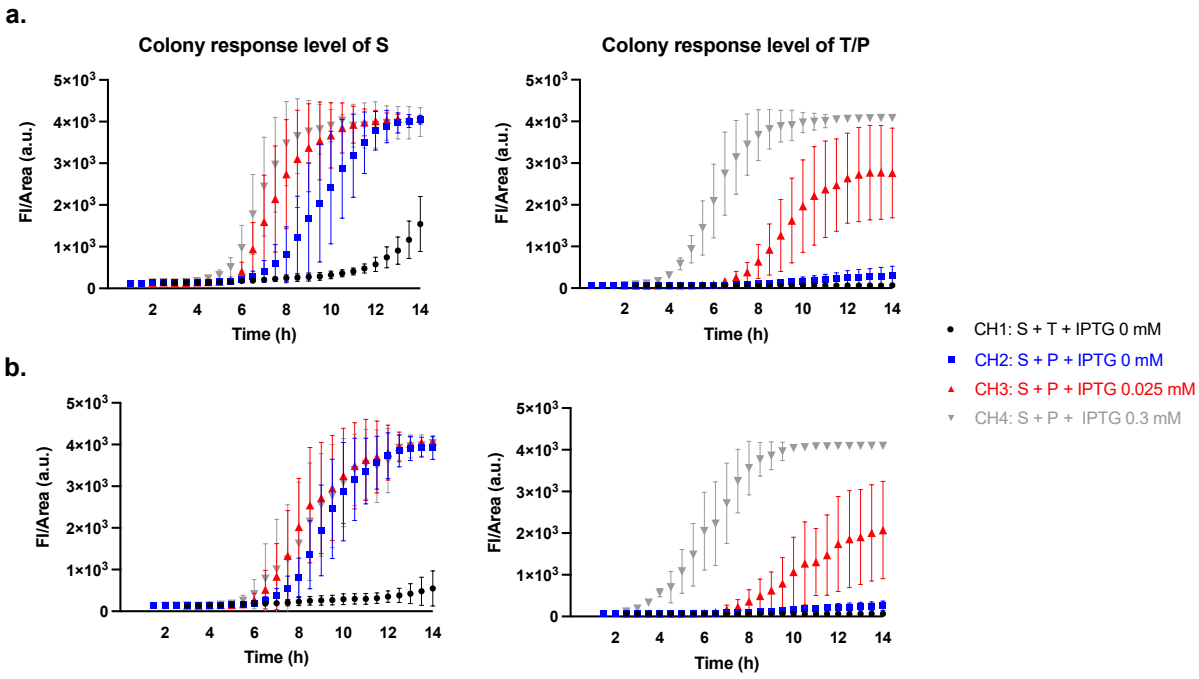

Figure 5. 7 Colony response levels of the sensor, Tuner (DE3), and producer strains upon induction. The colony response levels of the sensor strain (S) are shown in the 1st column. The colony response levels of the Tuner (DE3) (T) and producer (P) strains are shown in the 2nd column. (**a**) Scenario 5. (**b**) Scenario 10. Data are shown as the mean values with their standard deviations (shown as error bars) of three independent experiments.

The Wilcoxon test was performed for paired comparisons between the two scenarios (Table 5.5). The colony response levels of the Tuner (DE3) and producer were not expected to be significantly different between the two scenarios. However, the response levels of the Tuner (DE3) in channel 1 and of the producer in channel 3 showed significant differences (Table 5.5, 4th column). Moreover, the response levels of the sensor co-cultured with Tuner (DE3) in two scenarios, which were expected to be similar, showed to be significantly different (Table 5.5, 3rd column). One reason for these unexpected results may be due to the limitation of the measurement method used, as discussed above. The response level of the sensor induced by the non-induced producer was shown to be similar, while those of the sensor induced by the induced produced were shown to be significantly different (Table 5.5, 3rd column).

Table 5. 5 Comparison of colony response levels of the strains in scenario 5 and scenario 10. The Wilcoxon test was performed for paired comparisons between the two scenarios. NS = not significant, *p < 0.05, ***p < 0.001 and ****p < 0.0001

Channel	Treatment (IPTG induction)	Sensor	Tuner (DE3) or Producer
1	S + T (0 mM)	*	***
2	S + P (0 mM)	NS	NS
3	S + P (0.025 mM)	***	***
4	S + P (0.3 mM)	****	NS

In paired-bead experiments, the response levels of the sensor appeared to be around the measurement limit (4095) after it was activated by the producer for around 8 h. Although the experimental conditions were not identical, compared with response levels of the sensor in single-bead experiments, this result may suggest that under the tested microfluidic conditions, the activation ability of the producer reached levels greater than 10^{-8} M OHHL concentration in the tested period (comparing Figures 5.6 and 5.7). As discussed in Section 3.3.2, in planktonic experiments, the supernatants of the producer induced for 1 h showed greater ability to activate the sensor than OHHL concentration of 10^{-4} M. Therefore, the activation ability of the producer under the tested microfluidic condition may be lower than that of the producer in planktonic experiments. This result may be due to several reasons, such as the different initial states of the strains and different medium supply methods. Of note, the initial cell numbers of the producer in planktonic experiments (OD_{600} ~ 0.5) and in microfluidic experiments (newly inoculated cells) were greatly different.

5.3 Conclusions

In this chapter, compiled microscopic images collected from microfluidic experiments were digitised and assessed. In general, the sensor and producer strains showed inducer concentration-dependent expression under the tested microfluidic conditions. Moreover, the sensor strain may be able to detect an OHHL concentration down to 10^{-10} M. Under the tested microfluidic conditions, the activation ability of the producer reached levels greater than 10^{-8} M OHHL concentration in the tested period. The activation ability of the producer in microfluidic experiments may be lower than it was in planktonic experiments, which may be mainly due to the different initial states of the strains.

It should be noted that the accuracy of the digitised analysis was affected to varying degrees by several factors, such as the measurement limit of Fiji-ImageJ, the waiting time before taking the microscopic images, and the selection of the measured colonies and focal planes. More biological replicates are required to better assess the performance of the strains. Nonetheless, the obtained results could help to demonstrate the feasibility of studying cell-to-cell communication using a model bacterial consortium encapsulated in agarose hydrogel microbeads by analysing their fluorescent phenotypic changes. Future studies can build on the present work to develop algorithms for high-throughput analysis of microscopic images to fully exploit the potential of microfluidics for bacterial cultivation and visualisation.

Chapter 6 General discussion

An *E. coli* consortium consisting of three fluorescent strains (i.e., the sensor, producer, and regulator strains) was engineered based on the LuxI/LuxR system of *V. fischeri*. Fluorescent phenotypic changes were the basis for assessing the performance of the consortium both in the planktonic and encapsulated states.

The performance of the strains was first tested in the planktonic state. The cell response levels of the strains were assessed by normalising the fluorescence intensity with the optical density. The cell response levels of the sensor with basal or enhanced expression of LuxR were first tested upon OHHL induction. The sensor with basal LuxR expression showed an OHHL concentration-dependent response in the range of 10^{-7} to 10^{-4} M and may be able to detect OHHL concentrations greater than 10^{-4} M. Therefore, it was selected to test the performance of the producer and regulator strains. The producer also showed a concentration-dependent expression to IPTG induction and was able to activate the sensor's response by expressing LuxI that can catalyse the synthesis of OHHL. The regulator showed enhanced expression upon anhydrotetracycline (aTc) induction and was able to attenuate the sensor's response by producing AiiA that can degrade OHHL. As tracking the growth of each co-cultured strain based on optical density is currently not feasible, in planktonic experiments, supernatants of the producer and regulator were used to activate the sensor, respectively.
To assess the performance of co-cultured strains, the sensor and producer strains were encapsulated in agarose hydrogel microbeads and cultivated on a microfluidic platform. The colony response levels of the strains were assessed by normalising the fluorescence intensity with the sizes of the measured areas. The sensor and producer showed inducer concentration-dependent expression behaviours. The sensor may be able to detect OHHL concentration down to 10^{-10} M. The activation ability of the producer may be weaker under the tested microfluidic conditions compared with that of the producer in planktonic experiments, which may be mainly due to the different initial states of the strains.

In general, this work successfully engineered an *E. coli* consortium for studying QS and assessed the performance of the strains in the planktonic and encapsulated states. However, this work has several limitations.

Firstly, the fluorescence intensity detection at lower wavelengths was found to be more severely affected by the background fluorescence caused by the cells and LB (Amp) medium. Therefore, it was difficult to characterise the performance of the regulator strain over time and to test whether its expression could be regulated by aTc concentration. Besides, the ability of the regulator strain to attenuate the response level of the sensor also remains to be tested on the

microfluidic platform. Future studies could consider testing the expression behaviour of the regulator strain induced by different aTc concentrations using the Horiba FluoroMax-4 spectrofluorometer. Moreover, it should be interesting to adapt the current microfluidic protocol to co-culture the sensor and regulator strains to assess the attenuation ability of the regulator strain.

To be able to better track the activity of the regulator strain, it may be better to replace the fluorescent protein it uses. Given the plasmid was designed to be reconfigurable, it is possible to replace the insert by subcloning. Fluorescence protein mCherry used for the producer strain could be a choice if co-culturing the producer and regulator strains is not planned. If planning to image the three strains simultaneously, a yellow fluorescent protein whose excitation and emission wavelengths are intermediate between EGFP and mCherry could be considered. A possible option could be mBanana, whose excitation and emission maximum wavelengths were reported to be around 50 nm away from those of EGFP and mCherry, according to FPbase (https://www.fpbase.org/table/, accessed 30 January 2024) (Lambert, 2019). Additionally, *E. coli* expressing GFP, mBanana, and mCherry showed distinguishable clusters when sorting by flow cytometry (Shaner et al., 2004). Of note, mBanana shows lower brightness and slower maturation time compared with EGFP and mCherry (https://www.fpbase.org/table/, accessed 30 January 2024) (Lambert, 2019). Lower brightness may be advantageous considering the measurement limit of the used digitisation software. However, low brightness and slow maturation time may increase the waiting time before the fluorescent signal can be detected, which may prevent tracking the signal at early stages. Moreover, the colour of mBanana may be similar to the colour of the overlapping area of EGFP and mCherry. Bleed-through may also occur when detecting the three proteins. All of these factors may increase the difficulty of detecting fluorescent signals and performing microscopic analysis.

QS response analysis was mainly based on fluorescence intensity normalised by growth, namely cell response level or colony response level. However, the response level is an indirect indicator to estimate the environmental OHHL concentration or to assess the QS-related abilities of the strains. These assessments did not take into account several aspects, such as transcription and translation efficiency, maturation time of expressed proteins, and the emergence of different mutants. As it is much more complex to take these aspects into account to improve the accuracy of the analysis, all assessments remain at the estimation stage. One improvement could be to increase the number of replicates to improve the accuracy of the results. Especially in microscopic analysis, due to technical issues, such as microbeads being partially outside the imaging area, a number of positions were considered unmeasurable. When it comes to a specific configuration of strains (scenario), measurable positions were more limited. Increasing the number of replicates can increase the number of measurable positions,

which may improve the quality of the measurable positions and the quality of the digitised data. Additionally, future work could include upgrading the Positions Selection Tool used to determine the coordinates of the locations to be imaged, thereby increasing the number of positions that are correctly imaged.

Additionally, as discussed in Section 4.3.1, five focal planes (approximately 40 μm in height) within microbeads of approximately 80 μm in diameter were imaged. Single planes were selected for image digitisation. Limited imaging range was a compromise to meet appropriate imaging intervals. For a target colony, measurements were taken on one selected focal plane at all time points as a compromise to increase digitisation efficiency. Meanwhile, only scenarios 5 and 10 were measured for QS response analysis. To better understand how the strain configuration may affect the sensor's response, future work could include assessing other scenarios. Future studies could also consider using other software to analyse microscopic images, such as CellProfiler, which allows high-throughput analysis of microscopic images (Carpenter et al., 2006; Stirling et al., 2021).

As for the cell escape behaviour, increasing the agarose concentration to form stronger microbeads may be a way to delay the occurrence of this phenomenon. However, increasing the agarose concentration may affect not only microscopic analysis but also a number of factors, such as the size, weight, and softness of microbeads, which may affect the success of the trapping step. Nevertheless, a previous study found that changing the alginate concentration of alginate-based microcapsules could affect the QS responses of *V. harveyi* encapsulated in the microcapsules (Li et al., 2023). It may be interesting for future work to test the performance of the engineered strains in microbeads with higher agarose concentrations if efficient encapsulation and trapping can be ensured.

All constructed plasmids showed basal expression in the absence of inducers. For better analysis, in addition to LB medium and host strain controls, uninduced engineered strains could be cultivated in parallel as controls. Bacterial biosensors based on the LuxI/LuxR system of *V. fischeri* were reported to respond to other AHLs in addition to OHHL (Steindler and Venturi, 2007). Future studies could include testing the sensor's response to other AHLs. Future studies could also include testing the response of the sensor (ara^-) to OHHL induction at concentrations greater than 10^{-4} M in microplates. As for microfluidic experiments, future studies could include conducting more biological replicates to better characterise the performance of the sensor. The sensor could also be used to test the attenuation ability of other QQEs and inhibitors that can degrade OHHL. Replacing the used QS-related genes with other LuxI/LuxR-type genes could be considered to study other AI-1-mediated QS systems. Future studies could also modify the plasmids via subcloning to study other genes. New inserts could consider adding

appropriate restriction sites to flank the coding sequences (with RBSs) to increase flexibility in assembly and disassembly.

In conclusion, this work demonstrates the feasibility of engineering an *E. coli* consortium to study the activation and attenuation of QS responses. Experimental protocols were developed to assess the performance of the strains in the planktonic state. A workflow to encapsulate bacterial cells in agarose hydrogel microbeads and to visualise and analyse the development of bacterial communities in the microbeads was established. This work can serve as a basis for future studies of QS using an engineered bacterial consortium.

References

Anwar, H., Dasgupta, M.K. and Costerton, J.W. 1990. Testing the susceptibility of bacteria in biofilms to antibacterial agents. *Antimicrob Agents Chemother.* **34**(11), pp.2043-2046.

Ai, H.W., Shaner, N.C., Cheng, Z., Tsien, R.Y. and Campbell, R.E. 2007. Exploration of new chromophore structures leads to the identification of improved blue fluorescent proteins. *Biochemistry.* **46**(20), pp.5904-5910.

Abisado, R.G., Benomar, S., Klaus, J.R., Dandekar, A.A. and Chandler, J.R. 2018. Bacterial Quorum Sensing and Microbial Community Interactions. *mBio.* **9**(3), pp.10.1128/mbio.02331-02317.

Brennan, R.G. and Matthews, B.W. 1989. The helix-turn-helix DNA binding motif. *Journal of Biological Chemistry.* **264**(4), pp.1903-1906.

Bodman, S.B.v. and Farrand, S.K. 1995. Capsular polysaccharide biosynthesis and pathogenicity in Erwinia stewartii require induction by an N-acylhomoserine lactone autoinducer. *Journal of Bacteriology.* **177**(17), pp.5000-5008.

Berg, H.C. 2000. Motile Behavior of Bacteria. *Physics Today*. **53**(1), pp.24-29.

Byers, J.T., Lucas, C., Salmond, G.P.C. and Welch, M. 2002. Nonenzymatic Turnover of an Erwinia carotovora Quorum-Sensing Signaling Molecule. *Journal of Bacteriology.* **184**(4), pp.1163-1171.

Bahl, M.I., Sørensen, S.J. and Hestbjerg Hansen, L. 2004. Quantification of plasmid loss in Escherichia coli cells by use of flow cytometry. *FEMS Microbiology Letters.* **232**(1), pp.45-49.

Bose, J.L., Kim, U., Bartkowski, W., Gunsalus, R.P., Overley, A.M., Lyell, N.L., Visick, K.L. and Stabb, E.V. 2007. Bioluminescence in Vibrio fischeri is controlled by the redox-responsive regulator ArcA. *Molecular Microbiology.* **65**(2), pp.538-553.

Boles, B.R. and Horswill, A.R. 2008. Agr-mediated dispersal of Staphylococcus aureus biofilms. *PLoS Pathog*. **4**(4), pe1000052.

Burn, S.F. 2012. Detection of β-Galactosidase Activity: X-gal Staining. In: Michos, O. ed. *Kidney Development: Methods and Protocols.* Totowa, NJ: Humana Press, pp.241-250.

Blacker, T.S., Mann, Z.F., Gale, J.E., Ziegler, M., Bain, A.J., Szabadkai, G. and Duchen, M.R. 2014. Separating NADH and NADPH fluorescence in live cells and tissues using FLIM. *Nature Communications*. **5**(1), p3936.

Bulycheva, E.V., Korotkova, E.I., Voronova, O.A., Kustova, A.A. and Petrova, E.V. 2014. Fluorescence Analysis of E. coli Bacteria in Water. *Procedia Chemistry*. **10**, pp.179-183.

Brameyer, S., Kresovic, D., Bode, H.B. and Heermann, R. 2015. Dialkylresorcinols as bacterial signaling molecules. *Proceedings of the National Academy of Sciences*. **112**(2), pp.572-577.

Boo, A., Ledesma Amaro, R. and Stan, G.B. 2021. Quorum sensing in synthetic biology: A review. *Current Opinion in Systems Biology.* **28**, p100378.

Benchling [Biology Software]. 2024. Retrieved from https://benchling.com

Choi, S.H. and Greenberg, E.P. 1991. The C-terminal region of the Vibrio fischeri LuxR protein contains an inducer-independent lux gene activating domain. *Proceedings of the National Academy of Sciences.* **88**(24), pp.11115-11119.

Choi, S.H. and Greenberg, E.P. 1992. Genetic dissection of DNA binding and luminescence gene activation by the Vibrio fischeri LuxR protein. *J Bacteriol.* **174**(12), pp.4064-4069.

Cormack, B.P., Valdivia, R.H. and Falkow, S. 1996. FACS-optimized mutants of the green fluorescent protein (GFP). *Gene.* **173**(1), pp.33-38.

Carpenter, A.E., Jones, T.R., Lamprecht, M.R., Clarke, C., Kang, I.H., Friman, O., Guertin, D.A., Chang, J.H., Lindquist, R.A., Moffat, J., Golland, P. and Sabatini, D.M. 2006. CellProfiler: image analysis software for identifying and quantifying cell phenotypes. *Genome Biology.* **7**(10), pR100.

Cegelski, L., Marshall, G.R., Eldridge, G.R. and Hultgren, S.J. 2008. The biology and future prospects of antivirulence therapies. *Nat Rev Microbiol*. **6**(1), pp.17-27.

Choudhary, S. and Schmidt-Dannert, C. 2010. Applications of quorum sensing in biotechnology. *Applied Microbiology and Biotechnology.* **86**(5), pp.1267-1279.

Chen, Y.J., Liu, P., Nielsen, A.A.K., Brophy, J.A.N., Clancy, K., Peterson, T. and Voigt, C.A. 2013. Characterization of 582 natural and synthetic terminators and quantification of their design constraints. *Nature Methods.* **10**(7), pp.659-664.

Clark, K., Karsch-Mizrachi, I., Lipman, D.J., Ostell, J. and Sayers, E.W. 2015. GenBank. *Nucleic Acids Research*. **44**(D1), pp.D67-D72.

Devine, J.H., Countryman, C. and Baldwin, T.O. 1988. Nucleotide sequence of the luxR and luxI genes and structure of the primary regulatory region of the lux regulon of Vibrio fischeri ATCC 7744. *Biochemistry.* **27**(2), pp.837-842.

Dong, Y.H., Xu, J.L., Li, X.Z. and Zhang, L.H. 2000. AiiA, an enzyme that inactivates the acylhomoserine lactone quorum-sensing signal and attenuates the virulence of Erwinia carotovora. *Proceedings of the National Academy of Sciences.* **97**(7), pp.3526-3531.

Defoirdt, T., Boon, N., Sorgeloos, P., Verstraete, W. and Bossier, P. 2008. Quorum sensing and quorum quenching in Vibrio harveyi: lessons learned from in vivo work. *The ISME Journal.* **2**(1), pp.19-26.

Danino, T., Mondragón-Palomino, O., Tsimring, L. and Hasty, J. 2010. A synchronized quorum of genetic clocks. *Nature.* **463**(7279), pp.326-330.

Duan, F. and March, J.C. 2010. Engineered bacterial communication prevents Vibrio cholerae virulence in an infant mouse model. *Proceedings of the National Academy of Sciences.* **107**(25), pp.11260-11264.

Defoirdt, T., Brackman, G. and Coenye, T. 2013. Quorum sensing inhibitors: how strong is the evidence? *Trends in Microbiology.* **21**(12), pp.619-624.

Deng, Y., Lim, A., Lee, J., Chen, S., An, S., Dong, Y.H. and Zhang, L.H. 2014. Diffusible signal factor (DSF) quorum sensing signal and structurally related molecules enhance the antimicrobial efficacy of antibiotics against some bacterial pathogens. *BMC Microbiol*. **14**, p51.

Davis, R.M., Muller, R.Y. and Haynes, K.A. 2015. Can the Natural Diversity of Quorum-Sensing Advance Synthetic Biology? *Frontiers in Bioengineering and Biotechnology*. **3**.

Defoirdt, T. 2018. Quorum-Sensing Systems as Targets for Antivirulence Therapy. *Trends in Microbiology.* **26**(4), pp.313-328.

Di Martino, P. 2018. Extracellular polymeric substances, a key element in understanding biofilm phenotype. *AIMS Microbiol.* **4**(2), pp.274-288.

Duncker, K.E., Holmes, Z.A. and You, L. 2021. Engineered microbial consortia: strategies and applications. *Microbial Cell Factories.* **20**(1), p211.

Faruque, S.M., Albert, M.J. and Mekalanos, J.J. 1998. Epidemiology, genetics, and ecology of toxigenic Vibrio cholerae. *Microbiol Mol Biol Rev*. **62**(4), pp.1301-1314.

Federle, M.J. and Bassler, B.L. 2003. Interspecies communication in bacteria. *J Clin Invest*. **112**(9), pp.1291-1299.

Fetzner, S. 2015. Quorum quenching enzymes. *J Biotechnol.* **201**, pp.2-14.

Guzman, L.M., Belin, D., Carson, M.J. and Beckwith, J. 1995. Tight regulation, modulation, and high-level expression by vectors containing the arabinose PBAD promoter. *J Bacteriol.* **177**(14), pp.4121-4130.

García-Contreras, R., Maeda, T. and Wood, T.K. 2013. Resistance to quorum-quenching compounds. *Appl Environ Microbiol*. **79**(22), pp.6840-6846.

Holden, M.T.G., Ram Chhabra, S., De Nys, R., Stead, P., Bainton, N.J., Hill, P.J., Manefield, M., Kumar, N., Labatte, M., England, D., Rice, S., Givskov, M., Salmond, G.P.C., Stewart, G.S.A.B., Bycroft, B.W., Kjelleberg, S. and Williams, P. 1999. Quorum-sensing cross talk: isolation and chemical characterization of cyclic dipeptides from Pseudomonas aeruginosa and other Gram-negative bacteria. *Molecular Microbiology.* **33**(6), pp.1254-1266.

Hwang, I., Li, P.L., Zhang, L., Piper, K.R., Cook, D.M., Tate, M.E. and Farrand, S.K. 1994. TraI, a LuxI homologue, is responsible for production of conjugation factor, the Ti plasmid N-acylhomoserine lactone autoinducer. *Proc Natl Acad Sci U S A.* **91**(11), pp.4639-4643.

Hensel, Z. 2017. A plasmid-based Escherichia coli gene expression system with cell-to-cell variation below the extrinsic noise limit. *PLOS ONE.* **12**(10), pe0187259.

Han, Y. 2019. luxPR_4G12T. [Online]. [Accessed 30 January 2024]. Available from: http://parts.igem.org/Part:BBa_K3205005

International Organization for Standardization. 1998. ISO 15214:1998. *Microbiology of food and animal feeding stuffs — Horizontal method for the enumeration of mesophilic lactic acid bacteria — Colony-count technique at 30 °C.*

Ismail, A.S., Valastyan, J.S. and Bassler, B.L. 2016. A Host-Produced Autoinducer-2 Mimic Activates Bacterial Quorum Sensing. *Cell Host Microbe*. **19**(4), pp.470-480.

Kaplan, H.B. and Greenberg, E.P. 1985. Diffusion of autoinducer is involved in regulation of the Vibrio fischeri luminescence system. *Journal of Bacteriology.* **163**(3), pp.1210-1214.

Kingsford, C.L., Ayanbule, K. and Salzberg, S.L. 2007. Rapid, accurate, computational discovery of Rho-independent transcription terminators illuminates their relationship to DNA uptake. *Genome Biology.* **8**(2), pR22.

Kalia, V.C., Patel, S.K.S., Kang, Y.C. and Lee, J.K. 2019. Quorum sensing inhibitors as antipathogens: biotechnological applications. *Biotechnology Advances.* **37**(1), pp.68-90.

Kleine-Brüggeney, H., van Vliet, L.D., Mulas, C., Gielen, F., Agley, C.C., Silva, J.C.R., Smith, A., Chalut, K. and Hollfelder, F. 2019. Long-Term Perfusion Culture of Monoclonal Embryonic Stem Cells in 3D Hydrogel Beads for Continuous Optical Analysis of Differentiation. *Small.* **15**(5), p1804576.

Kleine-Brüggeney, H., Weingarten, R., Schulze Bockeloh, F., Engwer, C., Fartmann, V., Schäfer, J., Rezaei, M. and Bühren, S. 2021. A Macro-to-Micro Interface for Performing Comprehensive Microfluidic Cell Culture Assays. *Advanced Materials Interfaces.* **8**(21), p2100785.

Lilley, B.N. and Bassler, B.L. 2000. Regulation of quorum sensing in Vibrio harveyi by LuxO and Sigma-54. *Molecular Microbiology*. **36**(4), pp.940-954.

Lyczak, J.B., Cannon, C.L. and Pier, G.B. 2000. Establishment of Pseudomonas aeruginosa infection: lessons from a versatile opportunist. *Microbes and Infection.* **2**(9), pp.1051-1060.

Lee, S.J., Park, S.Y., Lee, J.J., Yum, D.Y., Koo, B.T. and Lee, J.K. 2002. Genes encoding the N-acyl homoserine lactone-degrading enzyme are widespread in many subspecies of Bacillus thuringiensis. *Appl Environ Microbiol.* **68**(8), pp.3919-3924.

Ledgham, F., Ventre, I., Soscia, C., Foglino, M., Sturgis, J.N. and Lazdunski, A. 2003. Interactions of the quorum sensing regulator QscR: interaction with itself and the other regulators of Pseudomonas aeruginosa LasR and RhlR. *Molecular Microbiology.* **48**(1), pp.199-210.

Li, C., Gao, M., Zheng, G., Ma, X., Liu, X. and Yu, W. 2023. Enhanced quorum sensing capacity via regulating microenvironment to facilitate stress resistance of probiotic in alginate-based microcapsules. *International Journal of Biological Macromolecules.* **225**, pp.605-614.

Lenz, D.H., Mok, K.C., Lilley, B.N., Kulkarni, R.V., Wingreen, N.S. and Bassler, B.L. 2004. The Small RNA Chaperone Hfq and Multiple Small RNAs Control Quorum Sensing in Vibrio harveyi and Vibrio cholerae. *Cell*. **118**(1), pp.69-82.

Lequette, Y., Lee, J.H., Ledgham, F., Lazdunski, A. and Greenberg, E.P. 2006. A distinct QscR regulon in the Pseudomonas aeruginosa quorum-sensing circuit. *J Bacteriol.* **188**(9), pp.3365-3370.

Lang, J. and Faure, D. 2014. Functions and regulation of quorum-sensing in Agrobacterium tumefaciens. *Frontiers in Plant Science.* **5**.

Lee, J.H., Wood, T.K. and Lee, J. 2015. Roles of Indole as an Interspecies and Interkingdom Signaling Molecule. *Trends in Microbiology.* **23**(11), pp.707-718.

Le, K.Y. and Otto, M. 2015. Quorum-sensing regulation in staphylococci—an overview. *Frontiers in Microbiology.* **6**.

Lu, H.D., Spiegel, A.C., Hurley, A., Perez, L.J., Maisel, K., Ensign, L.M., Hanes, J., Bassler, B.L., Semmelhack, M.F. and Prud'homme, R.K. 2015. Modulating Vibrio cholerae Quorum-Sensing-Controlled Communication Using Autoinducer-Loaded Nanoparticles. *Nano Letters.* **15**(4), pp.2235-2241.

Lambert, T.J. 2019. FPbase: a community-editable fluorescent protein database. *Nature Methods*. **16**(4), pp.277-278.

Lopreside, A., Wan, X., Michelini, E., Roda, A. and Wang, B. 2019. Comprehensive Profiling of Diverse Genetic Reporters with Application to Whole-Cell and Cell-Free Biosensors. *Analytical Chemistry.* **91**(23), pp.15284-15292.

McClean, K.H., Winson, M.K., Fish, L., Taylor, A., Chhabra, S.R., Camara, M., Daykin, M., Lamb, J.H., Swift, S., Bycroft, B.W., Stewart, G.S.A.B. and Williams, P. 1997. Quorum

sensing and Chromobacterium violaceum: exploitation of violacein production and inhibition for the detection of N-acylhomoserine lactones. *Microbiology.* **143**(12), pp.3703-3711.

Michael, B., Smith, J.N., Swift, S., Heffron, F. and Ahmer, B.M.M. 2001. SdiA of Salmonella enterica Is a LuxR Homolog That Detects Mixed Microbial Communities. *Journal of Bacteriology.* **183**(19), pp.5733-5742.

Martínez-Trujillo, M., Sánchez-Trujillo, A., Ceja, V., Avila-Moreno, F., Bermúdez-Cruz, R.M., Court, D. and Montañez, C. 2010. Sequences required for transcription termination at the intrinsic lambdatI terminator. *Can J Microbiol.* **56**(2), pp.168-177.

Merck KGaA. 2011. Competent Cells (User Protocol TB009 Rev. I 0416JSW). [Online]. [Accessed 8 July 2024]. Available from: https://www.emdmillipore.com/Web-US-Site/en_CA/-/USD/ShowDocument-File?ProductSKU=EMD_BIO-69450&DocumentId=TB009.pdf&DocumentType=USP&Language=EN&Country=US&Origin=PDP

Myers, J.A., Curtis, B.S. and Curtis, W.R. 2013. Improving accuracy of cell and chromophore concentration measurements using optical density. *BMC Biophysics.* **6**(1), p4.

Miyashiro, T. and Ruby, E.G. 2012. Shedding light on bioluminescence regulation in Vibrio fischeri. *Mol Microbiol.* **84**(5), pp.795-806.

Muthukrishnan, A.-B., Kandhavelu, M., Lloyd-Price, J., Kudasov, F., Chowdhury, S., Yli-Harja, O. and Ribeiro, A.S. 2012. Dynamics of transcription driven by the tetA promoter, one event at a time, in live Escherichia coli cells. *Nucleic Acids Research.* **40**(17), pp.8472-8483.

Morgan, K. and Patrick, M. 2014. Origin of Replication. In: Leeson, R., Tsang, J., LaManna, C. eds. *Plasmids 101*. [Online]. 4 ed., pp.14-16. [Accessed 14 June 2024]. Available from: https://www.addgene.org/educational-resources/ebooks/

Mühlmann, M., Forsten, E., Noack, S. and Büchs, J. 2017. Optimizing recombinant protein expression via automated induction profiling in microtiter plates at different temperatures. *Microbial Cell Factories.* **16**(1), p220.

Mehmood, A., Liu, G., Wang, X., Meng, G., Wang, C. and Liu, Y. 2019. Fungal Quorum-Sensing Molecules and Inhibitors with Potential Antifungal Activity: A Review. *Molecules.* **24**(10).

Mukherjee, S. and Bassler, B.L. 2019. Bacterial quorum sensing in complex and dynamically changing environments. *Nature Reviews Microbiology.* **17**(6), pp.371-382.

Miller, C. and Gilmore, J. 2020. Detection of Quorum-Sensing Molecules for Pathogenic Molecules Using Cell-Based and Cell-Free Biosensors. *Antibiotics (Basel).* **9**(5).

Nealson, K.H., Platt, T. and Hastings, J.W. 1970. Cellular control of the synthesis and activity of the bacterial luminescent system. *J Bacteriol.* **104**(1), pp.313-322.

Ng, W.L., Perez, L.J., Wei, Y., Kraml, C., Semmelhack, M.F. and Bassler, B.L. 2011. Signal production and detection specificity in Vibrio CqsA/CqsS quorum-sensing systems. *Molecular Microbiology.* **79**(6), pp.1407-1417.

Nisisako, T., Torii, T. and Higuchi, T. 2002. Droplet formation in a microchannel network. *Lab on a Chip.* **2**(1), pp.24-26.

Neubig, R.R., Spedding, M., Kenakin, T. and Christopoulos, A. 2003. International Union of Pharmacology Committee on Receptor Nomenclature and Drug Classification. XXXVIII. Update on terms and symbols in quantitative pharmacology. *Pharmacol Rev.* **55**(4), pp.597-606.

Namdev, P., Dar, H.Y., Srivastava, R.K., Mondal, R. and Anupam, R. 2019. Induction of T7 Promoter at Higher Temperatures May Be Counterproductive. *Indian Journal of Clinical Biochemistry.* **34**(3), pp.357-360.

Nwoko, E.Q.A. and Okeke, I.N. 2021. Bacteria autoaggregation: how and why bacteria stick together. *Biochem Soc Trans.* **49**(3), pp.1147-1157.

Pirhonen, M., Flego, D., Heikinheimo, R. and Palva, E.T. 1993. A small diffusible signal molecule is responsible for the global control of virulence and exoenzyme production in the plant pathogen Erwinia carotovora. *Embo j.* **12**(6), pp.2467-2476.

Pappas, K.M. and Winans, S.C. 2003. A LuxR-type regulator from Agrobacterium tumefaciens elevates Ti plasmid copy number by activating transcription of plasmid replication genes. *Mol Microbiol.* **48**(4), pp.1059-1073.

Patankar, A.V. and González, J.E. 2009. Orphan LuxR regulators of quorum sensing. *FEMS Microbiology Reviews.* **33**(4), pp.739-756.

Papenfort, K. and Bassler, B.L. 2016. Quorum sensing signal-response systems in Gram-negative bacteria. *Nat Rev Microbiol.* **14**(9), pp.576-588.

Papenfort, K., Silpe, J.E., Schramma, K.R., Cong, J.P., Seyedsayamdost, M.R. and Bassler, B.L. 2017. A Vibrio cholerae autoinducer–receptor pair that controls biofilm formation. *Nature Chemical Biology.* **13**(5), pp.551-557.

Pérez-Rodríguez, S., García-Aznar, J.M. and Gonzalo-Asensio, J. 2022. Microfluidic devices for studying bacterial taxis, drug testing and biofilm formation. *Microb Biotechnol.* **15**(2), pp.395-414.

Qin, X., Vila-Sanjurjo, C., Singh, R., Philipp, B. and Goycoolea, F.M. 2020. Screening of Bacterial Quorum Sensing Inhibitors in a Vibrio fischeri LuxR-Based Synthetic Fluorescent E. coli Biosensor. *Pharmaceuticals.* **13**(9), p263.

Rogozin, I.B. and Pavlov, Y.I. 2003. Theoretical analysis of mutation hotspots and their DNA sequence context specificity. *Mutat Res.* **544**(1), pp.65-85.

Ruby, E.G., Urbanowski, M., Campbell, J., Dunn, A., Faini, M., Gunsalus, R., Lostroh, P., Lupp, C., McCann, J., Millikan, D., Schaefer, A., Stabb, E., Stevens, A., Visick, K., Whistler, C. and Greenberg, E.P. 2005. Complete genome sequence of Vibrio fischeri: A symbiotic bacterium with pathogenic congeners. *Proceedings of the National Academy of Sciences.* **102**(8), pp.3004-3009.

Roy, V., Fernandes, R., Tsao, C.-Y. and Bentley, W.E. 2010. Cross Species Quorum Quenching Using a Native AI-2 Processing Enzyme. *ACS Chemical Biology*. 5(2), pp.223-232.

Rutherford, S.T. and Bassler, B.L. 2012. Bacterial quorum sensing: its role in virulence and possibilities for its control. *Cold Spring Harb Perspect Med.* **2**(11).

Slock, J., VanRiet, D., Kolibachuk, D. and Greenberg, E.P. 1990. Critical regions of the Vibrio fischeri luxR protein defined by mutational analysis. *J Bacteriol.* **172**(7), pp.3974-3979.

Shadel, G.S. and Baldwin, T.O. 1991. The Vibrio fischeri LuxR protein is capable of bidirectional stimulation of transcription and both positive and negative regulation of the luxR gene. *J Bacteriol*. **173**(2), pp.568-574.

Sturme, M.H.J., Kleerebezem, M., Nakayama, J., Akkermans, A.D.L., Vaughan, E.E. and de Vos, W.M. 2002. Cell to cell communication by autoinducing peptides in gram-positive bacteria. *Antonie van Leeuwenhoek.* **81**(1), pp.233-243.

Shaner, N.C., Campbell, R.E., Steinbach, P.A., Giepmans, B.N., Palmer, A.E. and Tsien, R.Y. 2004. Improved monomeric red, orange and yellow fluorescent proteins derived from Discosoma sp. red fluorescent protein. *Nat Biotechnol.* **22**(12), pp.1567-1572.

Schuster, M. and Peter Greenberg, E. 2006. A network of networks: Quorum-sensing gene regulation in Pseudomonas aeruginosa. *International Journal of Medical Microbiology.* **296**(2), pp.73-81.

Sandoz, K.M., Mitzimberg, S.M. and Schuster, M. 2007. Social cheating in Pseudomonas aeruginosa quorum sensing. *Proceedings of the National Academy of Sciences*. **104**(40), pp.15876-15881.

Steindler, L. and Venturi, V. 2007. Detection of quorum-sensing N-acyl homoserine lactone signal molecules by bacterial biosensors. *FEMS Microbiology Letters.* **266**(1), pp.1-9.

Schleif, R. 2010. AraC protein, regulation of the l-arabinose operon in Escherichia coli, and the light switch mechanism of AraC action. *FEMS Microbiology Reviews.* **34**(5), pp.779-796.

Schindelin, J., Arganda-Carreras, I., Frise, E., Kaynig, V., Longair, M., Pietzsch, T., Preibisch, S., Rueden, C., Saalfeld, S., Schmid, B., Tinevez, J.-Y., White, D.J., Hartenstein, V., Eliceiri, K., Tomancak, P. and Cardona, A. 2012. Fiji: an open-source platform for biological-image analysis. *Nature Methods*. **9**(7), pp.676-682.

Schuster, M., Sexton, D.J., Diggle, S.P. and Greenberg, E.P. 2013. Acyl-homoserine lactone quorum sensing: from evolution to application. *Annu Rev Microbiol.* **67**, pp.43-63.

Sackmann, E.K., Fulton, A.L. and Beebe, D.J. 2014. The present and future role of microfluidics in biomedical research. *Nature*. **507**(7491), pp.181-189.

Silva, J.P.N., Lopes, S.V., Grilo, D.J. and Hensel, Z. 2019. Plasmids for Independently Tunable, Low-Noise Expression of Two Genes. *mSphere.* **4**(3), pp.10.1128/msphere.00340-00319.

Sikdar, R. and Elias, M. 2020. Quorum quenching enzymes and their effects on virulence, biofilm, and microbiomes: a review of recent advances. *Expert Rev Anti Infect Ther.* **18**(12), pp.1221-1233.

Shao, B., Rammohan, J., Anderson, D.A., Alperovich, N., Ross, D. and Voigt, C.A. 2021. Single-cell measurement of plasmid copy number and promoter activity. *Nat Commun.* **12**(1), p1475.

Stirling, D.R., Swain-Bowden, M.J., Lucas, A.M., Carpenter, A.E., Cimini, B.A. and Goodman, A. 2021. CellProfiler 4: improvements in speed, utility and usability. *BMC Bioinformatics.* **22**(1), p433.

Tu, K.C. and Bassler, B.L. 2007. Multiple small RNAs act additively to integrate sensory information and control quorum sensing in Vibrio harveyi. *Genes Dev*. **21**(2), pp.221-233.

Theberge, A.B., Courtois, F., Schaerli, Y., Fischlechner, M., Abell, C., Hollfelder, F. and Huck, W.T.S. 2010. Microdroplets in Microfluidics: An Evolving Platform for Discoveries in Chemistry and Biology. *Angewandte Chemie International Edition.* **49**(34), pp.5846-5868.

Tsai, C.S. and Winans, S.C. 2010. LuxR-type quorum-sensing regulators that are detached from common scents. *Mol Microbiol.* **77**(5), pp.1072-1082.

Thompson, Jessica A., Oliveira, Rita A., Djukovic, A., Ubeda, C. and Xavier, Karina B. 2015. Manipulation of the Quorum Sensing Signal AI-2 Affects the Antibiotic-Treated Gut Microbiota. *Cell Reports.* **10**(11), pp.1861-1871.

Tan, L., Li, S.R., Jiang, B., Hu, X.M. and Li, S. 2018. Therapeutic Targeting of the Staphylococcus aureus Accessory Gene Regulator (agr) System. *Front Microbiol*. **9**, p55.

Thermo Fisher Scientific. 2018. *EVOS™ FL Auto 2 Imaging System For fluorescence and transmitted light applications*. [Online]. [Accessed 16 June 2024]. Available from: https://assets.fishersci.com/TFS-Assets/BID/manuals/MAN0016154_EVOS_FL_Auto_2_QR.pdf

Trunk, T., Khalil, H.S. and Leo, J.C. 2018. Bacterial autoaggregation. *AIMS Microbiol.* **4**(1), pp.140-164.

Tsoi, R., Wu, F., Zhang, C., Bewick, S., Karig, D. and You, L. 2018. Metabolic division of labor in microbial systems. *Proceedings of the National Academy of Sciences*. **115**(10), pp.2526-2531.

Tekel, S.J., Smith, C.L., Lopez, B., Mani, A., Connot, C., Livingstone, X. and Haynes, K.A. 2019. Engineered Orthogonal Quorum Sensing Systems for Synthetic Gene Regulation in Escherichia coli. *Front Bioeng Biotechnol*. **7**, p80.

Urbanowski, M.L., Lostroh, C.P. and Greenberg, E.P. 2004. Reversible acyl-homoserine lactone binding to purified Vibrio fischeri LuxR protein. *J Bacteriol.* **186**(3), pp.631-637.

Visick, K.L. and McFall-Ngai, M.J. 2000. An exclusive contract: specificity in the Vibrio fischeri-Euprymna scolopes partnership. *J Bacteriol.* **182**(7), pp.1779-1787.

Vendeville, A., Winzer, K., Heurlier, K., Tang, C.M. and Hardie, K.R. 2005. Making 'sense' of metabolism: autoinducer-2, LUXS and pathogenic bacteria. *Nature Reviews Microbiology.* **3**(5), pp.383-396.

Visick, K.L. and Ruby, E.G. 2006. Vibrio fischeri and its host: it takes two to tango. *Curr Opin Microbiol.* **9**(6), pp.632-638.

Verbeke, F., De Craemer, S., Debunne, N., Janssens, Y., Wynendaele, E., Van de Wiele, C. and De Spiegeleer, B. 2017. Peptides as Quorum Sensing Molecules: Measurement Techniques and Obtained Levels In vitro and In vivo. *Front Neurosci.* **11**, p183.

van Tatenhove-Pel, R.J., Hernandez-Valdes, J.A., Teusink, B., Kuipers, O.P., Fischlechner, M. and Bachmann, H. 2020. Microdroplet screening and selection for improved microbial production of extracellular compounds. *Current Opinion in Biotechnology*. **61**, pp.72-81.

Weston-Hafer, K. and Berg, D.E. 1991. Deletions in plasmid pBR322: replication slippage involving leading and lagging strands. *Genetics.* **127**(4), pp.649-655.

Wilson, T. and Hastings, J.W. 1998. BIOLUMINESCENCE. *Annual Review of Cell and Developmental Biology.* **14**(1), pp.197-230.

Whitehead, N.A., Barnard, A.M.L., Slater, H., Simpson, N.J.L. and Salmond, G.P.C. 2001. Quorum-sensing in Gram-negative bacteria. *FEMS Microbiology Reviews.* **25**(4), pp.365-404.

Watson, W.T., Minogue, T.D., Val, D.L., von Bodman, S.B. and Churchill, M.E.A. 2002. Structural Basis and Specificity of Acyl-Homoserine Lactone Signal Production in Bacterial Quorum Sensing. *Molecular Cell.* **9**(3), pp.685-694.

Weibel, D.B., DiLuzio, W.R. and Whitesides, G.M. 2007. Microfabrication meets microbiology. *Nature Reviews Microbiology.* **5**(3), pp.209-218.

Wen, K.Y., Cameron, L., Chappell, J., Jensen, K., Bell, D.J., Kelwick, R., Kopniczky, M., Davies, J.C., Filloux, A. and Freemont, P.S. 2017. A Cell-Free Biosensor for Detecting Quorum Sensing Molecules in P. aeruginosa-Infected Respiratory Samples. *ACS Synthetic Biology.* **6**(12), pp.2293-2301.

Yu, D., Zhao, L., Xue, T. and Sun, B. 2012. Staphylococcus aureus autoinducer-2 quorum sensing decreases biofilm formation in an icaR-dependent manner. *BMC Microbiology.* **12**(1), p288.

Yurtsev, E.A., Chao, H.X., Datta, M.S., Artemova, T. and Gore, J. 2013. Bacterial cheating drives the population dynamics of cooperative antibiotic resistance plasmids. *Mol Syst Biol*. **9**, p683.

Zhang, Z., Schwartz, S., Wagner, L. and Miller, W. 2000. A greedy algorithm for aligning DNA sequences. *J Comput Biol*. **7**(1-2), pp.203-214.

Zhu, J. and Winans, S.C. 2001. The quorum-sensing transcriptional regulator TraR requires its cognate signaling ligand for protein folding, protease resistance, and dimerization. *Proceedings of the National Academy of Sciences*. **98**(4), pp.1507-1512.

Zhang, R.G., Pappas, K.M., Brace, J.L., Miller, P.C., Oulmassov, T., Molyneaux, J.M., Anderson, J.C., Bashkin, J.K., Winans, S.C. and Joachimiak, A. 2002. Structure of a bacterial quorum-sensing transcription factor complexed with pheromone and DNA. *Nature.* **417**(6892), pp.971-974.

Zhu, J. and Mekalanos, J.J. 2003. Quorum Sensing-Dependent Biofilms Enhance Colonization in Vibrio cholerae. *Developmental Cell*. **5**(4), pp.647-656.

Zschiedrich, C.P., Keidel, V. and Szurmant, H. 2016. Molecular Mechanisms of Two-Component Signal Transduction. *J Mol Biol.* **428**(19), pp.3752-3775.

Zhao, X., Yu, Z. and Ding, T. 2020. Quorum-Sensing Regulation of Antimicrobial Resistance in Bacteria. *Microorganisms.* **8**(3).

Zhang, R., Goetz, H., Melendez-Alvarez, J., Li, J., Ding, T., Wang, X. and Tian, X.J. 2021. Winner-takes-all resource competition redirects cascading cell fate transitions. *Nature Communications.* **12**(1), p853.

Appendix A

Table A. 1 Information on the genetic materials

Gene	**Reference number**	**Source**	**Address**
pBAD24	87399	ATCC	Manassas, VA, USA
pET-21 (+)	-	Twist Bioscience	South San Francisco, CA, USA
Designed inserts	-		
pZH509	102664	Addgene	Watertown, MA, USA
tetR			
luxR	BBa_C0062	iGEM	https://parts.igem.org/Main_Page
luxPR_4G12T	BBa_K3205005		
aiiA	BBa_C0160		
Terminator rrnB T1	BBa_B0010		
Ribosome binding site	BBa_K3288007		
egfp	GenBank: U55761.1	GenBank	https://www.ncbi.nlm.nih.gov/genbank/
luxI	GenBank: M19039.1		
mCherry	GenBank: AY678264.1		
ebfp2	GenBank: EF517318.1		
Promoter P_{N25}	-	Muthukrishnan et al. (2012)	-
Terminator ECK120033736	-	Chen et al. (2013)	-
Terminator ECK120029600			
Terminator ECK120033737			
Terminator L3S2P21			
Terminator L3S3P21			

Table A. 2 Information on the main experimental materials and equipment

Item	**Reference number**	**Company**	**Address**
Glycerol	49767	Merck KGaA	Darmstadt, Germany
LB powder (Luria)	L3397		
Tuner (DE3) strain	70623		
LB power with agar (Luria)	L3272		
L (+) Arabinose	A3256		
OHHL	K3007		
Ampicillin	A0166		
Milli-Q water	-		
DH5alpha	18265017	Fisher Scientific	Waltham, MA, USA
Syringe filter	10268401		
Acetonitrile	A/0638/17		
TAE (10x)	AM9869	Thermo Fisher Scientific	
IPTG	R0392		
Invitrogen EVOS FL Auto 2 Imaging System	-		
Ethanol (>99.8%)	32221-2.5L	Honeywell	Charlotte, NC, USA
2 mL Syringe	720-2522	VWR	Radnor, PA, USA
LigaFast Rapid DNA Ligation System	M8221	Promega	Madison, WI, USA
Safe DNA Gel Stain	A8743-APE	Stratech Scientific	Ely, UK
Anhydrotetracycline	2-0401-002-IBA		
EcoRI-HF	R3101T	New England Biolabs	Ipswich, MA, USA
NheI-HF	R3131S		
PCR & DNA Cleanup Kit (5 µg)	T1030L		
1kb DNA Ladder Ready to Load	07-12-00050	Thistle Scientific	Rugby, UK
QIAquick Gel Extraction Kit	28704	Qiagen	Venlo, Netherlands
QIAprep Spin Miniprep Kit	27104		
Hi-Res Standard Agarose	AGD1-500GM	Cambridge Reagents/Geneflow	-/Lichfield, UK

96-well plate seal	PCR0548	Azenta Life Sciences	Burlington, MA, USA
96-well plate (black)	655090	Greiner Bio-One	Kremsmünster, Austria
Jenway 6715 UV/Visible Spectrophotometer	WZ-83056-70	Cole-Parmer	Vernon Hills, IL, USA
CLARIOstar Plate Reader	-	BMG LABTECH	Ortenberg, Germany
FluoroMax-4 spectrofluorometer	-	Horiba	Kyoto, Japan
CellCity Array Kit - Priming Solution - Hydrogel A (3% agarose) - Bead Formation Solution - Demulsification Solution - Trapping solution - Buffer B - Bead filter	-	Evorion Biotechnologies	Münster, Germany

Table A. 3 Information on the software

Software	**Version**	**Company/Publisher**	**Address**
Microsoft office for mac	16.86	Microsoft	Redmond, WA, USA
GraphPad Prism	10.2.2	GraphPad	Boston, MA, USA
CLARIOstar Reader Control	5.40 R3	BMG LABTECH	Ortenberg, Germany
MARS Data Analysis Software	3.32		
FluorEssence	-	Horiba	Kyoto, Japan
CellCity Tools	-	Evorion Biotechnologies	Münster, Germany
Invitrogen EVOS FL Auto 2 software	-	Thermo Fisher Scientific	Waltham, MA, USA
Fiji-ImageJ	2.14.0/1.54f	-	-
EndNote	X9 and 21	Clarivate	Philadelphia, PA, USA

Appendix B

Sequencing results of the three strains

Maps were generated using Benchling (2024). Maps were annotated based on information from iGEM (https://parts.igem.org/Main_Page), GenBank (https://www.ncbi.nlm.nih.gov/genbank/) (Clark et al., 2015), and Addgene (https://www.addgene.org/) accessed 30 January 2024, from NovoPro (https://www.novoprolabs.com/) and SnapGene (https://www.snapgene.com/) accessed 13 June 2024, and from Muthukrishnan et al. (2012) and Chen et al. (2013).

B.1 Sensor

B.1.1 Plasmid map

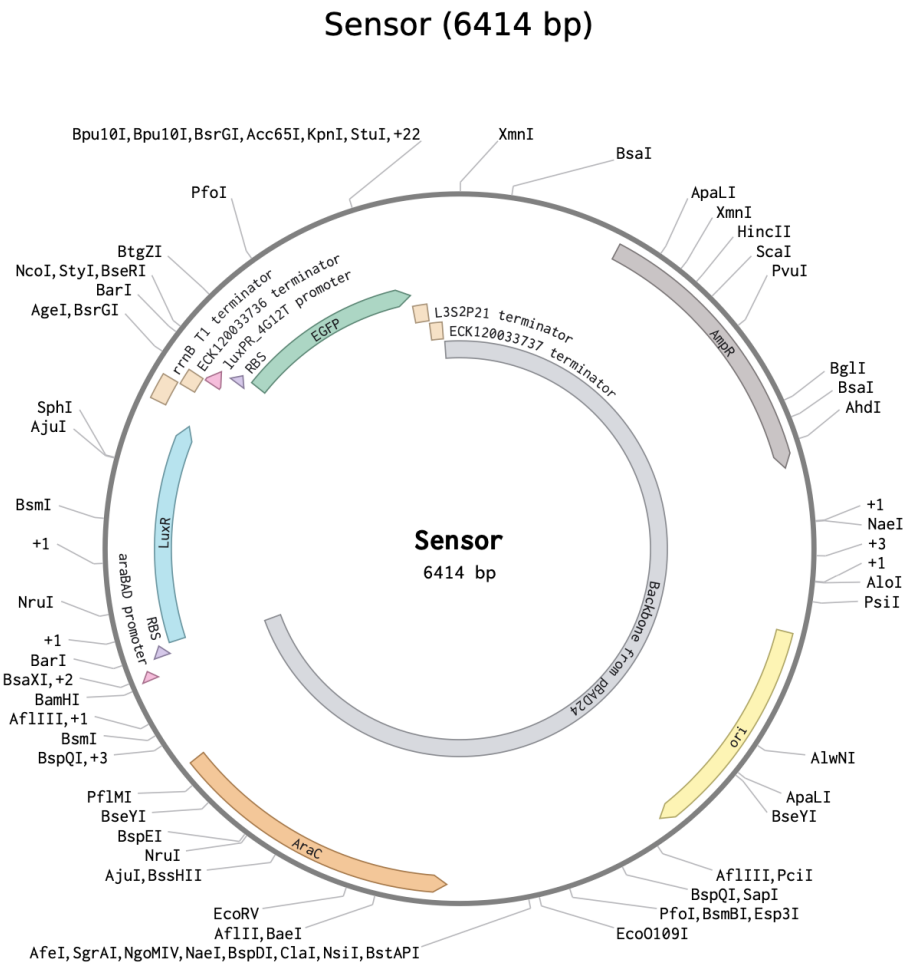

Figure B. 1 Plasmid map of the sensor strain

B.1.2 Sequence map

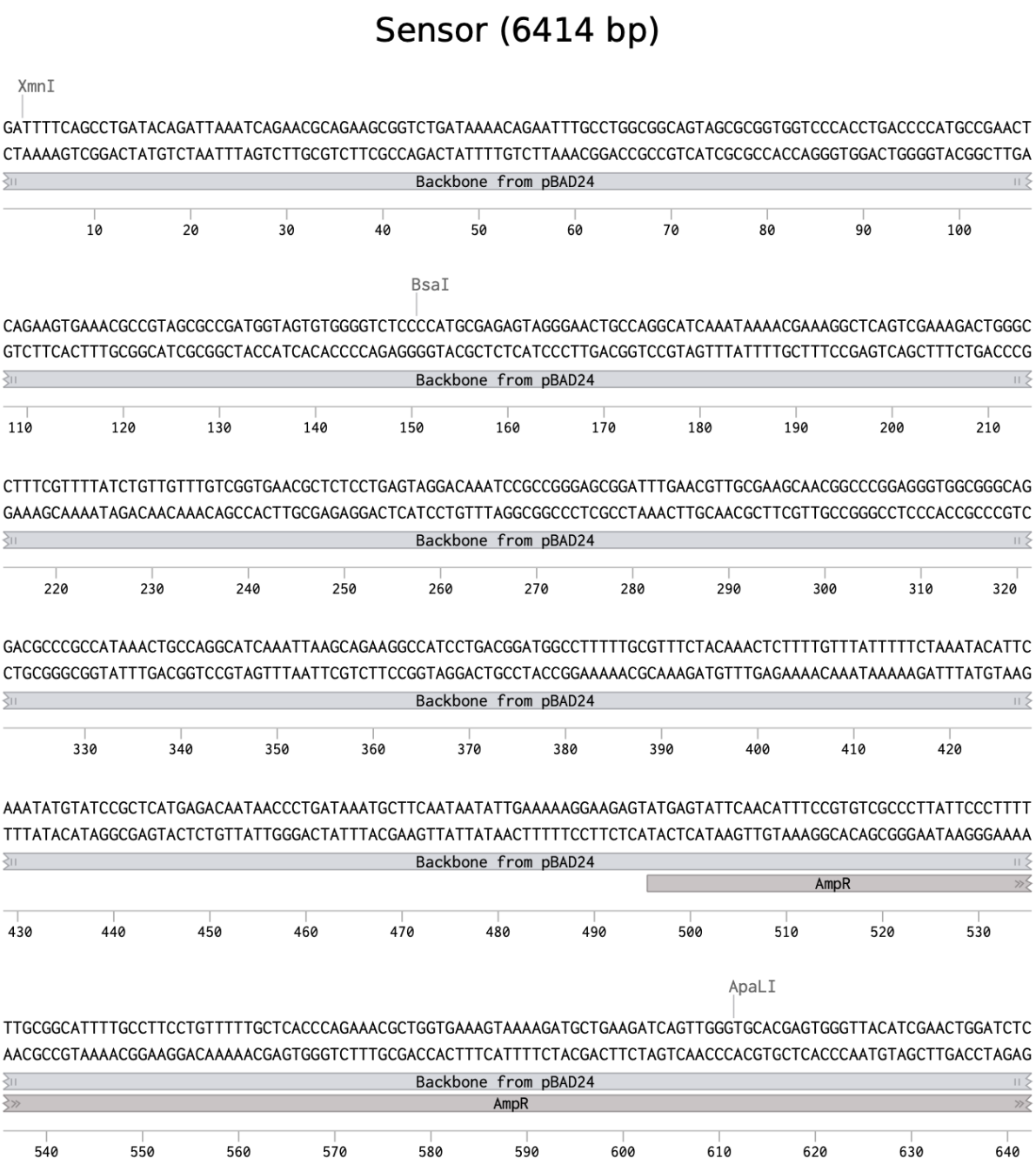

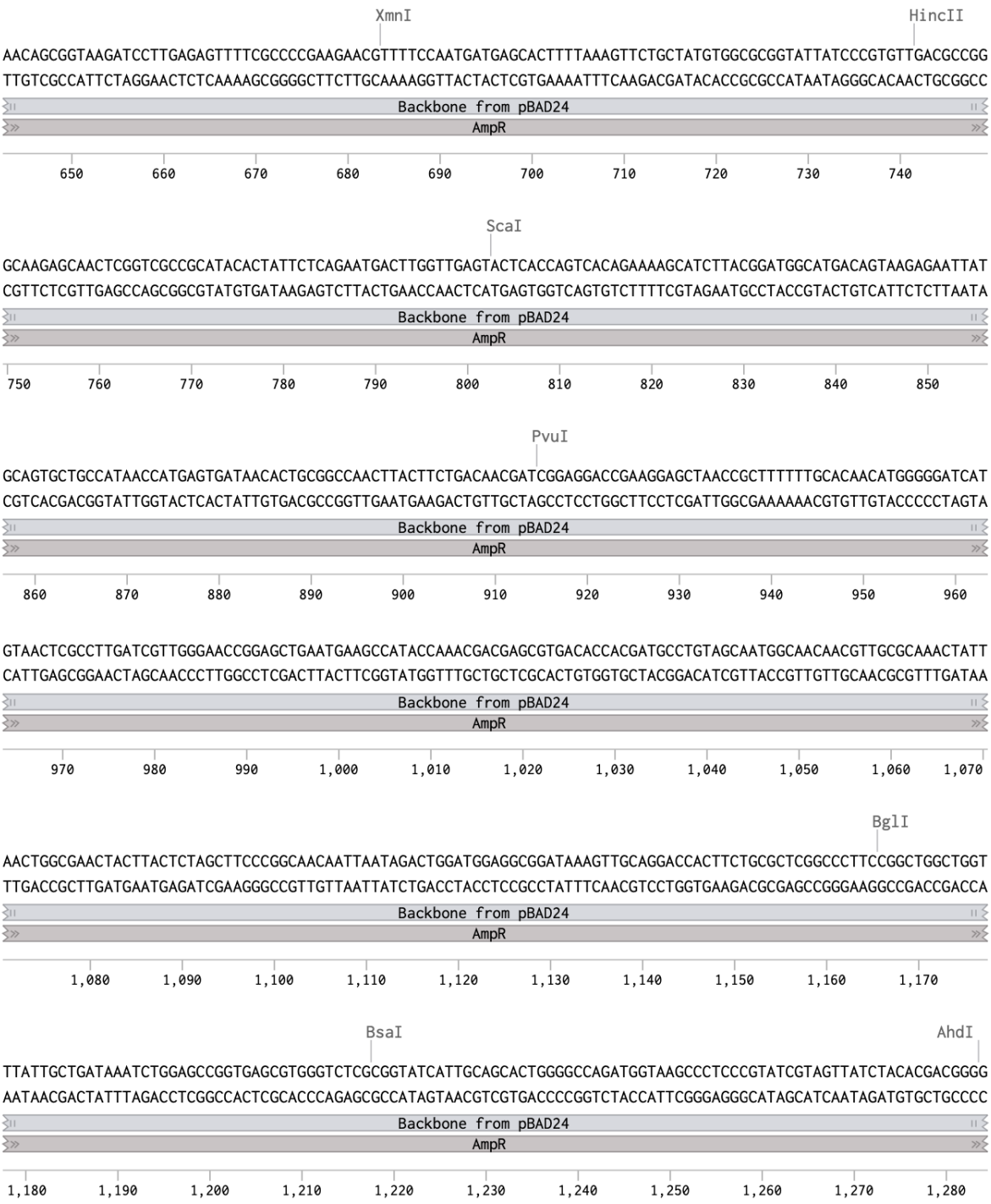
XmnI
HincII
AACAGCGGTAAGATCCTTGAGAGTTTTCGCCCCGAAGAACGTTTTCCAATGATGAGCACTTTTAAAGTTCTGCTATGTGGCGCGGTATTATCCCGTGTTGACGCCGG
TTGTCGCCATTCTAGGAACTCTCAAAAGCGGGGCTTCTTGCAAAAGGTTACTACTCGTGAAAATTTCAAGACGATACACCGCGCCATAATAGGGCACAACTGCGGCC
Backbone from pBAD24
AmpR
650
660
670
680
690
700
710
720
730
740
ScaI
GCAAGAGCAACTCGGTCGCCGCATACACTATTCTCAGAATGACTTGGTTGAGTACTCACCAGTCACAGAAAAGCATCTTACGGATGGCATGACAGTAAGAGAATTAT
CGTTCTCGTTGAGCCAGCGGCGTATGTGATAAGAGTCTTACTGAACCAACTCATGAGTGGTCAGTGTCTTTTCGTAGAATGCCTACCGTACTGTCATTCTCTTAATA
Backbone from pBAD24
AmpR
750
760
770
780
790
800
810
820
830
840
850
PvuI
GCAGTGCTGCCATAACCATGAGTGATAACACTGCGGCCAACTTACTTCTGACAACGATCGGAGGACCGAAGGAGCTAACCGCTTTTTTGCACAACATGGGGGATCAT
CGTCACGACGGTATTGGTACTCACTATTGTGACGCCGGTTGAATGAAGACTGTTGCTAGCCTCCTGGCTTCCTCGATTGGCGAAAAAACGTGTTGTACCCCCTAGTA
Backbone from pBAD24
AmpR
860
870
880
890
900
910
920
930
940
950
960
GTAACTCGCCTTGATCGTTGGGAACCGGAGCTGAATGAAGCCATACCAAACGACGAGCGTGACACCACGATGCCTGTAGCAATGGCAACAACGTTGCGCAAACTATT
CATTGAGCGGAACTAGCAACCCTTGGCCTCGACTTACTTCGGTATGGTTTGCTGCTCGCACTGTGGTGCTACGGACATCGTTACCGTTGTTGCAACGCGTTTGATAA
Backbone from pBAD24
AmpR
970
980
990
1,000
1,010
1,020
1,030
1,040
1,050
1,060
1,070
BglI
AACTGGCGAACTACTTACTCTAGCTTCCCGGCAACAATTAATAGACTGGATGGAGGCGGATAAAGTTGCAGGACCACTTCTGCGCTCGGCCCTTCCGGCTGGCTGGT
TTGACCGCTTGATGAATGAGATCGAAGGGCCGTTGTTAATTATCTGACCTACCTCCGCCTATTTCAACGTCCTGGTGAAGACGCGAGCCGGGAAGGCCGACCGACCA
Backbone from pBAD24
AmpR
1,080
1,090
1,100
1,110
1,120
1,130
1,140
1,150
1,160
1,170
BsaI
AhdI
TTATTGCTGATAAATCTGGAGCCGGTGAGCGTGGGTCTCGCGGTATCATTGCAGCACTGGGGCCAGATGGTAAGCCCTCCCGTATCGTAGTTATCTACACGACGGGG
AATAACGACTATTTAGACCTCGGCCACTCGCACCCAGAGCGCCATAGTAACGTCGTGACCCCGGTCTACCATTCGGGAGGGCATAGCATCAATAGATGTGCTGCCCC
Backbone from pBAD24
AmpR
1,180
1,190
1,200
1,210
1,220
1,230
1,240
1,250
1,260
1,270
1,280

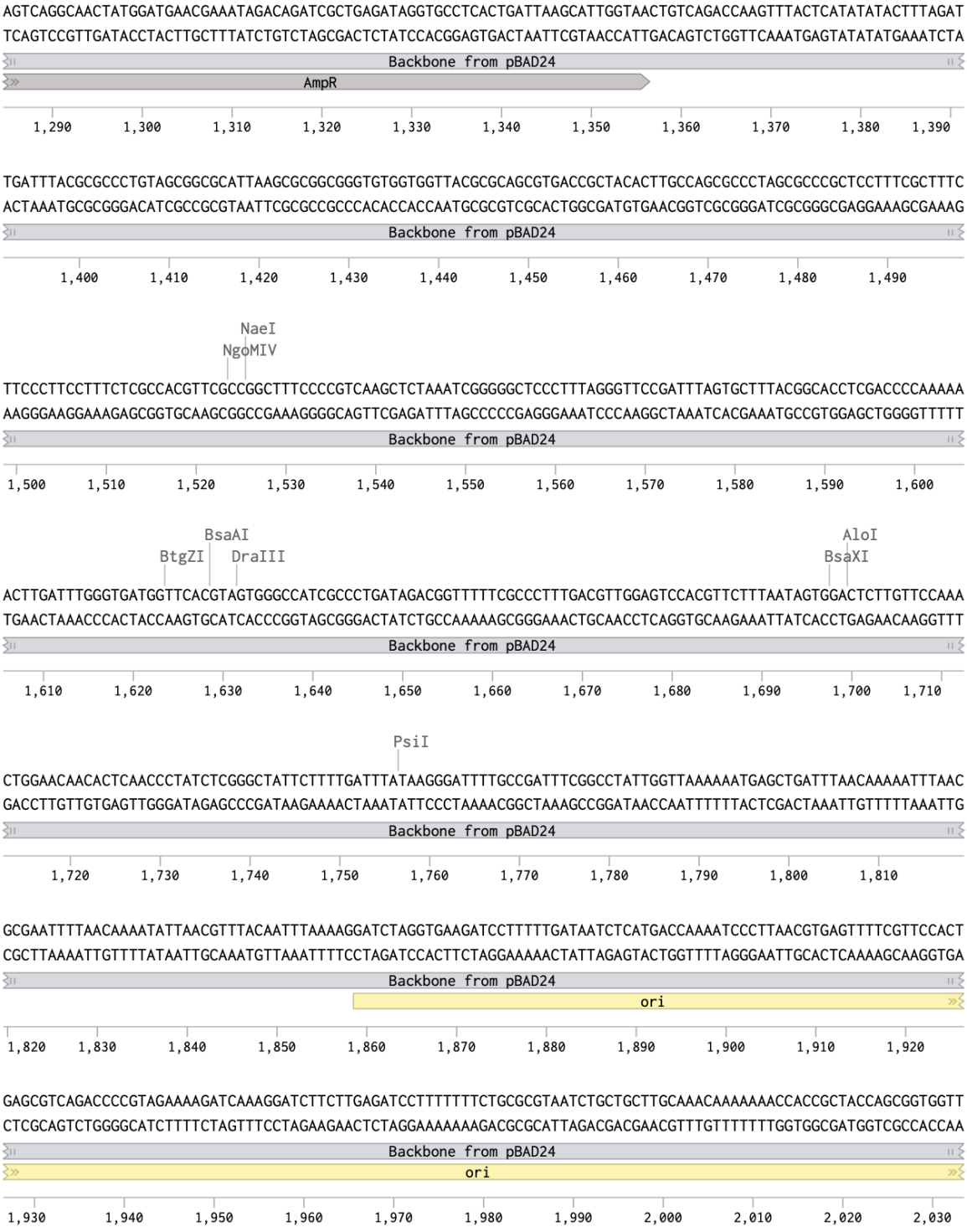
AGTCAGGCAACTATGGATGAACGAAATAGACAGATCGCTGAGATAGGTGCCTCACTGATTAAGCATTGGTAACTGTCAGACCAAGTTTACTCATATATACTTTAGAT
TCAGTCCGTTGATACCTACTTGCTTTATCTGTCTAGCGACTCTATCCACGGAGTGACTAATTCGTAACCATTGACAGTCTGGTTCAAATGAGTATATATGAAATCTA
Backbone from pBAD24
AmpR
1,290 1,300 1,310 1,320 1,330 1,340 1,350 1,360 1,370 1,380 1,390
TGATTTACGCGCCCTGTAGCGGCGCATTAAGCGCGGCGGGTGTGGTGGTTACGCGCAGCGTGACCGCTACACTTGCCAGCGCCCTAGCGCCCGCTCCTTTCGCTTTC
ACTAAATGCGCGGGACATCGCCGCGTAATTCGCGCCGCCCACACCACCAATGCGCGTCGCACTGGCGATGTGAACGGTCGCGGGATCGCGGGCGAGGAAAGCGAAAG
Backbone from pBAD24
1,400 1,410 1,420 1,430 1,440 1,450 1,460 1,470 1,480 1,490
NaeI
NgoMIV
TTCCCTTCCTTTCTCGCCACGTTCGCCGGCTTTCCCCGTCAAGCTCTAAATCGGGGGCTCCCTTTAGGGTTCCGATTTAGTGCTTTACGGCACCTCGACCCCAAAAA
AAGGGAAGGAAAGAGCGGTGCAAGCGGCCGAAAGGGGCAGTTCGAGATTTAGCCCCCGAGGGAAATCCCAAGGCTAAATCACGAAATGCCGTGGAGCTGGGGTTTTT
Backbone from pBAD24
1,500 1,510 1,520 1,530 1,540 1,550 1,560 1,570 1,580 1,590 1,600
BsaAI
BtgZI
DraIII
AloI
BsaXI
ACTTGATTTGGGTGATGGTTCACGTAGTGGGCCATCGCCCTGATAGACGGTTTTTCGCCCTTTGACGTTGGAGTCCACGTTCTTTAATAGTGGACTCTTGTTCCAAA
TGAACTAAACCCACTACCAAGTGCATCACCCGGTAGCGGGACTATCTGCCAAAAAGCGGGAAACTGCAACCTCAGGTGCAAGAAATTATCACCTGAGAACAAGGTTT
Backbone from pBAD24
1,610 1,620 1,630 1,640 1,650 1,660 1,670 1,680 1,690 1,700 1,710
PsiI
CTGGAACAACACTCAACCCTATCTCGGGCTATTCTTTTGATTTATAAGGGATTTTGCCGATTTCGGCCTATTGGTTAAAAAATGAGCTGATTTAACAAAAATTTAAC
GACCTTGTTGTGAGTTGGGATAGAGCCCGATAAGAAAACTAAATATTCCCTAAAACGGCTAAAGCCGGATAACCAATTTTTTACTCGACTAAATTGTTTTTAAATTG
Backbone from pBAD24
1,720 1,730 1,740 1,750 1,760 1,770 1,780 1,790 1,800 1,810
GCGAATTTTAACAAAATATTAACGTTTACAATTTAAAAGGATCTAGGTGAAGATCCTTTTTGATAATCTCATGACCAAAATCCCTTAACGTGAGTTTTCGTTCCACT
CGCTTAAAATTGTTTTATAATTGCAAATGTTAAATTTTCCTAGATCCACTTCTAGGAAAAACTATTAGAGTACTGGTTTTAGGGAATTGCACTCAAAAGCAAGGTGA
Backbone from pBAD24
ori
1,820 1,830 1,840 1,850 1,860 1,870 1,880 1,890 1,900 1,910 1,920
GAGCGTCAGACCCCGTAGAAAAGATCAAAGGATCTTCTTGAGATCCTTTTTTTCTGCGCGTAATCTGCTGCTTGCAAACAAAAAAACCACCGCTACCAGCGGTGGTT
CTCGCAGTCTGGGGCATCTTTTCTAGTTTCCTAGAAGAACTCTAGGAAAAAAAGACGCGCATTAGACGACGAACGTTTGTTTTTTTGGTGGCGATGGTCGCCACCAA
Backbone from pBAD24
ori
1,930 1,940 1,950 1,960 1,970 1,980 1,990 2,000 2,010 2,020 2,030

TGTTTGCCGGATCAAGAGCTACCAACTCTTTTTCCGAAGGTAACTGGCTTCAGCAGAGCGCAGATACCAAATACTGTCCTTCTAGTGTAGCCGTAGTTAGGCCACCA
ACAAACGGCCTAGTTCTCGATGGTTGAGAAAAAGGCTTCCATTGACCGAAGTCGTCTCGCGTCTATGGTTTATGACAGGAAGATCACATCGGCATCAATCCGGTGGT

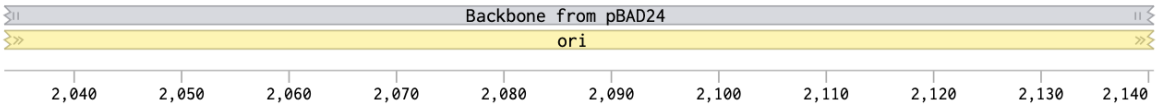

AlwNI

CTTCAAGAACTCTGTAGCACCGCCTACATACCTCGCTCTGCTAATCCTGTTACCAGTGGCTGCTGCCAGTGGCGATAAGTCGTGTCTTACCGGGTTGGACTCAAGAC
GAAGTTCTTGAGACATCGTGGCGGATGTATGGAGCGAGACGATTAGGACAATGGTCACCGACGACGGTCACCGCTATTCAGCACAGAATGGCCCAACCTGAGTTCTG

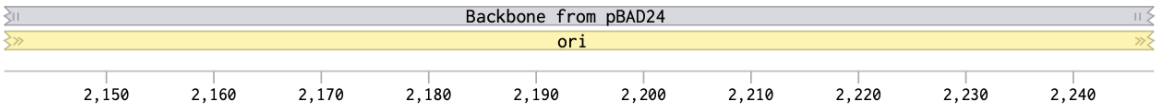

ApaLI BseYI

GATAGTTACCGGATAAGGCGCAGCGGTCGGGCTGAACGGGGGGTTCGTGCACACAGCCCAGCTTGGAGCGAACGACCTACACCGAACTGAGATACCTACAGCGTGAG
CTATCAATGGCCTATTCCGCGTCGCCAGCCCGACTTGCCCCCCAAGCACGTGTGTCGGGTCGAACCTCGCTTGCTGGATGTGGCTTGACTCTATGGATGTCGCACTC

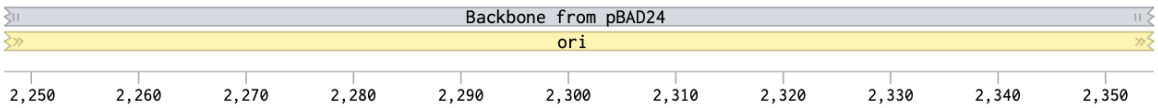

CTATGAGAAAGCGCCACGCTTCCCGAAGGGAGAAAGGCGGACAGGTATCCGGTAAGCGGCAGGGTCGGAACAGGAGAGCGCACGAGGGAGCTTCCAGGGGGAAACGC
GATACTCTTTCGCGGTGCGAAGGGCTTCCCTCTTTCCGCCTGTCCATAGGCCATTCGCCGTCCCAGCCTTGTCCTCTCGCGTGCTCCCTCGAAGGTCCCCCTTTGCG

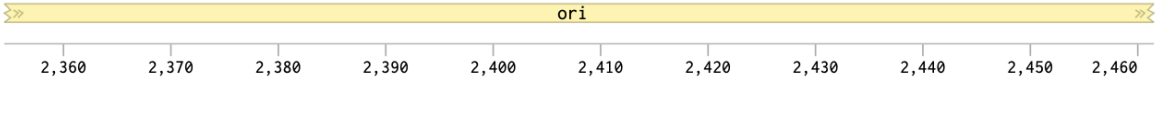

CTGGTATCTTTATAGTCCTGTCGGGTTTCGCCACCTCTGACTTGAGCGTCGATTTTTGTGATGCTCGTCAGGGGGCGGAGCCTATGGAAAAACGCCAGCAACGCGGC
GACCATAGAAATATCAGGACAGCCCAAAGCGGTGGAGACTGAACTCGCAGCTAAAAACACTACGAGCAGTCCCCCGCCTCGGATACCTTTTTGCGGTCGTTGCGCCG

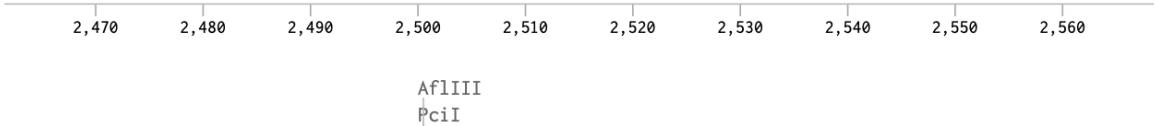

AflIII
PciI

CTTTTTACGGTTCCTGGCCTTTTGCTGGCCTTTTGCTCACATGTTCTTTCCTGCGTTATCCCCTGATTCTGTGGATAACCGTATTACCGCCTTTGAGTGAGCTGATA
GAAAAATGCCAAGGACCGGAAAACGACCGGAAAACGAGTGTACAAGAAAGGACGCAATAGGGGACTAAGACACCTATTGGCATAATGGCGGAAACTCACTCGACTAT

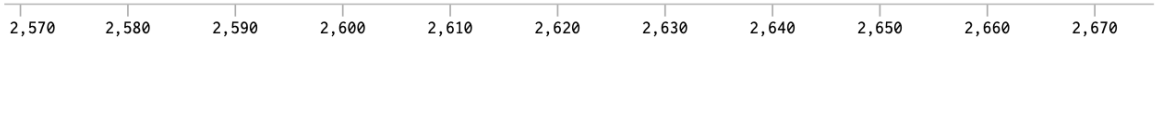

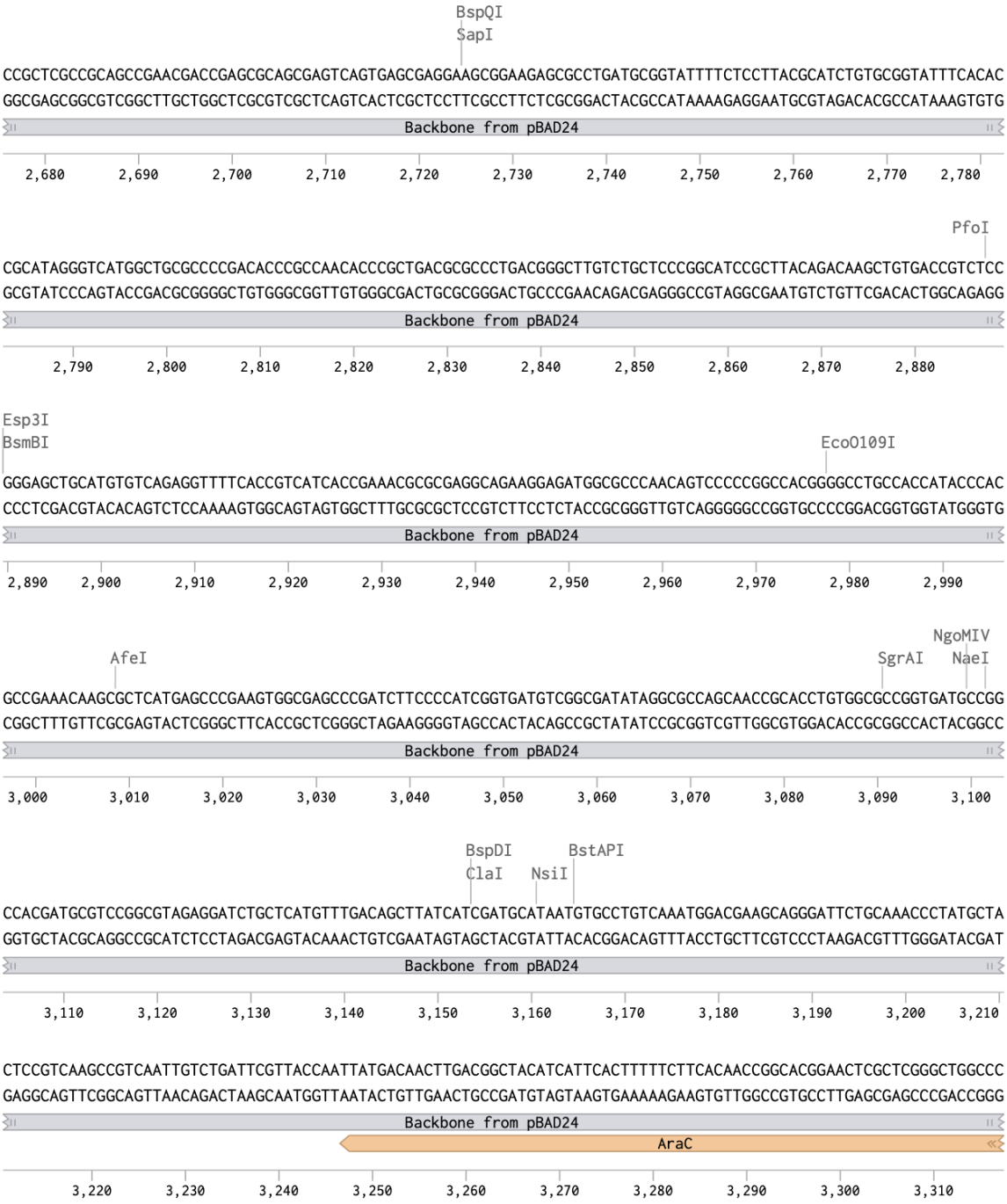
BspQI
SapI
CCGCTCGCCGCAGCCGAACGACCGAGCGCAGCGAGTCAGTGAGCGAGGAAGCGGAAGAGCGCCTGATGCGGTATTTTCTCCTTACGCATCTGTGCGGTATTTCACAC
GGCGAGCGGCGTCGGCTTGCTGGCTCGCGTCGCTCAGTCACTCGCTCCTTCGCCTTCTCGCGGACTACGCCATAAAAGAGGAATGCGTAGACACGCCATAAAGTGTG
Backbone from pBAD24
2,680 2,690 2,700 2,710 2,720 2,730 2,740 2,750 2,760 2,770 2,780
PfoI
CGCATAGGGTCATGGCTGCGCCCCGACACCCGCCAACACCCGCTGACGCGCCCTGACGGGCTTGTCTGCTCCCGGCATCCGCTTACAGACAAGCTGTGACCGTCTCC
GCGTATCCCAGTACCGACGCGGGGCTGTGGGCGGTTGTGGGCGACTGCGCGGGACTGCCCGAACAGACGAGGGCCGTAGGCGAATGTCTGTTCGACACTGGCAGAGG
Backbone from pBAD24
2,790 2,800 2,810 2,820 2,830 2,840 2,850 2,860 2,870 2,880
Esp3I
BsmBI
EcoO109I
GGGAGCTGCATGTGTCAGAGGTTTTCACCGTCATCACCGAAACGCGCGAGGCAGAAGGAGATGGCGCCCAACAGTCCCCCGGCCACGGGGCCTGCCACCATACCCAC
CCCTCGACGTACACAGTCTCCAAAAGTGGCAGTAGTGGCTTTGCGCGCTCCGTCTTCCTCTACCGCGGGTTGTCAGGGGGCCGGTGCCCCGGACGGTGGTATGGGTG
Backbone from pBAD24
2,890 2,900 2,910 2,920 2,930 2,940 2,950 2,960 2,970 2,980 2,990
NgoMIV
AfeI
SgrAI
NaeI
GCCGAAACAAGCGCTCATGAGCCCGAAGTGGCGAGCCCGATCTTCCCCATCGGTGATGTCGGCGATATAGGCGCCAGCAACCGCACCTGTGGCGCCGGTGATGCCGG
CGGCTTTGTTCGCGAGTACTCGGGCTTCACCGCTCGGGCTAGAAGGGGTAGCCACTACAGCCGCTATATCCGCGGTCGTTGGCGTGGACACCGCGGCCACTACGGCC
Backbone from pBAD24
3,000 3,010 3,020 3,030 3,040 3,050 3,060 3,070 3,080 3,090 3,100
BspDI
ClaI
NsiI
BstAPI
CCACGATGCGTCCGGCGTAGAGGATCTGCTCATGTTTGACAGCTTATCATCGATGCATAATGTGCCTGTCAAATGGACGAAGCAGGGATTCTGCAAACCCTATGCTA
GGTGCTACGCAGGCCGCATCTCCTAGACGAGTACAAACTGTCGAATAGTAGCTACGTATTACACGGACAGTTTACCTGCTTCGTCCCTAAGACGTTTGGGATACGAT
Backbone from pBAD24
3,110 3,120 3,130 3,140 3,150 3,160 3,170 3,180 3,190 3,200 3,210
CTCCGTCAAGCCGTCAATTGTCTGATTCGTTACCAATTATGACAACTTGACGGCTACATCATTCACTTTTTCTTCACAACCGGCACGGAACTCGCTCGGGCTGGCCC
GAGGCAGTTCGGCAGTTAACAGACTAAGCAATGGTTAATACTGTTGAACTGCCGATGTAGTAAGTGAAAAAGAAGTGTTGGCCGTGCCTTGAGCGAGCCCGACCGGG
Backbone from pBAD24
AraC
3,220 3,230 3,240 3,250 3,260 3,270 3,280 3,290 3,300 3,310

CGGTGCATTTTTTAAATACCCGCGAGAAATAGAGTTGATCGTCAAAACCAACATTGCGACCGACGGTGGCGATAGGCATCCGGGTGGTGCTCAAAAGCAGCTTCGCC
GCCACGTAAAAAATTTATGGGCGCTCTTTATCTCAACTAGCAGTTTTGGTTGTAACGCTGGCTGCCACCGCTATCCGTAGGCCCACCACGAGTTTTCGTCGAAGCGG

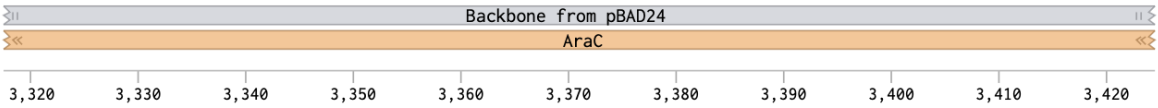

BaeI
AflII

TGGCTGATACGTTGGTCCTCGCGCCAGCTTAAGACGCTAATCCCTAACTGCTGGCGGAAAAGATGTGACAGACGCGACGGCGACAAGCAAACATGCTGTGCGACGCT
ACCGACTATGCAACCAGGAGCGCGGTCGAATTCTGCGATTAGGGATTGACGACCGCCTTTTCTACACTGTCTGCGCTGCCGCTGTTCGTTTGTACGACACGCTGCGA

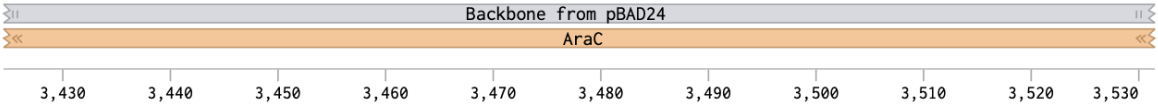

EcoRV

GGCGATATCAAAATTGCTGTCTGCCAGGTGATCGCTGATGTACTGACAAGCCTCGCGTACCCGATTATCCATCGGTGGATGGAGCGACTCGTTAATCGCTTCCATGC
CCGCTATAGTTTTAACGACAGACGGTCCACTAGCGACTACATGACTGTTCGGAGCGCATGGGCTAATAGGTAGCCACCTACCTCGCTGAGCAATTAGCGAAGGTACG

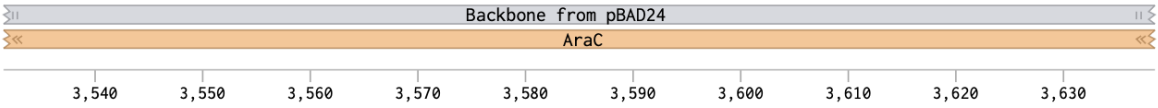

GCCGCAGTAACAATTGCTCAAGCAGATTTATCGCCAGCAGCTCCGAATAGCGCCCTTCCCCTTGCCCGGCGTTAATGATTTGCCCAAACAGGTCGCTGAAATGCGGC
CGGCGTCATTGTTAACGAGTTCGTCTAAATAGCGGTCGTCGAGGCTTATCGCGGGAAGGGGAACGGGCCGCAATTACTAAACGGGTTTGTCCAGCGACTTTACGCCG

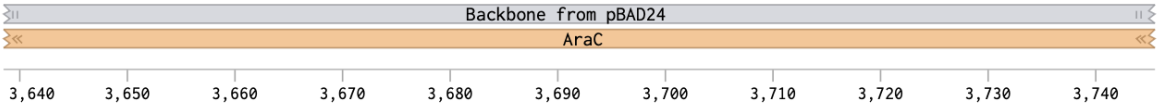

AjuI
BssHII

TGGTGCGCTTCATCCGGGCGAAAGAACCCCGTATTGGCAAATATTGACGGCCAGTTAAGCCATTCATGCCAGTAGGCGCGCGGACGAAAGTAAACCCACTGGTGATA
ACCACGCGAAGTAGGCCCGCTTTCTTGGGGCATAACCGTTTATAACTGCCGGTCAATTCGGTAAGTACGGTCATCCGCGCGCCTGCTTTCATTTGGGTGACCACTAT

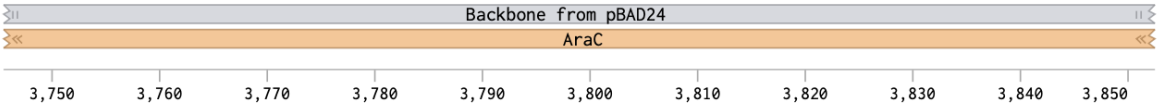

NruI
BspEI

CCATTCGCGAGCCTCCGGATGACGACCGTAGTGATGAATCTCTCCTGGCGGGAACAGCAAAATATCACCCGGTCGGCAAACAAATTCTCGTCCCTGATTTTTCACCA
GGTAAGCGCTCGGAGGCCTACTGCTGGCATCACTACTTAGAGAGGACCGCCCTTGTCGTTTTATAGTGGGCCAGCCGTTTGTTTAAGAGCAGGGACTAAAAAGTGGT

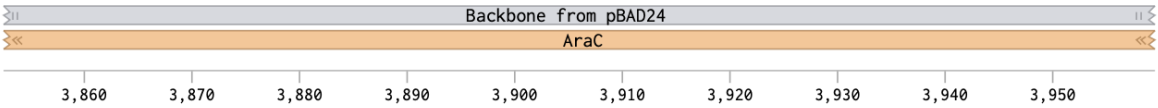

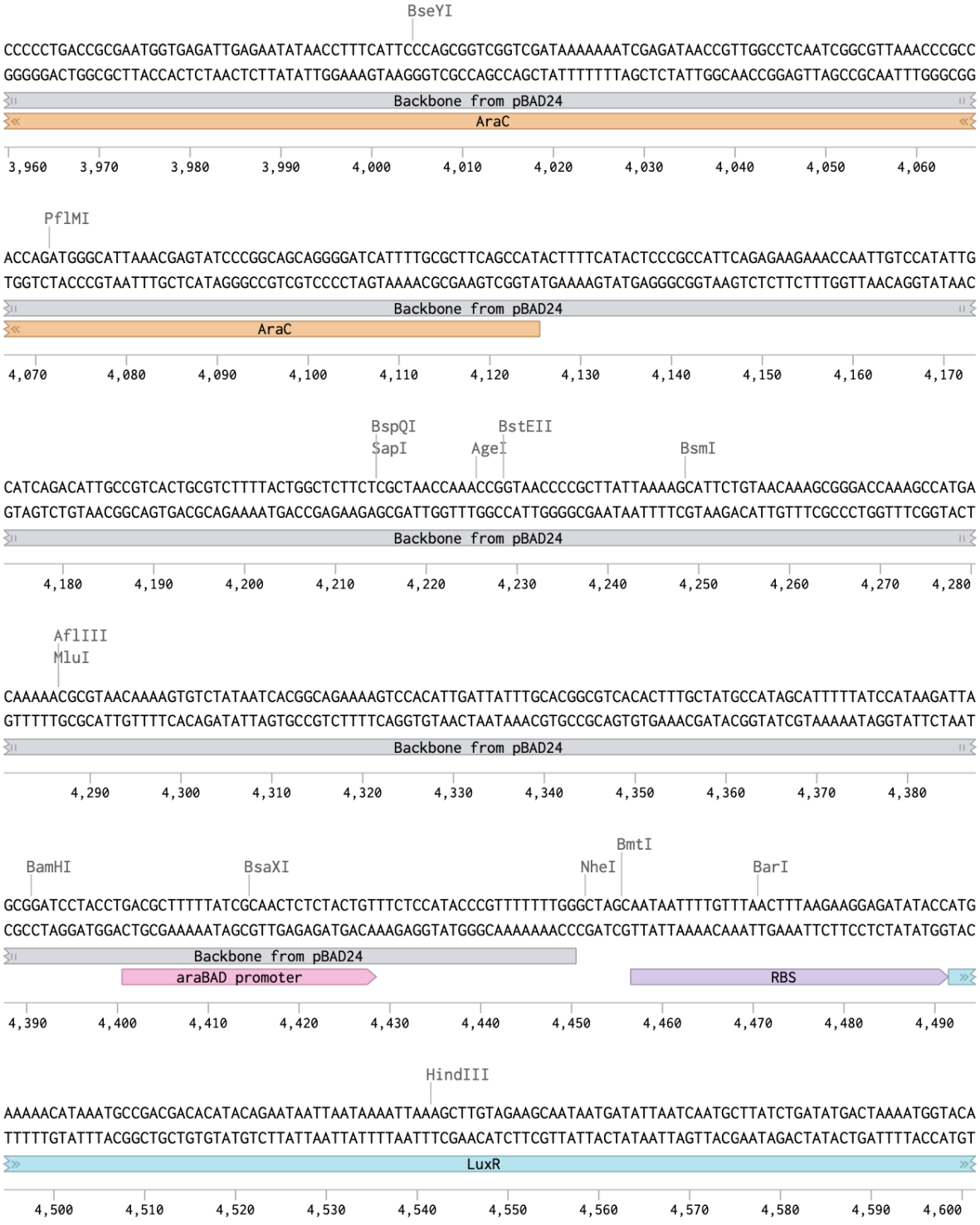
BseYI
CCCCCTGACCGCGAATGGTGAGATTGAGAATATAACCTTTCATTCCCAGCGGTCGGTCGATAAAAAAATCGAGATAACCGTTGGCCTCAATCGGCGTTAAACCCGCC
GGGGGACTGGCGCTTACCACTCTAACTCTTATATTGGAAAGTAAGGGTCGCCAGCCAGCTATTTTTTTAGCTCTATTGGCAACCGGAGTTAGCCGCAATTTGGGCGG
Backbone from pBAD24
AraC
3,960 3,970 3,980 3,990 4,000 4,010 4,020 4,030 4,040 4,050 4,060
PflMI
ACCAGATGGGCATTAAACGAGTATCCCGGCAGCAGGGGATCATTTTGCGCTTCAGCCATACTTTTCATACTCCCGCCATTCAGAGAAGAAACCAATTGTCCATATTG
TGGTCTACCCGTAATTTGCTCATAGGGCCGTCGTCCCCTAGTAAAACGCGAAGTCGGTATGAAAAGTATGAGGGCGGTAAGTCTCTTCTTTGGTTAACAGGTATAAC
Backbone from pBAD24
AraC
4,070 4,080 4,090 4,100 4,110 4,120 4,130 4,140 4,150 4,160 4,170
BspQI
SapI
BstEII
AgeI
BsmI
CATCAGACATTGCCGTCACTGCGTCTTTTACTGGCTCTTCTCGCTAACCAAACCGGTAACCCCGCTTATTAAAAGCATTCTGTAACAAAGCGGGACCAAAGCCATGA
GTAGTCTGTAACGGCAGTGACGCAGAAAATGACCGAGAAGAGCGATTGGTTTGGCCATTGGGGCGAATAATTTTCGTAAGACATTGTTTCGCCCTGGTTTCGGTACT
Backbone from pBAD24
4,180 4,190 4,200 4,210 4,220 4,230 4,240 4,250 4,260 4,270 4,280
AflIII
MluI
CAAAAACGCGTAACAAAAGTGTCTATAATCACGGCAGAAAAGTCCACATTGATTATTTGCACGGCGTCACACTTTGCTATGCCATAGCATTTTTATCCATAAGATTA
GTTTTTGCGCATTGTTTTCACAGATATTAGTGCCGTCTTTTCAGGTGTAACTAATAAACGTGCCGCAGTGTGAAACGATACGGTATCGTAAAAATAGGTATTCTAAT
Backbone from pBAD24
4,290 4,300 4,310 4,320 4,330 4,340 4,350 4,360 4,370 4,380
BmtI
BamHI
BsaXI
NheI
BarI
GCGGATCCTACCTGACGCTTTTTATCGCAACTCTCTACTGTTTCTCCATACCCGTTTTTTTGGGCTAGCAATAATTTTGTTTAACTTTAAGAAGGAGATATACCATG
CGCCTAGGATGGACTGCGAAAAATAGCGTTGAGAGATGACAAAGAGGTATGGGCAAAAAAACCCGATCGTTATTAAAACAAATTGAAATTCTTCCTCTATATGGTAC
Backbone from pBAD24
araBAD promoter
RBS
4,390 4,400 4,410 4,420 4,430 4,440 4,450 4,460 4,470 4,480 4,490
HindIII
AAAAACATAAATGCCGACGACACATACAGAATAATTAATAAAATTAAAGCTTGTAGAAGCAATAATGATATTAATCAATGCTTATCTGATATGACTAAAATGGTACA
TTTTTGTATTTACGGCTGCTGTGTATGTCTTATTAATTATTTTAATTTCGAACATCTTCGTTATTACTATAATTAGTTACGAATAGACTATACTGATTTTACCATGT
LuxR
4,500 4,510 4,520 4,530 4,540 4,550 4,560 4,570 4,580 4,590 4,600

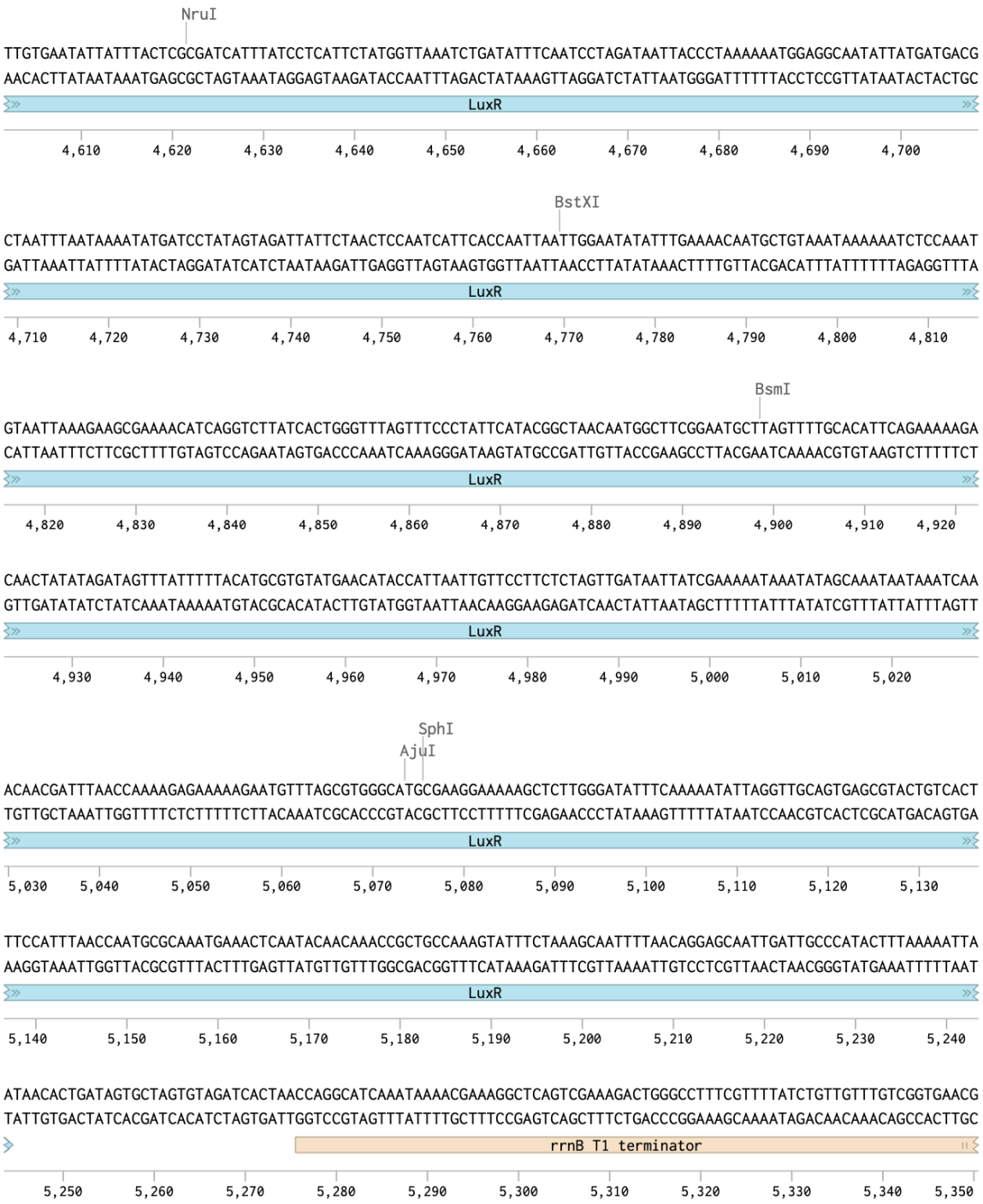
NruI
TTGTGAATATTATTTACTCGCGATCATTTATCCTCATTCTATGGTTAAATCTGATATTTCAATCCTAGATAATTACCCTAAAAAATGGAGGCAATATTATGATGACG
AACACTTATAATAAATGAGCGCTAGTAAATAGGAGTAAGATACCAATTTAGACTATAAAGTTAGGATCTATTAATGGGATTTTTTACCTCCGTTATAATACTACTGC
LuxR
4,610 4,620 4,630 4,640 4,650 4,660 4,670 4,680 4,690 4,700
BstXI
CTAATTTAATAAAATATGATCCTATAGTAGATTATTCTAACTCCAATCATTCACCAATTAATTGGAATATATTTGAAAACAATGCTGTAAATAAAAAATCTCCAAAT
GATTAAATTATTTTATACTAGGATATCATCTAATAAGATTGAGGTTAGTAAGTGGTTAATTAACCTTATATAAACTTTTGTTACGACATTTATTTTTTAGAGGTTTA
LuxR
4,710 4,720 4,730 4,740 4,750 4,760 4,770 4,780 4,790 4,800 4,810
BsmI
GTAATTAAAGAAGCGAAAACATCAGGTCTTATCACTGGGTTTAGTTTCCCTATTCATACGGCTAACAATGGCTTCGGAATGCTTAGTTTTGCACATTCAGAAAAAGA
CATTAATTTCTTCGCTTTTGTAGTCCAGAATAGTGACCCAAATCAAAGGGATAAGTATGCCGATTGTTACCGAAGCCTTACGAATCAAAACGTGTAAGTCTTTTTCT
LuxR
4,820 4,830 4,840 4,850 4,860 4,870 4,880 4,890 4,900 4,910 4,920
CAACTATATAGATAGTTTATTTTTACATGCGTGTATGAACATACCATTAATTGTTCCTTCTCTAGTTGATAATTATCGAAAAATAAATATAGCAAATAATAAATCAA
GTTGATATATCTATCAAATAAAAATGTACGCACATACTTGTATGGTAATTAACAAGGAAGAGATCAACTATTAATAGCTTTTTATTTATATCGTTTATTATTTAGTT
LuxR
4,930 4,940 4,950 4,960 4,970 4,980 4,990 5,000 5,010 5,020
SphI
AjuI
ACAACGATTTAACCAAAAGAGAAAAAGAATGTTTAGCGTGGGCATGCGAAGGAAAAAGCTCTTGGGATATTTCAAAAATATTAGGTTGCAGTGAGCGTACTGTCACT
TGTTGCTAAATTGGTTTTCTCTTTTTCTTACAAATCGCACCCGTACGCTTCCTTTTTCGAGAACCCTATAAAGTTTTTATAATCCAACGTCACTCGCATGACAGTGA
LuxR
5,030 5,040 5,050 5,060 5,070 5,080 5,090 5,100 5,110 5,120 5,130
TTCCATTTAACCAATGCGCAAATGAAACTCAATACAACAAACCGCTGCCAAAGTATTTCTAAAGCAATTTTAACAGGAGCAATTGATTGCCCATACTTTAAAAATTA
AAGGTAAATTGGTTACGCGTTTACTTTGAGTTATGTTGTTTGGCGACGGTTTCATAAAGATTTCGTTAAAATTGTCCTCGTTAACTAACGGGTATGAAATTTTTAAT
LuxR
5,140 5,150 5,160 5,170 5,180 5,190 5,200 5,210 5,220 5,230 5,240
ATAACACTGATAGTGCTAGTGTAGATCACTAACCAGGCATCAAATAAAACGAAAGGCTCAGTCGAAAGACTGGGCCTTTCGTTTTATCTGTTGTTTGTCGGTGAACG
TATTGTGACTATCACGATCACATCTAGTGATTGGTCCGTAGTTTATTTTGCTTTCCGAGTCAGCTTTCTGACCCGGAAAGCAAAATAGACAACAAACAGCCACTTGC
rrnB T1 terminator
5,250 5,260 5,270 5,280 5,290 5,300 5,310 5,320 5,330 5,340 5,350

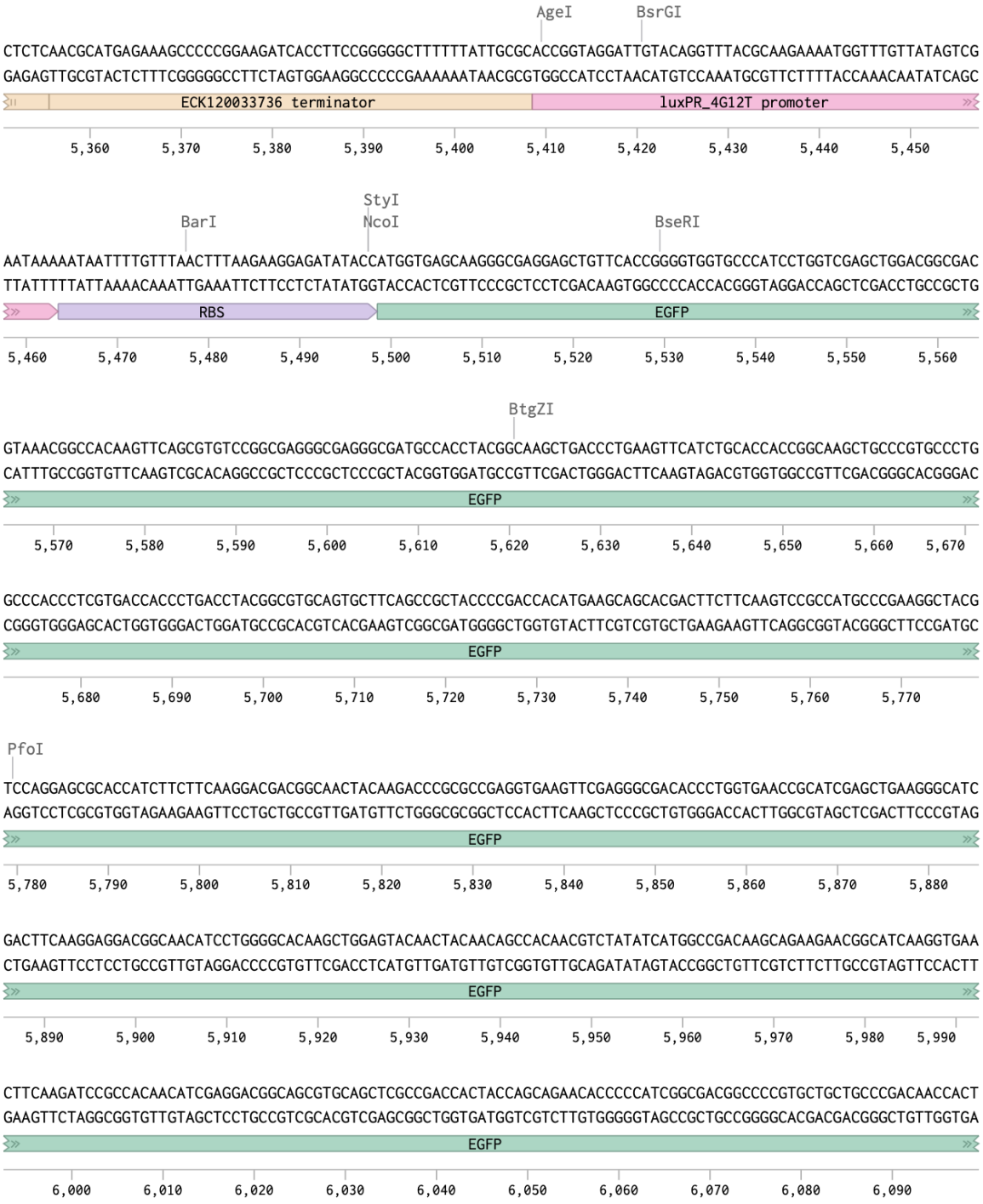
AgeI
BsrGI
CTCTCAACGCATGAGAAAGCCCCCGGAAGATCACCTTCCGGGGGCTTTTTTATTGCGCACCGGTAGGATTGTACAGGTTTACGCAAGAAAATGGTTTGTTATAGTCG
GAGAGTTGCGTACTCTTTCGGGGGCCTTCTAGTGGAAGGCCCCCGAAAAAATAACGCGTGGCCATCCTAACATGTCCAAATGCGTTCTTTTACCAAACAATATCAGC
ECK120033736 terminator
luxPR_4G12T promoter
5,360
5,370
5,380
5,390
5,400
5,410
5,420
5,430
5,440
5,450
StyI
NcoI
BarI
BseRI
AATAAAAATAATTTTGTTTAACTTTAAGAAGGAGATATACCATGGTGAGCAAGGGCGAGGAGCTGTTCACCGGGGTGGTGCCCATCCTGGTCGAGCTGGACGGCGAC
TTATTTTTATTAAAACAAATTGAAATTCTTCCTCTATATGGTACCACTCGTTCCCGCTCCTCGACAAGTGGCCCCACCACGGGTAGGACCAGCTCGACCTGCCGCTG
RBS
EGFP
5,460
5,470
5,480
5,490
5,500
5,510
5,520
5,530
5,540
5,550
5,560
BtgZI
GTAAACGGCCACAAGTTCAGCGTGTCCGGCGAGGGCGAGGGCGATGCCACCTACGGCAAGCTGACCCTGAAGTTCATCTGCACCACCGGCAAGCTGCCCGTGCCCTG
CATTTGCCGGTGTTCAAGTCGCACAGGCCGCTCCCGCTCCCGCTACGGTGGATGCCGTTCGACTGGGACTTCAAGTAGACGTGGTGGCCGTTCGACGGGCACGGGAC
EGFP
5,570
5,580
5,590
5,600
5,610
5,620
5,630
5,640
5,650
5,660
5,670
GCCCACCCTCGTGACCACCCTGACCTACGGCGTGCAGTGCTTCAGCCGCTACCCCGACCACATGAAGCAGCACGACTTCTTCAAGTCCGCCATGCCCGAAGGCTACG
CGGGTGGGAGCACTGGTGGGACTGGATGCCGCACGTCACGAAGTCGGCGATGGGGCTGGTGTACTTCGTCGTGCTGAAGAAGTTCAGGCGGTACGGGCTTCCGATGC
EGFP
5,680
5,690
5,700
5,710
5,720
5,730
5,740
5,750
5,760
5,770
PfoI
TCCAGGAGCGCACCATCTTCTTCAAGGACGACGGCAACTACAAGACCCGCGCCGAGGTGAAGTTCGAGGGCGACACCCTGGTGAACCGCATCGAGCTGAAGGGCATC
AGGTCCTCGCGTGGTAGAAGAAGTTCCTGCTGCCGTTGATGTTCTGGGCGCGGCTCCACTTCAAGCTCCCGCTGTGGGACCACTTGGCGTAGCTCGACTTCCCGTAG
EGFP
5,780
5,790
5,800
5,810
5,820
5,830
5,840
5,850
5,860
5,870
5,880
GACTTCAAGGAGGACGGCAACATCCTGGGGCACAAGCTGGAGTACAACTACAACAGCCACAACGTCTATATCATGGCCGACAAGCAGAAGAACGGCATCAAGGTGAA
CTGAAGTTCCTCCTGCCGTTGTAGGACCCCGTGTTCGACCTCATGTTGATGTTGTCGGTGTTGCAGATATAGTACCGGCTGTTCGTCTTCTTGCCGTAGTTCCACTT
EGFP
5,890
5,900
5,910
5,920
5,930
5,940
5,950
5,960
5,970
5,980
5,990
CTTCAAGATCCGCCACAACATCGAGGACGGCAGCGTGCAGCTCGCCGACCACTACCAGCAGAACACCCCCATCGGCGACGGCCCCGTGCTGCTGCCCGACAACCACT
GAAGTTCTAGGCGGTGTTGTAGCTCCTGCCGTCGCACGTCGAGCGGCTGGTGATGGTCGTCTTGTGGGGGTAGCCGCTGCCGGGGCACGACGACGGGCTGTTGGTGA
EGFP
6,000
6,010
6,020
6,030
6,040
6,050
6,060
6,070
6,080
6,090

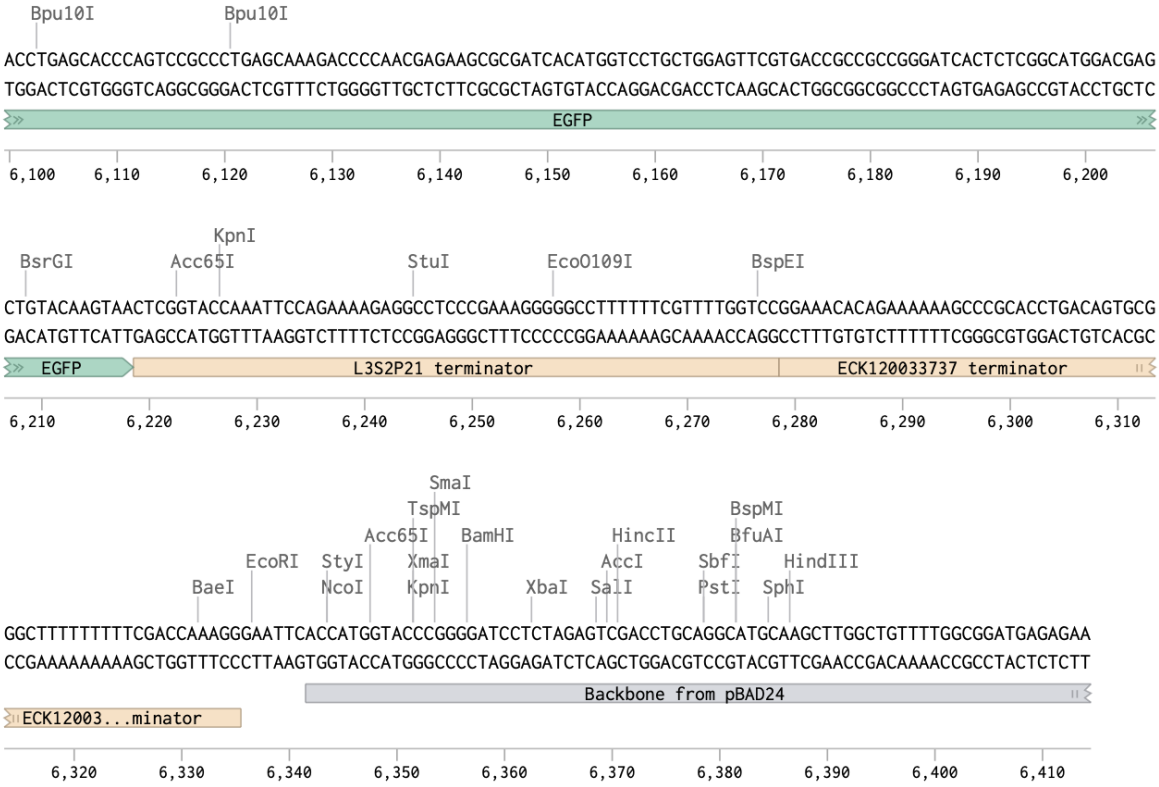

Figure B. 2 Sequence map of the sensor strain

B.2 Producer

B.2.1 Plasmid map

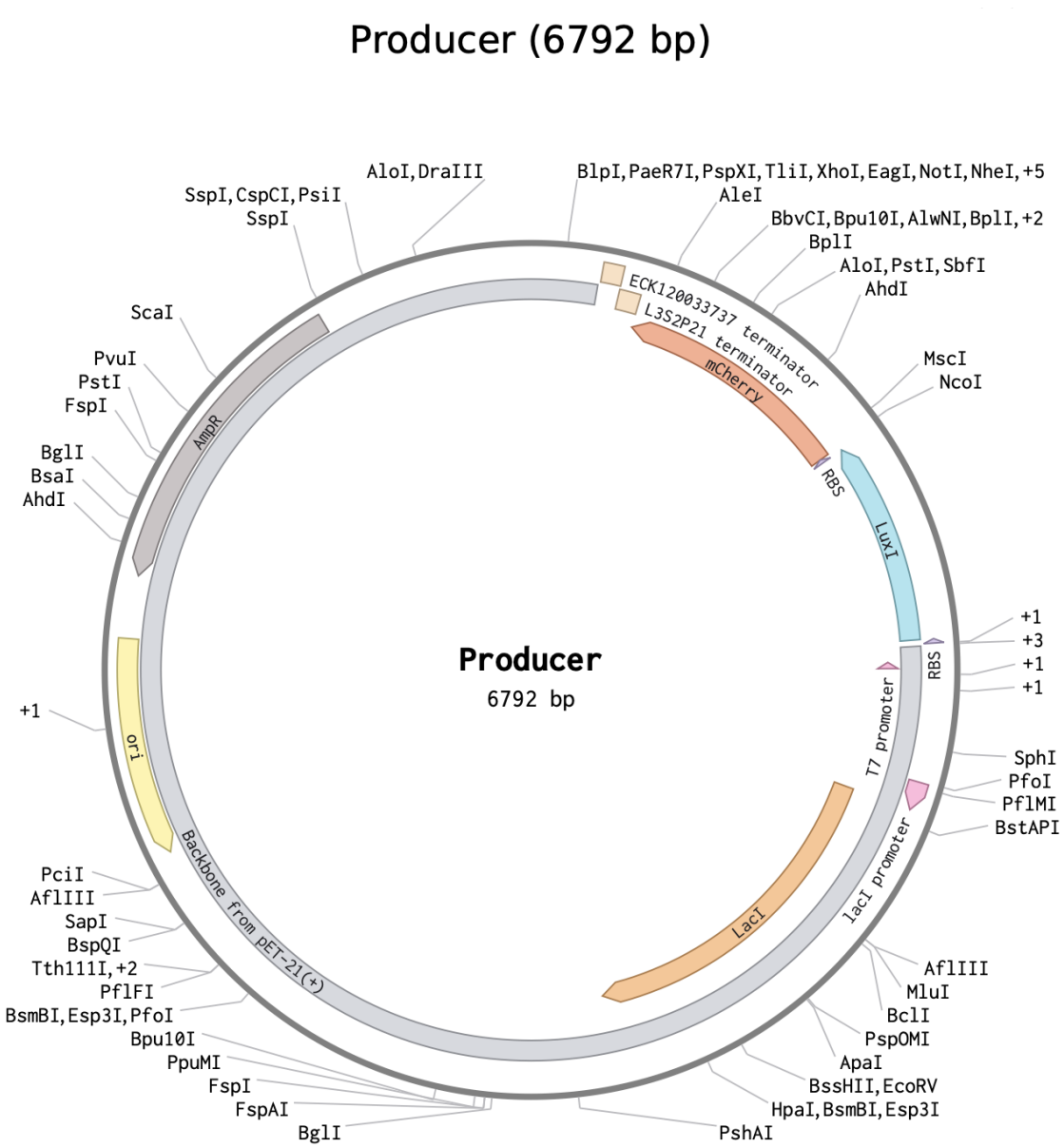

Figure B. 3 Plasmid map of the producer strain

B.2.2 Sequence map

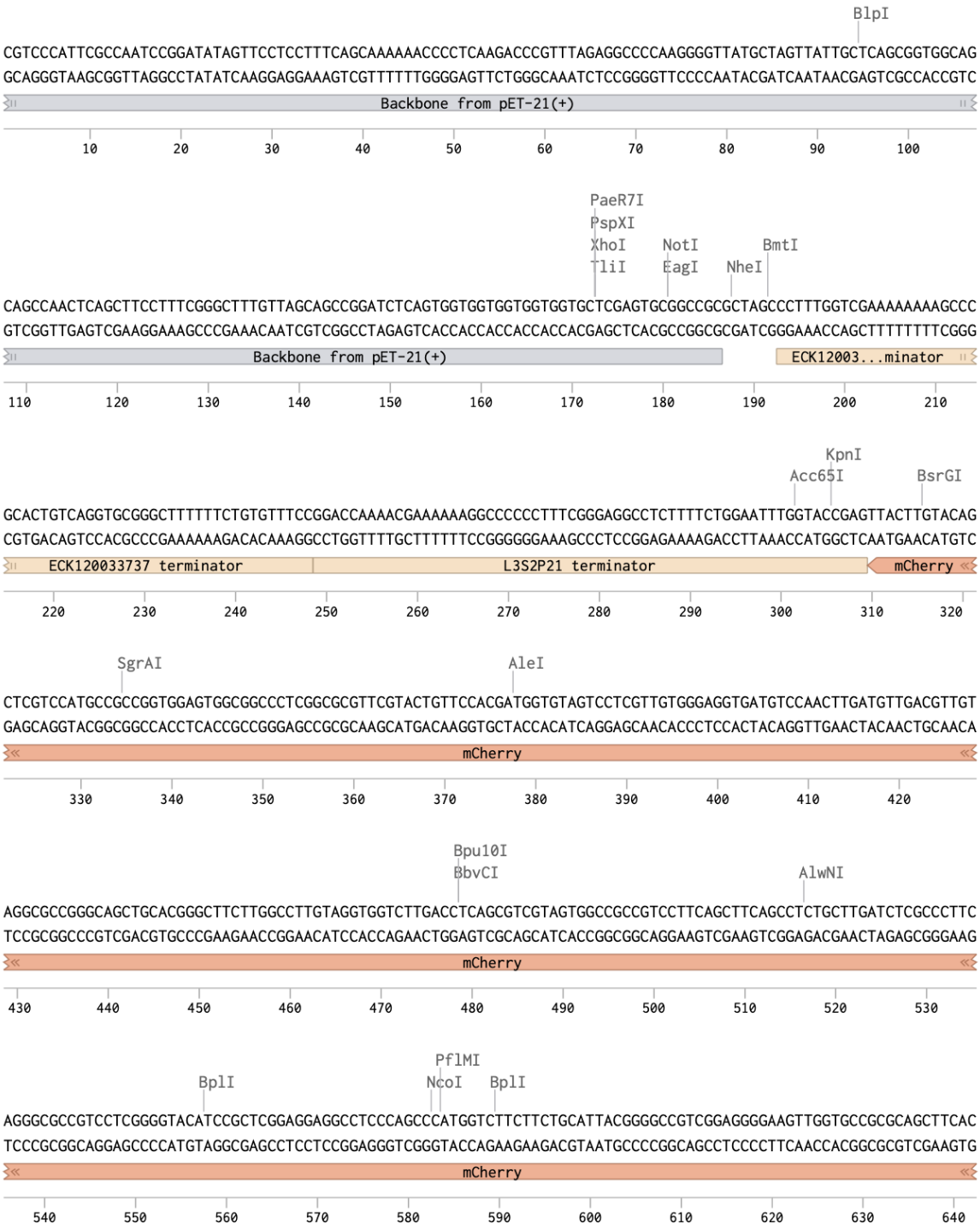

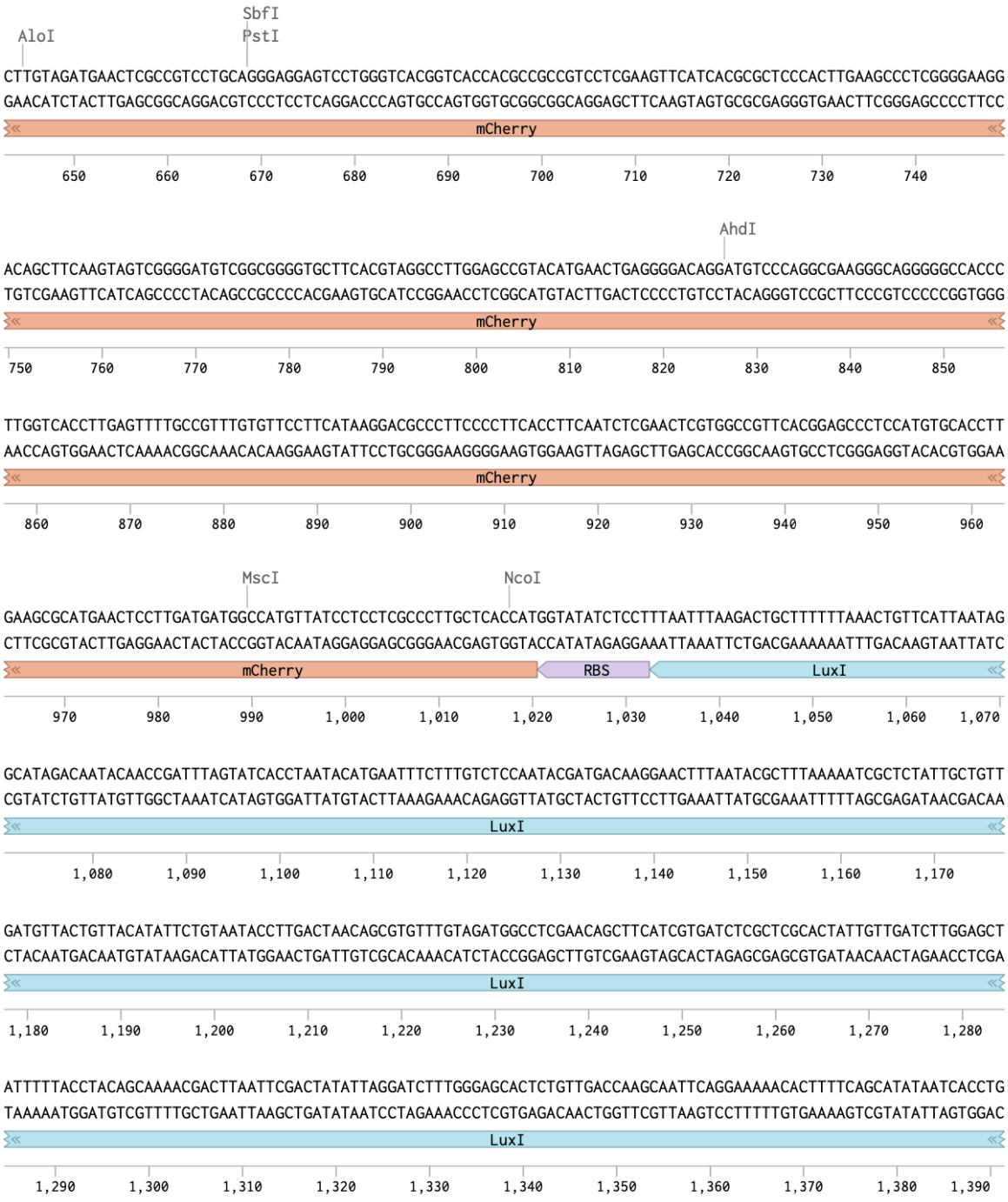
SbfI
AloI
PstI
CTTGTAGATGAACTCGCCGTCCTGCAGGGAGGAGTCCTGGGTCACGGTCACCACGCCGCCGTCCTCGAAGTTCATCACGCGCTCCCACTTGAAGCCCTCGGGGAAGG
GAACATCTACTTGAGCGGCAGGACGTCCCTCCTCAGGACCCAGTGCCAGTGGTGCGGCGGCAGGAGCTTCAAGTAGTGCGCGAGGGTGAACTTCGGGAGCCCCTTCC
mCherry
650
660
670
680
690
700
710
720
730
740
AhdI
ACAGCTTCAAGTAGTCGGGGATGTCGGCGGGGTGCTTCACGTAGGCCTTGGAGCCGTACATGAACTGAGGGGACAGGATGTCCCAGGCGAAGGGCAGGGGGCCACCC
TGTCGAAGTTCATCAGCCCCTACAGCCGCCCCACGAAGTGCATCCGGAACCTCGGCATGTACTTGACTCCCCTGTCCTACAGGGTCCGCTTCCCGTCCCCCGGTGGG
mCherry
750
760
770
780
790
800
810
820
830
840
850
TTGGTCACCTTGAGTTTTGCCGTTTGTGTTCCTTCATAAGGACGCCCTTCCCCTTCACCTTCAATCTCGAACTCGTGGCCGTTCACGGAGCCCTCCATGTGCACCTT
AACCAGTGGAACTCAAAACGGCAAACACAAGGAAGTATTCCTGCGGGAAGGGGAAGTGGAAGTTAGAGCTTGAGCACCGGCAAGTGCCTCGGGAGGTACACGTGGAA
mCherry
860
870
880
890
900
910
920
930
940
950
960
MscI
NcoI
GAAGCGCATGAACTCCTTGATGATGGCCATGTTATCCTCCTCGCCCTTGCTCACCATGGTATATCTCCTTTAATTTAAGACTGCTTTTTTAAACTGTTCATTAATAG
CTTCGCGTACTTGAGGAACTACTACCGGTACAATAGGAGGAGCGGGAACGAGTGGTACCATATAGAGGAAATTAAATTCTGACGAAAAAATTTGACAAGTAATTATC
mCherry
RBS
LuxI
970
980
990
1,000
1,010
1,020
1,030
1,040
1,050
1,060
1,070
GCATAGACAATACAACCGATTTAGTATCACCTAATACATGAATTTCTTTGTCTCCAATACGATGACAAGGAACTTTAATACGCTTTAAAAATCGCTCTATTGCTGTT
CGTATCTGTTATGTTGGCTAAATCATAGTGGATTATGTACTTAAAGAAACAGAGGTTATGCTACTGTTCCTTGAAATTATGCGAAATTTTTAGCGAGATAACGACAA
LuxI
1,080
1,090
1,100
1,110
1,120
1,130
1,140
1,150
1,160
1,170
GATGTTACTGTTACATATTCTGTAATACCTTGACTAACAGCGTGTTTGTAGATGGCCTCGAACAGCTTCATCGTGATCTCGCTCGCACTATTGTTGATCTTGGAGCT
CTACAATGACAATGTATAAGACATTATGGAACTGATTGTCGCACAAACATCTACCGGAGCTTGTCGAAGTAGCACTAGAGCGAGCGTGATAACAACTAGAACCTCGA
LuxI
1,180
1,190
1,200
1,210
1,220
1,230
1,240
1,250
1,260
1,270
1,280
ATTTTTACCTACAGCAAAACGACTTAATTCGACTATATTAGGATCTTTGGGAGCACTCTGTTGACCAAGCAATTCAGGAAAAACACTTTTCAGCATATAATCACCTG
TAAAAATGGATGTCGTTTTGCTGAATTAAGCTGATATAATCCTAGAAACCCTCGTGAGACAACTGGTTCGTTAAGTCCTTTTTGTGAAAAGTCGTATATTAGTGGAC
LuxI
1,290
1,300
1,310
1,320
1,330
1,340
1,350
1,360
1,370
1,380
1,390

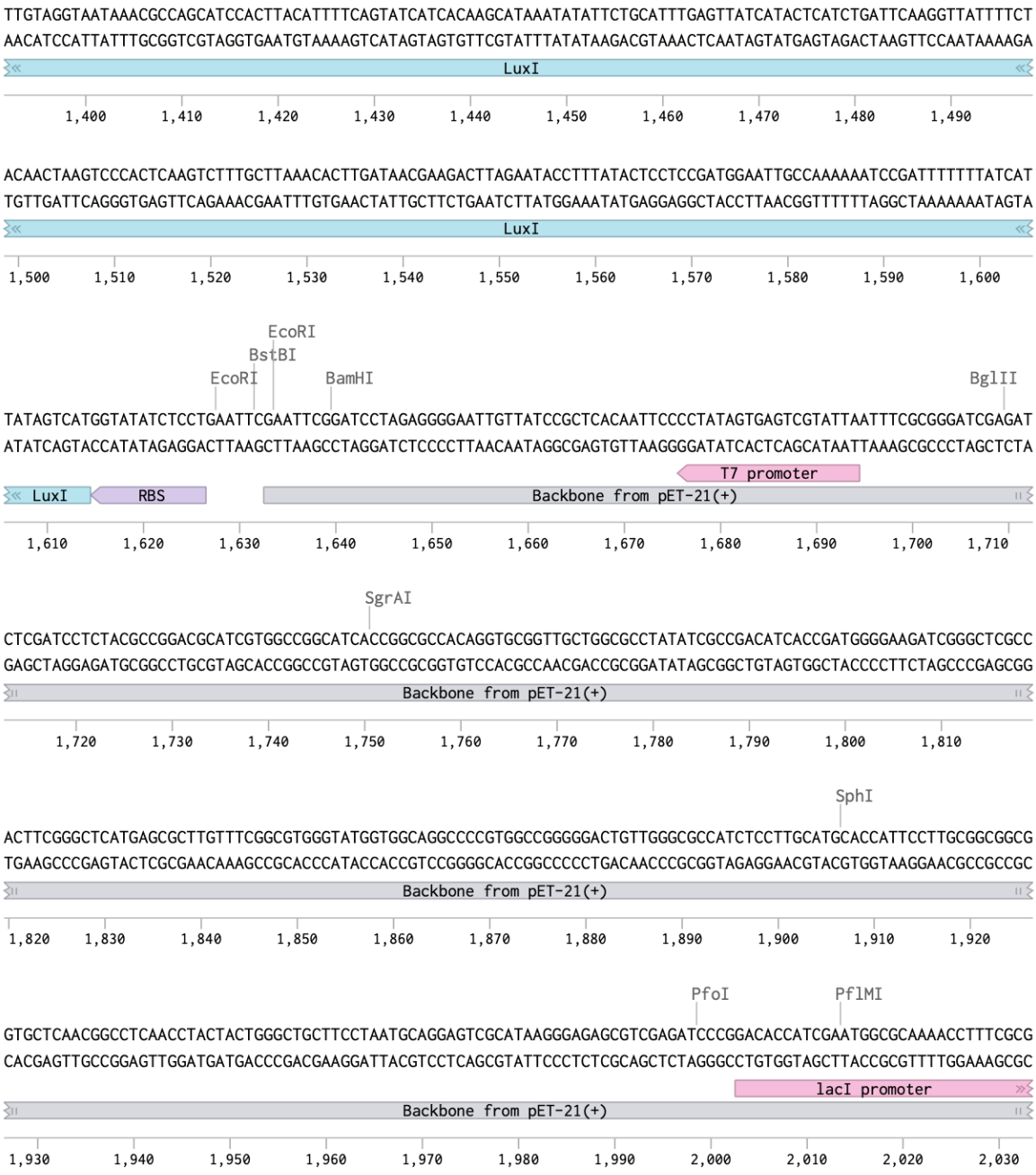
TTGTAGGTAATAAACGCCAGCATCCACTTACATTTTCAGTATCATCACAAGCATAAATATATTCTGCATTTGAGTTATCATACTCATCTGATTCAAGGTTATTTTCT
AACATCCATTATTTGCGGTCGTAGGTGAATGTAAAAGTCATAGTAGTGTTCGTATTTATATAAGACGTAAACTCAATAGTATGAGTAGACTAAGTTCCAATAAAAGA
LuxI
1,400 1,410 1,420 1,430 1,440 1,450 1,460 1,470 1,480 1,490
ACAACTAAGTCCCACTCAAGTCTTTGCTTAAACACTTGATAACGAAGACTTAGAATACCTTTATACTCCTCCGATGGAATTGCCAAAAAATCCGATTTTTTTATCAT
TGTTGATTCAGGGTGAGTTCAGAAACGAATTTGTGAACTATTGCTTCTGAATCTTATGGAAATATGAGGAGGCTACCTTAACGGTTTTTTAGGCTAAAAAAATAGTA
LuxI
1,500 1,510 1,520 1,530 1,540 1,550 1,560 1,570 1,580 1,590 1,600
EcoRI
BstBI
EcoRI
BamHI
BglII
TATAGTCATGGTATATCTCCTGAATTCGAATTCGGATCCTAGAGGGGAATTGTTATCCGCTCACAATTCCCCTATAGTGAGTCGTATTAATTTCGCGGGATCGAGAT
ATATCAGTACCATATAGAGGACTTAAGCTTAAGCCTAGGATCTCCCCTTAACAATAGGCGAGTGTTAAGGGGATATCACTCAGCATAATTAAAGCGCCCTAGCTCTA
T7 promoter
LuxI
RBS
Backbone from pET-21(+)
1,610 1,620 1,630 1,640 1,650 1,660 1,670 1,680 1,690 1,700 1,710
SgrAI
CTCGATCCTCTACGCCGGACGCATCGTGGCCGGCATCACCGGCGCCACAGGTGCGGTTGCTGGCGCCTATATCGCCGACATCACCGATGGGGAAGATCGGGCTCGCC
GAGCTAGGAGATGCGGCCTGCGTAGCACCGGCCGTAGTGGCCGCGGTGTCCACGCCAACGACCGCGGATATAGCGGCTGTAGTGGCTACCCCTTCTAGCCCGAGCGG
Backbone from pET-21(+)
1,720 1,730 1,740 1,750 1,760 1,770 1,780 1,790 1,800 1,810
SphI
ACTTCGGGCTCATGAGCGCTTGTTTCGGCGTGGGTATGGTGGCAGGCCCCGTGGCCGGGGGACTGTTGGGCGCCATCTCCTTGCATGCACCATTCCTTGCGGCGGCG
TGAAGCCCGAGTACTCGCGAACAAAGCCGCACCCATACCACCGTCCGGGGCACCGGCCCCCTGACAACCCGCGGTAGAGGAACGTACGTGGTAAGGAACGCCGCCGC
Backbone from pET-21(+)
1,820 1,830 1,840 1,850 1,860 1,870 1,880 1,890 1,900 1,910 1,920
PfoI
PflMI
GTGCTCAACGGCCTCAACCTACTACTGGGCTGCTTCCTAATGCAGGAGTCGCATAAGGGAGAGCGTCGAGATCCCGGACACCATCGAATGGCGCAAAACCTTTCGCG
CACGAGTTGCCGGAGTTGGATGATGACCCGACGAAGGATTACGTCCTCAGCGTATTCCCTCTCGCAGCTCTAGGGCCTGTGGTAGCTTACCGCGTTTTGGAAAGCGC
lacI promoter
Backbone from pET-21(+)
1,930 1,940 1,950 1,960 1,970 1,980 1,990 2,000 2,010 2,020 2,030

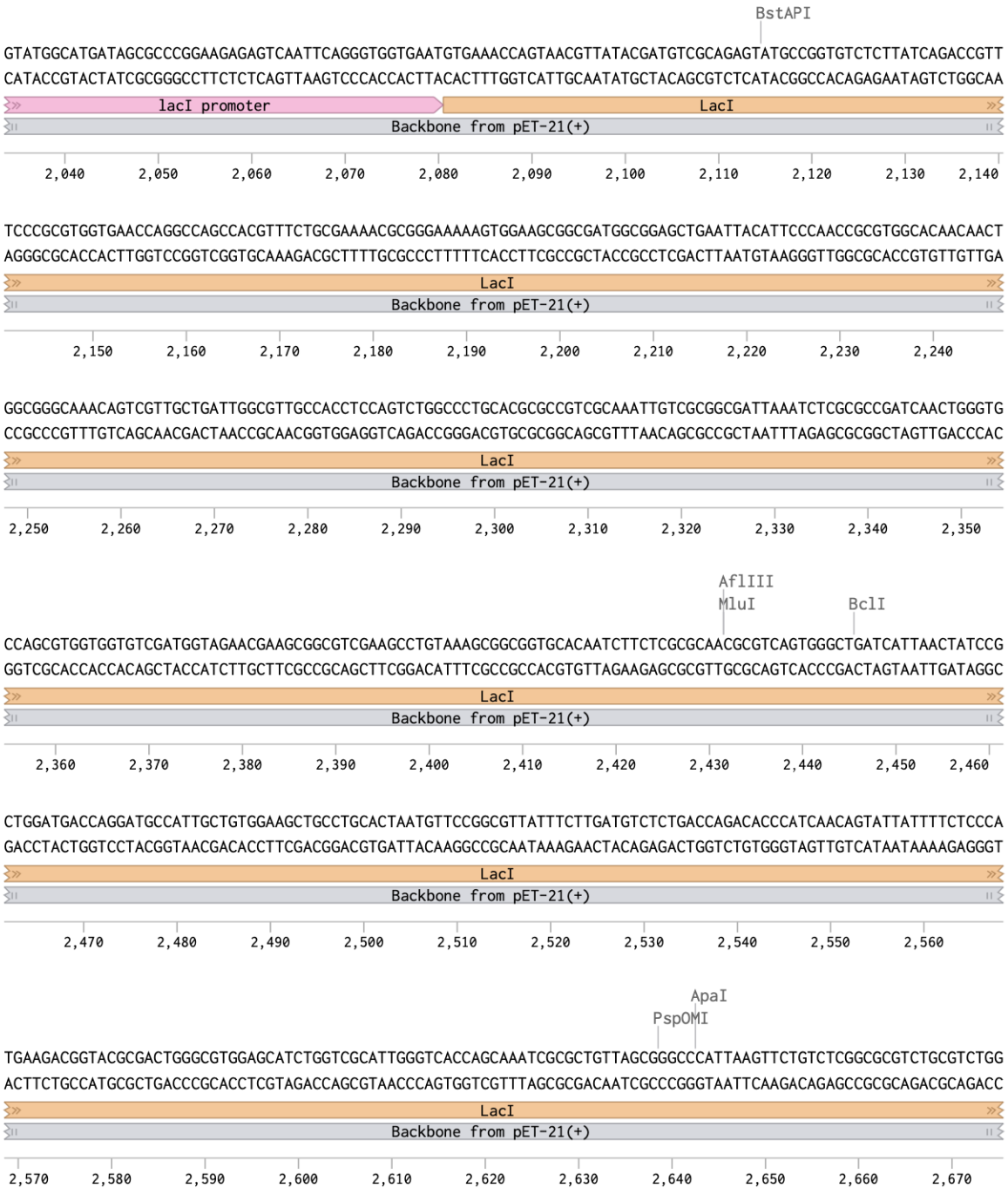
BstAPI
GTATGGCATGATAGCGCCCGGAAGAGAGTCAATTCAGGGTGGTGAATGTGAAACCAGTAACGTTATACGATGTCGCAGAGTATGCCGGTGTCTCTTATCAGACCGTT
CATACCGTACTATCGCGGGCCTTCTCTCAGTTAAGTCCCACCACTTACACTTTGGTCATTGCAATATGCTACAGCGTCTCATACGGCCACAGAGAATAGTCTGGCAA
lacI promoter
LacI
Backbone from pET-21(+)
2,040 2,050 2,060 2,070 2,080 2,090 2,100 2,110 2,120 2,130 2,140
TCCCGCGTGGTGAACCAGGCCAGCCACGTTTCTGCGAAAACGCGGGAAAAAGTGGAAGCGGCGATGGCGGAGCTGAATTACATTCCCAACCGCGTGGCACAACAACT
AGGGCGCACCACTTGGTCCGGTCGGTGCAAAGACGCTTTTGCGCCCTTTTTCACCTTCGCCGCTACCGCCTCGACTTAATGTAAGGGTTGGCGCACCGTGTTGTTGA
LacI
Backbone from pET-21(+)
2,150 2,160 2,170 2,180 2,190 2,200 2,210 2,220 2,230 2,240
GGCGGGCAAACAGTCGTTGCTGATTGGCGTTGCCACCTCCAGTCTGGCCCTGCACGCGCCGTCGCAAATTGTCGCGGCGATTAAATCTCGCGCCGATCAACTGGGTG
CCGCCCGTTTGTCAGCAACGACTAACCGCAACGGTGGAGGTCAGACCGGGACGTGCGCGGCAGCGTTTAACAGCGCCGCTAATTTAGAGCGCGGCTAGTTGACCCAC
LacI
Backbone from pET-21(+)
2,250 2,260 2,270 2,280 2,290 2,300 2,310 2,320 2,330 2,340 2,350
AflIII
MluI
BclI
CCAGCGTGGTGGTGTCGATGGTAGAACGAAGCGGCGTCGAAGCCTGTAAAGCGGCGGTGCACAATCTTCTCGCGCAACGCGTCAGTGGGCTGATCATTAACTATCCG
GGTCGCACCACCACAGCTACCATCTTGCTTCGCCGCAGCTTCGGACATTTCGCCGCCACGTGTTAGAAGAGCGCGTTGCGCAGTCACCCGACTAGTAATTGATAGGC
LacI
Backbone from pET-21(+)
2,360 2,370 2,380 2,390 2,400 2,410 2,420 2,430 2,440 2,450 2,460
CTGGATGACCAGGATGCCATTGCTGTGGAAGCTGCCTGCACTAATGTTCCGGCGTTATTTCTTGATGTCTCTGACCAGACACCCATCAACAGTATTATTTTCTCCCA
GACCTACTGGTCCTACGGTAACGACACCTTCGACGGACGTGATTACAAGGCCGCAATAAAGAACTACAGAGACTGGTCTGTGGGTAGTTGTCATAATAAAAGAGGGT
LacI
Backbone from pET-21(+)
2,470 2,480 2,490 2,500 2,510 2,520 2,530 2,540 2,550 2,560
ApaI
PspOMI
TGAAGACGGTACGCGACTGGGCGTGGAGCATCTGGTCGCATTGGGTCACCAGCAAATCGCGCTGTTAGCGGGCCCATTAAGTTCTGTCTCGGCGCGTCTGCGTCTGG
ACTTCTGCCATGCGCTGACCCGCACCTCGTAGACCAGCGTAACCCAGTGGTCGTTTAGCGCGACAATCGCCCGGGTAATTCAAGACAGAGCCGCGCAGACGCAGACC
LacI
Backbone from pET-21(+)
2,570 2,580 2,590 2,600 2,610 2,620 2,630 2,640 2,650 2,660 2,670

CTGGCTGGCATAAATATCTCACTCGCAATCAAATTCAGCCGATAGCGGAACGGGAAGGCGACTGGAGTGCCATGTCCGGTTTTCAACAAACCATGCAAATGCTGAAT
GACCGACCGTATTTATAGAGTGAGCGTTAGTTTAAGTCGGCTATCGCCTTGCCCTTCCGCTGACCTCACGGTACAGGCCAAAAGTTGTTTGGTACGTTTACGACTTA

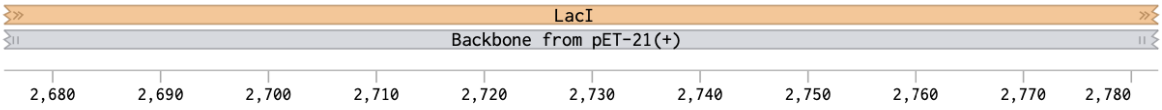

BssHII EcoRV

GAGGGCATCGTTCCCACTGCGATGCTGGTTGCCAACGATCAGATGGCGCTGGGCGCAATGCGCGCCATTACCGAGTCCGGGCTGCGCGTTGGTGCGGATATCTCGGT
CTCCCGTAGCAAGGGTGACGCTACGACCAACGGTTGCTAGTCTACCGCGACCCGCGTTACGCGCGGTAATGGCTCAGGCCCGACGCGCAACCACGCCTATAGAGCCA

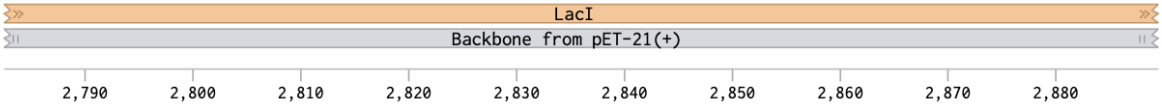

HpaI

AGTGGGATACGACGATACCGAAGACAGCTCATGTTATATCCCGCCGTTAACCACCATCAAACAGGATTTTCGCCTGCTGGGGCAAACCAGCGTGGACCGCTTGCTGC
TCACCCTATGCTGCTATGGCTTCTGTCGAGTACAATATAGGGCGGCAATTGGTGGTAGTTTGTCCTAAAAGCGGACGACCCCGTTTGGTCGCACCTGGCGAACGACG

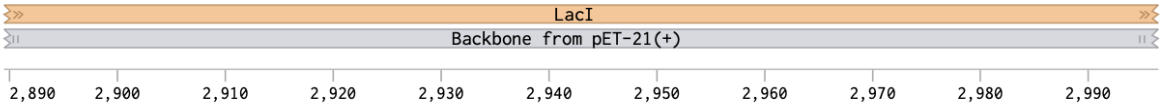

Esp3I
BsmBI

AACTCTCTCAGGGCCAGGCGGTGAAGGGCAATCAGCTGTTGCCCGTCTCACTGGTGAAAAGAAAAACCACCCTGGCGCCCAATACGCAAACCGCCTCTCCCCGCGCG
TTGAGAGAGTCCCGGTCCGCCACTTCCCGTTAGTCGACAACGGGCAGAGTGACCACTTTTCTTTTTGGTGGGACCGCGGGTTATGCGTTTGGCGGAGAGGGGCGCGC

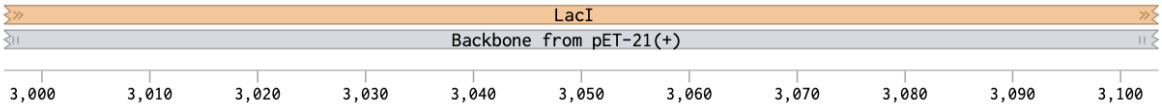

TTGGCCGATTCATTAATGCAGCTGGCACGACAGGTTTCCCGACTGGAAAGCGGGCAGTGAGCGCAACGCAATTAATGTAAGTTAGCTCACTCATTAGGCACCGGGAT
AACCGGCTAAGTAATTACGTCGACCGTGCTGTCCAAAGGGCTGACCTTTCGCCCGTCACTCGCGTTGCGTTAATTACATTCAATCGAGTGAGTAATCCGTGGCCCTA

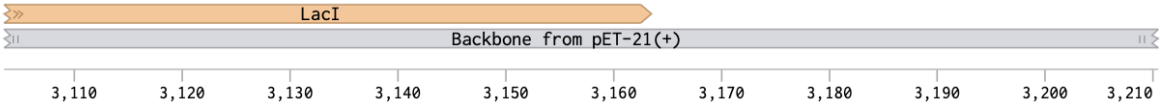

PshAI

CTCGACCGATGCCCTTGAGAGCCTTCAACCCAGTCAGCTCCTTCCGGTGGGCGCGGGGCATGACTATCGTCGCCGCACTTATGACTGTCTTCTTTATCATGCAACTC
GAGCTGGCTACGGGAACTCTCGGAAGTTGGGTCAGTCGAGGAAGGCCACCCGCGCCCCGTACTGATAGCAGCGGCGTGAATACTGACAGAAGAAATAGTACGTTGAG

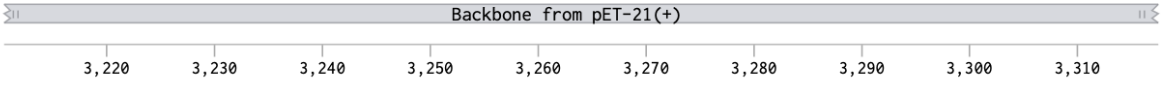

GTAGGACAGGTGCCGGCAGCGCTCTGGGTCATTTTCGGCGAGGACCGCTTTCGCTGGAGCGCGACGATGATCGGCCTGTCGCTTGCGGTATTCGGAATCTTGCACGC
CATCCTGTCCACGGCCGTCGCGAGACCCAGTAAAAGCCGCTCCTGGCGAAAGCGACCTCGCGCTGCTACTAGCCGGACAGCGAACGCCATAAGCCTTAGAACGTGCG

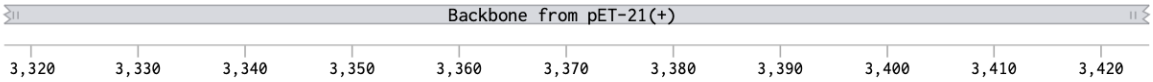

FspAI
BglI FspI

CCTCGCTCAAGCCTTCGTCACTGGTCCCGCCACCAAACGTTTCGGCGAGAAGCAGGCCATTATCGCCGGCATGGCGGCCCCACGGGTGCGCATGATCGTGCTCCTGT
GGAGCGAGTTCGGAAGCAGTGACCAGGGCGGTGGTTTGCAAAGCCGCTCTTCGTCCGGTAATAGCGGCCGTACCGCCGGGGTGCCCACGCGTACTAGCACGAGGACA

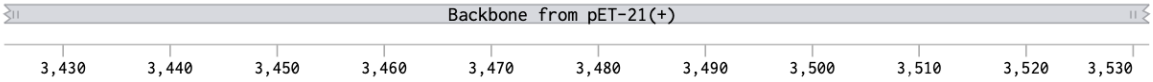

PpuMI

CGTTGAGGACCCGGCTAGGCTGGCGGGGTTGCCTTACTGGTTAGCAGAATGAATCACCGATACGCGAGCGAACGTGAAGCGACTGCTGCTGCAAAACGTCTGCGACC
GCAACTCCTGGGCCGATCCGACCGCCCCAACGGAATGACCAATCGTCTTACTTAGTGGCTATGCGCTCGCTTGCACTTCGCTGACGACGACGTTTTGCAGACGCTGG

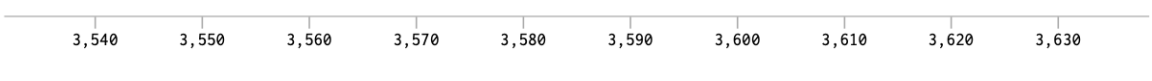

Bpu10I

TGAGCAACAACATGAATGGTCTTCGGTTTCCGTGTTTCGTAAAGTCTGGAAACGCGGAAGTCAGCGCCCTGCACCATTATGTTCCGGATCTGCATCGCAGGATGCTG
ACTCGTTGTTGTACTTACCAGAAGCCAAAGGCACAAAGCATTTCAGACCTTTGCGCCTTCAGTCGCGGGACGTGGTAATACAAGGCCTAGACGTAGCGTCCTACGAC

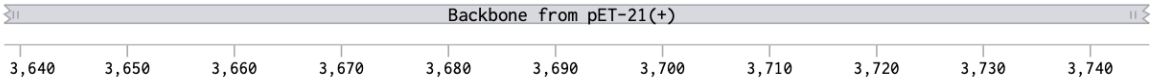

CTGGCTACCCTGTGGAACACCTACATCTGTATTAACGAAGCGCTGGCATTGACCCTGAGTGATTTTTCTCTGGTCCCGCCGCATCCATACCGCCAGTTGTTTACCCT
GACCGATGGGACACCTTGTGGATGTAGACATAATTGCTTCGCGACCGTAACTGGGACTCACTAAAAAGAGACCAGGGCGGCGTAGGTATGGCGGTCAACAAATGGGA

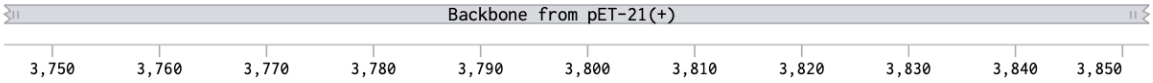

CACAACGTTCCAGTAACCGGGCATGTTCATCATCAGTAACCCGTATCGTGAGCATCCTCTCTCGTTTCATCGGTATCATTACCCCCATGAACAGAAATCCCCCTTAC
GTGTTGCAAGGTCATTGGCCCGTACAAGTAGTAGTCATTGGGCATAGCACTCGTAGGAGAGAGCAAAGTAGCCATAGTAATGGGGGTACTTGTCTTTAGGGGGAATG

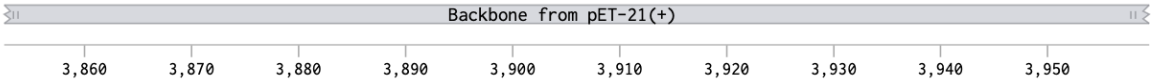

ACGGAGGCATCAGTGACCAAACAGGAAAAAACCGCCCTTAACATGGCCCGCTTTATCAGAAGCCAGACATTAACGCTTCTGGAGAAACTCAACGAGCTGGACGCGGA
TGCCTCCGTAGTCACTGGTTTGTCCTTTTTTGGCGGGAATTGTACCGGGCGAAATAGTCTTCGGTCTGTAATTGCGAAGACCTCTTTGAGTTGCTCGACCTGCGCCT

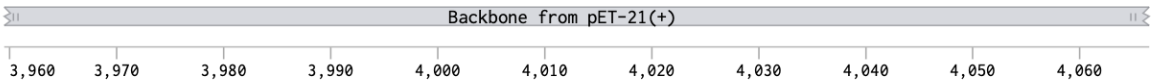

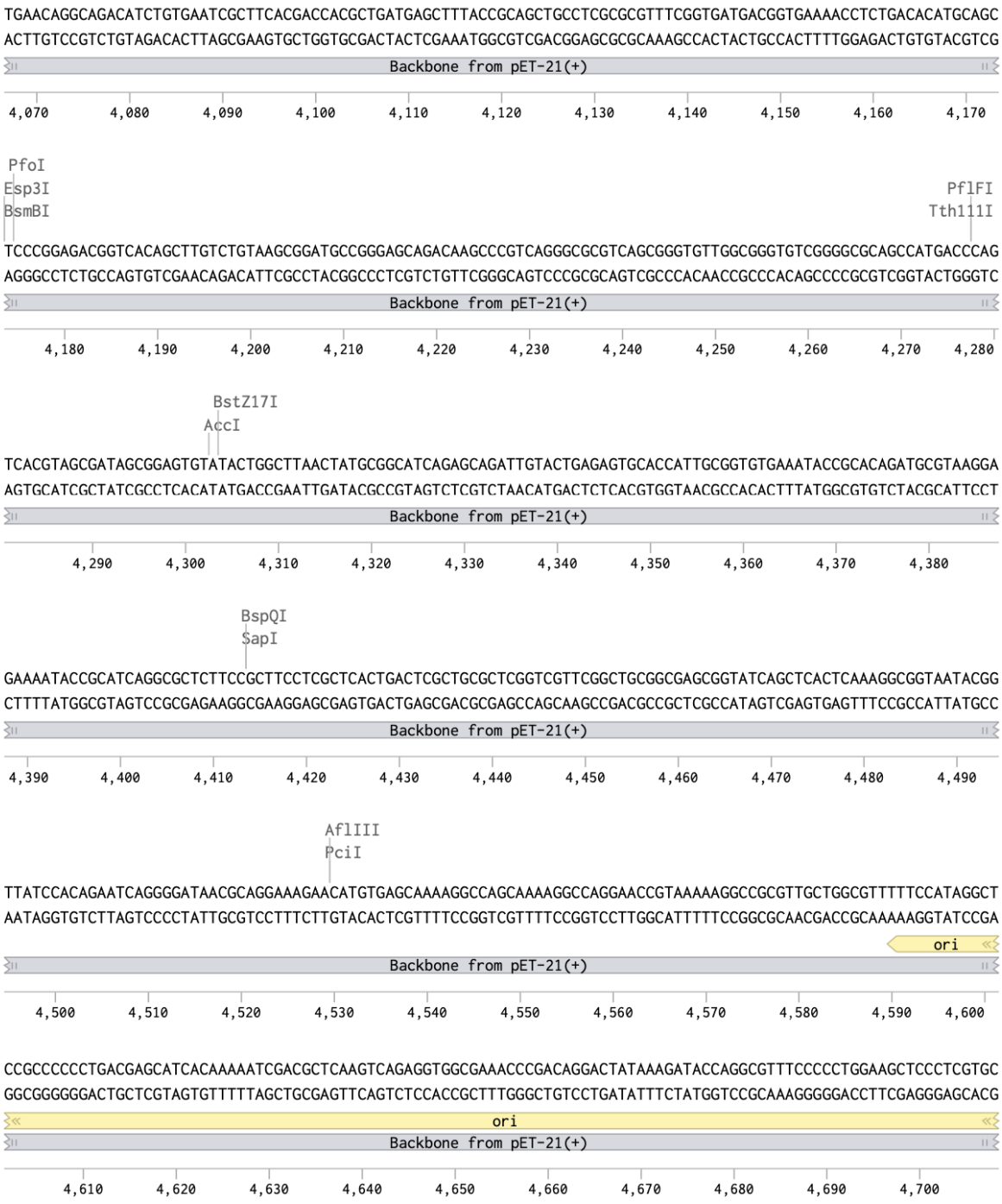
TGAACAGGCAGACATCTGTGAATCGCTTCACGACCACGCTGATGAGCTTTACCGCAGCTGCCTCGCGCGTTTCGGTGATGACGGTGAAAACCTCTGACACATGCAGC
ACTTGTCCGTCTGTAGACACTTAGCGAAGTGCTGGTGCGACTACTCGAAATGGCGTCGACGGAGCGCGCAAAGCCACTACTGCCACTTTTGGAGACTGTGTACGTCG
Backbone from pET-21(+)
4,070
4,080
4,090
4,100
4,110
4,120
4,130
4,140
4,150
4,160
4,170
PfoI
Esp3I
BsmBI
PflFI
Tth111I
TCCCGGAGACGGTCACAGCTTGTCTGTAAGCGGATGCCGGGAGCAGACAAGCCCGTCAGGGCGCGTCAGCGGGTGTTGGCGGGTGTCGGGGCGCAGCCATGACCCAG
AGGGCCTCTGCCAGTGTCGAACAGACATTCGCCTACGGCCCTCGTCTGTTCGGGCAGTCCCGCGCAGTCGCCCACAACCGCCCACAGCCCCGCGTCGGTACTGGGTC
Backbone from pET-21(+)
4,180
4,190
4,200
4,210
4,220
4,230
4,240
4,250
4,260
4,270
4,280
BstZ17I
AccI
TCACGTAGCGATAGCGGAGTGTATACTGGCTTAACTATGCGGCATCAGAGCAGATTGTACTGAGAGTGCACCATTGCGGTGTGAAATACCGCACAGATGCGTAAGGA
AGTGCATCGCTATCGCCTCACATATGACCGAATTGATACGCCGTAGTCTCGTCTAACATGACTCTCACGTGGTAACGCCACACTTTATGGCGTGTCTACGCATTCCT
Backbone from pET-21(+)
4,290
4,300
4,310
4,320
4,330
4,340
4,350
4,360
4,370
4,380
BspQI
SapI
GAAAATACCGCATCAGGCGCTCTTCCGCTTCCTCGCTCACTGACTCGCTGCGCTCGGTCGTTCGGCTGCGGCGAGCGGTATCAGCTCACTCAAAGGCGGTAATACGG
CTTTTATGGCGTAGTCCGCGAGAAGGCGAAGGAGCGAGTGACTGAGCGACGCGAGCCAGCAAGCCGACGCCGCTCGCCATAGTCGAGTGAGTTTCCGCCATTATGCC
Backbone from pET-21(+)
4,390
4,400
4,410
4,420
4,430
4,440
4,450
4,460
4,470
4,480
4,490
AflIII
PciI
TTATCCACAGAATCAGGGGATAACGCAGGAAAGAACATGTGAGCAAAAGGCCAGCAAAAGGCCAGGAACCGTAAAAAGGCCGCGTTGCTGGCGTTTTTCCATAGGCT
AATAGGTGTCTTAGTCCCCTATTGCGTCCTTTCTTGTACACTCGTTTTCCGGTCGTTTTCCGGTCCTTGGCATTTTTCCGGCGCAACGACCGCAAAAAGGTATCCGA
ori
Backbone from pET-21(+)
4,500
4,510
4,520
4,530
4,540
4,550
4,560
4,570
4,580
4,590
4,600
CCGCCCCCCTGACGAGCATCACAAAAATCGACGCTCAAGTCAGAGGTGGCGAAACCCGACAGGACTATAAAGATACCAGGCGTTTCCCCCTGGAAGCTCCCTCGTGC
GGCGGGGGGACTGCTCGTAGTGTTTTTAGCTGCGAGTTCAGTCTCCACCGCTTTGGGCTGTCCTGATATTTCTATGGTCCGCAAAGGGGGACCTTCGAGGGAGCACG
ori
Backbone from pET-21(+)
4,610
4,620
4,630
4,640
4,650
4,660
4,670
4,680
4,690
4,700

GCTCTCCTGTTCCGACCCTGCCGCTTACCGGATACCTGTCCGCCTTTCTCCCTTCGGGAAGCGTGGCGCTTTCTCATAGCTCACGCTGTAGGTATCTCAGTTCGGTG
CGAGAGGACAAGGCTGGGACGGCGAATGGCCTATGGACAGGCGGAAAGAGGGAAGCCCTTCGCACCGCGAAAGAGTATCGAGTGCGACATCCATAGAGTCAAGCCAC

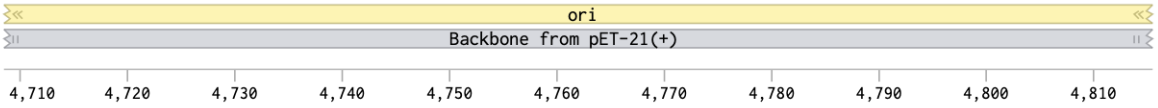

TAGGTCGTTCGCTCCAAGCTGGGCTGTGTGCACGAACCCCCCGTTCAGCCCGACCGCTGCGCCTTATCCGGTAACTATCGTCTTGAGTCCAACCCGGTAAGACACGA
ATCCAGCAAGCGAGGTTCGACCCGACACACGTGCTTGGGGGGCAAGTCGGGCTGGCGACGCGGAATAGGCCATTGATAGCAGAACTCAGGTTGGGCCATTCTGTGCT

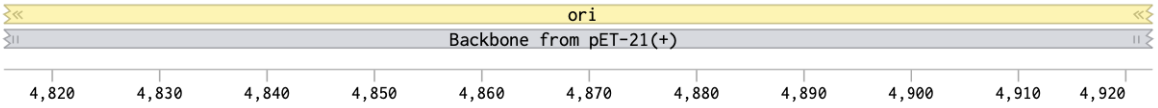

AlwNI

CTTATCGCCACTGGCAGCAGCCACTGGTAACAGGATTAGCAGAGCGAGGTATGTAGGCGGTGCTACAGAGTTCTTGAAGTGGTGGCCTAACTACGGCTACACTAGAA
GAATAGCGGTGACCGTCGTCGGTGACCATTGTCCTAATCGTCTCGCTCCATACATCCGCCACGATGTCTCAAGAACTTCACCACCGGATTGATGCCGATGTGATCTT

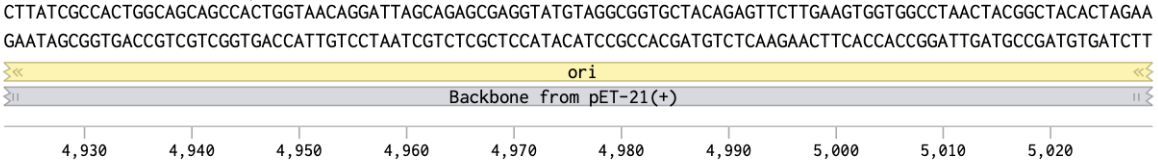

GGACAGTATTTGGTATCTGCGCTCTGCTGAAGCCAGTTACCTTCGGAAAAAGAGTTGGTAGCTCTTGATCCGGCAAACAAACCACCGCTGGTAGCGGTGGTTTTTTT
CCTGTCATAAACCATAGACGCGAGACGACTTCGGTCAATGGAAGCCTTTTTCTCAACCATCGAGAACTAGGCCGTTTGTTTGGTGGCGACCATCGCCACCAAAAAAA

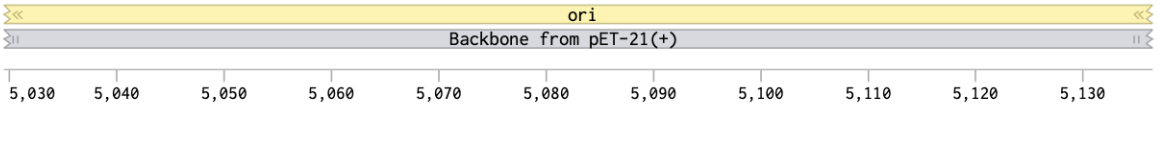

GTTTGCAAGCAGCAGATTACGCGCAGAAAAAAAGGATCTCAAGAAGATCCTTTGATCTTTTCTACGGGGTCTGACGCTCAGTGGAACGAAAACTCACGTTAAGGGAT
CAAACGTTCGTCGTCTAATGCGCGTCTTTTTTTCCTAGAGTTCTTCTAGGAAACTAGAAAAGATGCCCCAGACTGCGAGTCACCTTGCTTTTGAGTGCAATTCCCTA

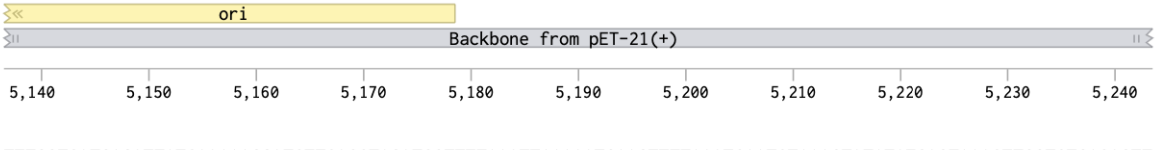

TTTGGTCATGAGATTATCAAAAAGGATCTTCACCTAGATCCTTTTAAATTAAAAATGAAGTTTTAAATCAATCTAAAGTATATATGAGTAAACTTGGTCTGACAGTT
AAACCAGTACTCTAATAGTTTTTCCTAGAAGTGGATCTAGGAAAATTTAATTTTTACTTCAAAATTTAGTTAGATTTCATATATACTCATTTGAACCAGACTGTCAA

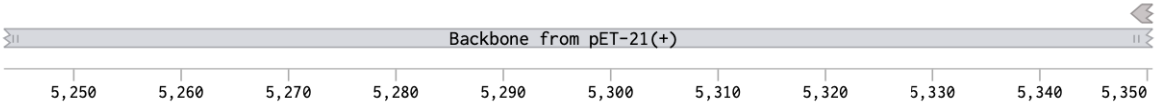

AhdI

ACCAATGCTTAATCAGTGAGGCACCTATCTCAGCGATCTGTCTATTTCGTTCATCCATAGTTGCCTGACTCCCCGTCGTGTAGATAACTACGATACGGGAGGGCTTA
TGGTTACGAATTAGTCACTCCGTGGATAGAGTCGCTAGACAGATAAAGCAAGTAGGTATCAACGGACTGAGGGGCAGCACATCTATTGATGCTATGCCCTCCCGAAT

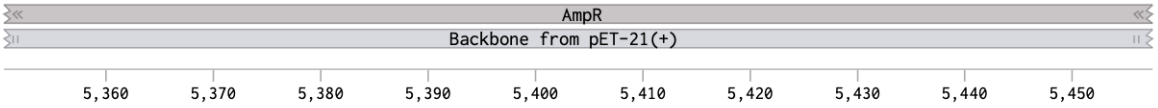

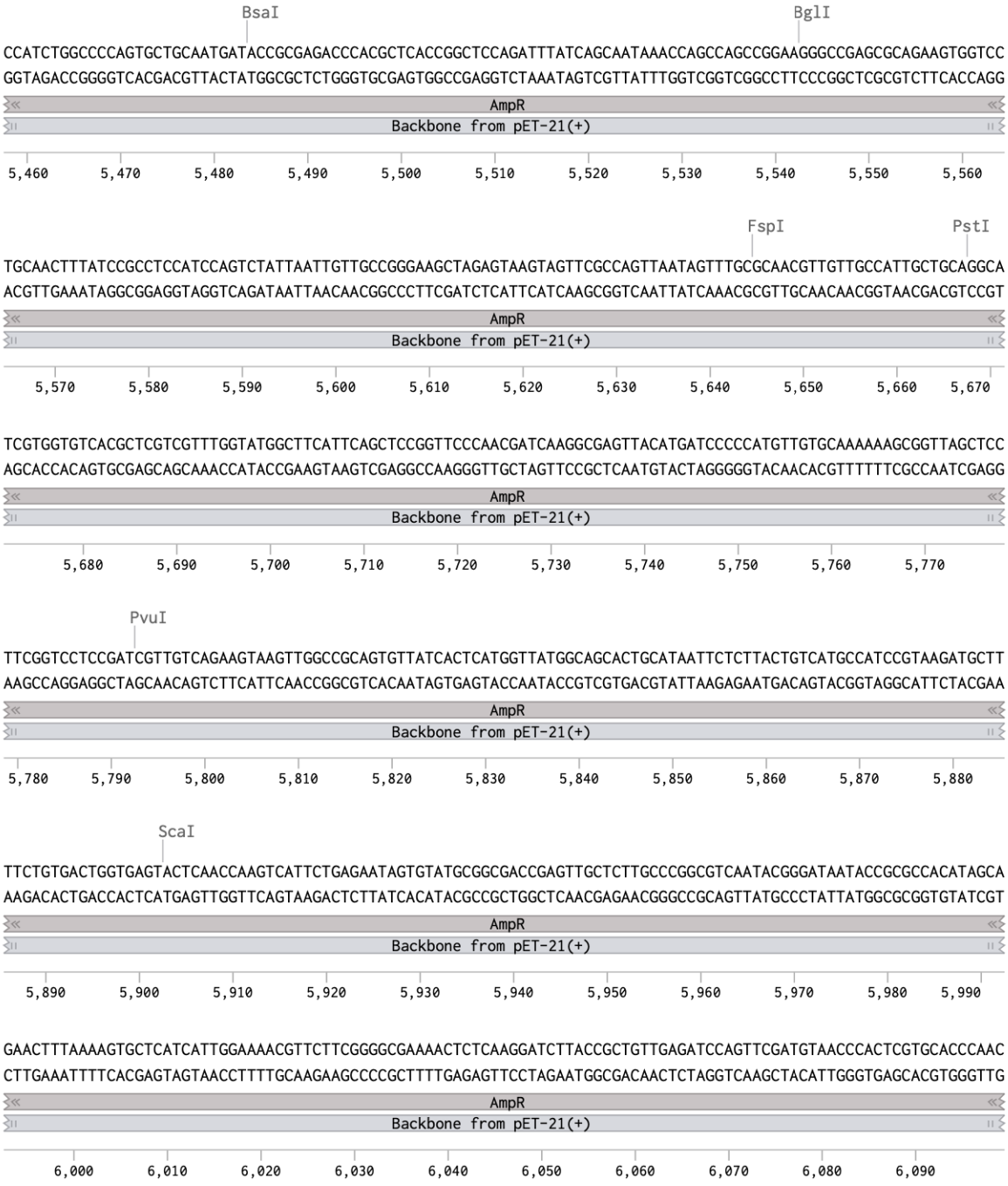
BsaI
BglI
CCATCTGGCCCCAGTGCTGCAATGATACCGCGAGACCCACGCTCACCGGCTCCAGATTTATCAGCAATAAACCAGCCAGCCGGAAGGGCCGAGCGCAGAAGTGGTCC
GGTAGACCGGGGTCACGACGTTACTATGGCGCTCTGGGTGCGAGTGGCCGAGGTCTAAATAGTCGTTATTTGGTCGGTCGGCCTTCCCGGCTCGCGTCTTCACCAGG
AmpR
Backbone from pET-21(+)
5,460
5,470
5,480
5,490
5,500
5,510
5,520
5,530
5,540
5,550
5,560
FspI
PstI
TGCAACTTTATCCGCCTCCATCCAGTCTATTAATTGTTGCCGGGAAGCTAGAGTAAGTAGTTCGCCAGTTAATAGTTTGCGCAACGTTGTTGCCATTGCTGCAGGCA
ACGTTGAAATAGGCGGAGGTAGGTCAGATAATTAACAACGGCCCTTCGATCTCATTCATCAAGCGGTCAATTATCAAACGCGTTGCAACAACGGTAACGACGTCCGT
AmpR
Backbone from pET-21(+)
5,570
5,580
5,590
5,600
5,610
5,620
5,630
5,640
5,650
5,660
5,670
TCGTGGTGTCACGCTCGTCGTTTGGTATGGCTTCATTCAGCTCCGGTTCCCAACGATCAAGGCGAGTTACATGATCCCCCATGTTGTGCAAAAAAGCGGTTAGCTCC
AGCACCACAGTGCGAGCAGCAAACCATACCGAAGTAAGTCGAGGCCAAGGGTTGCTAGTTCCGCTCAATGTACTAGGGGGTACAACACGTTTTTTCGCCAATCGAGG
AmpR
Backbone from pET-21(+)
5,680
5,690
5,700
5,710
5,720
5,730
5,740
5,750
5,760
5,770
PvuI
TTCGGTCCTCCGATCGTTGTCAGAAGTAAGTTGGCCGCAGTGTTATCACTCATGGTTATGGCAGCACTGCATAATTCTCTTACTGTCATGCCATCCGTAAGATGCTT
AAGCCAGGAGGCTAGCAACAGTCTTCATTCAACCGGCGTCACAATAGTGAGTACCAATACCGTCGTGACGTATTAAGAGAATGACAGTACGGTAGGCATTCTACGAA
AmpR
Backbone from pET-21(+)
5,780
5,790
5,800
5,810
5,820
5,830
5,840
5,850
5,860
5,870
5,880
ScaI
TTCTGTGACTGGTGAGTACTCAACCAAGTCATTCTGAGAATAGTGTATGCGGCGACCGAGTTGCTCTTGCCCGGCGTCAATACGGGATAATACCGCGCCACATAGCA
AAGACACTGACCACTCATGAGTTGGTTCAGTAAGACTCTTATCACATACGCCGCTGGCTCAACGAGAACGGGCCGCAGTTATGCCCTATTATGGCGCGGTGTATCGT
AmpR
Backbone from pET-21(+)
5,890
5,900
5,910
5,920
5,930
5,940
5,950
5,960
5,970
5,980
5,990
GAACTTTAAAAGTGCTCATCATTGGAAAACGTTCTTCGGGGCGAAAACTCTCAAGGATCTTACCGCTGTTGAGATCCAGTTCGATGTAACCCACTCGTGCACCCAAC
CTTGAAATTTTCACGAGTAGTAACCTTTTGCAAGAAGCCCCGCTTTTGAGAGTTCCTAGAATGGCGACAACTCTAGGTCAAGCTACATTGGGTGAGCACGTGGGTTG
AmpR
Backbone from pET-21(+)
6,000
6,010
6,020
6,030
6,040
6,050
6,060
6,070
6,080
6,090

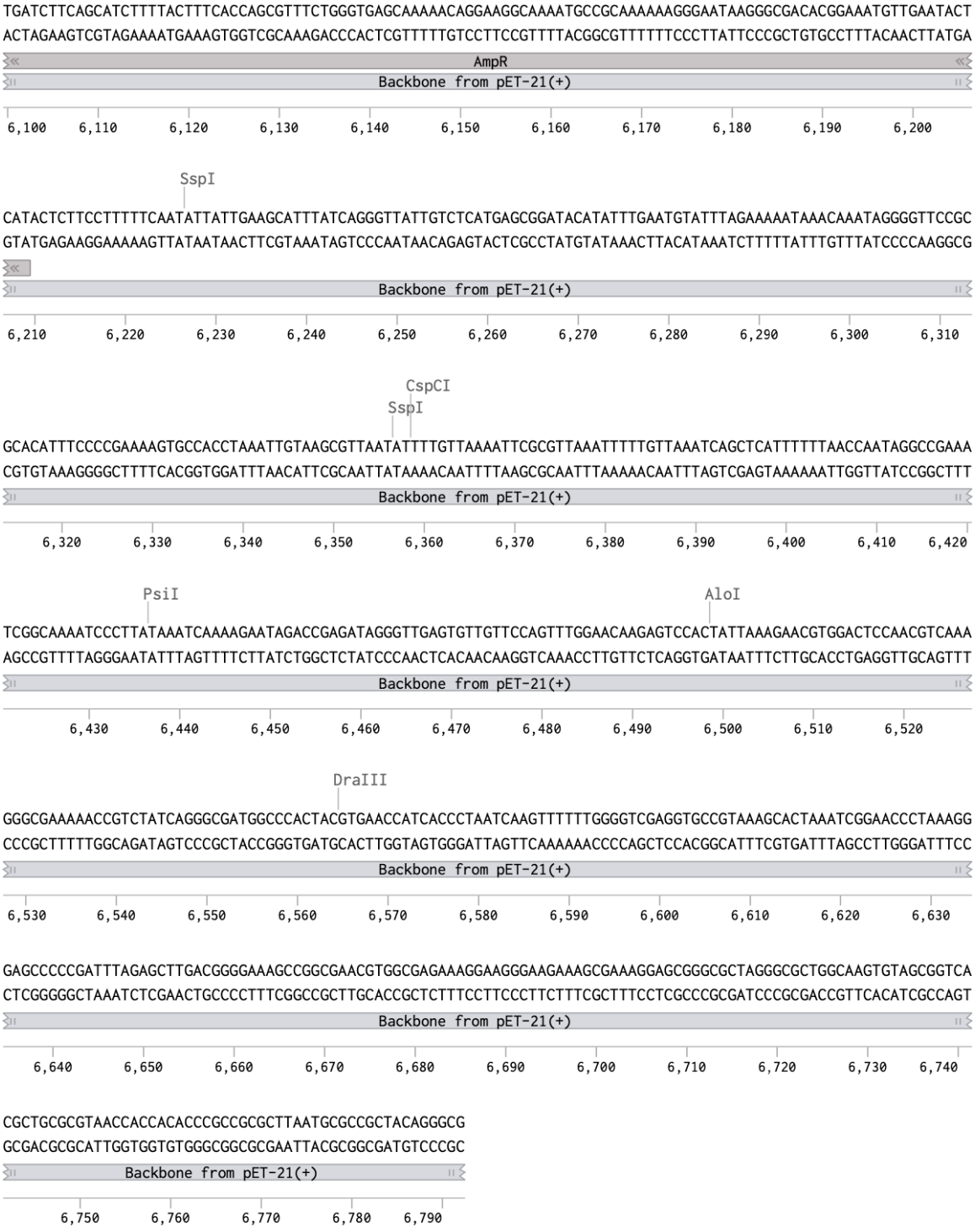

Figure B. 4 Sequence map of the producer strain

B.3 Regulator

B.3.1 Plasmid map

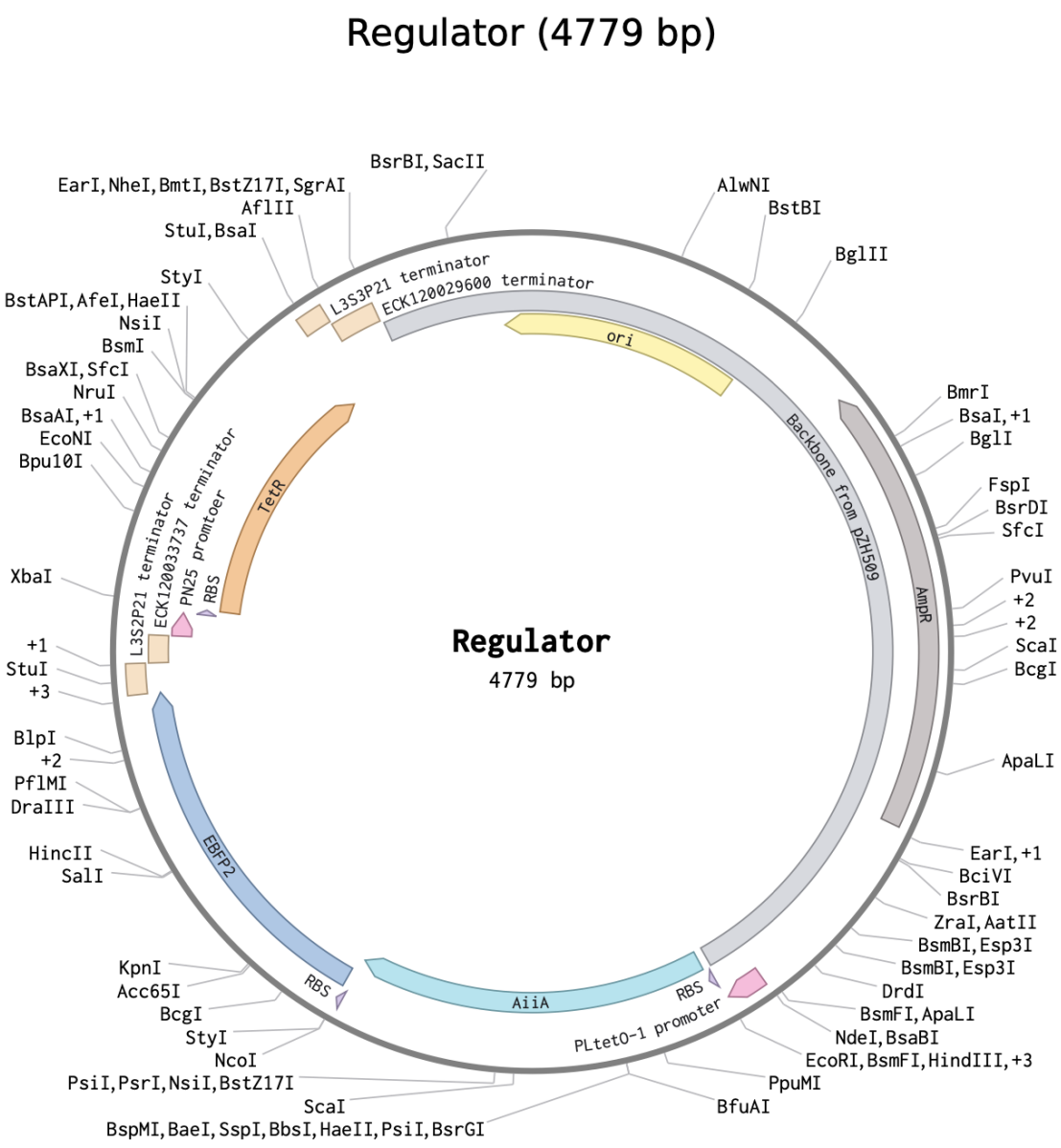

Figure B. 5 Plasmid map of the regulator strain

B.3.2 Sequence map

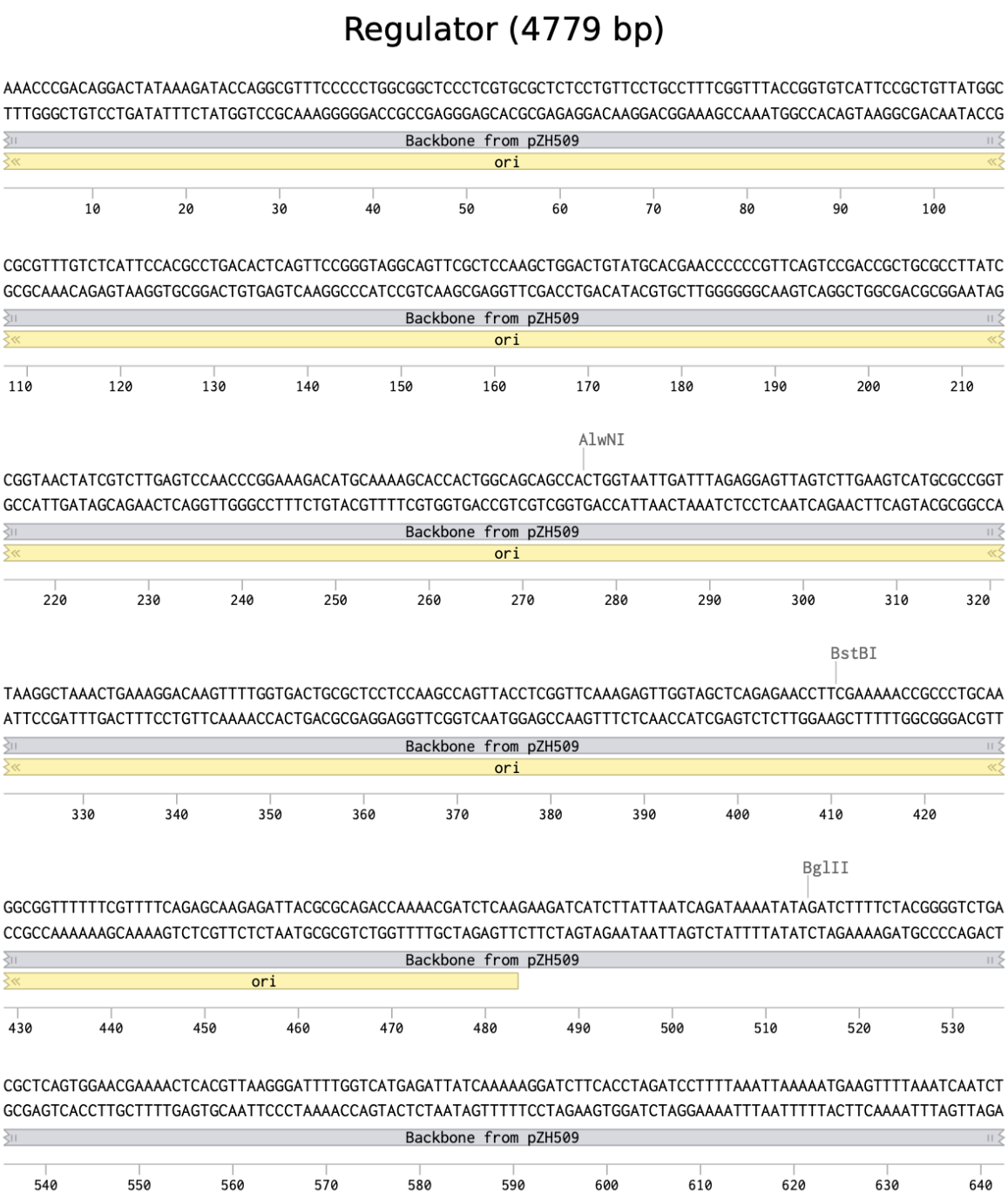

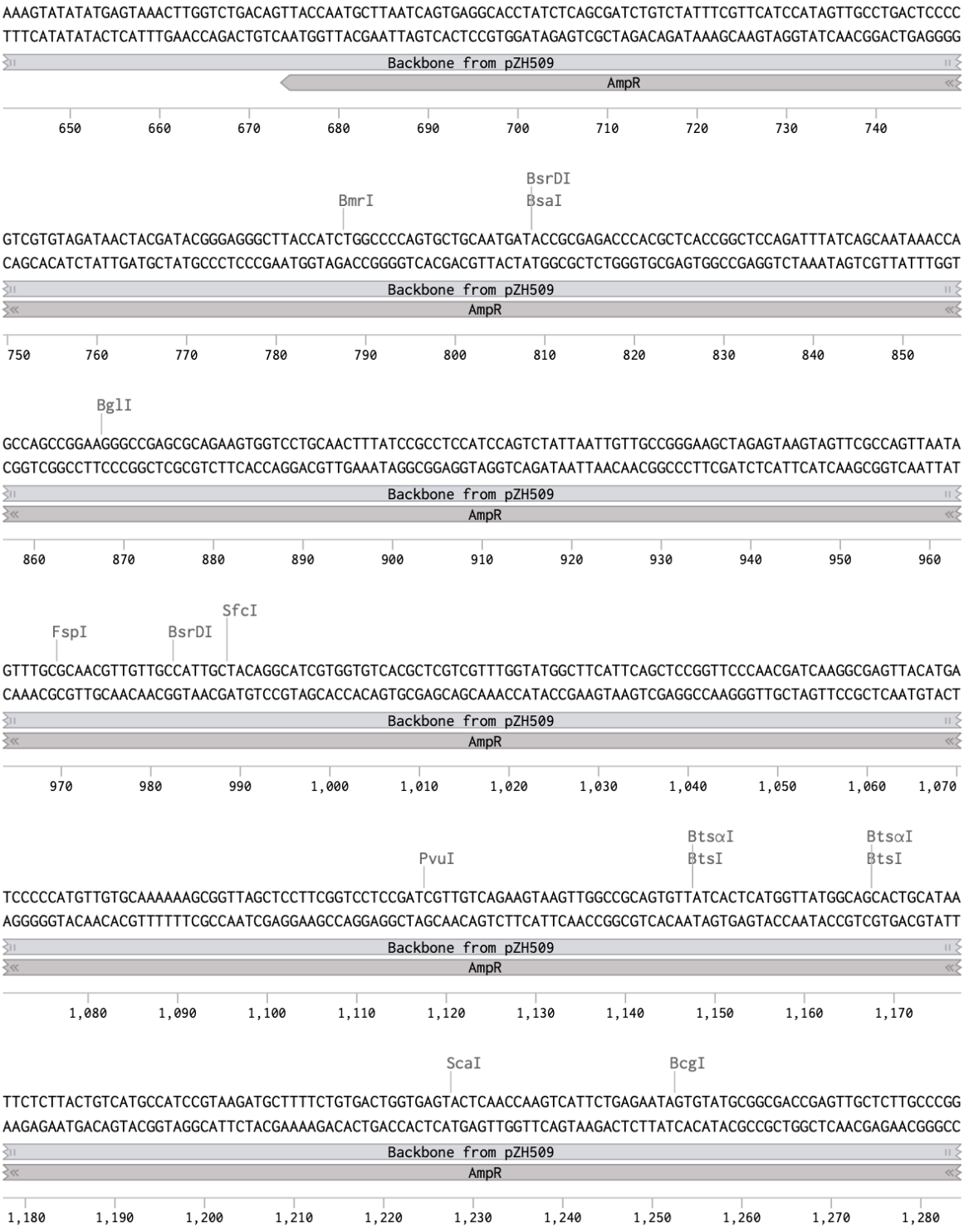
AAAGTATATATGAGTAAACTTGGTCTGACAGTTACCAATGCTTAATCAGTGAGGCACCTATCTCAGCGATCTGTCTATTTCGTTCATCCATAGTTGCCTGACTCCCC
TTTCATATATACTCATTTGAACCAGACTGTCAATGGTTACGAATTAGTCACTCCGTGGATAGAGTCGCTAGACAGATAAAGCAAGTAGGTATCAACGGACTGAGGGG
Backbone from pZH509
AmpR
650
660
670
680
690
700
710
720
730
740
BsrDI
BsaI
BmrI
GTCGTGTAGATAACTACGATACGGGAGGGCTTACCATCTGGCCCCAGTGCTGCAATGATACCGCGAGACCCACGCTCACCGGCTCCAGATTTATCAGCAATAAACCA
CAGCACATCTATTGATGCTATGCCCTCCCGAATGGTAGACCGGGGTCACGACGTTACTATGGCGCTCTGGGTGCGAGTGGCCGAGGTCTAAATAGTCGTTATTTGGT
Backbone from pZH509
AmpR
750
760
770
780
790
800
810
820
830
840
850
BglI
GCCAGCCGGAAGGGCCGAGCGCAGAAGTGGTCCTGCAACTTTATCCGCCTCCATCCAGTCTATTAATTGTTGCCGGGAAGCTAGAGTAAGTAGTTCGCCAGTTAATA
CGGTCGGCCTTCCCGGCTCGCGTCTTCACCAGGACGTTGAAATAGGCGGAGGTAGGTCAGATAATTAACAACGGCCCTTCGATCTCATTCATCAAGCGGTCAATTAT
Backbone from pZH509
AmpR
860
870
880
890
900
910
920
930
940
950
960
SfcI
FspI
BsrDI
GTTTGCGCAACGTTGTTGCCATTGCTACAGGCATCGTGGTGTCACGCTCGTCGTTTGGTATGGCTTCATTCAGCTCCGGTTCCCAACGATCAAGGCGAGTTACATGA
CAAACGCGTTGCAACAACGGTAACGATGTCCGTAGCACCACAGTGCGAGCAGCAAACCATACCGAAGTAAGTCGAGGCCAAGGGTTGCTAGTTCCGCTCAATGTACT
Backbone from pZH509
AmpR
970
980
990
1,000
1,010
1,020
1,030
1,040
1,050
1,060
1,070
BtsαI
BtsI
BtsαI
BtsI
PvuI
TCCCCCATGTTGTGCAAAAAAGCGGTTAGCTCCTTCGGTCCTCCGATCGTTGTCAGAAGTAAGTTGGCCGCAGTGTTATCACTCATGGTTATGGCAGCACTGCATAA
AGGGGGTACAACACGTTTTTTCGCCAATCGAGGAAGCCAGGAGGCTAGCAACAGTCTTCATTCAACCGGCGTCACAATAGTGAGTACCAATACCGTCGTGACGTATT
Backbone from pZH509
AmpR
1,080
1,090
1,100
1,110
1,120
1,130
1,140
1,150
1,160
1,170
ScaI
BcgI
TTCTCTTACTGTCATGCCATCCGTAAGATGCTTTTCTGTGACTGGTGAGTACTCAACCAAGTCATTCTGAGAATAGTGTATGCGGCGACCGAGTTGCTCTTGCCCGG
AAGAGAATGACAGTACGGTAGGCATTCTACGAAAAGACACTGACCACTCATGAGTTGGTTCAGTAAGACTCTTATCACATACGCCGCTGGCTCAACGAGAACGGGCC
Backbone from pZH509
AmpR
1,180
1,190
1,200
1,210
1,220
1,230
1,240
1,250
1,260
1,270
1,280

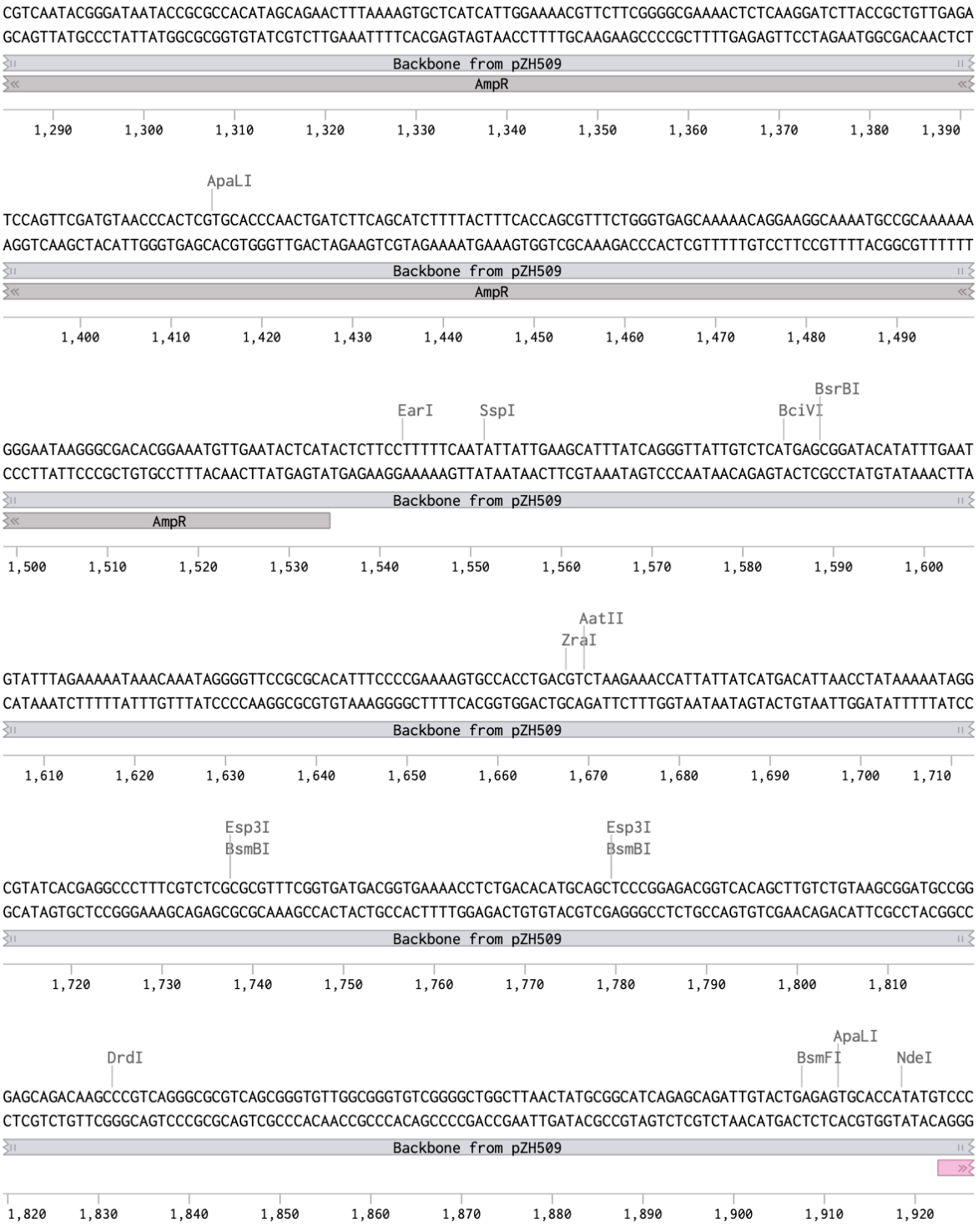
CGTCAATACGGGATAATACCGCGCCACATAGCAGAACTTTAAAAGTGCTCATCATTGGAAAACGTTCTTCGGGGCGAAAACTCTCAAGGATCTTACCGCTGTTGAGA
GCAGTTATGCCCTATTATGGCGCGGTGTATCGTCTTGAAATTTTCACGAGTAGTAACCTTTTGCAAGAAGCCCCGCTTTTGAGAGTTCCTAGAATGGCGACAACTCT
Backbone from pZH509
AmpR
1,290
1,300
1,310
1,320
1,330
1,340
1,350
1,360
1,370
1,380
1,390
ApaLI
TCCAGTTCGATGTAACCCACTCGTGCACCCAACTGATCTTCAGCATCTTTTACTTTCACCAGCGTTTCTGGGTGAGCAAAAACAGGAAGGCAAAATGCCGCAAAAAA
AGGTCAAGCTACATTGGGTGAGCACGTGGGTTGACTAGAAGTCGTAGAAAATGAAAGTGGTCGCAAAGACCCACTCGTTTTTGTCCTTCCGTTTTACGGCGTTTTTT
Backbone from pZH509
AmpR
1,400
1,410
1,420
1,430
1,440
1,450
1,460
1,470
1,480
1,490
BsrBI
EarI
SspI
BciVI
GGGAATAAGGGCGACACGGAAATGTTGAATACTCATACTCTTCCTTTTTCAATATTATTGAAGCATTTATCAGGGTTATTGTCTCATGAGCGGATACATATTTGAAT
CCCTTATTCCCGCTGTGCCTTTACAACTTATGAGTATGAGAAGGAAAAAGTTATAATAACTTCGTAAATAGTCCCAATAACAGAGTACTCGCCTATGTATAAACTTA
Backbone from pZH509
AmpR
1,500
1,510
1,520
1,530
1,540
1,550
1,560
1,570
1,580
1,590
1,600
AatII
ZraI
GTATTTAGAAAAATAAACAAATAGGGGTTCCGCGCACATTTCCCCGAAAAGTGCCACCTGACGTCTAAGAAACCATTATTATCATGACATTAACCTATAAAAATAGG
CATAAATCTTTTTATTTGTTTATCCCCAAGGCGCGTGTAAAGGGGCTTTTCACGGTGGACTGCAGATTCTTTGGTAATAATAGTACTGTAATTGGATATTTTTATCC
Backbone from pZH509
1,610
1,620
1,630
1,640
1,650
1,660
1,670
1,680
1,690
1,700
1,710
Esp3I
BsmBI
Esp3I
BsmBI
CGTATCACGAGGCCCTTTCGTCTCGCGCGTTTCGGTGATGACGGTGAAAACCTCTGACACATGCAGCTCCCGGAGACGGTCACAGCTTGTCTGTAAGCGGATGCCGG
GCATAGTGCTCCGGGAAAGCAGAGCGCGCAAAGCCACTACTGCCACTTTTGGAGACTGTGTACGTCGAGGGCCTCTGCCAGTGTCGAACAGACATTCGCCTACGGCC
Backbone from pZH509
1,720
1,730
1,740
1,750
1,760
1,770
1,780
1,790
1,800
1,810
ApaLI
DrdI
BsmFI
NdeI
GAGCAGACAAGCCCGTCAGGGCGCGTCAGCGGGTGTTGGCGGGTGTCGGGGCTGGCTTAACTATGCGGCATCAGAGCAGATTGTACTGAGAGTGCACCATATGTCCC
CTCGTCTGTTCGGGCAGTCCCGCGCAGTCGCCCACAACCGCCCACAGCCCCGACCGAATTGATACGCCGTAGTCTCGTCTAACATGACTCTCACGTGGTATACAGGG
Backbone from pZH509
1,820
1,830
1,840
1,850
1,860
1,870
1,880
1,890
1,900
1,910
1,920

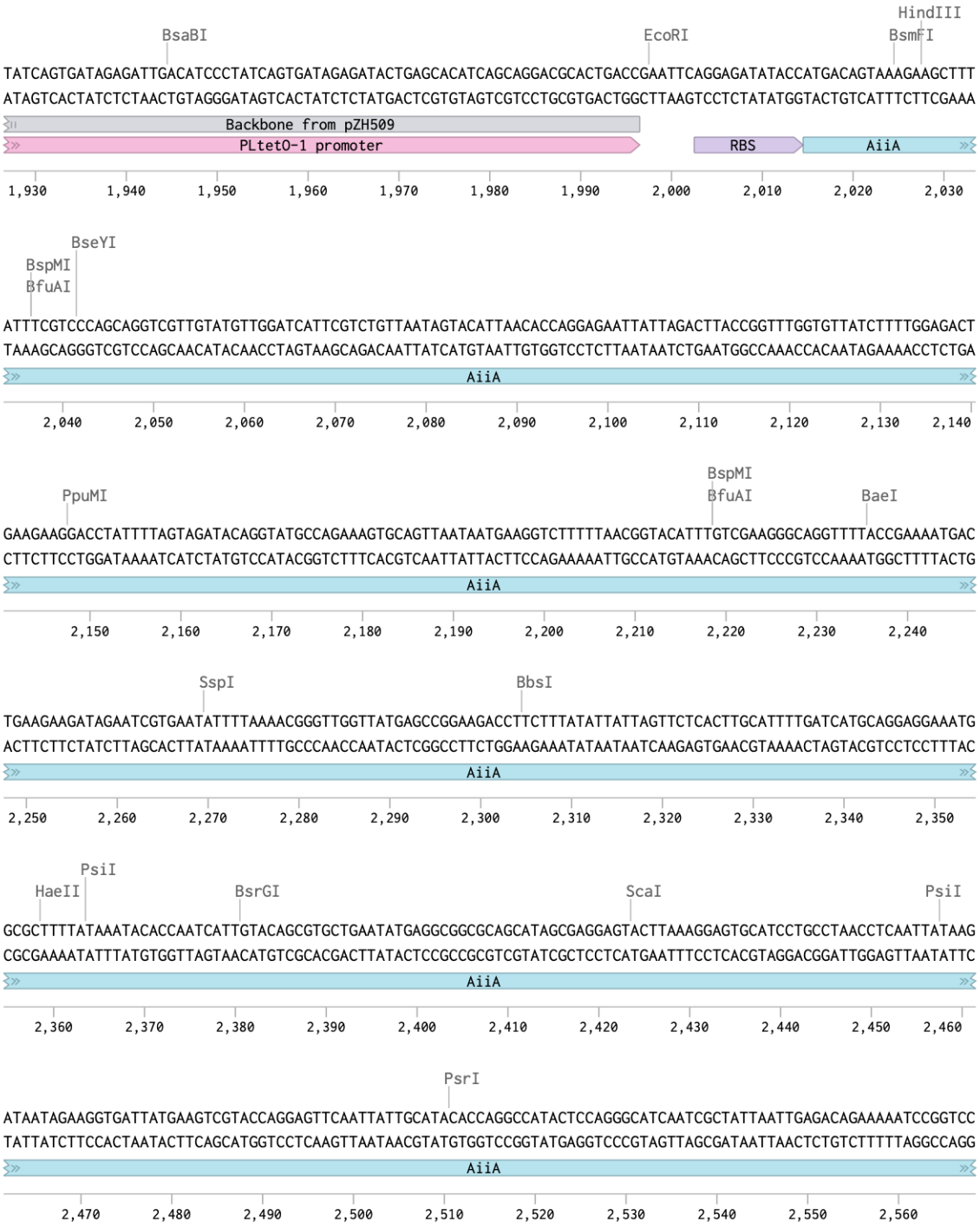
HindIII
BsaBI
EcoRI
BsmFI
TATCAGTGATAGAGATTGACATCCCTATCAGTGATAGAGATACTGAGCACATCAGCAGGACGCACTGACCGAATTCAGGAGATATACCATGACAGTAAAGAAGCTTT
ATAGTCACTATCTCTAACTGTAGGGATAGTCACTATCTCTATGACTCGTGTAGTCGTCCTGCGTGACTGGCTTAAGTCCTCTATATGGTACTGTCATTTCTTCGAAA
Backbone from pZH509
PLtetO-1 promoter
RBS
AiiA
1,930
1,940
1,950
1,960
1,970
1,980
1,990
2,000
2,010
2,020
2,030
BseYI
BspMI
BfuAI
ATTTCGTCCCAGCAGGTCGTTGTATGTTGGATCATTCGTCTGTTAATAGTACATTAACACCAGGAGAATTATTAGACTTACCGGTTTGGTGTTATCTTTTGGAGACT
TAAAGCAGGGTCGTCCAGCAACATACAACCTAGTAAGCAGACAATTATCATGTAATTGTGGTCCTCTTAATAATCTGAATGGCCAAACCACAATAGAAAACCTCTGA
AiiA
2,040
2,050
2,060
2,070
2,080
2,090
2,100
2,110
2,120
2,130
2,140
BspMI
PpuMI
BfuAI
BaeI
GAAGAAGGACCTATTTTAGTAGATACAGGTATGCCAGAAAGTGCAGTTAATAATGAAGGTCTTTTTAACGGTACATTTGTCGAAGGGCAGGTTTTACCGAAAATGAC
CTTCTTCCTGGATAAAATCATCTATGTCCATACGGTCTTTCACGTCAATTATTACTTCCAGAAAAATTGCCATGTAAACAGCTTCCCGTCCAAAATGGCTTTTACTG
AiiA
2,150
2,160
2,170
2,180
2,190
2,200
2,210
2,220
2,230
2,240
SspI
BbsI
TGAAGAAGATAGAATCGTGAATATTTTAAAACGGGTTGGTTATGAGCCGGAAGACCTTCTTTATATTATTAGTTCTCACTTGCATTTTGATCATGCAGGAGGAAATG
ACTTCTTCTATCTTAGCACTTATAAAATTTTGCCCAACCAATACTCGGCCTTCTGGAAGAAATATAATAATCAAGAGTGAACGTAAAACTAGTACGTCCTCCTTTAC
AiiA
2,250
2,260
2,270
2,280
2,290
2,300
2,310
2,320
2,330
2,340
2,350
PsiI
HaeII
BsrGI
ScaI
PsiI
GCGCTTTTATAAATACACCAATCATTGTACAGCGTGCTGAATATGAGGCGGCGCAGCATAGCGAGGAGTACTTAAAGGAGTGCATCCTGCCTAACCTCAATTATAAG
CGCGAAAATATTTATGTGGTTAGTAACATGTCGCACGACTTATACTCCGCCGCGTCGTATCGCTCCTCATGAATTTCCTCACGTAGGACGGATTGGAGTTAATATTC
AiiA
2,360
2,370
2,380
2,390
2,400
2,410
2,420
2,430
2,440
2,450
2,460
PsrI
ATAATAGAAGGTGATTATGAAGTCGTACCAGGAGTTCAATTATTGCATACACCAGGCCATACTCCAGGGCATCAATCGCTATTAATTGAGACAGAAAAATCCGGTCC
TATTATCTTCCACTAATACTTCAGCATGGTCCTCAAGTTAATAACGTATGTGGTCCGGTATGAGGTCCCGTAGTTAGCGATAATTAACTCTGTCTTTTTAGGCCAGG
AiiA
2,470
2,480
2,490
2,500
2,510
2,520
2,530
2,540
2,550
2,560

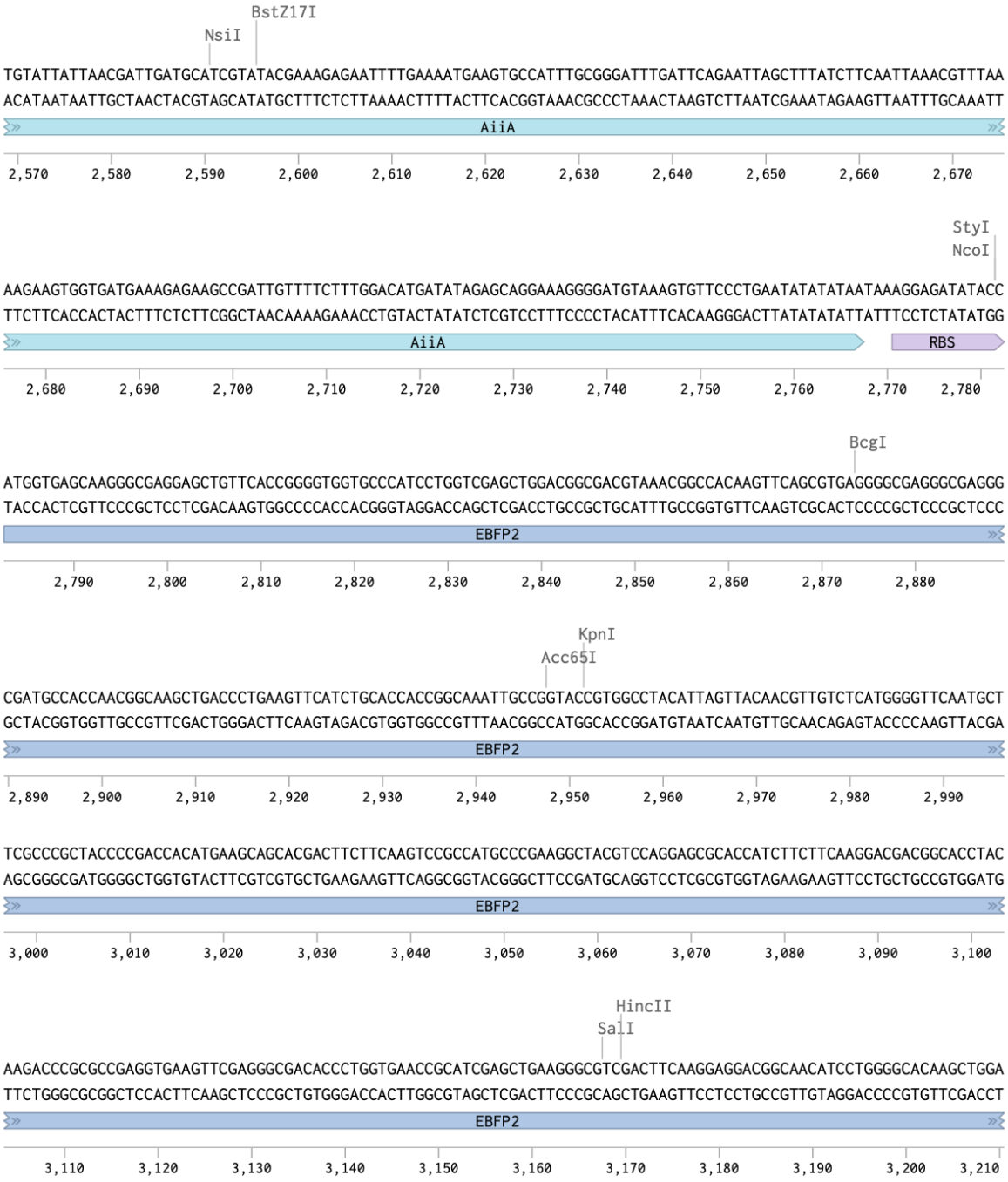
BstZ17I
NsiI
TGTATTATTAACGATTGATGCATCGTATACGAAAGAGAATTTTGAAAATGAAGTGCCATTTGCGGGATTTGATTCAGAATTAGCTTTATCTTCAATTAAACGTTTAA
ACATAATAATTGCTAACTACGTAGCATATGCTTTCTCTTAAAACTTTTACTTCACGGTAAACGCCCTAAACTAAGTCTTAATCGAAATAGAAGTTAATTTGCAAATT
AiiA
2,570 2,580 2,590 2,600 2,610 2,620 2,630 2,640 2,650 2,660 2,670
StyI
NcoI
AAGAAGTGGTGATGAAAGAGAAGCCGATTGTTTTCTTTGGACATGATATAGAGCAGGAAAGGGGATGTAAAGTGTTCCCTGAATATATATAATAAAGGAGATATACC
TTCTTCACCACTACTTTCTCTTCGGCTAACAAAAGAAACCTGTACTATATCTCGTCCTTTCCCCTACATTTCACAAGGGACTTATATATATTATTTCCTCTATATGG
AiiA
RBS
2,680 2,690 2,700 2,710 2,720 2,730 2,740 2,750 2,760 2,770 2,780
BcgI
ATGGTGAGCAAGGGCGAGGAGCTGTTCACCGGGGTGGTGCCCATCCTGGTCGAGCTGGACGGCGACGTAAACGGCCACAAGTTCAGCGTGAGGGGCGAGGGCGAGGG
TACCACTCGTTCCCGCTCCTCGACAAGTGGCCCCACCACGGGTAGGACCAGCTCGACCTGCCGCTGCATTTGCCGGTGTTCAAGTCGCACTCCCCGCTCCCGCTCCC
EBFP2
2,790 2,800 2,810 2,820 2,830 2,840 2,850 2,860 2,870 2,880
KpnI
Acc65I
CGATGCCACCAACGGCAAGCTGACCCTGAAGTTCATCTGCACCACCGGCAAATTGCCGGTACCGTGGCCTACATTAGTTACAACGTTGTCTCATGGGGTTCAATGCT
GCTACGGTGGTTGCCGTTCGACTGGGACTTCAAGTAGACGTGGTGGCCGTTTAACGGCCATGGCACCGGATGTAATCAATGTTGCAACAGAGTACCCCAAGTTACGA
EBFP2
2,890 2,900 2,910 2,920 2,930 2,940 2,950 2,960 2,970 2,980 2,990
TCGCCCGCTACCCCGACCACATGAAGCAGCACGACTTCTTCAAGTCCGCCATGCCCGAAGGCTACGTCCAGGAGCGCACCATCTTCTTCAAGGACGACGGCACCTAC
AGCGGGCGATGGGGCTGGTGTACTTCGTCGTGCTGAAGAAGTTCAGGCGGTACGGGCTTCCGATGCAGGTCCTCGCGTGGTAGAAGAAGTTCCTGCTGCCGTGGATG
EBFP2
3,000 3,010 3,020 3,030 3,040 3,050 3,060 3,070 3,080 3,090 3,100
HincII
SalI
AAGACCCGCGCCGAGGTGAAGTTCGAGGGCGACACCCTGGTGAACCGCATCGAGCTGAAGGGCGTCGACTTCAAGGAGGACGGCAACATCCTGGGGCACAAGCTGGA
TTCTGGGCGCGGCTCCACTTCAAGCTCCCGCTGTGGGACCACTTGGCGTAGCTCGACTTCCCGCAGCTGAAGTTCCTCCTGCCGTTGTAGGACCCCGTGTTCGACCT
EBFP2
3,110 3,120 3,130 3,140 3,150 3,160 3,170 3,180 3,190 3,200 3,210

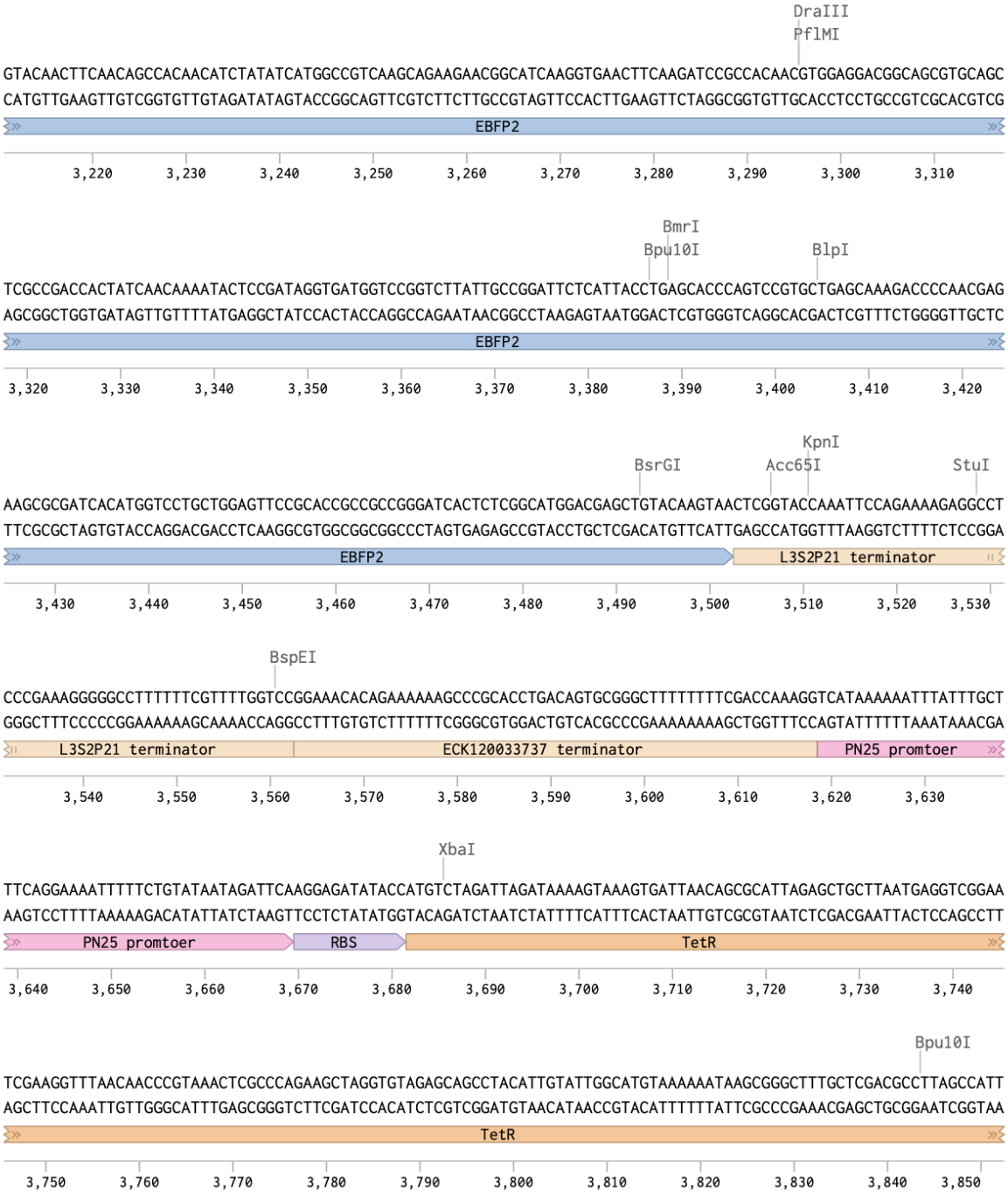
DraIII
PflMI
GTACAACTTCAACAGCCACAACATCTATATCATGGCCGTCAAGCAGAAGAACGGCATCAAGGTGAACTTCAAGATCCGCCACAACGTGGAGGACGGCAGCGTGCAGC
CATGTTGAAGTTGTCGGTGTTGTAGATATAGTACCGGCAGTTCGTCTTCTTGCCGTAGTTCCACTTGAAGTTCTAGGCGGTGTTGCACCTCCTGCCGTCGCACGTCG
EBFP2
3,220
3,230
3,240
3,250
3,260
3,270
3,280
3,290
3,300
3,310
BmrI
Bpu10I
BlpI
TCGCCGACCACTATCAACAAAATACTCCGATAGGTGATGGTCCGGTCTTATTGCCGGATTCTCATTACCTGAGCACCCAGTCCGTGCTGAGCAAAGACCCCAACGAG
AGCGGCTGGTGATAGTTGTTTTATGAGGCTATCCACTACCAGGCCAGAATAACGGCCTAAGAGTAATGGACTCGTGGGTCAGGCACGACTCGTTTCTGGGGTTGCTC
EBFP2
3,320
3,330
3,340
3,350
3,360
3,370
3,380
3,390
3,400
3,410
3,420
KpnI
BsrGI
Acc65I
StuI
AAGCGCGATCACATGGTCCTGCTGGAGTTCCGCACCGCCGCCGGGATCACTCTCGGCATGGACGAGCTGTACAAGTAACTCGGTACCAAATTCCAGAAAAGAGGCCT
TTCGCGCTAGTGTACCAGGACGACCTCAAGGCGTGGCGGCGGCCCTAGTGAGAGCCGTACCTGCTCGACATGTTCATTGAGCCATGGTTTAAGGTCTTTTCTCCGGA
EBFP2
L3S2P21 terminator
3,430
3,440
3,450
3,460
3,470
3,480
3,490
3,500
3,510
3,520
3,530
BspEI
CCCGAAAGGGGGCCTTTTTTCGTTTTGGTCCGGAAACACAGAAAAAAGCCCGCACCTGACAGTGCGGGCTTTTTTTTCGACCAAAGGTCATAAAAAATTTATTTGCT
GGGCTTTCCCCCGGAAAAAAGCAAAACCAGGCCTTTGTGTCTTTTTTCGGGCGTGGACTGTCACGCCCGAAAAAAAAGCTGGTTTCCAGTATTTTTTAAATAAACGA
L3S2P21 terminator
ECK120033737 terminator
PN25 promtoer
3,540
3,550
3,560
3,570
3,580
3,590
3,600
3,610
3,620
3,630
XbaI
TTCAGGAAAATTTTTCTGTATAATAGATTCAAGGAGATATACCATGTCTAGATTAGATAAAAGTAAAGTGATTAACAGCGCATTAGAGCTGCTTAATGAGGTCGGAA
AAGTCCTTTTAAAAAGACATATTATCTAAGTTCCTCTATATGGTACAGATCTAATCTATTTTCATTTCACTAATTGTCGCGTAATCTCGACGAATTACTCCAGCCTT
PN25 promtoer
RBS
TetR
3,640
3,650
3,660
3,670
3,680
3,690
3,700
3,710
3,720
3,730
3,740
Bpu10I
TCGAAGGTTTAACAACCCGTAAACTCGCCCAGAAGCTAGGTGTAGAGCAGCCTACATTGTATTGGCATGTAAAAAATAAGCGGGCTTTGCTCGACGCCTTAGCCATT
AGCTTCCAAATTGTTGGGCATTTGAGCGGGTCTTCGATCCACATCTCGTCGGATGTAACATAACCGTACATTTTTTATTCGCCCGAAACGAGCTGCGGAATCGGTAA
TetR
3,750
3,760
3,770
3,780
3,790
3,800
3,810
3,820
3,830
3,840
3,850

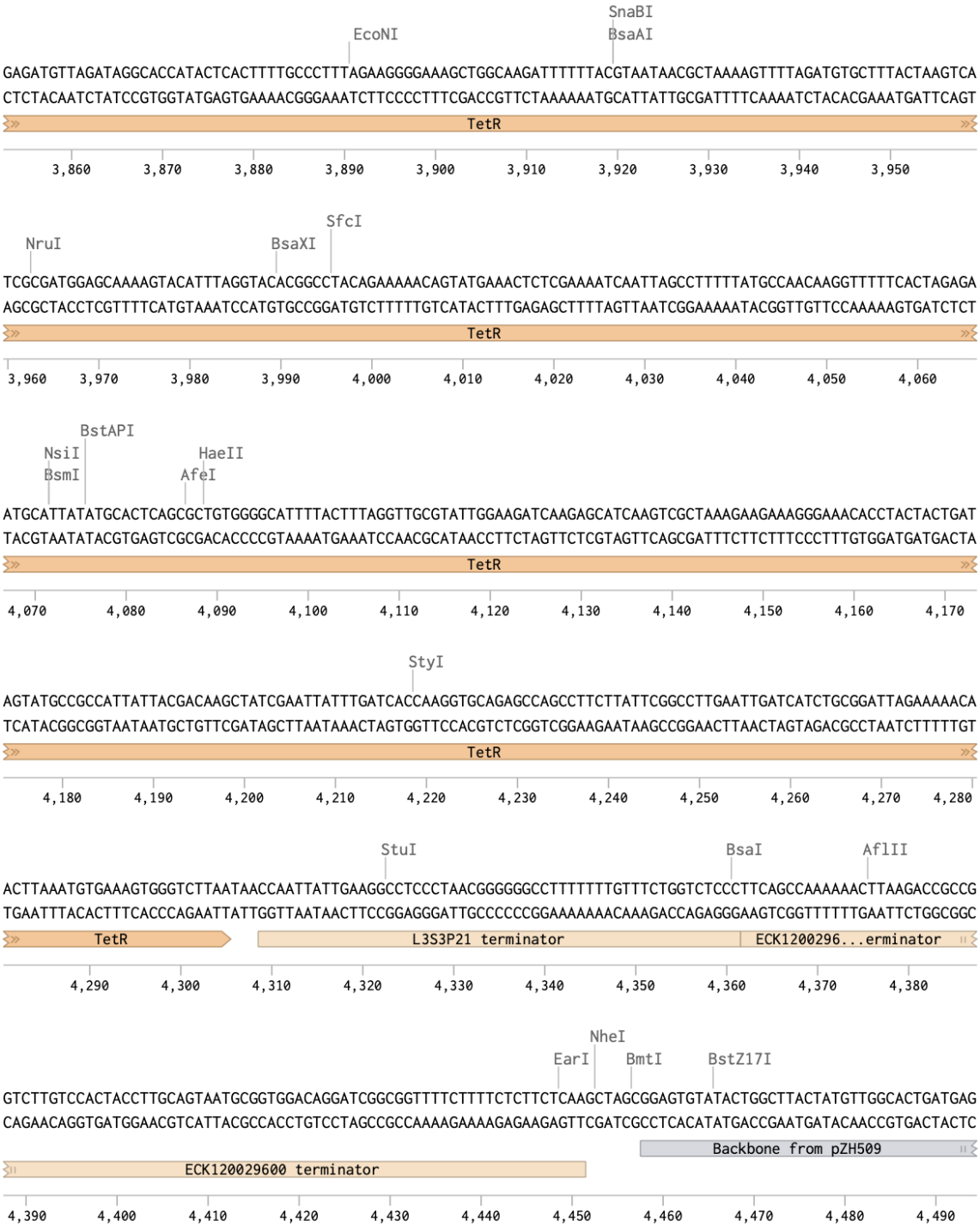
SnaBI
BsaAI
EcoNI
GAGATGTTAGATAGGCACCATACTCACTTTTGCCCTTTAGAAGGGGAAAGCTGGCAAGATTTTTTACGTAATAACGCTAAAAGTTTTAGATGTGCTTTACTAAGTCA
CTCTACAATCTATCCGTGGTATGAGTGAAAACGGGAAATCTTCCCCTTTCGACCGTTCTAAAAAATGCATTATTGCGATTTTCAAAATCTACACGAAATGATTCAGT
TetR
3,860
3,870
3,880
3,890
3,900
3,910
3,920
3,930
3,940
3,950
SfcI
NruI
BsaXI
TCGCGATGGAGCAAAAGTACATTTAGGTACACGGCCTACAGAAAAACAGTATGAAACTCTCGAAAATCAATTAGCCTTTTTATGCCAACAAGGTTTTTCACTAGAGA
AGCGCTACCTCGTTTTCATGTAAATCCATGTGCCGGATGTCTTTTTGTCATACTTTGAGAGCTTTTAGTTAATCGGAAAAATACGGTTGTTCCAAAAAGTGATCTCT
TetR
3,960
3,970
3,980
3,990
4,000
4,010
4,020
4,030
4,040
4,050
4,060
BstAPI
NsiI
BsmI
HaeII
AfeI
ATGCATTATATGCACTCAGCGCTGTGGGGCATTTTACTTTAGGTTGCGTATTGGAAGATCAAGAGCATCAAGTCGCTAAAGAAGAAAGGGAAACACCTACTACTGAT
TACGTAATATACGTGAGTCGCGACACCCCGTAAAATGAAATCCAACGCATAACCTTCTAGTTCTCGTAGTTCAGCGATTTCTTCTTTCCCTTTGTGGATGATGACTA
TetR
4,070
4,080
4,090
4,100
4,110
4,120
4,130
4,140
4,150
4,160
4,170
StyI
AGTATGCCGCCATTATTACGACAAGCTATCGAATTATTTGATCACCAAGGTGCAGAGCCAGCCTTCTTATTCGGCCTTGAATTGATCATCTGCGGATTAGAAAAACA
TCATACGGCGGTAATAATGCTGTTCGATAGCTTAATAAACTAGTGGTTCCACGTCTCGGTCGGAAGAATAAGCCGGAACTTAACTAGTAGACGCCTAATCTTTTTGT
TetR
4,180
4,190
4,200
4,210
4,220
4,230
4,240
4,250
4,260
4,270
4,280
StuI
BsaI
AflII
ACTTAAATGTGAAAGTGGGTCTTAATAACCAATTATTGAAGGCCTCCCTAACGGGGGGCCTTTTTTTGTTTCTGGTCTCCCTTCAGCCAAAAAACTTAAGACCGCCG
TGAATTTACACTTTCACCCAGAATTATTGGTTAATAACTTCCGGAGGGATTGCCCCCCGGAAAAAAACAAAGACCAGAGGGAAGTCGGTTTTTTGAATTCTGGCGGC
TetR
L3S3P21 terminator
ECK1200296...erminator
4,290
4,300
4,310
4,320
4,330
4,340
4,350
4,360
4,370
4,380
NheI
EarI
BmtI
BstZ17I
GTCTTGTCCACTACCTTGCAGTAATGCGGTGGACAGGATCGGCGGTTTTCTTTTCTCTTCTCAAGCTAGCGGAGTGTATACTGGCTTACTATGTTGGCACTGATGAG
CAGAACAGGTGATGGAACGTCATTACGCCACCTGTCCTAGCCGCCAAAAGAAAAGAGAAGAGTTCGATCGCCTCACATATGACCGAATGATACAACCGTGACTACTC
Backbone from pZH509
ECK120029600 terminator
4,390
4,400
4,410
4,420
4,430
4,440
4,450
4,460
4,470
4,480
4,490

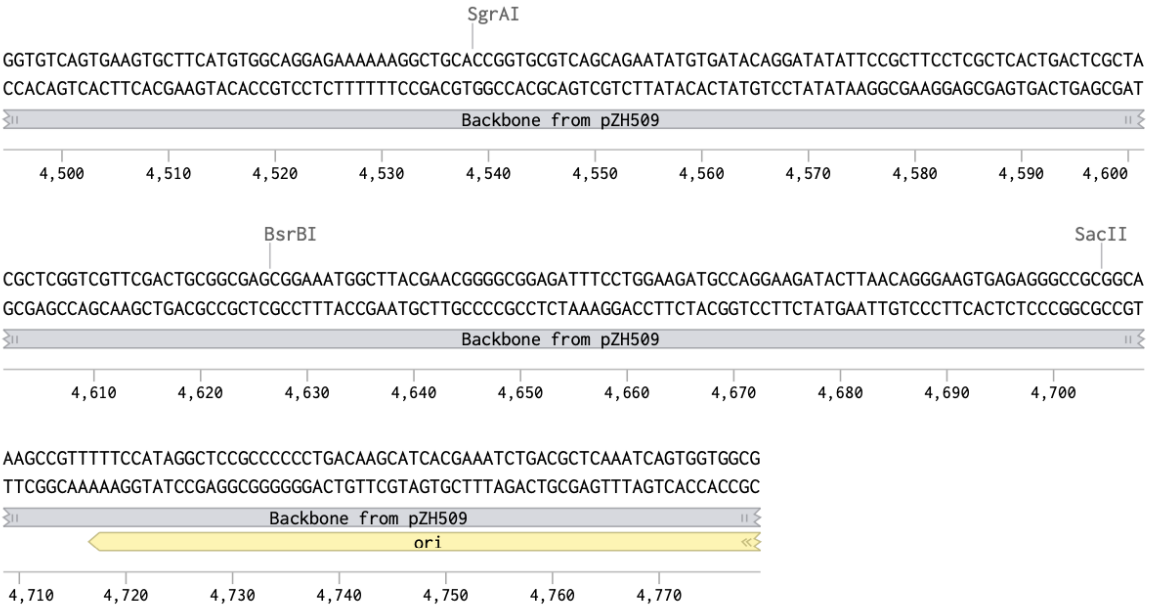

Figure B. 6 Sequence map of the regulator strain

Appendix C

Table C. 1 Positions measured in the single-bead experiment on Day 1

Channel	Treatment (OHHL induction)	Position				
1	10^{-10} M	12	19	31	33	42
2	10^{-8} M	55	58	66	70	72
3	10^{-6} M	103	106	110	125	126
4	0 M	151	154	174	176	190

Table C. 2 Time points when the sizes of the measured areas were last adjusted in the single-bead experiment on Day 1 (correspond to Table C.1)

Channel	Treatment (OHHL induction)	Time point				
1	10^{-10} M	17	16	17	17	18
2	10^{-8} M	14	17	15	19	15
3	10^{-6} M	21	16	16	17	17
4	0 M	18	17	18	19	17

Table C. 3 Area sizes when the sizes of the measured areas were last adjusted in the single-bead experiment on Day 1 (correspond to Table C.2)

Channel	Treatment (OHHL induction)	Area size (a.u.)				
1	10^{-10} M	6056	4156	4670	6285	5319
2	10^{-8} M	7805	4068	3576	4309	9294
3	10^{-6} M	4770	5682	4835	4132	3576
4	0 M	4749	6412	5554	5701	7078

Table C. 4 Positions measured in the single-bead experiment on Day 2

Channel	Treatment (OHHL induction)	Position				
1	10^{-9} M	2	6	7	12	16
2	10^{-7} M	30	33	38	43	46
3	10^{-5} M	66	76	79	82	85
4	0 M	108	109	115	121	126

Table C. 5 Time points when the sizes of the measured areas were last adjusted in the single-bead experiment on Day 2 (correspond to Table C.4)

Channel	Treatment (OHHL induction)	Time point				
1	10^{-9} M	14	15	12	30	12
2	10^{-7} M	10	18	13	13	14
3	10^{-5} M	13	16	13	12	7
4	0 M	12	13	18	16	11

Table C. 6 Area sizes when the sizes of the measured areas were last adjusted in the single-bead experiment on Day 2 (correspond to Table C.5)

Channel	Treatment (OHHL induction)	Area size (a.u.)				
1	10^{-9} M	4678	12142	7891	7106	10422
2	10^{-7} M	4645	9108	3778	12186	9698
3	10^{-5} M	16408	14269	9941	10671	4765
4	0 M	4744	8775	11671	14769	8262

Table C. 7 Positions and corresponding time points when the sizes of the measured areas were last adjusted in the paired-bead experiment on Day 1

Scenario	5			10			
Treatment (IPTG induction)	Position	Time point		Treatment (IPTG induction)	Position	Time point	
		S	T/P			S	T/P
S + T (0 mM)	253	16	12	S + T (0 mM)	242	12	15
S + P (0 mM)	178	14	18		272	16	18
	192	17	14		278	12	14
	224	13	14		298	18	19
	234	18	17	S + P (0 mM)	170	15	15
S + P (0.025 mM)	81	13	17		177	13	26
	104	14	20		179	13	16
	112	17	20		205	18	23
	115	18	11		217	16	23
	116	14	21		228	14	16
	130	17	25		235	14	22
	134	12	14	S + P (0.025 mM)	95	23	26
	147	14	22		98	28	25
	155	15	15		120	15	28
	156	15	20		122	20	17
S + P (0.3 mM)	5	13	23		133	14	16
	8	25	27		142	14	27
	26	20	24		152	19	20
	66	17	14	S + P (0.3 mM)	16	16	24
	67	20	15		74	23	26
	71	20	19				
	73	19	16				
	78	14	21				

Table C. 8 Positions and corresponding area sizes when the sizes of the measured areas were last adjusted in the paired-bead experiment on Day 1 (correspond to Table C.7)

Scenario	**5**			**10**			
Treatment (IPTG induction)	**Position**	**Area size (a.u.)**		**Treatment (IPTG induction)**	**Position**	**Area size (a.u.)**	
		S	**T/P**			**S**	**T/P**
S + T (0 mM)	253	11305	7362	S + T (0 mM)	242	1325	3224
S + P (0 mM)	178	17170	4832		272	2873	2497
	192	6529	15993		278	10196	9249
	224	27522	21336		298	3588	4963
	234	20718	16742	S + P (0 mM)	170	7385	10921
S + P (0.025 mM)	81	4856	22290		177	9693	8159
	104	22976	12281		179	5406	4433
	112	3503	17362		205	11534	8416
	115	8220	12051		217	17032	12104
	116	11900	13303		228	4464	6118
	130	4825	17862		235	4434	1372
	134	14400	12484	S + P (0.025 mM)	95	2885	16031
	147	15870	6478		98	566	15226
	155	9239	16063		120	2338	1606
	156	4978	8451		122	1170	2763
S + P (0.3 mM)	5	13016	5575		133	1866	4150
	8	22894	6395		142	13652	2244
	26	29825	8614		152	1601	2801
	66	11520	6062	S + P (0.3 mM)	16	8652	2063
	67	5829	3087		74	2499	1444
	71	11834	4785				
	73	12929	5721				
	78	17309	2562				

Table C. 9 Positions and corresponding time points when the sizes of the measured areas were last adjusted in the paired-bead experiment on Day 2

Scenario	5			10			
Treatment (IPTG induction)	Position	Time point		Treatment (IPTG induction)	Position	Time point	
		S	T/P			S	T/P
S + T (0 mM)	247	18	24	S + T (0 mM)	255	25	16
	253	19	14		309	22	22
	258	20	13	S + P (0 mM)	166	17	26
	314	22	22		227	17	17
S + P (0 mM)	160	16	21	S + P (0.025 mM)	80	25	27
	184	13	17		134	22	18
	185	26	15		136	17	24
	188	20	16	S + P (0.3 mM)	5	24	23
	205	17	15		54	21	15
	238	26	25		61	24	16
S + P (0.025 mM)	141	24	17		62	20	27
S + P (0.3 mM)	24	16	21				
	74	17	18				

Table C. 10 Positions and corresponding area sizes when the sizes of the measured areas were last adjusted in the paired-bead experiment on Day 2 (correspond to Table C.9)

Scenario	5			10			
Treatment (IPTG induction)	Position	Area size (a.u.)		Treatment (IPTG induction)	Position	Area size (a.u.)	
		S	T/P			S	T/P
S + T (0 mM)	247	4148	5772	S + T (0 mM)	255	2030	10464
	253	11211	10971		309	3933	1810
	258	12849	12106	S + P (0 mM)	166	6944	1634
	314	17402	6479		227	2428	3699
S + P (0 mM)	160	8872	3723	S + P (0.025 mM)	80	5033	4509
	184	7789	7677		134	7466	8400
	185	7138	8636		136	4989	1202
	188	11194	9263	S + P (0.3 mM)	5	2428	1354
	205	7300	10405		54	12437	3635
	238	12834	4581		61	1780	8162
S + P (0.025 mM)	141	8324	2824		62	2390	1441
S + P (0.3 mM)	24	12335	5053				
	74	2515	9397				

Table C. 11 Positions and corresponding time points when the sizes of the measured areas were last adjusted in the paired-bead experiment on Day 3

Scenario	**5**			**10**			
Treatment (IPTG induction)	**Position**	**Time point**		**Treatment (IPTG induction)**	**Position**	**Time point**	
		S	**T/P**			**S**	**T/P**
S + T (0 mM)	-	-	-	S + T (0 mM)	259	15	14
S + P (0 mM)	-	-	-	S + P (0 mM)	216	17	15
S + P (0.025 mM)	83	16	18	S + P (0.025 mM)	-	-	-
	149	18	15	S + P (0.3 mM)	22	16	19
	157	13	16				
S + P (0.3 mM)	13	15	16				

Table C. 12 Positions and corresponding area sizes when the sizes of the measured areas were last adjusted in the paired-bead experiment on Day 3 (correspond to Table C.11)

Scenario	**5**			**10**			
Treatment (IPTG induction)	**Position**	**Area size (a.u.)**		**Treatment (IPTG induction)**	**Position**	**Area size (a.u.)**	
		S	**T/P**			**S**	**T/P**
S + T (0 mM)	-	-	-	S + T (0 mM)	259	3519	1677
S + P (0 mM)	-	-	-	S + P (0 mM)	216	5363	3345
S + P (0.025 mM)	83	12112	5085	S + P (0.025 mM)	-	-	-
	149	1000	5840	S + P (0.3 mM)	22	5066	2267
	157	8282	9434				
S + P (0.3 mM)	13	12605	3209				